12-2011

Preparation and Characterization of Biomimetic Hydroxyapatite-Resorbable Polymer Composites for Hard Tissue Repair

Kristopher R. Hiebner
University of Nebraska-Lincoln, kris.hiebner@huskers.unl.edu

Preparation and Characterization of Biomimetic Hydroxyapatite-Resorbable Polymer Composites for Hard Tissue Repair

By

Kristopher Robert Hiebner

A Dissertation

Presented to the Faculty of

The Graduate College at the University of Nebraska

In Partial Fulfillment of Requirements

For the Degree of Doctor of Philosophy

Major: Chemistry

Under the Supervision of Professor Jody G. Redepenning

Lincoln, Nebraska

December 2011

Preparation and Characterization of Biomimetic

Hydroxyapatite-Resorbable Polymer Composites for Hard Tissue Repair

Kristopher Robert Hiebner, Ph.D.

University of Nebraska, 2011

Advisor: Jody G. Redepenning

Autografts are the orthopedic "gold standard" for repairing bone voids. Autografts are osteoconductive and do not elicit an immune response, but they are in short supply and require a second surgery to harvest the bone graft. Allografts are currently the most common materials used for the repair of segmental defects in hard tissue. Unlike autografts, allografts can cause an undesirable immune response and the possibility of disease transmission is a major concern. As an alternative to the above approaches, recent research efforts have focused on the use of composite materials made from hydroxyapatite (HA) and bioresorbable polymers, such as poly-L-lactide (PLLA). Recent results have shown that the surface hydroxides on HA can initiate the ring opening polymerization (ROP) of L-lactide and other lactones creating a composite with superior interfacial strength.

This thesis demonstrates that the surface of porous biologically derived HA substrates, such as coralline HA and trabecular bone, can be used to initiate the ROP of L-lactide and other lactones from the vapor phase. This process increases the strength of the porous scaffold through the deposition of a thin, uniform polymer coating, while maintaining the porous structure. The kinetics of the chemical vapor deposition

polymerization (CVDP) are described using a quartz crystal microbalance (QCM). The reaction temperature and monomer vapor pressure are found to affect the rate of the polymerization. Also described in this thesis is the preparation of a porous polymer scaffold that mimics the structure of demineralized bone matrix (DBM). This demineralized bone matrix simulant (DBMS) is created using anorganic bovine bone as a template to initiate the polymerization of various lactones, followed by the removal of the HA scaffold. This material retained its shape and exhibits mechanical properties superior to DBM. Finally it is shown that HA can be used to initiate the ROP of ε-caprolactam and the biocompatibility of various HA/bioresorbable polymer composites are described through the use of cell cultures run in collaboration with a research group specializing in immunology.

Dedication

This dissertation is dedicated to my parents, Robert and Denese. Without your support, guidance, and sacrifices this would not have been possible. I thank you for encouraging and supporting me and my siblings in our pursuit of higher education.

Love,

Kristopher

Acknowledgements

I would like to acknowledge and thank everyone was has helped and supported me as I have completed my dissertation. First and foremost, I would like to thank Crystal, my parents, Robert and Denese, my brothers and sisters, Braden, Grant, Whitney, Jordan, Mattison, and the rest of my family and friends for the support over the past several years.

I would especially like to thank my advisor, Professor Jody G. Redepenning, for his support, guidance, and encouragement. He has helped me develop and evolve as an independent thinker and has provided the opportunity to work on a fascinating research project. I would also like to extend my thanks to my doctoral committee Dr. Christian Binek, Dr. Wonyoung Choe, Dr. David Hage, and Dr. Robert Powers for their support.

I would also like to thank my current and former lab members, Dr. Nathan Stafford, Dr. Chun Juan Zhang, Dr. Jeremy Karr, Dr. Rajesh Rajasekaran, Dr. Troy Wiegand, Dr. Chris Schwartz, Paul Goodman, Ben Wymore, Haoming Li, and Lukasz Guaza for their help. Additionally I would like to thank Dr. Andrei Sokolov for his help with sputtering and lithography, Dr. Natale J. Ianno for his help with sputtering and questions regarding the quartz crystal microbalance, Dr. You (Joe) Zhou and Dr. Han Chen for their help with scanning electron microscopy, Dr. Mark Beatty and Bobby Simetich for their help with mechanical testing, and Les Marquart for his help in the machine shop. Also I would like to acknowledge Dr. Paul Wooley, director of research at Orthopaedic Research Institute at Via Christi Hospital in Wichita, KS, Dr. Haiying Yu, and Zheng Song for performing the cell culture studies.

The funding that made this research possible was provided by the United States Army Medical Research and Materiel Command (USAMRMC) and the University of Nebraska Department of Chemistry. Additional thanks to Biomet, Inc. for donating Pro Osteon and coral samples and Premium Protein Products for donating bovine femurs.

Figures, Equations, and Tables

Table of Contents

Chapter One

Introduction

The repair and replacement of hard tissue is a challenge that has intrigued humans throughout history. Neolithic man was known to perform trephination, the surgical creation of a hole in the cranium.[1] Pre-Incans in Peru not only performed trephination but also cranioplasty, the repair of defects in the skull. Several skulls have been discovered with shells, gourds, and silver or gold plates implanted.[2, 3] For broken bones that would not heal through splinting and fitting together, the Aztecs recommended using an intramedullary graft of wood.[4] The first bone graft procedure was performed in 1501 by an Iranian surgeon, Muhammad Baha' al-Dawla. He reported the surgical treatment of osteomyelitis of the skull through the removal of a portion of the sick bone and replacing it with a piece of bone from a dog.[5, 6] The outcome of that surgery is not known, and Job van Meekeren is often credited with the first successful bone graft procedure in 1668.[7] A defect in a Russian man's skull was repaired by van Meekeren with a piece of bone from a dog. The church considered this unchristian and the man was excommunicated. The recipient of the graft asked to have it removed, but by that point his skull had healed.[8] The first clinical autograft was performed in 1820 by Philips von Walter in Germany.[9] The first allograft was performed in 1880 by William Macewen from Scotland,[10] but it wasn't until 1915 and the publication of F.H. Albee's work on bone graft surgery that bone transplantation became more routinely preformed.[11]

Today, the repair and replacement of hard tissue remains an important issue. Since the beginning of Operation Enduring Freedom (OEF) and Operation Iraqi Freedom (OIF), more than 34,300 (19%) of troops have been wounded. Musculoskeletal injuries

make up 70% of war wounds and 55% are to the extremities. Fractures are 26% of combat injuries, and 82% of all fractures are open fractures.[12, 13] Many of these injuries are caused by improvised explosive devices (IEDs). The average wound caused by an IED requires five surgeries, resulting in an estimated 30,000 surgeries.[14] Fortunately, the survival rate of these injuries is now 90%, higher than any previous conflict. This can be attributed to improvements in body armor, military tactics, improved medical techniques, and rapid evacuations.[15] With the majority of the trauma occurring in OEF and OIF being orthopedic-related, the United States army has placed an emphasis on improving treatment and outcomes of these injuries. The first mission statement listed on the United States Army Institute of Surgical Research Orthopaedic Trauma Research Program (USAISR OTRP) website is "Improved Healing of Segmental Bone Defects: Develop a treatment for fractures likely to become non-unions due to the size of the defect, concomitant neural/vascular injury, or lack of soft tissue coverage. Tissue engineering or regenerative medicine approaches to discover treatments that are capable of working in the face of contamination / infection are desired."[16]

This issue is no less important to the civilian population. As the U.S. population ages, the need to repair damaged bone and tissues due to osteoporosis and other diseases increases. It is estimated that in 2010, 52 million Americans over the age of 50 had osteoporosis or low bone mass.[17] In 2005 alone there were more than 2 million fractures due to osteoporosis, costing a total of $17 billion.[18] In total there are more than 6.5 million fractures a year in the U.S., of which approximately 15% are difficult to heal. This includes both delayed unions and nonunions.[19] Although not as prevalent, bone and joint cancer affects 0.08% of the U.S. population, with a relative survival rate of 66.3%.[20]

The survivors are left with large defects in the bone due to the resection of the tumor, which often require the use of a bone graft to aid in the repair.[21, 22]

The vast majority of bone trauma can be healed through the common treatment of fixation. This involves the alignment, immobilization and stabilization of the bone so the fracture can heal. For simple fractures, this can be achieved using external slings, splints, or casts. More complex open or comminuted fractures may require the use of external fixators. This involves placing pins or wires into the bone above and below the fracture site that are connected to clamps and rods on the outside of the skin. The three most common external fixators are the standard pin fixator, the ring fixator, and the hybrid fixator. No secondary surgery is required to remove the external fixators. Internal fixation can also be used for complex or comminuted fractures. This is achieved through the use of metal wires, pins, screws, plates, and intramedullary mails or rods. Although some devices are left in, a second surgery is often required to remove the device.[23] In cases where the device is left in, the healed bone is not as strong as the preinjury bone due to the differences in flexural properties between the bone and the supporting device.[24] This is known as stress-shielding and can lead to bone atrophy.[25] In addition, even though the fixation device is biologically inert, it is not integrated into the bone. This results in phase boundaries between the bone and the device, which increases the chances of future fractures at the site.[26, 27]

Some traumatic bone injuries lead to segmental bone defects. A segmental bone defect is defined as a gap or fracture in the bone that is too large to be repaired through the normal mechanism used to fuse the two segments.[28-30] The minimum size of this defect, known as the critical size defect, is loosely defined as 2-2.5 times the diameter of

the affected bone.[31, 32] Actual critical size defects vary to some extent based on a variety of factors, including species, defect location, biomechanical conditions, and age, among others.[33] The result is a permanent gap in the bone that requires a graft composed of a bioinert or biocompatible material to aid in the healing process.

An ideal bone graft should not produce an immune response but should provide mechanical support, be osteoconductive and osteoinductive, promote osteogenesis, and eventually be osseointegrated. An osteoconductive graft is one that permits bone growth on its surface and into its pores.[34] It has been argued that the minimum graft porosity needed for regenerating bone is 100 μm,[35, 36] with the optimum macroscopic porosity being between 100 and 500 μm.[37, 38] The pores promote vascularization and aid in the transport of materials and waste. Osteoinduction is defined as the stimulation of osteoprogenitor cells to differentiate into osteoblasts in an extraskeletal site. A bone graft is considered osteogenic if it contains cells that help form new bone.[39] Osseointegration is defined as direct contact between the living bone and implant through the ingrowth of new bone into the graft.[34] Gradually the graft is replaced by the new bone in a process known as creeping substitution.[40]

The material that is the closest to containing all of these properties, and is considered the "gold standard" of bone grafts, is autograft bone. An autograft is defined as bone from one area of the skeleton that is transferred to a different location within the same individual. Ironically, autograft bone does not exhibit the so-called optimum porosity described above. Common autograft preparations include nonvascularized cortical, vascularized cortical, and cancellous bone. Cortical bone is typically harvested from the fibula, rib, or tibia and is used in defects of greater than 5 to 6 cm that require

structural support. Cancellous bone is harvested from the iliac crest and is useful in voids where structural support is not needed. Nonvascularized cortical grafts are osteoconductive but contain little osteoinductive or osteogenic properties.[39] Necrosis and resorption are seen early after transplantation, while new bone growth proceeds at a much slower pace.[41] Vascularized cortical grafts are capable of overcoming the problems associated with necrosis in the early stages in nonvascularized grafts. Studies have shown that after 24 weeks both types of cortical autografts are similarly incorporated, but there is a larger amount of necrotic tissue in the nonvascularized graft.[42] Cancellous autografts are osteoconductive and again provide limited osteogenic properties.[39] Their advantages include rapid revascularization and quick integration times when compared to cortical bone.[42] The advantages of autografts are optimum incorporation, no disease transmission, and histocompatibility, meaning tissue rejection is not an issue; but there are major disadvantages as well. Perhaps the greatest issue is donor site morbidity. Many studies have reported complications when harvesting bone from the iliac crest,[43, 44] as well as lingering pain.[45, 46] Additionally, the supply of autograft bone is limited.[39]

One alternative to an autograft is an allograft. An allograft comes from a donor that is the same species as the recipient. Compared to autografts, there is a very large supply of allograft material and donor site morbidity is not an issue;[47] however, there are several problems with fresh allografts. The first is disease transmission. Second, fresh allografts provoke an immune response that threatens the incorporation or destruction of the graft.[48-54] The antigens of the major histocompatibility complex (MHC) are primarily responsible for the immune response. [55] This response can be reduced if the tissue of the host and graft are properly matched,[49-51] but preservation has been shown to be most

effective in reducing the immune response, improving the incorporation, and reducing disease transmission.[56] Preservation is typically achieved by freezing the material below -60 ^{o}C or by using freeze drying.[57] Although these processes reduce immunogenicity and antigenicity, they also destroy the osteoprogenitor cells and reduce the osteoinductive properties, leaving behind an osteoconductive scaffold. The revascularization and incorporation of the allograft is generally slower compared to autografts, but the process is similar.[58] Complications that can cause failure of the allograft include infection, delayed healing, fractures, significant resorption, or a "walling off" of the allograft.[59-64] The immune response is thought to be the primary cause of these complications. Infection rates have been reported to be as high as 14%, but this is not a result of the transfer process. Instead, it is due to the large amount of necrotic tissue that remains in the graft for an extended period of time.[56, 65, 66] Nonunion has been seen in 11% of cases using frozen allografts.[67] Fractures occur in about 16% of cases, typically two to three years after implantation.[62, 68] The fractures are thought to occur where revascularization and new bone growth are absent. There are numerous long term studies on the outcome of bone allografts.[60, 69, 70] One noteworthy recent study showed a good or excellent result in 77% of patients treated with a massive allograft after the removal of a tumor.[71]

Allograft bone is also often processed as demineralized bone matrix (DBM). DBM was originally produced as a solution to preservation problems in countries where power outages are common.[57, 72, 73] DBM is prepared by the removal of the mineral phase of the bone, hydroxyapatite (HA). The demineralization process leaves behind an organic matrix consisting of noncollagenous proteins, bone growth factors, and collagen.[57, 74, 75] The resulting organic matrix is osteoconductive and osteoinductive but

has no structural strength.[57, 76] Because it has no mechanical strength, it is often used in powder or putty form. The complex mechanism by which DBM stimulates new bone growth is dependent on many factors, including the extent of demineralization, particle size, donor related effects, preparation of the matrix, and degradation of the matrix during demineralization.[75, 77, 78] Due to these many variables, the clinical outcome is often difficult to predict. DBM does not elicit an immune response.[72]

Another less viable alternative to the options summarized earlier is a xenograft. A xenograft is defined as tissue from a member of one species that is transplanted into a member of a different species. The major attraction of xenografts is their large supply. Over the last few decades bone from numerous species has been transplanted into man. The results have generally been poor.[79] Much like allografts, the fresh xenograft produces an immune response that results in inflammation, sequestration, and resorption of the graft.[80-82] Freeze-dried samples show no decrease in the undesirable immunological response.[83, 84] Another problem when using xenografts is disease transmission. One example is when bovine bone is used as the grafting material. It is important to limit exposure to the prion protein (PrP^{Sc}) which is responsible for bovine spongiform encephalitis in cows and Creutzfeldt-Jakob disease in humans. Current products produced from bovine bone are deproteinized through either chemical treatment or sintering at high temperatures, leaving behind the inorganic HA matrix.[79] This deproteinized bovine bone (DBB) has reduced mechanical strength.[85, 86] Biodegradability of these materials differs depending on whether they were sintered or not.[86] Additionally, religious and ethical concerns with transplantation of tissue from other species can pose a problem.[87, 88]

The disadvantages associated with using autografts and allografts have led to research into alternative materials that still possess many of the properties desired in an ideal bone graft substitute. A large amount of research has focused on using a bioactive ceramic, synthetic hydroxyapatite ($Ca_{10}(PO_4)_6(OH)_2$).[89, 90] HA has a similar composition to the mineral portion of bone. Biological HA is prone to ion substitution and is usually calcium deficient and always carbonate substituted. Therefore, an appropriate way to write the formula for biological HA is $(Ca, M)_{10}(PO_4, Y)_6(OH, X)_2$, where M represents cations besides Ca^{2+} (Mg^{2+}, Na^+, K^+, Sr^{2+}, Ba^{2+}); Y represents carbonates, acid phosphate, and sulfates; and X represents F^-, Cl^-, and carbonates.[91] HA can be prepared as dense or macroporous forms. Dense HA is defined as having a maximum porosity of 5% by volume, with micropores of about 1 μm in diameter.[92] It is prepared through a three step process: preparation of the HA powder, compacting or compressing into the desired shape, and sintering. HA can be prepared through precipitation,[93, 94] hydrolysis, solid-state, or hydrothermal reactions.[92, 95] The powder is then compressed at a pressure of 60 to 80 MPa and heated to 950 to 1300 ^oC.[95] Alternative hot-pressing techniques, in which heat and pressure are applied at the same time, can be used.[96] Dense HA is biocompatible,[92] osteoconductive,[97-100] and exhibits good interfacial strength between the bone and the implant.[101, 102] But dense HA is a typical fragile and brittle ceramic. It has a Young's modulus of 35-120 GPa, a bending strength of 38-250 MPa, a compressive strength of 120-900 MPa, and a tensile strength of 38-300 MPa. The listed range of values is due to the different conditions used to prepare the dense HA. All of these values are comparable to bone, but dense HA has a low fracture toughness (K_{IC} = 0.8-1.2 MPa $m^{1/2}$), a Weibull's modulus of 5-18, and a decelerated crack propagation coefficient

that is 26-80 in a dry atmosphere and 12 to 49 in a humid atmosphere. These mechanical parameters make dense HA highly susceptible to slow crack growth and make it unreliable under load. Implants with a Weibull's modulus of 10-20 are expected to fail in several months, meaning dense HA is not suitable for load bearing applications. [91, 92, 95] In addition to inadequate mechanical properties, dense HA is slowly resorbed in the body.[103, 104]

An alternative to using a synthetic dense HA implant is to use a synthetic porous HA implant. There are several methods available to produce porous, synthetic HA scaffolds.[105] One method involves mixing HA powders with volatile particles that burn off when sintered at high temperatures. This method usually produces closed pores.[106, 107] Another method involves mixing HA with water-soluble porogens. This method does not require sintering and produces an interconnected porous structure.[108] A third method produces porous HA by a technique called foaming. Gas evolving reactions are carried out within the HA slurry, causing it to foam. Monomers in the foam are then polymerized and the entire mixture is sintered.[109-111] Other synthetic methods include phase mixing[112] and the polymeric sponge method.[113, 114]

When dense HA scaffolds and porous HA scaffolds are compared, far more fibrous tissue is found within the porous implant and at earlier stages after surgery.[115] There are two reasons the porous HA provides better conditions for new bone growth than dense HA. First, porous HA allows migration and proliferation of osteoblasts and mesenchymal cells to take place. In addition, vascularization can occur within the pores.[116] Second, porous HA provides greater mechanical stability between the surrounding bone and the implant.[117] As stated earlier, Hulbert and Klawitter argue that

the minimum pore size required for regenerating bone is 100 μm. This corresponds well with the average size of the pores in the haversian system, which have diameters between 100 and 200 μm.[35, 36] In addition to pore size, interconnectivity is also important.[118-123] Interconnected pores allow cells to penetrate into the scaffold and vascularization to take place throughout so that bone growth occurs within.[124-127] Although larger pores and greater interconnectivity produce more bone ingrowth, the mechanical strength decreases as these properties increase.[105, 128, 129] For example, increasing the pore volume from 10 to 20% results in a decrease in the mechanical strength by a factor of four.[130, 131, 132] The porosity also increases the surface area of the HA implant, which leads to greater resorption than dense HA.[133]

The materials described above are attempts to mimic the bone structure produced by nature.[134] An alternative to producing synthetic structures is to use materials already provided by nature. One example of a natural porous substrate is coral. Coral is composed of calcium carbonate, usually in the mineral form aragonite. The two genera of coral that receive the most attention are *Porites* and *Goniopora* because of their structural similarities to human bone. *Porites* has a void volume of 66%, a pore size of 230 μm, and an interconnecting pore size of 190 μm. *Goniopora* has a pore size of 600 μm and an interconnecting pore size of 220 to 260 μm.[135] Although the unaltered coral can be used as a bone graft scaffold, it is usually considered inadequate due to its high dissolution rate and poor longevity and stability.[134] It is possible to convert the calcium carbonate in coral to hydroxyapatite via hydrothermal exchange while maintaining the macroscopic structure.[136] The new material is often called coralline hydroxyapatite and has been shown to be an effective osteoconductive scaffold for the generation of new

bone.[122, 137-140] Conversion to 100% HA is possible, but the reaction can also be terminated early to produce a material with a calcium carbonate core and a thin HA layer. Scaffolds that are not completely converted to HA dissolve faster than scaffolds composed completely of HA.[97]

Porous HA can also be derived from bovine bone. This scaffold is produced by removing the organic material, generally through the use of one of two methods. The first method involves using highly caustic solutions to dissolve and hydrolyze the organic material. The second method involves removal of the organic material through heating at high temperatures.[89, 90, 141-143] These methods can be used to produce anorganic bone with a porous scaffold that is identical in structure and composition to the original bone while exhibiting good osteoconduction.[144-147]

Bioresorbable polymers have also been used in a variety of ways for bone fixation and repair. Among synthetic polymers, polyesters have been extensively researched. This class of polymers includes poly-L-lactide (PLLA), polyglycolide (PGA), poly-ε-caprolactone (PCLN), poly-p-dioxanone (PD), and copolymers of these polymers. The attractiveness of these polymers lies with their ability to undergo hydrolysis at the ester linkage, eventually leading to the complete breakdown of the implanted material.[148] The degradation mechanism is regarded as bulk erosion, as evident by the large molecular weight decrease that precedes the release of the monomer.[149] Currently, these materials are most commonly used in sutures, rotator cuff repair, and as fixation plates and screws for non-load bearing applications.[150-156] The downside to solid implants composed completely of PLLA is slow bone ingrowth, fibrous encapsulation of the implant, and localized acidosis due to polymer degradation.[157-161] In addition, such solid polymer

devices remain in the recipient for several years and can actually inhibit the healing process.[162] One study saw local inflammatory reactions and intraosseous cysts in the bone where bioresorbable polymer implants were placed.[163] Recent work has focused on creating highly porous scaffolds to promote bone growth. These porous polymer matrixes can be created by a variety of methods, including fiber bonding, solvent casting/particulate leaching, gas foaming, and phase separation.[164-166] The polymer scaffolds often exhibit good osteocompatibilty[167] and osteoconductivity.[168] Local acidosis is generally not a problem with highly porous scaffolds because they have a low polymer mass per unit volume and, in general,[161] the buffering capacity of biological fluids is able to compensate for the acidic products of the degradation. Furthermore, the movement of these fluids dilutes and diffuses the products away from the implant site.[160, 169, 170] Of concern when using bioresorbable polymer scaffolds is the mechanical strength over time. The bulk degradation mechanism can lead to a large decrease in the mechanical properties over a short period of time because of the large surface area of the porous scaffold.[167] The mass and strength loss depend on many factors, including polymer properties, implant configuration, *in vitro* test conditions, and *in vivo* conditions.[148, 171, 172] Ideally the degradation rate and mechanical strength loss compliments the healing rate of the bone to prevent failure of the device.[173]

Unfortunately, ceramic and polymer implants alone don't accurately mimic the structure of bone. Bone is composed of an organic matrix (30-35% by weight), made up of mainly type I collagen, with an inorganic mineral phase (65-70% by weight) dispersed throughout. The inorganic material, HA, provides the mechanical strength and rigidity, while the organic matrix provides flexibility and elasticity.[174] To more closely mimic the

unique structural characteristics of bone, researchers have investigated using HA as a filler within a matrix of a bioresorbable polymer. The polymer helps to overcome the brittleness of the HA, and the ceramic improves the mechanical properties and osteoconductivity of the polymer matrix.[175-178] Several studies have examined the efficacy of PLLA/HA composites in animal models.[179-186] One study where PLLA/HA composites were implanted in the tibias of rabbits found bony ingrowth into the implant. The polymer was absorbed gradually over time and no adverse reactions were seen.[180] Early composites were formed by taking a high molecular weight polymer and combining it with HA through various methods, such as solvent solution casting, melt mixing, and mechanical pressing.[187] Although the results were promising, a lack of interfacial bonding and adhesion between the two phases limited the mechanical strength of the composite materials.[188-191] Because the HA was not bonded to the polymer, the interface served as a point of failure and failure propagation.[192] To overcome this problem, several researchers have attempted to modify the surface of HA to improve the interfacial bonding between the HA and the polymer matrix.[193-195]

Typically, the ring opening polymerization of lactones is performed using tin(II) octoate ($Sn(oct)_2$) as a catalyst and an alcohol as an initiator. This polymerization occurs via coordination insertion with the final polymer having an alcohol and ester end group, which prevents the polymer from bonding to the surface of HA.[196-201] Recently an alternative method for the production of HA/polymer composites has been developed. This method uses the nucleophilic hydroxides on the surface of HA to initiate the ring opening polymerization of various lactones. This polymerization process is anionic.[202-204] In the resulting composite, the bioresorbable polymer is directly bonded to the surface of

the HA. This improved interfacial interaction between HA and the bioresorbable polymer produces a composite with superior mechanical properties. One recent study used an anorganic bone scaffold to initiate the polymerization of L-lactide. The monomer polymerized within the porous framework and the resulting composite had a macroscopic morphology similar to the original bone, with the polymer replacing the original organic matrix. The composites exhibited compressive strength and an elastic modulus similar to that of human femoral bone.[205]

The research presented in this dissertation is based on a continuing effort in our research group to use the nucleophilic surface of HA to initiate the ring opening polymerization of L-lactide and other lactones. The resulting composite material can potentially be used for the repair of hard tissues. Previous work has focused on using synthetic and biological powdered HA and anorganic cortical bone to initiate the polymerization of lactones. These reactions were performed with the HA in direct contact with the molten monomer and resulted in a nonporous composite. The anorganic bone/PLLA composites exhibited a macroscopic morphology and mechanical properties similar to that of the original bone.[205-207]

My efforts, described in the proceeding chapters, will mainly focus on the creation of porous polymer/ceramic materials that can potentially be used for hard tissue repair. Interconnected porosity is a highly desirable trait of bone graft substitutes because it improves the osteoconductivity of the material by allowing cells to penetrate into the scaffold and provide vascularization throughout so that bone growth occurs within the scaffold.[124-127] Many attempts have been made to produce a synthetic porous scaffold that mimics the structure of bone. Alternatively, nature provides numerous porous

ceramic scaffolds that resemble the structure of bone. These include coral and anorganic bone. The problem with both synthetic and naturally occurring ceramic porous scaffolds is the mechanical properties are often ill suited for load bearing applications. Improvements in the mechanical properties can be made by introducing a polymer coating onto the scaffold; however, there is not a direct bond between the ceramic and the polymer, and the coating processes can leave behind uneven polymer films and partially filled pores. Chapter 2 will describe my efforts to use the nucleophilic surface of various biologically derived porous substrates to initiate the polymerization of lactones. The process produces thin, even polymer films and leaves the pores intact. The attachment of the polymer to the surface creates a better interfacial strength and increases the mechanical properties of the scaffold. Chapter 3 examines the kinetics of the polymerization process through the use of a quartz crystal microbalance.

A different type of porous material is described in Chapter 4. As in previous work within our group, anorganic bone is used to initiate the polymerization of various lactones. Removal of the inorganic material leaves a porous polymer substrate. Because anorganic bone was used as the template, the resulting polymer matrix has a structure similar to DBM. Unlike DBM, the material maintains its original structure and exhibits improved mechanical properties.

In addition to the production of the porous substitutes described above, Chapter 5 focuses on using HA and anorganic bone to initiate the polymerization of the lactam ε-caprolactam. ε-Caprolactam is structurally similar to ε-caprolactone but contains an amide group in place of the ester group. Poly-ε-caprolactam (PCLM) degrades slower in

the body than polylactones, which could be advantageous in load bearing applications where implant strength is needed over an extended period of time.

Any material that will potentially be implanted into the body for hard tissue repair must be biocompatible. Chapter 6 describes preliminary results based on cell culture experiments designed to assess the cytotoxicity and inflammatory response toward the HA/polymer composites. In summary, the research in this dissertation describes my efforts to create various biocompatible HA/polymer composites that can potentially be used for hard tissue repair.

References

1. Sanan, A.; Haines, S.J., Repairing holes in the head: A history of cranioplasty. *Neurosurgery* **1997**, 40, 588-602.

2. Pietrzak, W.S., Musculoskeletal and wound treatment through the ages: A brief historical tour. In *Musculoskeletal Tissue Regeneration: Biological Materials and Methods*, Pietrzak, W.S., ed.; Humana Press: Totowa, New Jersey, 2008.

3. Longacre, J.J.; de Stefano, G.A., Reconstruction of extensive defects of the skull with split rib grafts. *Plastic and Reconstructive Surgery* **1957**, 19, 186-200.

4. Burwell, R.G., History of bone grafting and bone substitutes with special reference to osteogenic induction. In *Bone Grafts, Derivatives and Substitutes*, Urist, M.R.; O'Connor, B.T.; Burwell, R.G., eds.; Butterworth-Heinemann: Oxford, England, 1994.

5. Rodriguez, U.H., Grafting of bone from a dog into the human skull: An historical note. *Plastic and Reconstructive Surgery* **1995**, 96, 1481.

6. Deschamps, J.-Y.; Roux, F.A.; Saï, P.; Gouin, E., History of xenotransplantation. *Xenotransplantation* **2005**, 12, 91-109.

7. van Meekeren, J., *Heel en geneeskonstige aanmerkingen*. C. Commelijn: Amsterdam, The Netherlands, 1668**.**

8. de Boer, H.H., The history of bone grafts. *Clinical Orthopaedics and Related Research* **1988**, 226, 292-298.

9. von Walter, P., Wiedereinheilung der bei der trepanation ausgebohrten Knochenscheibe. *Journal der Chirurgie und Augen-Heilkunde* **1821**, 2, 571.

10. Macewen, W., Observations concerning transplantation on bone. *Proceedings of the Royal Society of London* **1881**, 32, 232.

11. Albee, F.H., *Bone Graft Surgery*. W.B. Saunders: Philadelphia, Pennsylvania, 1915.

12. Ling, G.S.F.; Rhee, P.; Ecklund, J.M., Surgical innovations arising from the Iraq and Afghanistan wars. *Annual Review of Medicine* **2010**, 61, 457-468.

13. Owens, B.D.; Kragh, J.F.; Macaitis, J.; Svoboda, S.J., Characterization of extremity wounds in Operation Iraqi Freedom and Operation Enduring Freedom. *Journal of Orthopaedic Trauma* **2007**, 21, 254-257.

14. Hyer, R., Iraq and Afghanistan producing new pattern of extremity war injuries, http://www.medscape.com/viewarticle/528624, March 2006, Accessed July 26, 2011.

15. Pollack, P.; Rogers, C., A brief background of combat injuries. *American Academy of Orthopaedic Surgeons (AAOS) Now* **2007**, Mar/Apr. http://www.aaos.org/news/bulletin/marapr07/research2.asp, Accessed July 26, 2011.

16. United States Army Institute of Surgical Research Orthopaedic Trauma Research Program, http://www.usaisr.amedd.army.mil/otrp.html, November 2010, Accessed July 26, 2011.

17. National Osteoporosis Foundation, Prevalence Report. http://www.nof.org/advocacy/resources/prevalencereport, Accessed July 27, 2011.

18. Burge, R.; Dawson-Hughes, B.; Solomon, D.H.; Wong, J.B.; King, A.; Tosteson, A., Incidence and economic burden of osteoporosis-related fractures in the United States, 2005-2025. *Journal of Bone and Mineral Research* **2007**, 22, 465-475.

19. Braddock, M.; Houston, P.; Campbell, C.; Ashcroft, P., Born again bone: Tissue engineering for bone repair. *News in Physiological Sciences* **2001**, 16, 208-213.

20. National Cancer Institute, Surveillance Epidemiology and End Results (SEER) Stat Fact Sheets: Bone and Joint. http://seer.cancer.gov/statfacts/html/bones.html#incidence-mortality, Accessed July 27, 2011.

21. Mankin, H.J.; Gebhardt, M.C.; Jennings, L.C.; Dempsey, S.; Tomford, W.W., Long-term results of allograft replacement in the management of bone tumors. *Clinical Orthopaedics and Related Research* **1996**, 324, 86-97.

22. Enneking, W.F.; Eady, J.L.; Burchardt, H., Autogenous cortical bone grafts in the reconstruction of segmental skeletal defects. *Journal of Bone and Joint Surgery* **1980**, 62A, 1039-1057.

23. Taljanovic, M.S.; Jones, M.D.; Ruth J.T.; Benjamin, J.B.; Sheppard, J.E.; Hunter, T.B., Fracture fixation. *RadioGraphics* **2003**, 23, 1569-1590.

24. Friedlaender, G.E.; Horowitz, M.C., Immune responses to osteochondral allografts: nature and significance. *Orthopedics* **1992**, 15, 1171-1175.

25. Ramakrishna, S.; Huang, Z.-M. Kumar, G.V.; Batchelor, A.W.; Mayer, J., *An Introduction to Biocomposites*; Imperial College: London, England, 2004.

26. Rokkanen, P.U.; Bostman, O.; Hirvensalo, E.; Makela, E.A.; Partio, E.K.; Patiala, H.; Vanionpaa, S.; Vihtonen, K.; Tormala, P., Bioresorbable fixation in orthopedic surgery and traumatology. *Biomaterials* **2000**, 21, 2607-2613.

27. Sivakumar, M.; Mudali, U.K.; Rajeswari, S., Investigation of failures in stainless steel orthopedic implant devices: Fatigue failure due to improper fixation of a compression bone plate. *Journal of Materials Science Letters* **1994**, 13, 142-145.

28. Egol, K.; Koval, K.J.; Zuckerman, J.D., *Handbook of Fractures*, 4th ed.; Lippincott Williams and Wilkins: Philadelphia, Pennsylvania, 2010.

29. Ip, D., *Orthopedic Traumatology – A Resident's Guide*, 2nd ed.; Springer: Berlin, Germany, 2008.

30. Delahay, J.N.; Wiesel, S.W., *Essential of Orthopedic Surgery*, 3rd ed.; Springer: Berlin, Germany, 2006.

31. Lindsey, R.W.; Gugala, Z.; Milne, E.; Sun, M.; Gannon, F.H.; Latta, L.L., The efficacy of cylindrical titanium mesh cage for the reconstruction of a critical-size canine segmental femoral diaphyseal defect. *Journal of Orthopaedic Research* **2006**, 24, 1438-1453.

32. Gugala, Z.; Lindsey, R.W.; Gogolewski, S., New approaches in the treatment of critical-size segmental defects in long bones. *Macromolecular Symposia* **2007**, 253, 147-161.

33. Reichert, J.C.; Saifzadeh, S.; Wullschleger, M.E.; Epari, D.R.; Schütz, M.A.; Duda, G.N.; Schell, H.; van Griensven, M.; Redl, H.; Hutmacher, D.W., The challenge of establishing preclinical models for segmental bone defect research. *Biomaterials* **2009**, 30, 2149-2163.

34. Albrektsson, T.; Johansson, C., Osteoinduction, osteoconduction and osseointegration. *European Spine Journal* **2001**, 10, S96-S101.

35. Hulbert, S.F.; Young, F.A.; Mathews, R.S.; Klawitter, J.J.; Talbert, C.D.; Stelling, F.H., Potential of ceramic materials as permanently implantable skeletal prostheses. *Journal of Biomedical Materials Research* **1970**, 4, 433-456.

36. Klawitter, J.J.; Hulbert, S.F., Application of porous ceramics for the attachment of load bearing internal orthopedic applications. *Journal of Biomedical Materials Research* **1971**, 5, 161-229.

37. Daculsi, G.; Passuti, N., Effect of the macroporosity for osseous substitution of calcium phosphate ceramics. *Biomaterials* **1990**, 11, 86-87.

38. Feng, B.; Jinkang, Z.; Zhen, W.; Jianxi, L.; Jiang, C.; Jian, L.; Guolin, M.; Xin, D., The effect of pore size on the tissue ingrowth and neovascularization in porous bioceramics of controlled architecture in vivo. *Biomedical Materials* **2011**, 6, 015007.

39. Fujishiro, T.; Kobayashi, H.; Bauer, T.W., Autograft bone. In *Musculoskeletal Tissue Regeneration: Biological Materials and Methods*, Pietrzak, W.S., ed.; Humana Press: Totowa, New Jersey, 2008.

40. Goldberg, V.M.; Akhavan, S., Biology of bone grafts. In *Bone Regeneration and Repair: Biology and Clinical Applications*, Lieberman, J.R.; Friedlaender, G.F., eds.; Humana Press: Totowa, New Jersey, 2005.

41. Goldberg, V.M.; Stevenson, S., Natural history of autografts and allografts. *Clinical Orthopaedics and Related Research* **1987**, 225, 7-16.

42. Dell, P. C.; Burchardt, H.; Glowczewskie, F. P., Jr., A roentgenographic, biomechanical, and histological evaluation of vascularized and non-vascularized segmental fibular canine autografts. *Journal of Bone and Joint Surgery-American Volume* **1985,** 67, 105-112.

43. Finkemeier, C. G., Bone-grafting and bone-graft substitutes. *Journal of Bone and Joint Surgery-American Volume* **2002,** 84-A, 454-464.

44. Arrington, E. D.; Smith, W. J.; Chambers, H. G.; Bucknell, A. L.; Davino, N. A., Complications of iliac crest bone graft harvesting. *Clinical Orthopaedics and Related Research* **1996,** 329, 300-309.

45. Sasso, R.C.; LeHuec, J.C.; Shaffrey, C., Iliac crest bone graft donor site pain after lumbar interbody fusion: A prospective patient satisfaction outcome assessment. *Journal of Spinal Disorders and Techniques* **2005**, 18, S77-S81.

46. Summers, B.N.; Eisenstein, S.M., Donor site pain from the ilium. A complication of lumber spine fusion. *Journal of Bone and Joint Surgery – British Volume* **1989**, 71, 677-680.

47. Bauer, T.W.; Muschler, G.F., Bone graft materials. *Clinical Orthopaedics* **2000**, 371, 10-27**.**

48. Goldberg, V.M., Biology of bone allograft and clinical application. In *Musculoskeletal Tissue Regeneration: Biological Materials and Methods*, Pietrzak, W.S., ed.; Humana Press: Totowa, New Jersey, 2008.

49. Bos G.; Goldberg, V.M.; Powell, A.E.; Heiple, K.G.; Zika, J.M., The effect of histocompatibility matching on canine frozen bone allograft. *Journal of Bone and Joint Surgery* **1983**, 65A, 89-96.

50. Goldberg, V.M.; Bos, G.D.; Heiple, K.G.; Zika, J.M.; Powell, A.E., Improved acceptance of frozen bone allografts in genetically mismatched dogs by immunosuppression. *Journal of Bone and Joint Surgery* **1984**, 66, 937-950.

51. Goldberg, V.M.; Powell, A.; Shaffer, J.W.; Zika, J.; Bos, G.D.; Heiple, K.G., Bone grafting: Role of histocompatibility in transplantation. *Journal of Orthopaedic Research* **1985**, 3, 389-404.

52. Bos, G.D.; Goldberg, V.M.; Gordon, N.H.; Dollinger, B.M.; Zika, J.M.; Powell, A.E.; Heiple, K.G., The long-term fate of fresh and frozen orthotopic bone allografts in genetically defined rats. *Clinical Orthopaedics* **1985**, 197, 245-254.

53. Stevenson, S., The immune response to osteochondral allografts in dogs. *Journal of Bone and Joint Surgery* **1987**, 69A, 573-582.

54. Stevenson, S.; Li, S.; Martin, B., The fate of cancellous and cortical bone after transplantation of fresh and frozen tissue-antigen-matched and mismatched osteochondral allografts in dogs. *Journal of Bone and Joint Surgery* **1991**, 73A, 1143-1156.

55. Stevenson, S.; Horowitz, M., Current concepts review: The response of bone allografts. *Journal of Bone and Joint Surgery* **1992**, 74A, 939-950.

56. Tomford, W.W.; Thongphasuk, J.; Mankin, H.J.; Ferraro, M.J., Frozen musculoskeletal allografts. A study of the clinical incidence and causes of infection associated with their use. *Journal of Bone and Joint Surgery* **1990**, 72A, 657-663.

57. Sutherland, D.; Bostrom, M., Grafts and bone graft substitutes. In *Bone Regeneration and Repair: Biology and Clinical Applications*, Lieberman, J.R.; Friedlaender, G.F., eds.; Humana Press: Totowa, New Jersey, 2005.

58. Nunamaker, D.M.; Rhinelander, F.W., Bone grafting. In *Textbook of Small Animal Orthopaedics*, Newton, C.D.; Nunamaker, D.M., eds.; J.B. Lippincott: Philadelphia, Pennsylvania, 1985.

59. Mankin, H.J., Complications in allograft surgery. In *Osteochondral Allografts*, Friedlaender, G.E.; Mankin, H.J.; Sell, K.W., eds.; Little, Brown: Boston, Massachusetts, 1983.

60. Mankin, H.J.; Gebhardt, M.C.; Jennings, L.C.; Springfield, D.S.; Tomford, W.W., Long-term results of allograft replacement in the management of bone tumors. *Clinical Orthopaedics* **1996**, 324, 86-87.

61. Temple, H.T.; Scully, S.P.; O'Keefe, R.J.; Kattapurum, S.; Mankin, H.J., Clinical outcome in 38 patients with juxacortical osteosarcoma. *Clinical Orthopaedics* **2000**, 373, 208-217.

62. Berrey Jr., W.H.; Lord, C.F.; Gebhardt, M.C.; Mankin, H.J., Fractures of allografts: Frequency, treatment, and end results. *Journal of Bone and Joint Surgery* **1990**, 72A, 825-833.

63. Sorger, J.I.; Hornicek, F.J.; Zavatta, M.; Menzner, J.P.; Gebhardt, M.C.; Tomford, W.W.; Mankin, H.J., Allograft fractures revisited. *Clinical Orthopaedics* **2001**, 382, 66-74.

64. Delloye, C.; Cornu, O.; Druez, V.; Barbier, O., Bone allografts: What they can offer and what they cannot. *Journal of Bone and Joint Surgery* **2007**, 89-B, 575-579.

65. Donati, D.; Di Bella, C.; Col Angeli, M.; Bianchi, G.; Mercuri, M., The use of massive bone allografts in bone tumor surgery of the limb. *Current Orthopaedics* **2005**, 19, 393-399.

66. Mankin, H.; Hornicek, F.; Raskin, K., Infection in massive bone allografts. *Clinical Orthopaedics* **2005**, 432, 210-216.

67. Vander Griend, R., The effect of internal fixation on the healing of large allografts. *Journal of Bone and Joint Surgery* **1994**, 76A, 657-663.

68. Thompson, R.; Pickvance, E.; Garry, D., Fractures in large-segment allografts. *Journal of Bone and Joint Surgery* **1993**, 75A, 1663-1673.

69. Enneking, W.F.; Mindell, E.R., Observations on massive retrieved human allograft. *Journal of Bone and Joint Surgery* **1991**, 73A, 1123-1142.

70. Aho, A.J.; Ekfors, T.; Dean, P.B.; Incorporation and clinical results of large allografts of the extremities and pelvis. *Clinical Orthopaedics* **1994**, 307, 200-213.

71. Mankin, H.J.; Hornicek, F.J.; Gebhradt, M.C.; Tomford, W.W., Bone allograft transplantation: Theory and practice. In *Bone Regeneration and Repair: Biology and Clinical Applications*, Lieberman, J.R.; Friedlaender, G.F., eds.; Humana Press: Totowa, New Jersey, 2005.

72. Goel, S.C.; Tuli, S.M. Use of decalbone in healing of osseous cystic defects. In *Bone Grafts, Derivatives and Substitutes*, Urist, M.R., O'Conner, B.T., Burwell, R.G., eds.; Butterworth-Heinemann: Oxford, England, **1994**.

73. Joyce, M.J.; Joyce, D.M., Musculoskeletal allograft tissue banking and safety. In *Bone Graft Substitutes*, Laurencin, C.T., ed.; ASTM International: West Conshohocken, Pennsylvania, **2003**.

74. Walsh, W.R.; Christiansen, D.L., Demineralized bone matrix as a template for mineral-organic composites. *Biomaterials* **1995**, 16, 1363-1371.

75. Wolfinbarger Jr., L.; Eisenlohr, L.M.; Ruth, K., Demineralized bone matrix: Maximizing new bone formation for successful bone implantation. In *Musculoskeletal Tissue Regeneration: Biological Materials and Methods*; Pietrzak, W.S., Ed.; Humana Press: Totowa, New Jersey, **2008**.

76. Urist, M.R.; Silverman, B.F.; Buring, K.; Dubuc, F.L.; Rosenberg, J.M., The bone induction principle. *Clinical Orthopaedics and Related Research* **1967**, 53, 243-283.

77. Zhang, M.; Powers Jr., R.M.; Wolfinbarger Jr., L., Effect(s) of the demineralization process on the osteoinductivity of demineralized bone matrix. *Journal of Periodontology* **1997**, 68, 1085-1092.

78. Russell, J.L.; Block, J.E., Clinical utility of demineralized bone matrix for osseous defects, arthrodesis and reconstruction: Impact of processing techniques and study methodology. *Orthopaedics* **1999**, 22, 524-531.

79. Stavropoulos, A., Deproteinized bovine bone xenograft. In *Musculoskeletal Tissue Regeneration: Biological Materials and Methods*; Pietrzak, W.S., Ed.; Humana Press: Totowa, New Jersey, **2008**.

80. Burchardt, H., The biology of bone graft repair. *Clinical Orthopaedics* **1983**, 174, 28-42.

81. Salama, R., Xenogenic bone grafting in humans. *Clinical Orthopaedics* **1983**, 174, 113-121.

82. Bach, F.H., Xenotransplantation: Problems and prospects. *Annual Review of Medicine* **1998**, 49, 301-310.

83. Heiple, K.G.; Kendrick, R.E.; Herndon, C.H.; Chase, S.W., A critical evaluation of processed calf bone. *Journal of Bone and Joint Surgery* **1967**, 49A, 1119-1127.

84. Pieron, A.P.; Bigelow, D.; Hamonic, M., Bone grafting with Boplant. Results in thirty-three cases. *Journal of Bone and Joint Surgery* **1968**, 50B, 364-368.

85. Jarcho, M., Calcium phosphate ceramics as hard tissue prosthetics. *Clinical Orthopaedics and Related Research* **1981**, 157, 259-278.

86. LeGeros, R.Z., Properties of osteoconductive biomaterials: calcium phosphates. *Clinical Orthopaedics and Related Research* **2002**, 395, 81-98.

87. Albar, M.A., Islamic ethics of organ transplantation and brain death. *Saudi Journal of Kidney Diseases and Transplantation* **1996**, 7, 109-114.

88. Xenotransplantation and the “yuk” factor. *Nature Biotechnology* **1996**, 14, 403-404.

89. Araujo, M. V. F.; Mendes, V. C.; Chattopadhyay, P.; Davies, J. E., Low-temperature particulate calcium phosphates for bone regeneration. *Clinical Oral Implants Research* **2010,** 21, 632-641.

90. Fulmer, N. L.; Bussard, G. M.; Gampper, T. J.; Edlich, R. F., Anorganic bovine bone and analogs of bone mineral as implants for craniofacial surgery: a literature review. *Journal of Long-Term Effects of Medical Implants* **1998,** 8, 69-78.

91. Shi, D.; Wen, X., Bioactive ceramics: Structure, synthesis, and mechanical properties. In *Introduction to Biomaterials*, Shi, D., ed.; Tsinghua University Press: Beijing, China, 2006.

92. LeGeros, R.Z.; LeGeros, J.P., Dense Hydroxyapatite. In *An Introduction to Bioceramics*, Hench, L.L.; Wilson, J., eds.; World Scientific: Singapore, 1993.

93. Rathje, W., Zur kenntnis der phosphate I. Über hydroxylapatit. *Bodenk Pflernah* **1939**, 12, 121-128.

94. Hayek, E.; Newesely, H., Pentacalcium monohydroxyorthophosphate. *Inorganic Synthesis* **1963**, 7, 63-65.

95. Orlovskii, V.P.; Komlev, V.S.; Barinov, S.M., Hydroxyapatite and hydroxyapatite-based ceramics. *Inorganic Materials* **2002**, 38, 973-984.

96. Li, J.; Hashida, T., Preparation of hydroxyapatite ceramics by hydrothermal hot-pressing method at 300 ^{o}C. *Journal of Materials Science* **2007**, 42, 5013-5019.

97. Bucholz, R.W., Nonallograft osteoconductive bone graft substitutes. *Clinical Orthopaedics and Related Research* **2002**, 395, 44-52.

98. LeGeros, R.Z.; Properties of osteoconductive biomaterials: Calcium phosphates. *Clinical Orthopaedics and Related Research* **2002**, 395, 81-98.

99. Oonishi, H.; Hench, L.L.; Wilson, J.; Sugihara F., Quantitative comparison of bone growth behavior in granules of Bioglass^{R}, A-W glass-ceramic, and hydroxyapatite. *Journal of Biomedical Materials Research* **2000**, 51, 37-46.

100. Imaizumi, H.; Sakurai, M.; Kashimoto, O.; Kikawa, T.; Suzuki, O., Comparative study on the osteoconductivity by synthetic octacalcium phosphate and sintered hydroxyapatite in rabbit bone marrow. *Calcified Tissue International* **2006**, 78, 45-54.

101. Osborn, J.F.; Neweseley, H., The material science of calcium phosphate ceramics. *Biomaterials* **1980**, 1, 108-111.

102. Niki, M.; Ito, T.; Matsuda, T.; Ogino, M., Comparative push-out data of bioactive and non-bioactive materials of similar rugosity. In *The Bone-Biomaterial Interface*, Davies, J.E., ed.; University of Toronto Press: Toronto, Canada, 1991.

103. Okuda, T.; Ioku, K.; Yonezawa, I.; Minagi, H.; Gonda, Y.; Kawachi, G.; Kamitakahara, M.; Shibata, Y.; Murayama, H.; Kurosawa, H.; Ikeda, T., The slow resorption with replacement by bone of a hydrothermally synthesized pure calcium-deficient hydroxyapatite. *Biomaterials* **2008,** 29, 2719-2728.

104. LeGeros, R.Z.; Bautista, C.; Styner, D.; LeGeros, J.P.; Vijayraghavan, T.V.; Retino, M.; Valdecanas, A., Comparative properties of bioactive bone graft materials. *Bioceramics* **1995**, 8, 81-87.

105. Sopyan, M.; Mel, M.; Ramesh, S.; Khalid, K.A., Porous hydroxyapatite for artificial bone applications. *Science and Technology of Advanced Materials* **2007**, 8, 116-123.

106. Aoki, S.; Yamaguchi, S.; Nakahira, A.; Suganuma, K., Preparation of porous calcium phosphates using a ceramic foaming technique combined with a hydrothermal treatment and the cell response with incorporation of osteoblast-like cells. *Journal of the Ceramic Society of Japan* **2004**, 112, 193-199.

107. Wilson, C.E.; de Bruijn, J.D.; van Blitterswijk, C.A.; Verbout, A.J.; Dhert, W.J.A., Design and fabrication of standardized hydroxyapatite scaffolds with a defined macro-architecture by rapid prototyping for bone-tissue-engineering research. *Journal of Biomedical Materials Research Part A* **2003**, 68A, 123-132.

108. Tadic, D.; Beckmann, F.; Schwarz, K.; Epple, M., A novel method to produce hydroxyapatite objects with interconnecting porosity that avoids sintering. *Biomaterials* **2004**, 25, 3335-3340.

109. Tamai, N.; Myoui, A.; Tomita, T.; Nakase, T.; Tanaka, J.; Ochi, T.; Yoshikawa, H., Novel hydroxyapatite ceramics with an interconnective porous structure exhibit superior osteoconduction in vivo. *Journal of Biomedical Materials Research* **2002**, 59, 110-117.

110. Sepulveda, P.; Binner, J.G.; Rogero, S.O.; Higa, O.Z.; Bressiani, J.C., Production of porous hydroxyapatite by the gel-casting of foams and cytotoxic evaluation. *Journal of Biomedical Materials Research* **2000**, 50, 27-34.

111. Rejda, B.V.; Peelen, J.G.; de Groot, K., Tri-calcium phosphate as a bone substitute. *Journal of Bioengineering* **1977**, 1, 93-97.

112. Li, S.H.; De Wijn, J.R.; Layrolle, P.; De Groot, K., Synthesis of macroporous hydroxyapatite scaffolds for bone tissue engineering. *Journal of Biomedical Materials Research* **2002**, 61, 109-120.

113. Tian, J.; Tian, J., Preparation of porous hydroxyapatite. *Journal of Materials Science* **2001**, 36, 3061-3066.

114. Woyansky, J.S.; Scott, C.E.; Minnear, W.P., Processing of porous ceramics. *American Ceramic Society Bulletin* **1992**, 71, 1674-1682.

115. Andrade, J.C.T.; Camilli, J.A.; Kawachi, E.Y.; Bertran, C.A., Behavior of dense and porous hydroxyapatite implants and tissue response in rat femoral defects. *Journal of Biomedical Materials Research* **2002**, 62, 30-36.

116. Kuboki, Y.; Takita, H.; Kobayashi, D.; Tsuruga, E.; Inoue, M.; Murata, M.; Nagai, N.; Dohi, Y.; Ohgushi, H., BMP-induced osteogenesis on the surface of hydroxyapatite with geometrically feasible and nonfeasible structures: Topology of osteogenesis. *Journal of Biomedical Materials Research* **1998**, 39, 190-199.

117. Story, B.J.; Wagner, W.R.; Gaisser, D.M.; Cook, S.D.; Rust-Dawicki, A.M., In vivo performance of a modified CSTi dental implant coating. *International Journal of Oral and Maxillofacial Implants* **1998**, 13, 749-757.

118. Simske, S.J.; Ayers, R.A.; Bateman, T.A., Porous materials for bone engineering. *Materials Science Forum* **1997**, 250, 151-182.

119. Hing, K.A.; Best, S.M.; Bonfield, W., Characterization of porous hydroxyapatite. *Journal of Materials Science: Materials in Medicine* **1999**, 10, 135-145.

120. Kühne, J.-H.; Bartl, R.; Frisch, B.; Hammer, C., Bone formation in coralline hydroxyapatite. *Acta Orthopaedica Scandinavica* **1994**, 65, 246-252.

121. Eggli, P.S.; Müller, W.; Schenk, R.K., Porous hydroxyapatite and tricalcium phosphate cylinders with two different pore size ranges implanted in the cancellous bone of rabbits. A comparative histomorphometric and histologic study of bony ingrowth and implant substitution. *Clinical Orthopaedics and Related Research* **1988**, 232, 127-138.

122. Holmes, R.; Mooney, V.; Bucholz, R.; Tencer, A., A coralline hydroxyapatite bone graft substitute. *Clinical Orthopaedics and Related Research* **1984**, 188, 252-262.

123. Holmes, R.E.; Bucholz, R.W.; Mooney, V., Porous hydroxyapatite as a bone-graft substitute in metaphyseal defects. A histometric study. *Journal of Bone and Joint Surgery* **1986**, 68, 904-911.

124. Lu, J.; Flautre, B.; Anselme, K., Role of interconnections in porous bioceramics on bone re-colonization in-vitro and in-vivo. *Journal of Materials Science: Materials in Medicine* **1999,** 10, 111-120.

125. Flautre, B.; Descamps, M.; Delecourt, M., Porous HA ceramic for bone replacement: Role of the pore and interconnections: Experimental study in the rabbit. *Journal of Materials Science: Materials in Medicine* **2001,** 12, 679-682.

126. Chang, B.S.; Lee, C.K.; Youn, H.J., Osteoconduction at porous hydroxyapatite with various pore configurations. *Biomaterials* **2000,** 21, 1291-1298.

127. Hollister, S.J.; Maddox, R.D.; Taboas, J.M., Optimal design and fabrication of scaffolds to mimic tissue properties and satisfy biological constraints. *Biomaterials* **2002,** 23, 4095-4103.

128. Karageorgiou, V.; Kaplan, D., Porosity of 3D scaffolds and osteogenesis. *Biomaterials* **2005**, 26, 5474-5491.

129. Richart, O.; Descamps, M.; Liebetrau, A., Preparation and mechanical characterization of hydroxyapatite monodispersed macroporous structure. Influence of interconnection and macropores diameters. *Key Engineering Materials* **2002**, 218-220, 9-12.

130. Blokhuis, T.J.; Termaat, M.F.; den Boer, F.C.; Patka, P., Properties of calcium phosphate ceramics in relation to their in vivo behavior. *Journal of Trauma: Injury, Infection, and Critical Care* **2000**, 48, 179-186.

131. Le Huec, J.C.; Schaeverbeke, T.; Clement, D.; Faber, J.; Le Rebeller, A., Influence of porosity on the mechanical resistance of hydroxyapatite ceramics under compressive stress. *Biomaterials* **1995,** 16, 113-118.

132. Liu, D.-M., Influence of porosity and pore size on the compressive strength of porous hydroxyapatite ceramic. *Ceramics International* **1997**, 23, 135-139.

133. Shors, E.C.; Holmes, R.E., Porous hydroxyapatite. In *An Introduction to Bioceramics*, Hench, L.L.; Wilson, J., eds.; World Scientific: Singapore, 1993.

134. Ben-Nissan, B., Natural bioceramics: From coral to bone and beyond. *Current Opinion in Solid State and Materials Science* **2003**, 7, 283-288.

135. Vikram, D.; Nather, A.; Khalid, K.A., Role of ceramics as bone graft substitutes. In *Bone Grafts and Bone Substitutes: Basic Science and Clinical Applications*, Nather, A., ed.; World Scientific: Hackensack, New Jersey, 2005.

136. Roy, D.M.; Linnehan, S.K., Hydroxyapatite formed from coral skeletal carbonate by hydrothermal exchange. *Nature* **1974**, 247, 220-222.

137. Shors, E.C., Coralline bone graft substitutes. *Orthopedic Clinics of North America* **1999**, 30, 599-613.

138. Chiroff, R.T.; White, E.W.; Weber, K.N.; Roy, D.M., Tissue ingrowth of replamineform implants. *Journal of Biomedical Materials Research* **1975**, 9, 29-45.

139. Damien, E.; Revell, P.A., Coralline hydroxyapatite bone graft substitute: A review of experimental studies and biomedical applications. *Journal of Applied Biomaterials and Biomechanics* **2004**, 2, 65-73.

140. Holmes, R.E., Bone regeneration within a coralline hydroxyapatite implant. *Plastic and Reconstructive Surgery* **1979**, 63, 626-633.

141. Bassett, C. A. L.; Hurley, L. A.; Stinchfield, F. E., Fate of long-term anorganic bone implants. *Transplant Biology* **1962,** 29, 51-55.

142. Rapkin, E. Anorganic bone. 2,968,593, January 17, 1961.

143. Williams, J. B.; Irvine, J. W., Jr., Preparation of the inorganic matrix of bone. *Science* **1954,** 119, 771-2.

144. Joschek, S.; Nies, B.; Krotz, R.; Göpferich, A., Chemical and physicochemical characterization of porous hydroxyapatite ceramics made of natural bone. *Biomaterials* **2000**, 21, 1645-1658.

145. Lin, F.H.; Liao, C.J.; Chen, K.S.; Sun, J.S.; Lin, C.Y., Preparation of beta TCP/HAP biphasic ceramics with natural bone structure by heating bovine cancellous bone with the addition of $(NH_4)_2HPO_4$. *Journal of Biomedical Materials Research* **2000**, 51, 157-163.

146. Mushipe, M.T.; Revell, P.A.; Shelton, J.C., Cancellous bone repair using bovine trabecular bone matrix particulates. *Biomaterials* **2002**, 23, 365-370.

147. Mushipe, M.T.; Revell, P.A.; Shelton, J.C., The effects if bovine trabecular bone matrix particulates on cortical bone repair. *Journal of Materials Science: Materials in Medicine* **2002**, 13, 99-105.

148. Pietrzak, W.S., Bioabsorbable polymer applications in musculoskeletal fixation and healing. In *Musculoskeletal Tissue Regeneration: Biological Materials and Methods*, Pietrzak, W.S., ed.; Humana Press: Totowa, New Jersey, 2008.

149. Gombotz, W.R.; Pettit, D.K., Biodegradable polymers for protein and peptide drug delivery. *Bioconjugate Chemistry* **1995**, 6, 332-351.

150. Ascherman, J. A.; Foo, R.; Nanda, D.; Parisien, M., Reconstruction of cranial bone defects using a quick-setting hydroxyapatite cement and absorbable plates. *Journal of Craniofacial Surgery* **2008,** 19, 1131-1135.

151. Curtis, N.; Zoellner, H., Resection of an orbital rim intraosseous cavernous hemangioma and reconstruction by chin graft and resorbable fixation plate. *Ophthalmic Plastic and Reconstructive Surgery* **2007,** 23, 232-234.

152. Eppley, B. L.; Pietrzak, W. S., A resorbable rivet system for pediatric craniofacial surgery: Biomechanical testing and clinical experience. *Journal of Craniofacial Surgery* **2006,** 17, 11-14.

153. Kessler, K. J.; Bullens-Borrow, A. E.; Zisholtz, J., LactoSorb plates for rotator cuff repair. *Arthroscopy-the Journal of Arthroscopic and Related Surgery* **2002,** 18, 279-283.

154. Roncevic, R., Lactosorb panel and screws for repair of large orbital floor defects. *Journal of Cranio-Maxillofacial Surgery* **1998,** 26, 191-192.

155. Torre, M.; Jasonni, V.; Asquasciati, C.; Costanzo, S.; Romanini, M. V.; Varela, P., Absorbable Stabilisation of the Bar in Minimally Invasive Repair of Pectus Excavatum. *European Journal of Pediatric Surgery* **2008,** 18, 407-409.

156. Noda, K.; Tanikawa, R.; Sugimura, T.; Kawasaki, K.; Kimura, T.; Izumi, N.; Hashimoto, M., Use of Bioabsorbable Plates for Cranial Fixation -Technical Note. *Neurologia Medico-Chirurgica* **2009,** 49, 559-562.

157. Matsusue, Y.; Nakamura, T.; Iida, H.; Shimizu, K., A long-term clinical study on drawn poly-L-lactide implants in orthopaedic surgery. *Journal of Long-Term Effects of Medical Implants* **1997,** 7, 119-137.

158. Matsusue, Y.; Hanafusa, S.; Yamamuro, T.; Shikinami, Y.; Ikada, Y., Tissue reaction of bioabsorbable ultra high strength poly (L-lactide) rod. A long-term study in rabbits. *Clinical Orthopaedics and Related Research* **1995**, 317, 246-253.

159. Yamamuro, T.; Matsusue, Y.; Uchida, A.; Shimada, K.; Shimozaki, E.; Kitaoka, K., Bioabsorbable osteosynthetic implants of ultra high strength poly-L-lactide. A clinical study. *International Orthopaedics* **1994,** 18, 332-40.

160. Boyan, B.D.; McMillan, J.; Lohmann, C.H.; Ranly, D.M.; Schwartz, Z., Bone graft substitutes: Basic information for successful clinical use with special focus on synthetic graft substitutes. In *Bone Graft Substitutes*, Laurencin, C.T., ed.; ASTM International: West Conshohocken, Pennsylvania, 2003.

161. Wong, W.H.; Mooney, D., Synthesis and properties of biodegradable polymers used as synthetic matrices for tissue engineering. In *Synthetic Biodegradable Polymer Scaffolds*, Atala, A.; Mooney, D.; Vacanti, J.P.; Langer, R., eds.; Birkhäuser: Boston, Massachusetts, 1997.

162. Walton, M.; Cotton, N. J., Long-term in vivo degradation of poly-L-lactide (PLLA) in bone. *Journal of Biomaterials Applications* **2007,** 21, 395-411.

163. Bostman, O.M.; Pihlajamaki, H.K., Adverse tissue reaction to bioabsorbable fixation devices. *Clinical Orthopaedics and Related Research* **2000**, 371, 216-227.

164. Mikos, A.G.; Temenoff, J.S., Formation of highly porous biodegradable scaffolds for tissue engineering. *Electronic Journal of Biotechnology* **2000**, 3, 114-119.

165. Laurencin, C.T.; Borden, M.; Attawia, M.; El-Almin, S., Structural assessment of a tissue engineered scaffold for bone repair. *Engineering in Medicine and Biology Society, 2001. Proceedings of the 23rd Annual International Conference of the IEEE* **2001**, 3, 2975-2978.

166. Ge, Z.; Jin, Z.; Cao, T., Manufacture of degradable polymeric scaffolds for bone regeneration. *Biomedical Materials* **2008**, 3, 022001.

167. Nair, L.S.; Laurencin, C.T., Polymers as biomaterials for tissue engineering and controlled drug delivery. *Advances in Biochemical Engineering/Biotechnology* **2006**, 102, 47-90.

168. Murphy, W.L.; Kohn, D.H.; Mooney, D.J., Growth of continuous bonelike mineral within porous poly(lactide-co-glycolide) scaffolds in vitro. *Journal of Biomedical Materials Research* **2000**, 50, 50-58.

169. Vasenius, J.; Majola, A.; Miettinen, E.-L.; Törmälä, P.; Rokkanen, P., Do intramedullary rods of self-reinforced poly-L-lactide or poly-DL/L-lactide cause lactic acid acidosis in rabbits? *Clinical Materials* **1992**, 10, 213-218.

170. Pihlajamäki, H.; Böstman, O.; Tynninen, O.; Laitinen, O., Long-term tissue response to bioabsorbable poly-L-lactide and metallic screws: An experimental study. *Bone* **2006**, 39, 932-937.

171. Pietrzak, W., Principles of development and use of absorbable internal fixation. *Tissue Engineering* **2000**, 6, 425-433.

172. Mukherjee, D.P.; Pietrzak, W.S., Bioabsorbable fixation: Scientific, technical, and clinical concepts. *Journal of Craniofacial Surgery* **2011**, 22, 679-689.

173. Pietrzak, W.S.; Caminear, D.S.; Perns, S.V., Mechanical characteristics of an absorbable copolymer internal fixation pin. *Journal of Foot and Ankle Surgery* **2002**, 41, 379-388.

174. Kalfas, I.H., Principles of bone healing. *Neurosurgical Focus* **2001**, 10, (4), 7-10.

175. Rizzi, S.C.; Heath, D.J.; Coombes, A.G.A.; Bock, N.; Textor, M.; Downes, S., Biodegradable polymer/hydroxyapatite composites: Surface analysis and initial attachment of human osteoblasts. *Journal of Biomedical Materials Research* **2001**, 55, 475-486.

176. Coombes, A.G.A.; Meikle, M.C., Resorbable synthetic polymers as replacements for bone graft. *Clinical Materials* **1994**, 17, 35-67.

177. Kikuchi, M.; Cho, S.-B.; Suetsugu, Y.; Tanaka, J., In vitro tests and in vivo tests developed TCP/CPLA composites. *Bioceramics* **1997**, 10, 407-410.

178. Reis, R.L.; Cunha, A.M.; Fernandes, M.H.; Correia, R.N., Bioinert and biodegradable polymeric matrix composites filled with bioactive SiO_2-$3CaO{\cdot}P_2O_5$-MgO glasses and glass-ceramics. *Bioceramics* **1997**, 10, 415-418.

179. Furukawa, T.; Matsusue, Y.; Yasunaga, T.; Shikinami, Y.; Okuno, M.; Nakamura, T., Biodegradation behavior of ultra-high-strength hydroxyapatite/poly (L-lactide) composite rods for internal fixation of bone fractures. *Biomaterials* **2000,** 21, 889-898.

180. Hasegawa, S.; Ishii, S.; Tamura, J.; Furukawa, T.; Neo, M.; Matsusue, Y.; Shikinami, Y.; Okuno, M.; Nakamura, T., A 5-7 year in vivo study of high-strength hydroxyapatite/poly(L-lactide) composite rods for the internal fixation of bone fractures. *Biomaterials* **2006,** 27, 1327-1332.

181. Kotani, Y.; Abumi, K.; Shikinami, Y.; Takahata, M.; Kadoya, K.; Kadosawa, T.; Minami, A.; Kaneda, K., Two-year observation of artificial intervertebral disc replacement: results after supplemental ultra-high strength bioresorbable spinal stabilization. *Journal of Neurosurgery* **2004,** 100, 337-342.

182. Cehreli, M. C.; Sahin, S.; Kesenci, K.; Tuzlakoglu, K.; Piskin, E.; Ozturk, S.; Ruacan, S.; Caner, B.; Bozkurt, M. F., Biological reactions to a poly(L-lactide)-hydroxyapatite composite: A study in canine mandible. *Journal of Biomaterials Applications* **2003,** 17, 265-276.

183. Furukawa, T.; Matsusue, Y.; Yasunaga, T.; Nakagawa, Y.; Okada, Y.; Shikinami, Y.; Okuno, M.; Nakamura, T., Histomorphometric study on high-strength hydroxyapatite/poly(L-lactide) composite rods for internal fixation of bone fractures. *Journal of Biomedical Materials Research* **2000,** 50, 410-419.

184. Ishii, S.; Tamura, J.; Furukawa, T.; Nakamura, T.; Matsusue, Y.; Shikinami, Y.; Okuno, M., Long-term study of high-strength hydroxyapatite/poly(L-lactide) composite rods for the internal fixation of bone fractures: A 2-4-year follow-up study in rabbits. *Journal of Biomedical Materials Research Part B-Applied Biomaterials* **2003,** 66B, 539-547.

185. Yasunaga, T.; Matsusue, Y.; Furukawa, T.; Shikinami, Y.; Okuno, M.; Nakamura, T., Bonding behavior of ultrahigh strength unsintered hydroxyapatite particles/poly(L-lactide) composites to surface of tibial cortex in rabbits. *Journal of Biomedical Materials Research* **1999,** 47, 412-419.

186. Ignjatovic, N.; Plavsic, M.; Najman, S.; Savic, V.; Uskokovic, D., Analysis of in vivo substitution of bone tissue by HAp/PLLA composite biomaterial with PLLA of different molecular weights using FTIR spectroscopy. *Materials Science Forum* **2000**, 352, 143-150.

187. Todo, M.; Park, S.D.; Arakawa, K.; Takenoshita, Y., Relationship between microstructure and fracture behavior of bioabsorbable HA/PLLA composites. *Composites: Part A*, **2006**, 37, 2221-2225.

188. Shikinami, Y.; Okuno, M., Bioresorbable devices made of forged composites of hydroxyapatite (HA) particles and poly-L-lactide (PLLA): Part I. Basic characteristics. *Biomaterials* **1999**, 20, 859-877.

189. Verheyen, C.C.P.M.; De Wijn, J.R.; Van Blitterswijk, C.A.; De Groot, K., Evaluation of hydroxylapatite/poly(l-lactide) composites: Mechanical behavior. *Journal of Biomedical Materials Research* **1992**, 26, 1277-1296.

190. Ignjatovic, N.; Tomic, S.; Dakic, M.; Miljkovic, M.; Plavsic, M.; Uskokovic, D., Synthesis and properties of hydroxyapatite/poly-L-lactide composite biomaterials. *Biomaterials* **1999**, 20, 809-816.

191. Gultekin, N.; Tihminlioglu, F.; Ciftcioglu, R.; Ciftcioglu, M.; Harsa, S., Preparation and characterization of polylactide-hydroxyapatite biocomposites. *Key Engineering Materials* **2004**, 264-268, 1953-1956.

192. Kagawa, T.; Todo, M.; Takenoshita, Y.; Myoui, A., Effect of press process on the fracture behavior of HA/PLLA biocomposite material. *16th International Conference on Composite Materials* **2007**, Kyoto, Japan, 1-5.

193. Hong, Z.; Qiu, X.; Sun, J.; Deng, M.; Chen, X.; Jing, X., Grafting polymerization of L-lactide on the surface of hydroxyapatite nano-crystals. *Polymer* **2004**, 45, 6699-6706.

194. Zhang, S.; Luo, Q.; Cao, R.; Li, S., Molecular modification of hydroxyapatite to introduce interfacial bonding with poly (lactic acid) in biodegradable composites. *Key Engineering Materials* **2005**, 288-289, 227-230.

195. Wang, M.; Deb, S.; Bonfield, W., Chemically couple hydroxyapatite-polyethylene composites: Processing and characterization. *Materials Letters* **2000**, 44, 119-124.

196. Li, H.; Liao, L.; Wang, Q.; Liu, L., Flash-heating-enhanced ring-opening polymerizations of epsilon-caprolactone under conventional conditions. *Macromolecular Chemistry and Physics* **2006,** 207, 1789-1793.

197. Kaihara, S.; Matsumura, S.; Mikos, A. G.; Fisher, J. P., Synthesis of poly(L-lactide) and polyglycolide by ring-opening polymerization. *Nature Protocols* **2007,** 2, 2767-2771.

198. Kowalski, A.; Duda, A.; Penczek, S., Mechanism of cyclic ester polymerization initiated with tin(II) octoate. 2. Macromolecules fitted with tin(II) alkoxide species observed directly in MALDI-TOF spectra. *Macromolecules* **2000,** 33, 689-695.

199. Kricheldorf, H. R.; Kreiser-Saunders, I.; Damrau, D. O., Resorbable initiators for polymerizations of lactones. *Macromolecular Symposia* **2000,** 159, 247-257.

200. Ryner, M.; Stridsberg, K.; Albertsson, A. C.; von Schenck, H.; Svensson, M., Mechanism of ring-opening polymerization of 1,5-dioxepan-2-one and L-lactide with stannous 2-ethylhexanoate. A theoretical study. *Macromolecules* **2001,** 34, 3877-3881.

201. Helwig, E.; Sandner, B.; Gopp, U.; Vogt, F.; Wartewig, S.; Henning, S., Ring-opening polymerization of lactones in the presence of hydroxyapatite. *Biomaterials* **2001,** 22, 2695-2702.

202. Sugiyama, N.; Kunibu, R.; Yoshizawa-Fujita, M.; Takeoka, Y.; Aizawa, M.; Rikukawa, M., Ring-opening bulk polymerization of L-lactide in porous hydroxyapatite. *Chemistry Letters* **2007,** 36, 1476-1477.

203. Helwig, E.; Sandner, B.; Gopp, U.; Vogt, F.; Wartewig, S.; Henning, S., Ring-opening polymerization of lactones in the presence of hydroxyapatite. *Biomaterials* **2001,** 22, 2695-2702.

204. Guerra, G. D.; Cerrai, P.; Tricoli, M.; Krajewski, A.; Ravaglioli, A.; Mazzocchi, M.; Barbani, N., Composites between hydroxyapatite and poly(epsilon-caprolactone) synthesized in open system at room temperature. *Journal of Materials Science-Materials in Medicine* **2006,** 17, 69-79.

205. Wiegand, T.; Karr, J.; Steinkruger, J. D.; Hiebner, K.; Simetich, B.; Beatty, M.; Redepenning, J., Reconstruction of anorganic mammalian bone by surface-initiated polymerization of L-lactide. *Chemistry of Materials* **2008,** 20, 5016-5022.

206. Karr, J.J., Preparation and Characterization of Ceramic/Polymer Biomaterials, Ph.D. dissertation, University of Nebraska, Lincoln, Nebraska, 2007.

207. Wiegand, T.E., Resorbable Polymer-Hydroxyapatite Composites for Bone Trauma Treatment: Synthesis and Properties, Ph.D. dissertation, University of Nebraska, Lincoln, Nebraska, 2011.

Chapter Two

Chemical Vapor Deposition Polymerization of Common Biocompatible Monomers and Polymers Initiated by the Nucleophilic Surface of Biologically Derived Porous Substrates

Introduction and Background

As was described in the introduction, an extensive body of research has examined the use of ceramics, such as hydroxyapatite (HA), biodegradable polymers, and composites of the two materials as an alternative to autografts and allografts as bone grafts for the repair of large defects in bone. After biocompatibility and osteoconductivity, perhaps the most important property of a bone graft substitute is compositional similarity to the bone it is replacing, and its efficacy in mimicking the macro- and microscopic morphology of bone.[1-5] Bone is composed of an inorganic material, highly substituted hydroxyapatite, within an organic matrix. The porosity of cortical bone is 3-12% and the porosity of cancellous bone is 50-90%. The pores within cancellous bone can be as large as 1 mm whereas the voids within cortical bone are much smaller. For example, the series of interconnected pores that comprise the haversian canals in cortical bone have a cross-sectional area of 2500-12000 μm^2.[2]

HA is often the material of choice for bone defect repair due to its similar composition ($Ca_{10}(PO_4)_6(OH)_2$) to bone. The original sintered HA ceramic grafts were dense and mechanically strong, but poorly resorbed, brittle, and difficult to handle.[6] Several studies have shown a lack of fibrous tissue surrounding implanted dense HA scaffolds,[7, 8] while others have observed fibrous tissue surrounding the implant.[9, 10] Often lacking in these early studies was demonstration of tissue regeneration inside the implant.

When comparing dense HA scaffolds to porous HA scaffolds, Andrade et al. observed far more fibrous tissue within the porous implant and at earlier stages after surgery.[11] The pores were found to be desirable for the development of new bone growth for two reasons. First, they allow the migration and proliferation of osteoblasts and mesenchymal cells to take place, followed by vascularization within the pores.[12] Second, the pores were found to promote greater mechanical stability between the surrounding bone and the implant.[13] Hulbert and Klawitter showed that the minimum pore size required for regenerating bone was 100 μm. This corresponds well with the average size of the pores in the haversian system, which have a diameter between 100 and 200 μm.[14, 15] The optimum range for macroscopic porosity is between 100 and 500 μm.[16, 17] In addition to pore size, interconnectivity of the pores is also important.[18-23] Interconnected pores allow cells to penetrate into the scaffold so that vascularization and mature bone growth can occur throughout.[24-27] Three factors that are considered important when optimizing bone growth within a porous scaffold are the permeability, tortuosity, and the mean equivalent diameter of the interconnecting pathways.[28] Microporosity (less than 5 μm) and surface roughness are also important in regard to the bioresorbability of the ceramic bone graft. The desirable influence of high surface roughness has been attributed to high levels of adsorbed bone producing proteins and cells, both of which facilitate resorption of the scaffold.[2, 29, 30] Although larger pores and greater interconnectivity produce more bone ingrowth, the mechanical strength decreases as these properties increase.[1, 2, 31] For example, increasing the pore volume from 10 to 20% results in a decrease of the mechanical strength by a factor of four.[29, 32, 33] The optimum scaffold therefore must strike a balance between the porosity of the implant and strength. Although scaffolds

with high porosity may lead to high rates of new bone growth, their poor mechanical stability can limit their utility to non-load bearing applications.

Synthetic HA scaffolds have been prepared using a variety of methods.[1] One method involves mixing HA powders with volatile particles that burn off when sintered at high temperatures. This method usually produces closed pores.[34, 35] Another method involves mixing HA with water-soluble porogens. This does not require sintering and produces an interconnected porous structure.[36] A third method produces porous HA by a technique called foaming. Gas evolving reactions are carried out within a slurry containing HA and a polymerizable monomer, causing it to foam. The monomer is then polymerized and the composite sintered.[37-39] Other synthetic methods include phase mixing[40] and the polymeric sponge method.[41, 42]

The methods described above were designed to produce porous HA scaffolds that mimic the bone structure provided by nature.[43] An alternative to producing synthetic structures is to use natural materials as templates. One example of a natural porous substrate is coral. Coral is composed of calcium carbonate, usually in the mineral form aragonite. The two genera that receive the most attention are *Porites* and *Goniopora* because of their structural similarities to human bone. *Porites* has a void volume of 66%, a pore size of 230 μm, and an interconnecting pore size of 190 μm. *Goniopora* has a pore size of 600 μm and an interconnecting pore size of 220 to 260 μm.[6] Although unaltered coral can be used as a bone graft scaffold, it is usually considered inadequate due to its high dissolution rate, poor longevity and poor mechanical properties.[43] The calcium carbonate coral can be converted to hydroxyapatite via hydrothermal exchange while

maintaining the macroscopic structure.[44] The exchange that takes place is shown in equation 2.1.

$$10CaCO_3 + 6(NH_4)_2HPO_4 + 2H_2O \rightarrow Ca_{10}(PO_4)_6(OH)_2 + 6(NH_4)_2CO_3 + 4H_3CO_3 \quad (2.1)$$

The new material, commonly called coralline hydroxyapatite and has been shown to be an effective osteoconductive scaffold for the generation of new bone.[22, 45-48] Complete conversion of the calcium carbonate in coral to HA is possible, but the reaction can also be terminated early to produce a material with a calcium carbonate core and a thin HA layer. One commercially available product of this composition is Pro-Osteon 500R produced by Biomet, Inc. Because it is not completely converted to HA, the dissolution is faster than a scaffold composed completely of HA.[49] The hydrothermal conversion can also be used to convert other marine species such as Australian coral,[50] cuttlefish bone (CFB),[51] and gastropod (Abalone) nacre[52] from calcium carbonate to HA. CFB is of interest because it is readily available worldwide. Although the structure of cuttlefish bone is different from that of bone, it does contain highly ordered layers of interconnected, 80 μm x 100 μm, pores.[51]

Another commercial HA scaffold derived from a natural source is modified bovine trabecular bone. This scaffold is produced by removing the organic material and then sintering the remaining anorganic bone. An example of a commercially available product is Endobon produced by Biomet, Inc. (Warsaw, IN).[53] The advantage of using bovine trabecular bone is that its composition is virtually identical to that of human bone, and it possesses good osteoconduction.[54-57]

As was mentioned earlier, the major problem associated with porous ceramic scaffolds is a decrease in mechanical strength as the porosity increases. One method aimed at increasing the mechanical strength is filling microscopic pores in the ceramic with a biodegradable polymer, such as poly-L-lactide (PLLA) or polyglycolide (PGA), creating a composite polymer/HA material. The HA scaffold is reinforced and the limited bioactivity of the polymer is countered by combining the two materials.[58-63] Such polymer coatings should evenly coat the entire substrate while maintaining the open porous structure. This is traditionally achieved by dipping the scaffold into a solution or liquid melt of the polymer after which it is removed and dried. Thin polymer coatings can also be achieved through other methods, including spraying or spin-on processes.[62] The processes described above can result in non-uniform thicknesses, pinholes, and residual solvent left behind.[64] In addition, such techniques do not produce a chemical bond between the scaffold and the polymer. One might conclude that such a bond would increase the interfacial strength of the composite, and improve the mechanical properties of the entire device.

Chemical vapor deposition polymerization (CVDP) is one method capable of producing thin, even polymer films that can be bonded to the surface on complex substrates. In CVDP, a monomer precursor is heated in the presence of a substrate. The monomer enters the vapor phase where it comes into contact with the substrate. At the substrate surface it adsorbs and one of two results can occur. The monomer can react at the surface or desorb and reenter the vapor phase. Over time a thin polymer film is produced that becomes thicker as the reaction proceeds. Because the substrate does not come into contact with the liquid monomer, excess monomer does not accumulate and

consequently need not be removed. Additionally one does not have to worry about filling the pores with liquid monomer through capillary action. Finally, for coatings formed by CVDP, one can often identify discrete bonds between the surface and the polymer chains in the coating. In other words, CVDP coatings do not merely cover the surface; they are attached to it.[64]

Recently it has been shown that the ring opening polymerization of several lactones can be initiated by the nucleophilic surface of HA in the absence of any other solvent or catalysts.[65-67] With this result in mind, one can hypothesize that the polymerization could occur out of the vapor phase. In this chapter I describe the use of CVDP to create composites of porous HA scaffolds with polylactones and polylactams. More specifically, the work in this chapter describes the use of various biologically derived porous scaffolds, including cuttlefish bone, coral, coralline HA, and trabecular bone, to initiate the polymerization of lactones and lactams via CVDP.

Experimental

Chemicals: Ammonia dihydrogen phosphate ($NH_4H_2PO_4$, from Sigma Aldrich, St. Louis, MO), calcium hydroxide ($Ca(OH)_2$, $\geq$ 95% from Sigma Aldrich), calcium hypochlorite ($Ca(OCl)_2$ from Sigma Aldrich), cuttlefish bone (CFB, from Petsmart, Lincoln, NE), deuterated chloroform ($CDCl_3$, 99.8% D from Sigma-Aldrich), ε-caprolactam (99%+ from Acros Organics, Geel, Belgium), ε-caprolactone (99% from Acros Organics), ethylenediamine (99% from Sigma Aldrich), glycolide (GL, 99.9% from Polysciences Inc., Warrington, PA), 1,1,1,3,3,3-hexafluoro-2-propanol (HFIP, 99.5%+, from Acros Organics), polystyrene (PolyCAL™ gel permeation chromatography (GPC) standards from Viscotek, Worchestershire, U.K.), sodium

hypochlorite ($Na(OCl)_2$, 5.25% solution from HyVee, Lincoln, NE), tetrahydrofuran (THF, HPLC grade from Sigma Aldrich), and 2,2,2-trifluoroethanol (TFE, ≥ 99% from Sigma Aldrich) were used as purchased from the respective supplier. L-Lactide (from Purac, Lincolnshire, IL) was sublimed at 90 ^oC and then transferred into a $N_{2(g)}$ atmosphere glove box for subsequent use. Anorganic trabecular bone was derived from bovine femur donated by Premium Protein Products (Lincoln, NE). *Goniopora* coral, Pro Osteon 500R, and Pro Osteon 200R were provided by Biomet® in 6 mm x 12 mm cylinders and 13 mm x 14 mm x 17 mm blocks.

Preparation of cuttlefish bone/poly-L-lactide (PLLA) composites via CVDP: CFB was hydrothermally converted from calcium carbonate, present in the mineral form aragonite, to HA. The CFB was placed in a 0.6 M $NH_4H_2PO_4$ solution. The molar ratio of calcium from the CFB to phosphorus from the $NH_4H_2PO_4$ solution was maintained at 10 to 6, the ratio present in HA. The CFB and ammonium phosphate solution were placed in a Teflon tube, plugged with Teflon plugs and then inserted into a high pressure reactor (Figure 2.1). The reactor was sealed with a torque wrench, applying 40 ft/lbs to each screw. The reactor was heated at 200 ^oC for 9 hr and then allowed to cool to room temperature. CFB hydroxyapatite (CFBHA) samples were rinsed with water and dried in air. Prior to reacting with L-lactide, CFBHA samples were heated at either 700 ^oC for 16 hr or 800 ^oC to remove organic material. After heating, samples were transferred to a vacuum desiccator and allowed to cool before being transferred to a $N_{2(g)}$ atmosphere glove box. In the glove box, L-lactide (approximately 200 mg) was loaded into a Pyrex glass tube. The tube typically had a diameter between 7 and 9.5 mm, and was constructed with an hour glass constriction near the center. This constriction prevented

Figure 2.1. High pressure reactor used to hydrothermally convert cuttlefish bone ($CaCO_3$) to hydroxyapatite. It has an outer diameter of 65 mm, an inner diameter of 39 mm, a height of 36 cm, and a volume of approximately 310 cm^3.

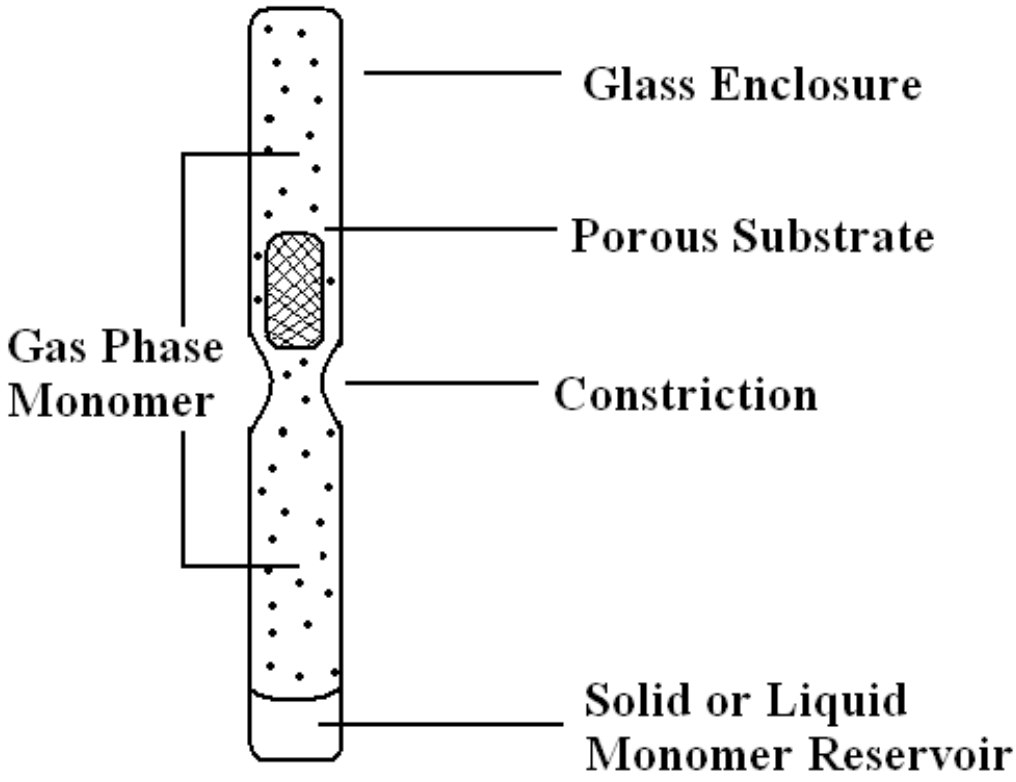

Figure 2.2. Typical reaction vessel used for the CVDP of L-lactide onto porous substrates.

the sample from coming in contact with the liquid monomer in the bottom of the vessel (Figure 2.2). The sample was then inserted in the tube, coming to rest above the constriction. A rubber septum was placed on the open end of the tube and the reaction tube and contents were then attached to a rotary vane pump. The pressure in the tube dropped to 20 mTorr over 10-15 min. Once the reaction vessel was evacuated, its bottom was immersed in liquid N_2 to lower the vapor pressure of the monomer. The reaction tube was then sealed under vacuum using a glass blowing torch. The tube was then transferred to a convection oven and the reaction was allowed to proceed at 130 ^{o}C. Reaction times were either 10 days or 14 days. The reaction tube was then removed from the oven. Before it was opened, the bottom of the reaction tube was immersed in liquid N_2 to condense excess L-lactide from the vapor phase into the bottom of the vessel away from the sample.

Pre-reaction treatment for *Goniopora* coral and Pro Osteon: Prior to using coral and Pro Osteon samples to initiate cyclic lactone polymerizations, I investigated a number of sample pretreatments in search for optimum conditions that would produce a composite with desired visual and physical properties. The temperature at which the sample is heated at prior to reacting with L-lactide affects the sample color, its composition, and subsequent polymerization rates. Heating samples to 400-500 ^{o}C turns the samples from white to brown and eventually grey. This is due to residual organic material.[68, 69] The sample can be returned to white by heating it to 550 ^{o}C or greater. At 600 ^{o}C the sample, which is primarily the aragonite polymorph of calcium carbonate ($CaCO_3$), is converted to calcium oxide (CaO) with the concomitant elimination of carbon dioxide (CO_2) (Equation 2.2).

$$CaCO_{3(s)} \rightarrow CaO_{(s)} + CO_{2(g)} \quad (2.2)$$

CaO is a strong nucleophile that is capable of initiating the polymerization of L-lactide, whereas $CaCO_3$ is a weak nucleophile that does not initiate the polymerization. As described later, the generation of additional nucleophiles leads to an increase in the observed polymerization rates.

Preparation of *Goniopora* coral/PLLA composites via CVDP: Cylinder coral samples with a diameter of 6 mm and a length of 12 mm were treated at a variety of temperatures prior to being reacted. These include drying at room temperature under vacuum, drying at 200 ^{o}C in air, and heating to 400 ^{o}C, 550 ^{o}C, and 600 ^{o}C in air. The length of time was varied as well. Samples were dried at room temperature for 16 hours, at 200 ^{o}C for 2 hours, heated to 400 ^{o}C for 3 hours, and various lengths of time from 6 to 43 hours at 550 ^{o}C and 600 ^{o}C. Reaction and sample preparation was the same as described above. In a typical reaction, between 300 and 400 mg of L-lactide was loaded into the reaction tube. Reactions were generally carried out at 130 ^{o}C, but occasionally as high as 160 ^{o}C. Reaction times varied from 22 hr to 119 hr. Some of the samples were briefly immersed for 2 hours in liquid L-lactide before being inverted and allowed to react via CVDP. The reaction tube was then removed from the oven. Post reaction steps were performed as described above.

Preparation of Pro Osteon 500R and 200R cylinder/PLLA composites via CVDP: The pre-reaction treatment of Pro Osteon 500R and 200R cylinder samples with a diameter of 6 mm and a length of 12 mm was limited to two temperatures. One set of

samples was heated to 400 ^{o}C for 3 hours and the second set was heated to 600 ^{o}C for 19 hours in air. Three hours at 400 ^{o}C proved to be sufficient to drive off the organic material while only turning the sample light brown in color. Nineteen hours at 600 ^{o}C converts roughly 85-90% of the $CaCO_3$ to CaO. The overall reaction and sample preparation is the same as described above. For 500R samples, 200 mg of L-lactide was added to the reaction tube. 200R samples heated to 400 ^{o}C were placed in reaction tubes with one of four different amounts of L-lactide: 100 mg, 150 mg, 200 mg, or 250 mg. For 200R samples heated to 600 ^{o}C, 200 mg of L-lactide was added to the reaction tube. Samples heated to 600 ^{o}C were allowed to react at 130 ^{o}C for 5 days via CVDP. Samples heated to 400 ^{o}C were reacted for 10 days via CVDP. The termination of the reaction occurred as described above.

Preparation of Pro Osteon 500R block/PLLA composites via CVDP: Pro Osteon 500R blocks with dimensions of 13 mm x 14 mm x 17 mm were exposed to a variety of pre-reaction treatments in an attempt to produce a visually appealing product and a composite with superior compressive strength compared to uncoated Pro Osteon. The majority of the samples were dried under vacuum at room temperature for 16 hours. Others were subjected to heating at 500 ^{o}C in various environments including air, a stream of oxygen, and vacuum conditions. Additionally, chemical treatments were executed to attempt to remove residual organic material without heating. These chemical treatments included placing the sample in solutions of calcium hypochlorite and sodium hypochlorite followed by rinsing in deionized water and vacuum drying at room temperature. Polymerizations of cyclic lactones were then carried out as described above. A large diameter tube was needed to accommodate for these large samples, and a

minimum of 4 g of L-lactide was added to the reaction tubes. This amount was sufficient to ensure that adequate monomer was present to fill the void volume of the Pro Osteon if the reaction proceeded long enough. Typical reaction times were 6 days, but these periods varied from 3 days to a maximum of 27 days. Some of the samples were briefly immersed in L-lactide for either 2 hr or 3 days before the CVDP process. For these samples, a modified procedure was used to remove the samples from the oven while isolating the coated sample from excess monomer. A hole was cut in the bottom of the oven and covered while heating samples. When the reactions were terminated, the bottom reservoir of the reaction vessel was dropped through the hole and cooled in liquid N_2 while the sample continued to be heated at the reaction temperature. This proved to be a highly effective method for condensing the vapor phase monomer into the bottom of the reaction vessel and for making sure that any excess monomer was removed from the surface of the sample.

Preparation of bovine trabecular bone (TB)/PLLA, poly-ε-caprolactam (PCLM), polyglycolide (PG), poly-ε-caprolactone (PCLN) composites via CVDP: Cylindrical plugs, with a diameter of 6 mm and a length between 12 and 20 mm, of trabecular bone were cut from the proximal end of a bovine femur. The plugs were placed into a Soxhlet extractor to remove the majority of the organic material. The solvent mixture used for the extraction was 80% ethylenediamine and 20 % deionized water (v/v).[70] This solvent refluxed at 119 ^{o}C. The samples were extracted for approximately 48 hr. Fresh solvent cycled through approximately every 10 min. After the extraction period, the solvent/organic bone material mixture was replaced with deionized water. Soxhlet extraction of the bone with water was continued until the water was neutral pH. The

water was replaced 3-4 times during this process. The now white, porous trabecular bone was removed and allowed to air dry. Samples were further heated to temperatures between 600 ^{o}C and 700 ^{o}C in air to remove the residual organic material before being used in a reaction with one of the monomers. The length of this heating was varied from 16 hr to 66.5 hr. Reactions were executed as described above using excess monomer. CVDP of L-lactide, ε-caprolactam, and glycolide were conducted at 130 ^{o}C, 250 ^{o}C, and 100 ^{o}C, respectively. Termination of the reactions was executed as described above.

Scanning electron microscopy (SEM) images were obtained using a Hitachi (Tokyo, Japan) S4700 Field-Emission Scanning Electron Microscope (Morrison Microscopy Core Research Facility, University of Nebraska-Lincoln (UNL)). X-Ray powder diffraction (XRD) patterns were obtained on a Rigaku (Tokyo, Japan) D-Max/B θ/2θ Horizontal X-Ray Diffractometer (Nebraska Center for Materials and Nanoscience (NCMN), UNL). X-Rays are produced by a 2 kW copper target with K_{α} of λ = 154.4 pm. Obtained patterns were compared to and confirmed with a database of standard XRD patterns. NMR spectra were obtained using either a Bruker (Billerica, MA) 300 MHz NMR or Bruker Avance 400 MHz NMR instrument. Spectral processing was done using Bruker Topspin 3.0.b.8 (Research Instrumentation Facility, Department of Chemistry, UNL). Samples were dissolved in $CDCl_3$ and spectra were referenced to the solvent singlet at 7.27 ppm. Gel permeation chromatography (GPC) was used to determine M_p. GPC was performed using a Viscotek VE 2001 GPC solvent/sample module (Department of Chemistry, UNL). The instrument was equipped with a 7.8 mm x 30 cm Jordi-Gel DVB 10,000 Å organic GPC column that was heated to 35 ^{o}C. The detector was a Viscotek VE 3589 refractive index detector. HPLC grade THF was used as the eluent at

a flow rate of 1 mL/min. A series of polystyrene standards were used to create a calibration plot from which the molecular weight of the sample could be determined. Mechanical testing was performed using a Single Axis Instron Model 1123 Fatigue Testing Machine at a crosshead speed of 1 mm/min (College of Dentistry and Department of Chemistry, UNL). Instrument control, data acquisition, and data processing were performed by Blue Hill version 2.23 software (Norwood, MA).

Results and Discussion

CFBHA/PLLA composites via CVDP: Although the structure is quite different from mammalian bone, CFB does possess layers of channeling pores that are 80 μm wide and 100 μm tall,[51] making it potentially useful as a porous bone graft scaffold. The porous structure and a top view of the channeling pores are shown in the SEM images in Figure 2.3. The CFB was converted to morphologically similar HA for two reasons. First, the primary inorganic component of CFB, $CaCO_3$, is a weak nucleophile that does not initiate the polymerization of L-lactide. Second, upon being heated to 400 ^{o}C, the CFB loses an average mass of 10 ± 2% and delaminates into individual layers. Consequently, heating to higher temperatures in hope of generating well-structured CaO was not feasible. CFB was converted hydrothermally to HA as summarized by Equation 2.1. Confirmation of successful conversion was demonstrated using XRD (Figure 2.4). As seen in Figure 2.4, the hydrothermal conversion results in complete conversion from aragonite $CaCO_3$ to HA. The structure after the conversion is maintained as well (Figure 2.5).

Although the CFB and, subsequently, the CFBHA have a porosity of around 90%, the CFB's compressive strength of approximately 2.75 MPa[71] is not ideal for use as a

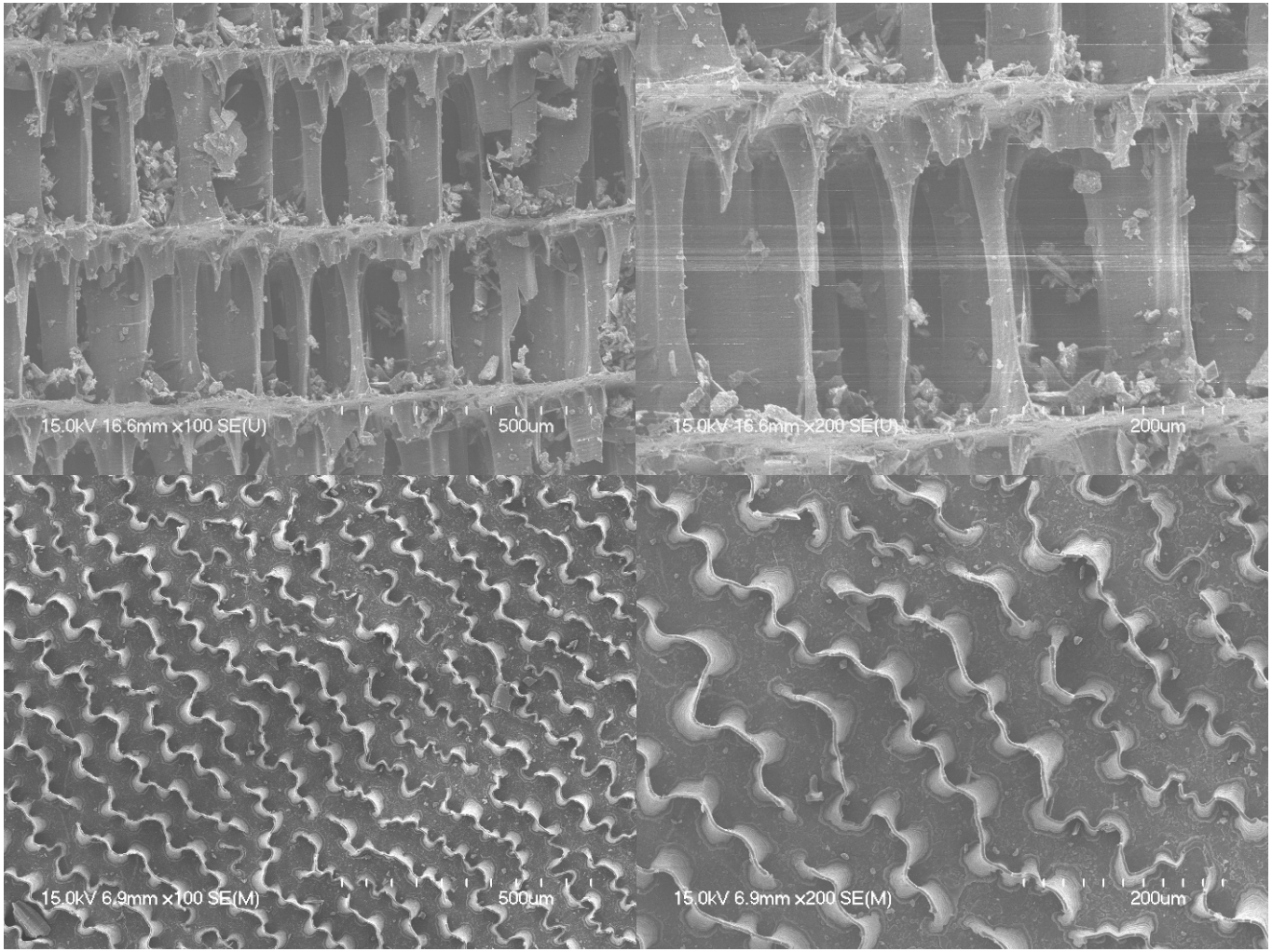

Figure 2.3. Scanning electron microscopy images of cuttlefish bone displaying the layered porous structure and the channeling pores from above.

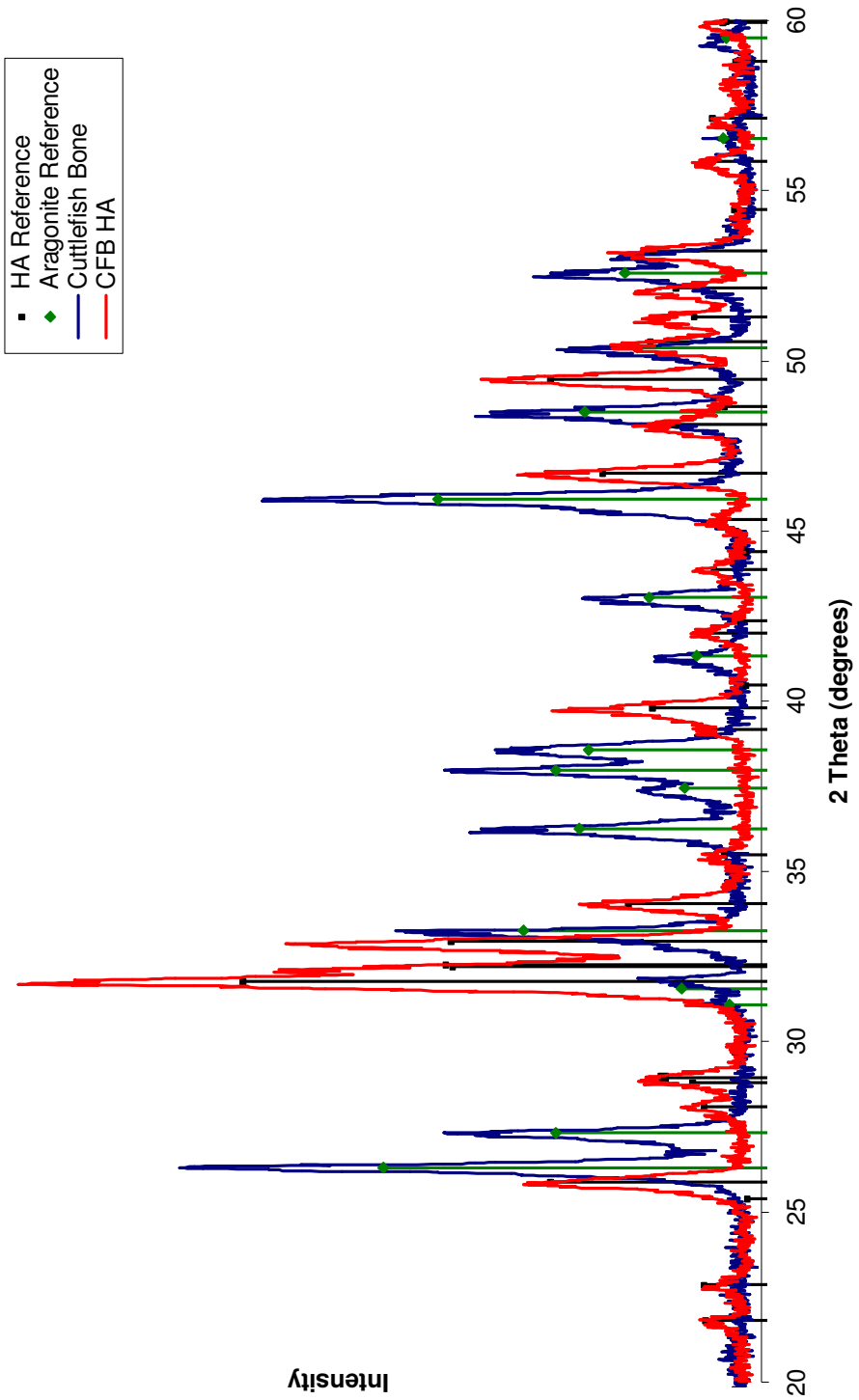

Figure 2.4. X-ray powder diffraction patterns showing the conversion of cuttlefish bone from aragonite $CaCO_3$ to hydroxyapatite.

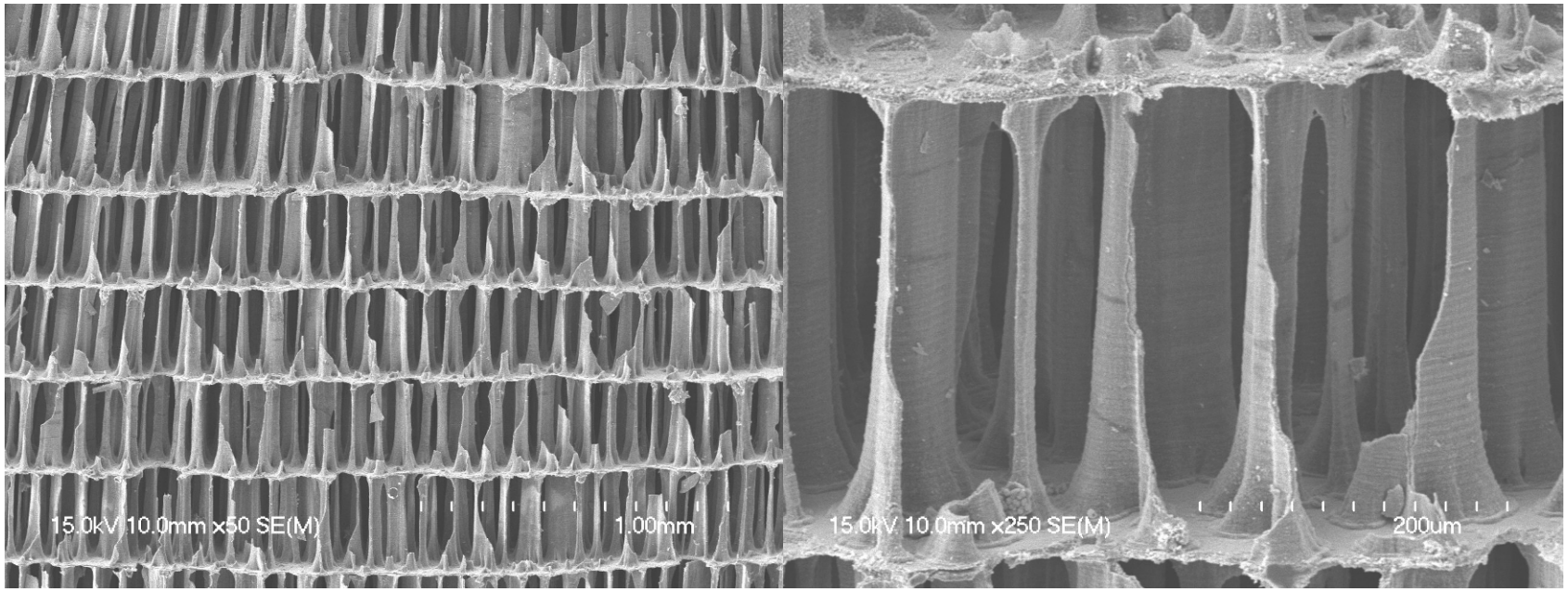

Figure 2.5. Scanning electron microscopy images of the porous structure of cuttlefish bone after it was converted to hydroxyapatite. The structure of the original cuttlefish bone is maintained (see Figure 2.3).

bone graft scaffold. To strengthen the CFBHA, I attempted to use it to initiate the CVDP of L-lactide. The goal was to reinforce the structure with a thin polymer layer. The reaction was carried out at 130 ^{o}C for 10 or 14 days. The results of the CVDP can be seen in the SEM images in Figure 2.6. Although some pores remain open, it appears that the majority of them are filled with PLLA. The CVDP of L-lactide by CFBHA was verified by ^{1}H NMR (Figure 2.7). Peak assignments for L-lactide and PLLA were compared to literature values.[72-76] Comparison of the integrated areas of the quartets at approximately 5.17 and 5.03 ppm provide information on the amount of polymer compared to monomer in the composite. The quartet at 5.17 ppm is due to the internal methine proton in the polymer and the quartet at 5.03 ppm is due to the methine proton of L-lactide. The quartet at 4.36 ppm is due to the methine protons at the hydroxyl end of the polymer. Doublets at approximately 1.53 ppm and 1.66 ppm are due to the methyl protons in PLLA and L-lactide respectively. Comparison of these integrated peak areas shows this particular composite contains approximately 91% polymer. These preliminary results indicate that the CVDP of L-lactide can be initiated by CFBHA. The reaction times were too long and the majority of the pores were filled. It is possible that shortening the reaction time will prevent this issue. It is also possible that the pore structure of the CFB does not lend itself well to the CVDP of L-lactide while at the same time maintaining the original porosity.

Goniopora coral/PLLA composites via CVDP: As mentioned earlier in the experimental section, the coral samples are predominantly $CaCO_3$, specifically the mineral form aragonite. At elevated temperatures (above 500 ^{o}C) it is possible to convert the $CaCO_3$ to CaO through the loss of CO_2 (Equation 2.2). This was originally deemed

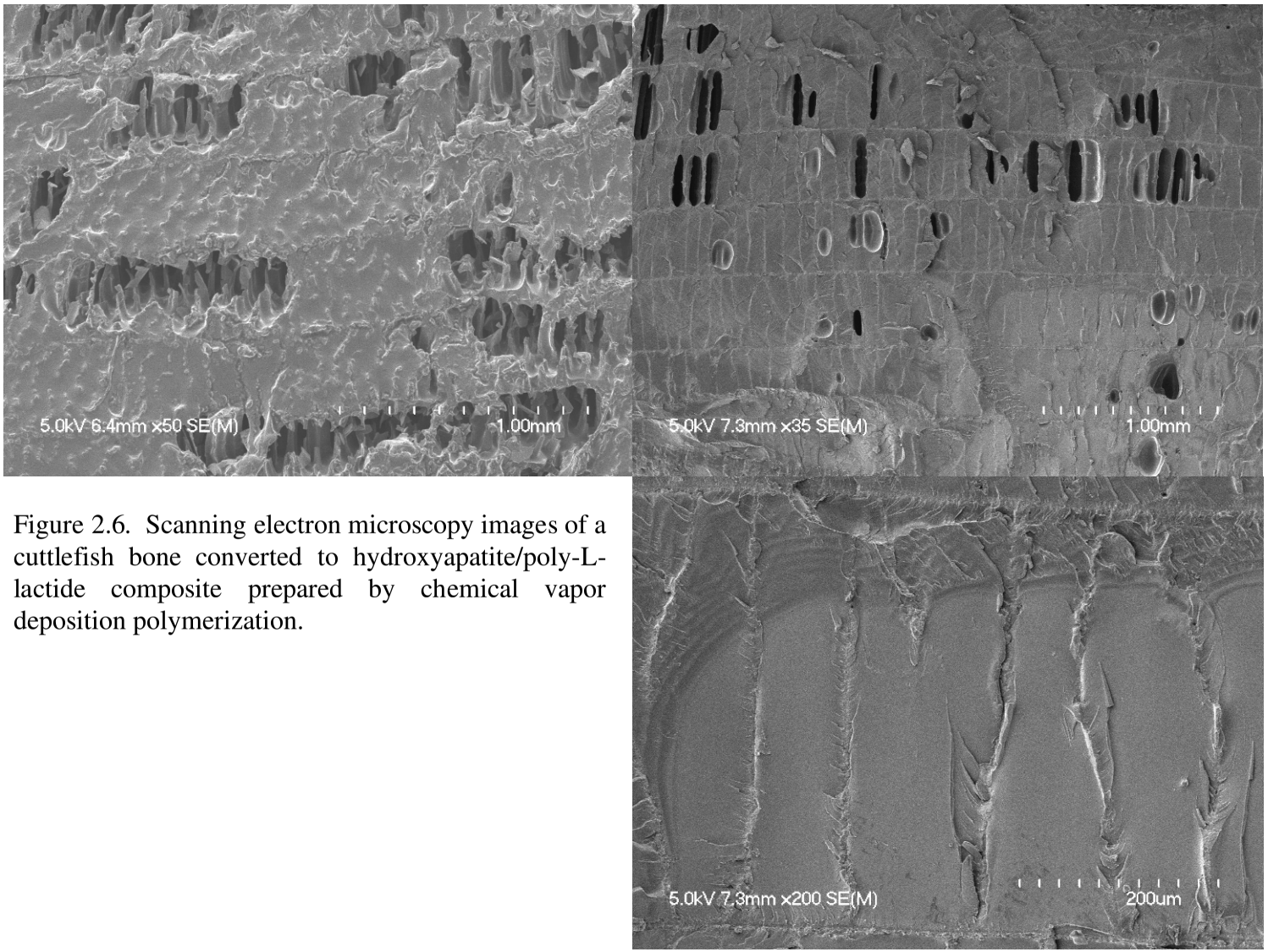

Figure 2.6. Scanning electron microscopy images of a cuttlefish bone converted to hydroxyapatite/poly-L-lactide composite prepared by chemical vapor deposition polymerization.

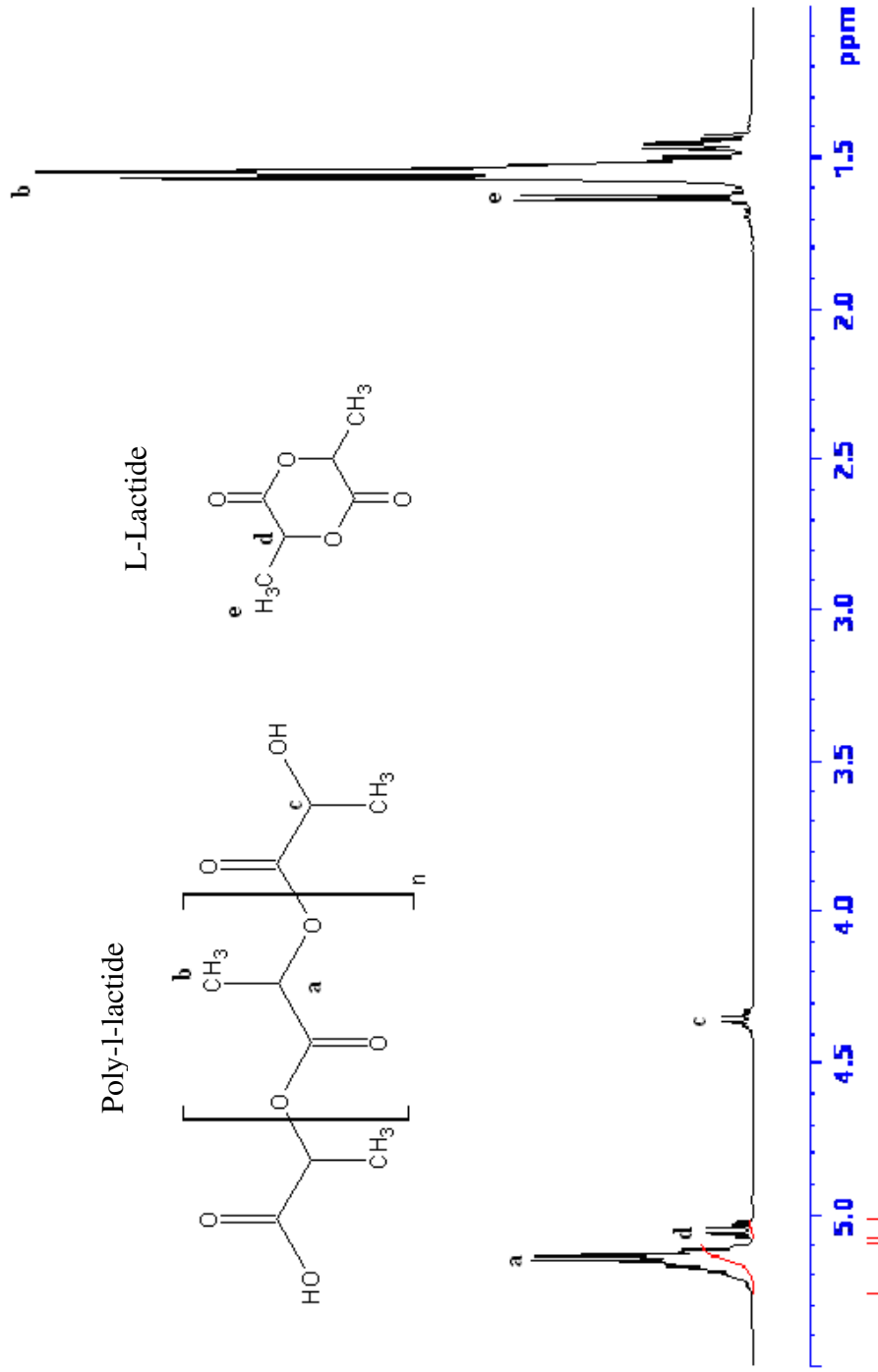

Figure 2.7. Representative ^{1}H NMR spectrum of a CFBHA/PLLA composite.

necessary as $CaCO_3$ is a weak nucleophile not capable of initiating the polymerization of L-lactide and CaO is capable of initiating the reaction. Figure 2.8 shows the time dependent mass loss of *Goniopora* coral upon heating it in air at 600 ^oC. Between t = 0 hr and approximately t = 20 hr the rate of weight loss proceeds at a constant rate. The point at t = 0 hr is the mass of coral obtained by thermally pretreating it at 400 ^oC for 3 hr. As a result of this thermal pretreatment the average percent mass loss of four samples heated to 400 ^oC was 2.56 ± 0.29%, where the reported uncertainty is one standard deviation (SD). This plot shown in Figure 2.8 indicates that at 600 ^oC, the decomposition of the aragonite in coral is a zero order reaction for which the weight of the coral decreases by approximately 2% of the original weight for each hour it is heated. This zero order process continues until the mass loss nears 44%, at which point nearly all of the $CaCO_3$ (Formula Weight (F.W.) = 100.09 g/mol) has been converted to CaO (F.W. = 56.08 g/mol). Figure 2.8 shows that the extent of the conversion process can be controlled by terminating the heating process at a given time. As expected, heating the coral at higher temperatures results in a faster rate of conversion and at much lower temperatures a much slower rate of conversion occurs. For example, two samples heated at 550 ^oC for 25 and 43 hours produced a mass loss of 6.07 and 7.36% respectively. At 500 ^oC for a period of 43 hr, no conversion of $CaCO_3$ to CaO was observed. The conversion from aragonite to CaO can be observed over time using XRD. Figure 2.9 shows a series of XRD patterns of coral heated at 600 ^oC for 12 and 24 hr. It also shows an unheated sample and a coral sample heated to 400 ^oC for 3 hr. Although no conversion of $CaCO_3$ to CaO occurs at 400 ^oC, the coral originally present in the mineral phase aragonite, is completely converted to the mineral phase calcite. This was not

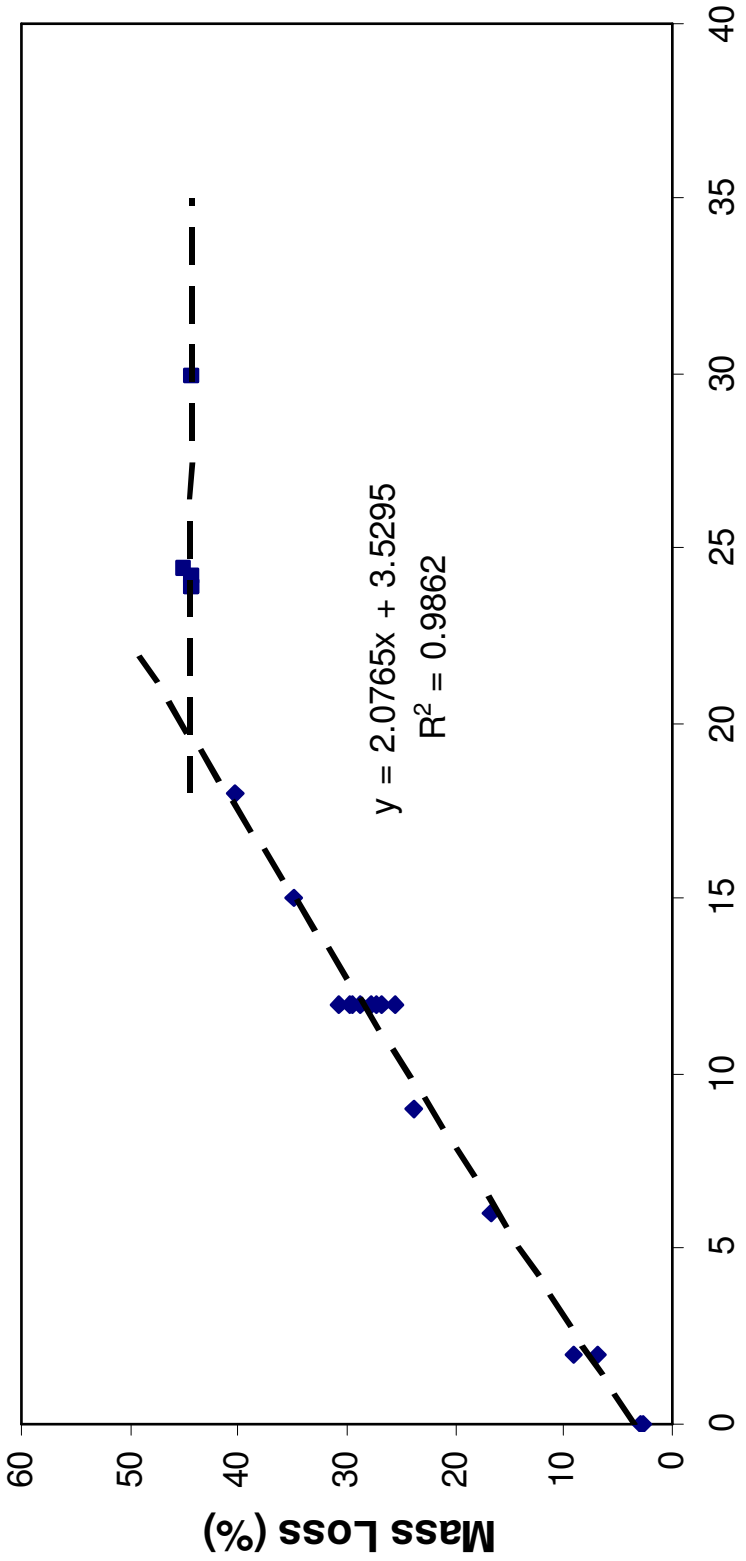

Figure 2.8. Time dependent mass loss of *Goniopora* coral heated at 600 °C.

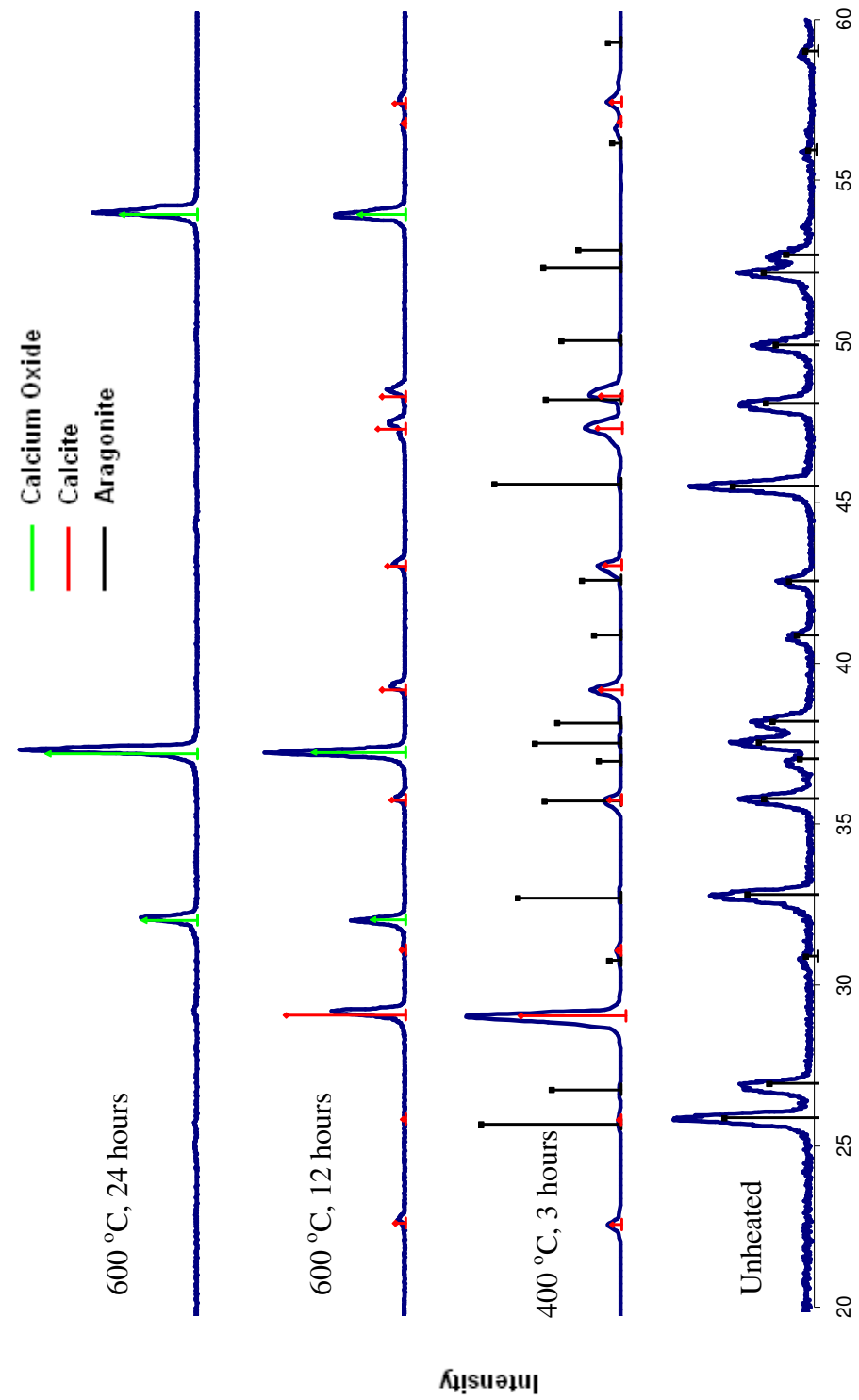

Figure 2.9. X-Ray powder diffraction patterns for *Goniopora* coral heated at 400 °C for 3 hr and 600 °C for 12 and 24 hr.

observed when heating at 300 °C or below. Heating the sample at 600 °C for 12 hr, results in an approximately 25% mass loss, meaning approximately 55% of its original $CaCO_3$ is converted to CaO. The peaks at 32, 37.5, and 54 degrees that are absent from the patterns of the coral samples treated at lower temperatures are due to CaO. For the sample that was heated for 24 hr at 600 °C, the conversion is complete and the only peaks present are those of CaO.

The effect heating at 600 °C has on the microporosity of the coral is readily apparent in SEM images. Figure 2.10 displays SEM images of a coral sample as received from Biomet, Inc. and a coral sample that has been heated to 600 °C for 24 hr in air. The development of small pores a few micrometers in diameter can clearly be seen after heating. Samples heated at this temperature and length were extremely brittle due to the loss of 44% of the original mass and increase in microporosity.

Although the mechanical properties of the sample suffered upon its conversion to CaO, this conversion did create a nucleophile suitable to polymerize L-lactide by CVDP, and hopefully strengthen the sample. SEM images in Figure 2.11 show a coral sample heated to 600 °C for 24 hours in air and the same coral sample coated with PLLA by CVDP. The thin, even polymer coating appears smooth when compared to the uncoated sample. A few of the macroscopic pores appear to be filled with PLLA, most notably in the upper left corner, but the majority of the pores remained unfilled and the interconnected porous network is largely preserved. The influence of thermal pretreatment and reaction conditions are summarized in Table 2.1. There are two general trends that can be observed based on this data. First, longer reaction times produced larger amounts of deposited polymer when samples were pretreated for the same length

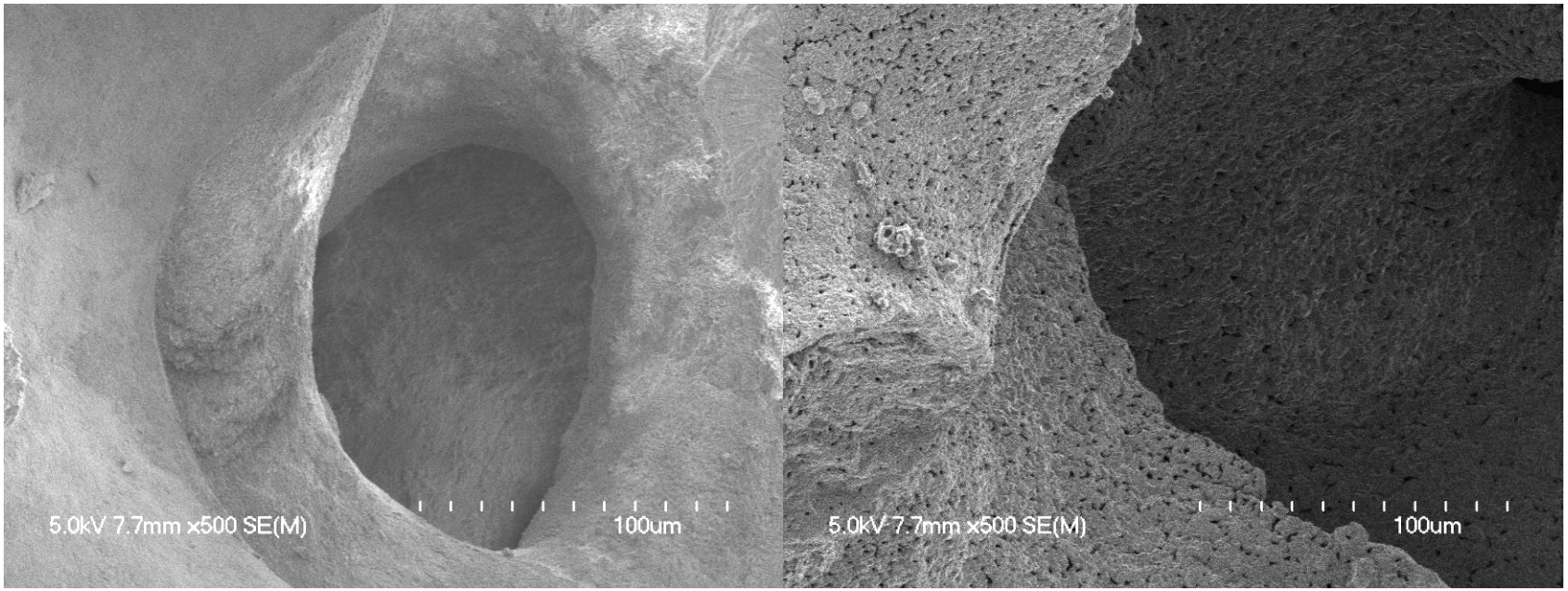

Figure 2.10. Scanning electron microscopy images of (left) *Goniopora* coral as received from Biomet, Inc. and (right) *Goniopora* coral heated at 600 ^{o}C for 24 hr in air.

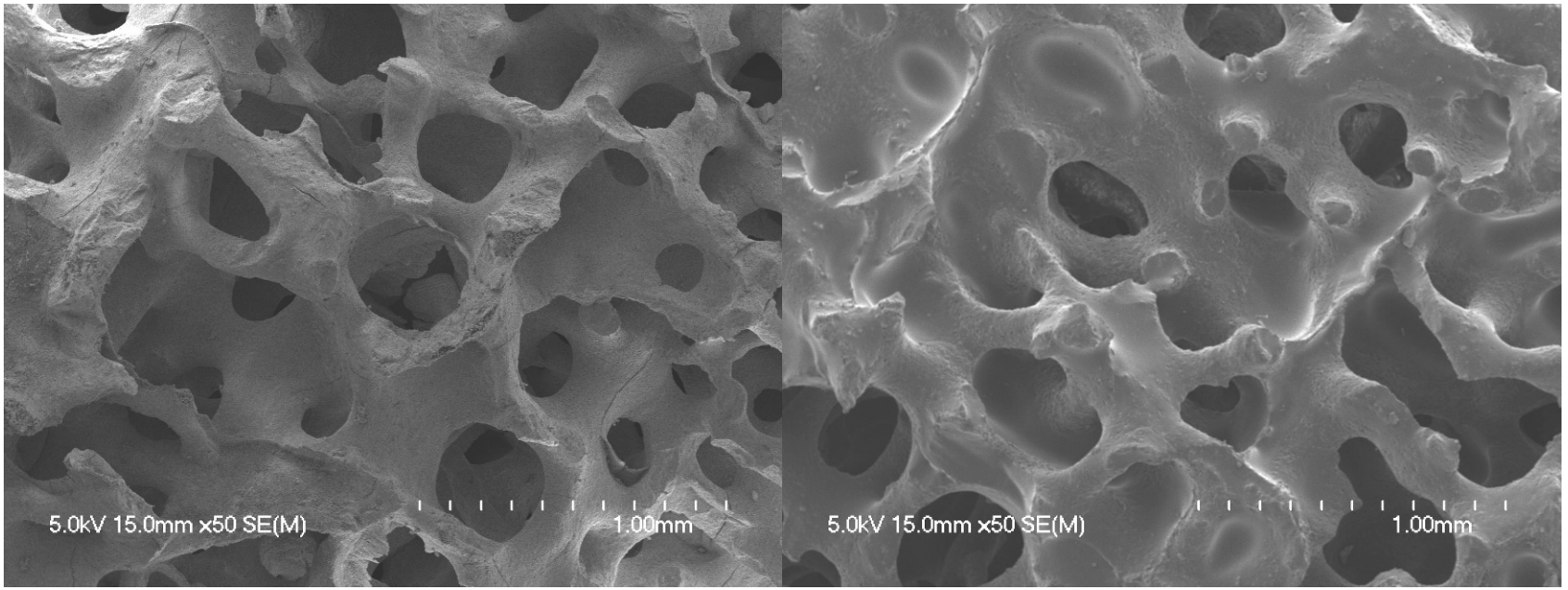

Figure 2.11. Scanning electron microscopy images of (left) coral heated at 600 ^{o}C for 24 hours in air and (right) coral heated at 600 ^{o}C for 24 hours in air followed by CVDP of L-lactide to PLLA for 24 hours.

Sample	Time heated at 600 °C (hr)	Reaction temperature (°C)	Reaction time (hr)	Mass gain (%)
1	12	130	40.75	91
2	12	130	57	130
3	12	130	70.5	138
4	12	130	70.5	159
5	6	130	24	31
6	15	130	24	73
7	18	130	24	70
8	30	130	24	87
9	24	130	137	120
10	24	160	26	180

Table 2.1. Raw data for several individual coral/PLLA composites heated at 600 °C for various lengths of time followed by CVDP of L-lactide to PLLA for various lengths of time.

of time at 600 ^{o}C. Second, as the length of the pretreatment was increased, an increase in the amount of polymer deposited was observed when the reactions were conducted for the same length of time at 130 ^{o}C. Additionally, reactions conducted at 160 ^{o}C instead of 130 ^{o}C proceeded faster, producing thicker polymer films and greater polymer masses for reactions run for the same period of time. A representative ^{1}H NMR spectrum for coral/PLLA composites prepared via CVDP is shown in Figure 2.12. There are only PLLA peaks present in this spectrum. Note that the absence of extraneous peaks in the spectrum indicates that it is a relatively pure sample of PLLA. The spectrum indicates that the sample is >99% PLLA and that no excess monomer can be detected.

The generation of CaO is advantageous because it initiates the polymerization of L-lactide, but once in the body any excess CaO will readily dissolve forming strongly basic $Ca(OH)_2$ in the presence of water.[77] If the dissolution were to happen quickly, the structural integrity of the implant might be compromised and there would probably be an undesirable response to the strong base. Consequently I sought to convert the CaO generated during the heating of the coral samples at 600 ^{o}C back to the original $CaCO_3$ while maintaining the interconnected porous structure. The conversion of CaO to $CaCO_3$ can be accomplished in two steps. The first step involves converting the CaO to $Ca(OH)_2$ and the second involves converting the $Ca(OH)_2$ to $CaCO_3$. Recently, it has been shown that $Ca(OH)_2$ can be converted to $CaCO_3$ in supercritical CO_2 containing small amounts of water (wet-sCO_2).[78] I placed my coral derived CaO/PLLA composites in a desiccator with a vial of water at 50 ^{o}C for 20 hr. This step converted the CaO to $Ca(OH)_2$, but I also observed that the polymer layer on the sample became highly swollen and more elastic than its original form. The sample was then placed in a supercritical CO_2 dryer

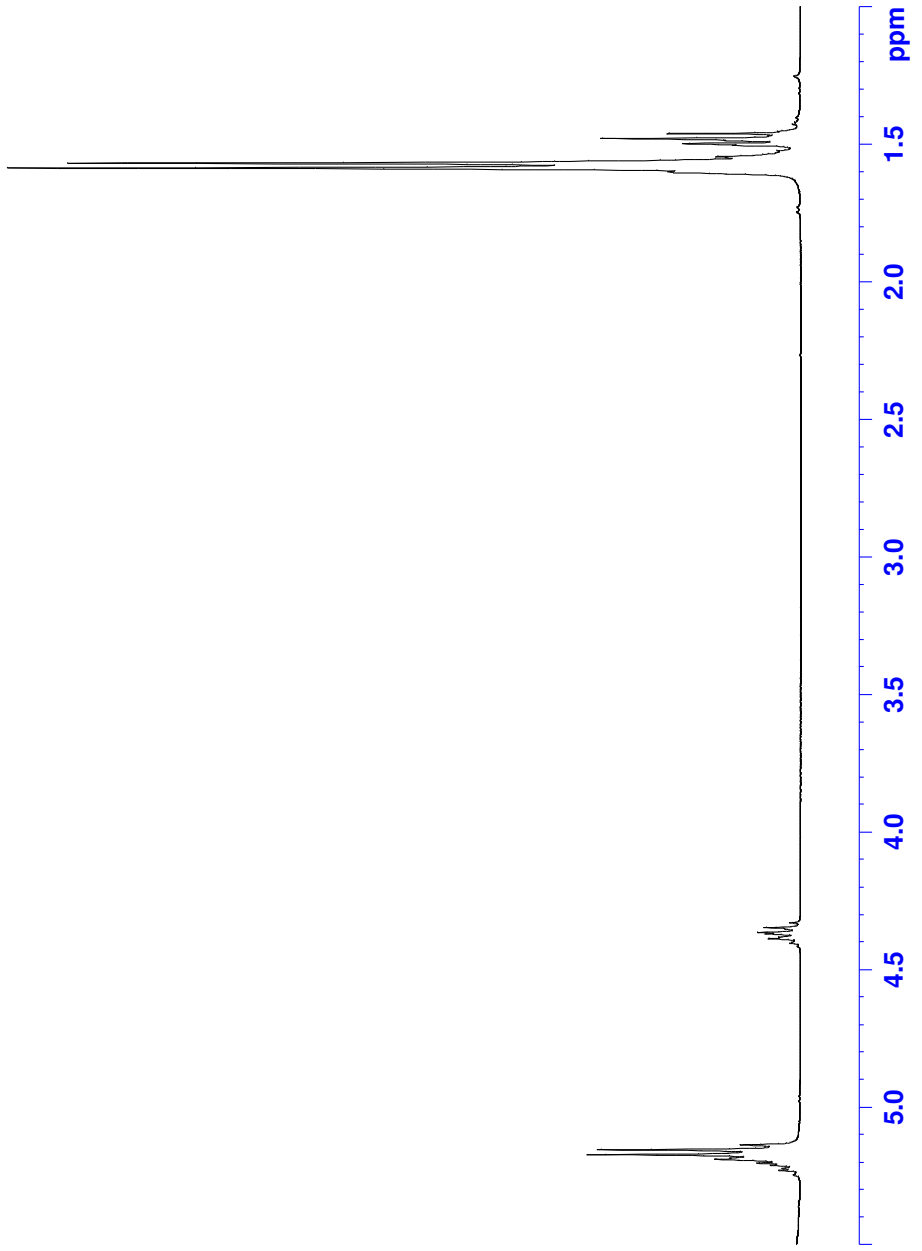

Figure 2.12. Representative ^{1}H NMR spectrum of a coral/PLLA composite.

with a damp Kimwipe, containing approximately 1 ml of deionized water. The pressure was increased to 1250 psi and the temperature to 42 ^{o}C over a period of 15 min. The pressure and temperature were then allowed to drop below the critical point. The XRD pattern in Figure 2.13 confirms that the original CaO was converted back to $CaCO_3$, but the resulting polymorph was calcite, not the desired aragonite. This process does hold potential for converting CaO to $CaCO_3$ in composites such as these. The porous structure is retained after the conversion. The downside of the conversion process is that the physical characteristics of the polymer (and probably its molecular weight) are altered. It may be possible to convert uncoated samples, but the brittleness of such samples presents a different challenge.

Alternatively, it was possible to demonstrate the polymerization of L-lactide using coral dried at room temperature under vacuum or at 400 ^{o}C in air instead of heating the coral samples to 600 ^{o}C and converting them to CaO. Although $CaCO_3$ does not effectively initiate the polymerization of L-lactide, I investigated the possible use of hypochlorite or hydroxide remaining from the process used to remove the organic constituents. The disadvantage would be the rate of the reaction would slow considerably because of the small number of potential nucleophiles. The advantage would be the possible avoidance of brittleness I observed upon heating the coral to 600 ^{o}C. Two coral samples were heated at 400 ^{o}C for 3 hr to remove water and any other residual organic material. The mass loss due to this process was 2.69 ± 0.07%. The pretreated samples were then used to attempt to initiate the CVDP of L-lactide. The reactions were carried out at 130 ^{o}C for 113 hr. I was somewhat surprised by the success of these reactions. The average percent mass gain was 37 ± 5%, and the peak molecular weight (M_p) of one

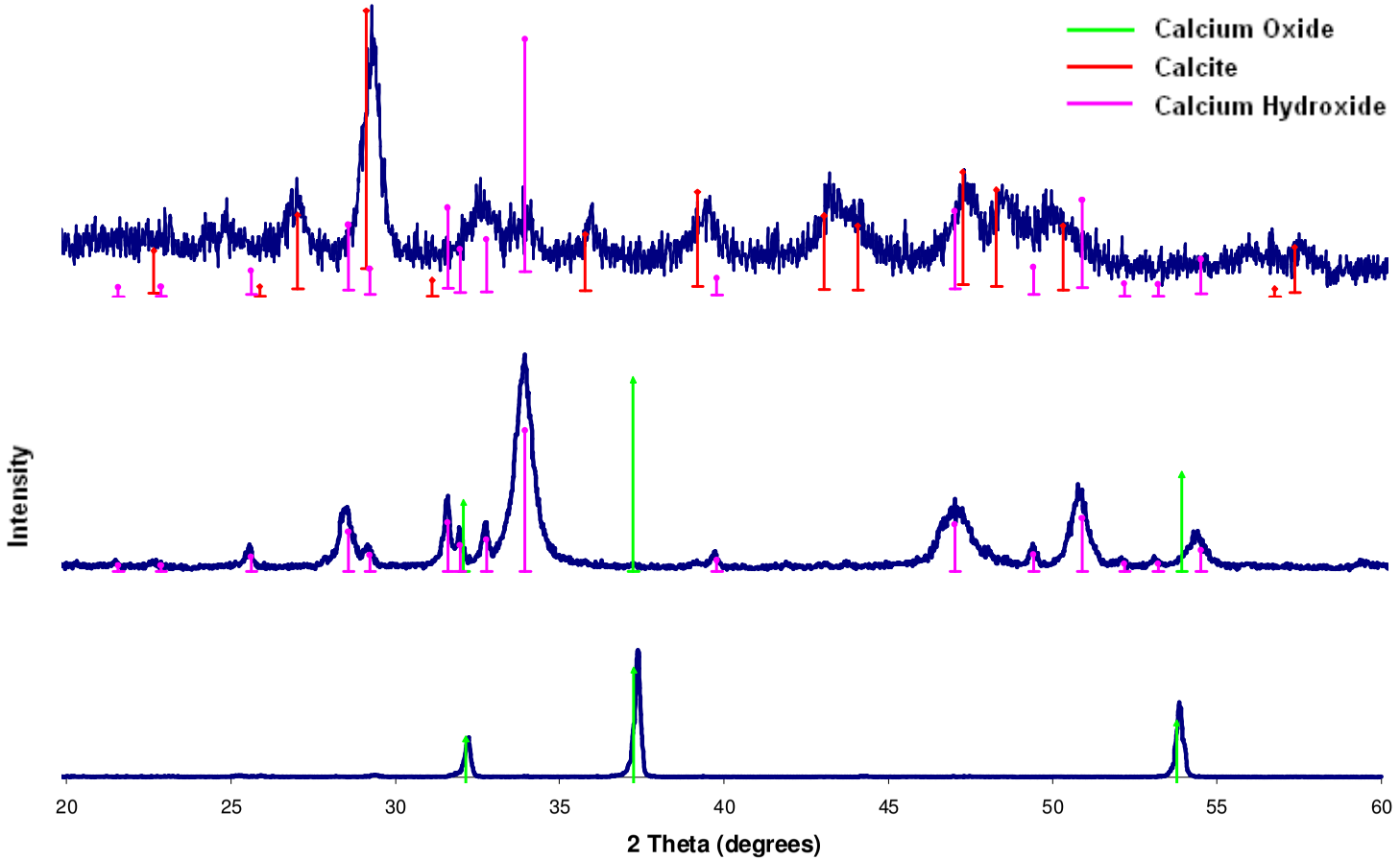

Figure 2.13. X-Ray powder diffraction patterns for a coral/PLLA sample. Coral had been previously converted to CaO at 600 ^{o}C for 24 hours (bottom). It was then converted to $Ca(OH)_2$ (middle) and finally calcite ($CaCO_3$) (top) using wet-sCO_2.

of these two samples was measured to be 45,000 Da by GPC. SEM images shown in Figure 2.14 confirm the presence of a smooth PLLA coating. In Figure 2.14 a SEM image of an uncoated coral sample heated to 400 ^{o}C is compared to a SEM image of the coral sample with a thin, even layer of PLLA. Again, like the coral heated to 600 ^{o}C, a thin, even layer of polymer is deposited via CVDP without filling up the macroscopic pores.

Additionally, four coral samples, two of which were placed in a solution of $Ca(OH)_2$ for three days and then rinsed in water, were dried at room temperature under vacuum for 16 hr. These treated coral samples were then used to polymerize L-lactide via CVDP. The reaction was carried out at 130 ^{o}C for 5 days. At the end of this period, polymer was observed to have deposited on the coral. The average percent mass gained for the four samples was 74 ± 3%. The M_p was 5200 ± 600 Da. These four coral/PLLA samples also underwent mechanical testing. The average compressive strength was 18 ± 3 MPa and the average elastic modulus was 1.2 ± 0.3 GPa. An additional coral sample was heated to 500 ^{o}C for 16 hr and reacted in the same manner as the preceding four samples. This sample had a 93.22% mass gain, a M_p of 17,700 Da, a compressive strength of 11.4 MPa, and an elastic modulus of 0.5 GPa. For comparison purposes, one source in the literature lists the compressive strength for *Goniopora* coral at 2.64 MPa[79] and trabecular bone between 1 and 12 MPa depending on the location of the bone.[80] Consequently, these results from my exploratory experiments suggest that these coral/PLLA composites are approximately 7 times stronger than the original coral and also mechanically stronger than trabecular bone. This increase in strength can be attributed to the deposited polymer reinforcing the coral structure. It can also be

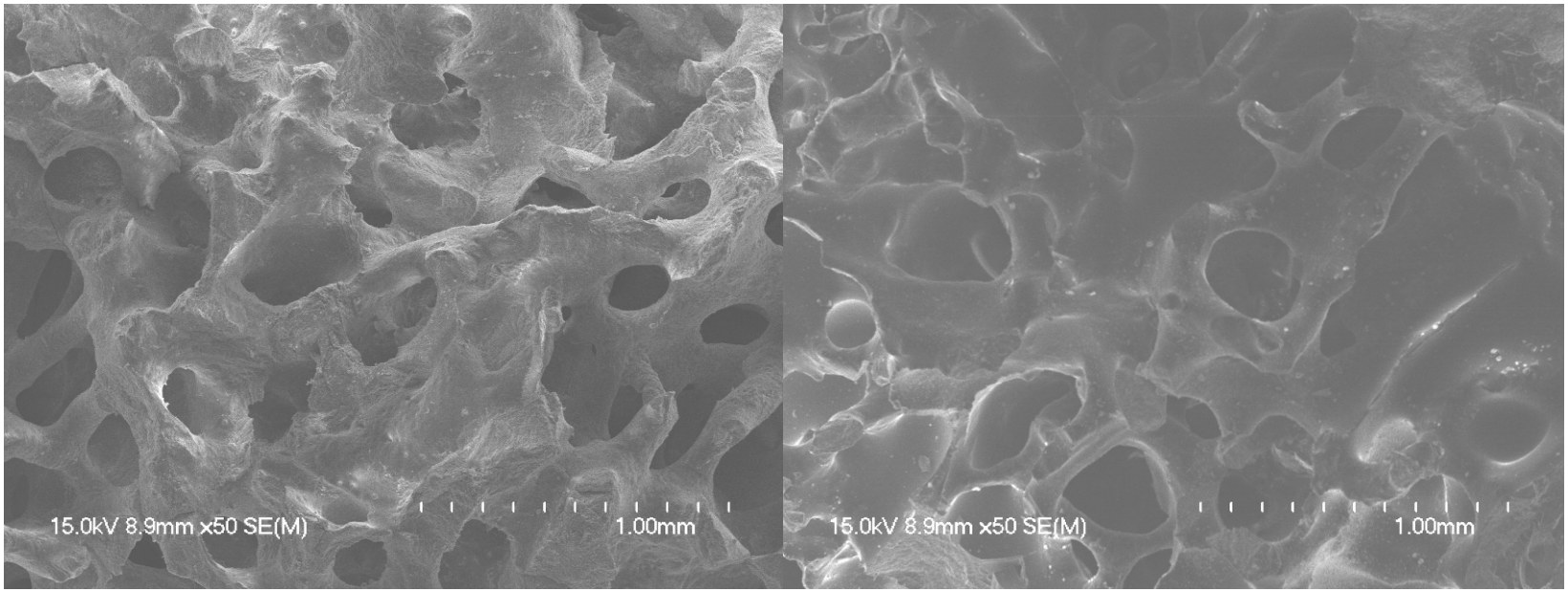

Figure 2.14. Scanning electron microscopy images of (left) coral heated to 400 ^{o}C for 3 hours and (right) a coral/PLLA composite after CVDP at 130 ^{o}C for 113 hr.

attributed to partially filling the void volume of the sample. As mentioned earlier, the higher the porosity, the lower the compressive strength for porous ceramic scaffolds. The coral samples had a void volume of 72 ± 1%. After coating the samples with PLLA, this void volume was 67 ± 6% filled. Increasing the compressive strength is important, but the interconnected porosity needs to be maintained for optimum bone ingrowth. These preliminary results suggest that I have succeeded in improving the compressive strength without compromising the desired porosity.

Pro Osteon 500R and 200R cylinder/PLLA composites via CVDP: Pro Osteon is a coralline hydroxyapatite marketed by Biomet, Inc. Instead of completely converting the entire coral scaffold to HA, only a thin layer of the surface is converted by terminating the hydrothermal exchange early.[44] This maintains the $CaCO_3$ core which is resorbed faster than HA and also the interconnected porous structure. The 200R and 500R samples differ in their pore size and porosity. Pro Osteon 200R has an average pore size of 200 μm and an average porosity of 50%. Pro Osteon 500R has an average pore size of 500 μm and an average porosity of 65%.[81] Biomet expressed interest in improving the mechanical properties of the Pro Osteon bone graft substitute by using the CVDP method developed in our group. The goal was to increase the strength while maintaining the interconnected porosity. Based on results of the coral samples described above, I opted to focus on two different pre-reaction treatments. Heating samples at 400 ^{o}C in air for three hours was previously shown to remove the residual organic material without converting the sample to CaO. The downside of this treatment is a slight color change from white to light brown or grey. The second treatment examined was to heat the samples in air at 600 ^{o}C for 43 hours. The samples were white after this period of

time and the $CaCO_3$ was quantitatively converted to CaO. Polymerizations of L-lactide were performed over 10 days at 130 ^oC for the samples pretreated at 400 ^oC, and over 5 days at 130 ^oC for the samples pretreated at 600 ^oC. For all of the reactions with Pro Osteon 500R, 200 mg of L-lactide was used. For reactions with Pro Osteon 200R, L-lactide sample sizes of 100 mg, 150 mg, 200 mg, or 250 mg were used. A representative ^1H NMR of the polymer product formed using Pro Osteon 500R as the initiator is shown in Figure 2.15. The polymerization of L-lactide is confirmed by the polymer methine quartet at 5.17 ppm and the absence of the monomer methine quartet at 5.03 ppm. The percent mass loss after heating, percent mass gain after the CVDP, and the M_p of the Pro Osteon 500R and 200R samples can be seen in Table 2.2. The compressive strength and elastic modulus of the samples can be seen in Table 2.3. Mechanical testing was performed by Biomet. The reported values are those provided by them. It is unknown why they tested only half of the samples heated to 400 ^oC. As expected the Pro Osteon samples heated to 400 ^oC lost around 2 % of their mass and the samples heated to 600 ^oC lost around 37 %. This additional mass loss is due to the conversion of $CaCO_3$ to CaO. These additional nucleophiles explain the higher percent mass increase (due to polymer) that occurred in a shorter reaction time for the samples heated to 600 ^oC. It was also observed that as the amount of L-lactide in the reaction vessel was increased, so too did the percent mass increase of Pro Osteon 200R samples. By limiting the amount of L-lactide available for polymerization, I was able to control the mass deposited on the surface of the Pro Osteon. Of great interest is the compressive strength of the samples in Table 2.3. Literature values for the compressive strengths of uncoated Pro Osteon 500R and 200R samples are 6 MPa and 10 MPa respectively.[82] Four Pro Osteon 500R samples

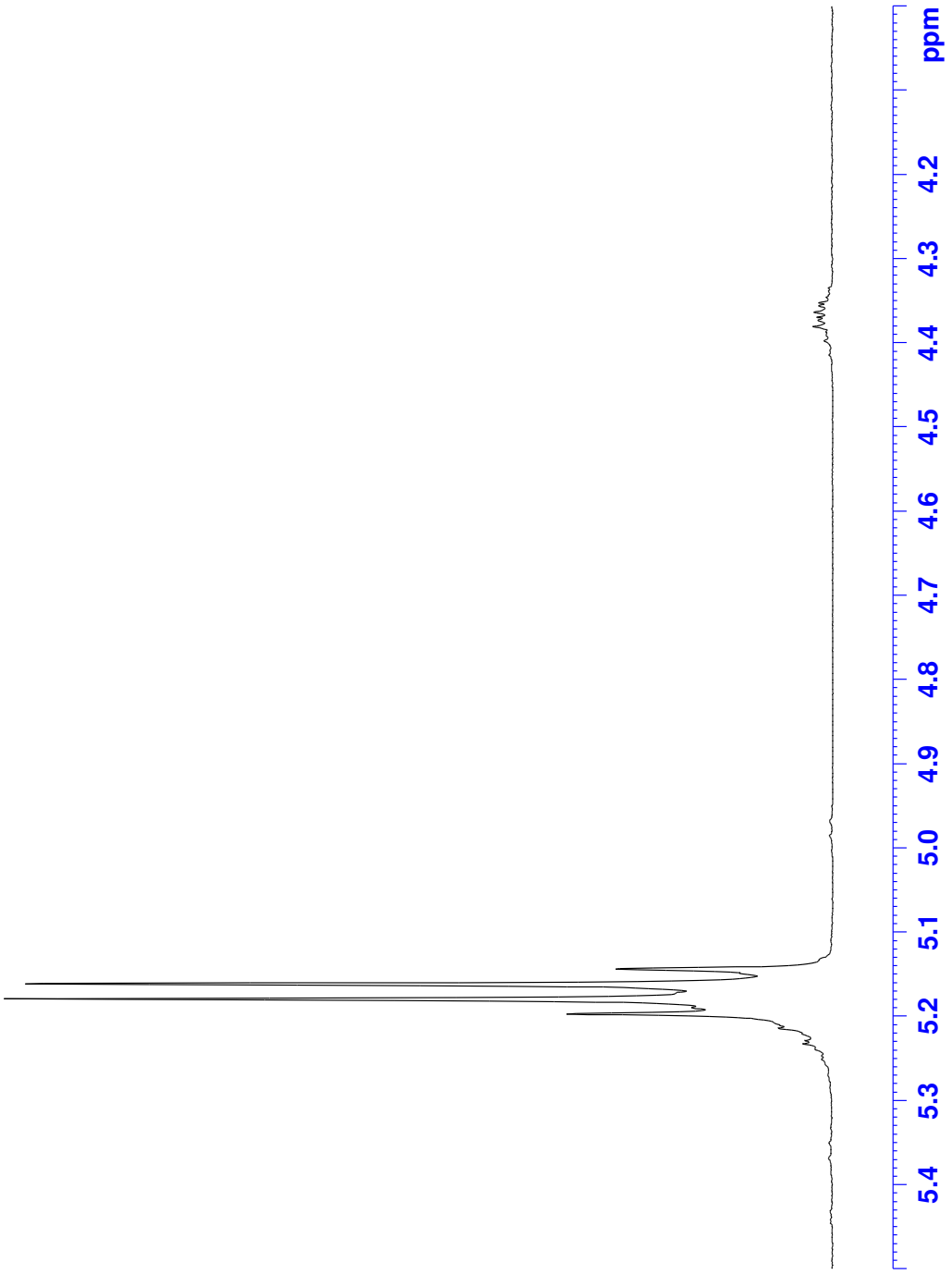

Figure 2.15. Representative ^{1}H NMR spectrum of a Pro Osteon 500R/PLLA composite.

Pro Osteon type	Pre-treatment temperature (°C)	Mass loss (%)	L-lactide (mg)	Mass gain (%)	Peak molecular weight (Da)
500R	400 (n = 20)	2.0 ±0.4	200	53 ± 8	11000 ± 3000 (n = 18)
	600 (n = 5)	36.9 ± 0.6	200	100 ± 14	9000 ± 3000
200R	400 (n = 12)	2.2 ± 1.2	100 (n = 3)	22.0 ± 0.6	22000 ± 8000
			150 (n = 3)	29.1 ± 4.2	13000 ± 8000
			200 (n = 3)	44.1 ± 6.2	12000 ± 3000
			250 (n = 3)	49.0 ± 9.9	15000 ± 3000
	600 (n = 3)	38.6 ± 1.5	200 (n = 3)	69.6 ± 5.9	4000 ± 400

Table 2.2. Mass loss of Pro Osteon 500R and 200R and mass gain and molecular weight of Pro Osteon 500R and 200R/PLLA composites prepared by CVDP. The values listed for the mass loss, mass gain, and peak molecular weight are the averages with an uncertainty of one SD ($\bar{x}$ ± 1 SD).

Pro Osteon type	Pre-treatment temperature (^{o}C)	Compressive strength (MPa)	Modulus (GPa)
500R	400 (n = 10)	5.9 ± 2.0	0.2 ± 0.05
500R	600 (n = 5)	5.5 ± 2.7	0.1 ± 0.05
200R	400 (n = 6)	26.0 ± 11.3	0.3 ± 0.08
200R	600 (n = 3)	11.5 ± 10.0	0.2 ± 0.09

Table 2.3 Compressive strength and elastic modulus of Pro Osteon 500R and 200R/PLLA composites prepared via CVDP. The values listed for compressive strength and modulus are the averages with an uncertainty of one SD ($\bar{x}$ ± 1 SD).

tested by Biomet had a compressive strength of 2.6 ± 1.0 MPa. The compressive strength of Pro Osteon 500R/PLLA composites is similar to or double the value for uncoated samples depending on the value used for uncoated Pro Osteon samples. No difference was seen between the samples heated at 400 ^{o}C and 600 ^{o}C. The additional mass loss of the 600 ^{o}C is possibly offset by the larger mass gained during the CVDP due to the increase in the number of nucleophiles. The compressive strength of Pro Osteon 200R samples heated to 400 ^{o}C are approximately 2.5 times that of uncoated samples. The samples heated to 600 ^{o}C showed compressive strengths similar to uncoated samples. The data of the individual samples was examined in an attempt to find a correlation between the compressive strength and the variables of percent mass loss, percent mass gain, and the molecular weight of the polymer coating. No correlations were observed. There are two possible reasons for this. First, the structure of coral is anisotropic[83] and the technicians at Biomet who did the mechanical testing did not record the orientation of the native macroscopic pores in Pro Osteon with respect to the axis along which their measurements were made. By examining other Pro Osteon samples, I observed that the orientation of these columnar structures was not the same in each sample. Since the samples are compressed along the same axis in each mechanical test (the long axis of the cylinder), the compressive strength of the sample will be different depending on which way the porous columns run through the sample. This was a possible source of scatter in the compressive strength values. Second, the variables (percent mass loss, percent mass gain, and molecular weight) examined were most likely not the best choices when looking for an explanation into the compressive strength values. As mentioned earlier in the chapter, the compressive strength of porous scaffolds increases as the porosity

decreases. A better method for examining the change in porosity would be to examine how the percent void volume of the sample changes with the deposition of the polymer. The percent void volume is calculated by first calculating the volume of the sample, which for a cube is

$$V = l * w * h \tag{2.3}$$

and for a cylinder is

$$V = \pi * r^2 * h \tag{2.4}$$

where V is the volume, l is the length of the cube, w is the width of the cube, h is the height of the cube or the cylinder and r is the radius of the cylinder. Once the volume of the sample is known, its void volume (V_{void}) can be calculated by subtracting the volume of the cube or cylinder that is occupied by the HA/$CaCO_3$ scaffold.

$$V_{void} = V - (\frac{m_{sample}}{d_{CaCO_3}}) \tag{2.5}$$

In equation 2.5, m_{sample} is the mass of the sample and d_{CaCO_3} is the density of $CaCO_3$ with units of g/mm^3. The percent void volume ($\%V_{void}$) is then calculated by dividing the void volume from equation 2.5 by the total volume of the cube or the cylinder from equation 2.3 or 2.4 and multiplying by 100.

$$\%V_{void} = (\frac{V_{void}}{V}) * 100 \tag{2.6}$$

The mass of PLLA (m_{total}) needed to fill the void volume can be calculated by multiplying the density of PLLA (d_{PLLA}) by the void volume of the sample.

$$m_{total} = V_{void} * d_{PLLA} \tag{2.7}$$

The percent of the void volume that is filled ($\%V_{filled}$) with PLLA after the CVDP can be calculated by dividing the deposited mass of the polymer (m_{PLLA}) by m_{total} and multiplying by 100.

$$\%\,V_{filled} = \left(\frac{m_{PLLA}}{m_{total}}\right) * 100 \tag{2.8}$$

As can be seen by the equations above, the dimensions of the sample are needed to determine the void volume and therefore the percent void volume filled. Unfortunately the exact dimensions were not recorded by the technicians who performed the mechanical studies. Consequently, additional studies were necessary. For the Pro Osteon 500R blocks used to initiate the CVDP in the next section, the dimensions were known and the percent void volume was calculated. Additionally the orientation of the porous columns was noted and was used to interpret the results of the mechanical testing. If a correlation between the compressive strength and one of the variables can be established, then an adequate amount of polymer can be deposited to create composites with the desired properties and compressive strength.

Pro Osteon 500R block/PLLA composites via CVDP: Pro Osteon 500R block samples were subjected to a variety of pre-reaction conditions as was described in the experimental section. This was done in an attempt to achieve three things: remove the residual organic material, maintain the original white/off-white color of the Pro Osteon samples, and to create a substrate that would initiate the CVDP of L-lactide to deposit desired quantities of polymer in a relatively short period of time. As before, the overall goal was to maintain the interconnected porosity of the Pro Osteon while improving the compressive strength. In addition to varying the pre-reaction conditions, I also varied the reaction temperatures in attempts to increase the rate of the CVDP. The influence of

various pre-reaction and reaction conditions on the color of the Pro Osteon 500R/PLLA samples can be seen in Figure 2.16. Samples D, R, and Y were dried at room temperature under vacuum. Samples D and R were reacted at 130 ^{o}C for 6 and 27 days respectively while sample Y was reacted at 160 ^{o}C for 6 days. A representative ^{1}H NMR of a Pro Osteon 500R block/PLLA composite prepared by CVDP is shown in Figure 2.17. Although room temperature drying under vacuum did not remove the organic material, the samples maintained their original coloration. Sample Y appeared slightly yellow due to the higher polymerization temperature. Overall, regardless of reaction temperature and length, little polymer was deposited when the Pro Osteon samples were dried at room temperature under vacuum. The average percent mass gain for these samples was 16 ± 15% (n = 16). The average M_p for the samples dried at room temperature under vacuum was 5,000 ± 3,000 Da. The remaining samples in Figure 2.16 were all heated to 500 ^{o}C. Sample W was heated for 640 hr, samples K and V for 16 hr in air, and sample H was heated for 16 hr under a flow of $O_{2(g)}$. The samples heated in air gradually turned grey in color, and the sample heated under a flow of $O_{2(g)}$ turned dark grey/brown. In addition to being heated at 500 ^{o}C, sample K was bleached in a 5.25% by weight solution of sodium hypochlorite in an attempt to remove the residual pyrolyzed organic material. This sample appears to be whiter than the others heated to 500 ^{o}C. The percent mass loss appears to support the contention that additional material was removed through the bleaching process. Samples heated in air or oxygen lost an average of 2.6 ± 0.1% (n = 4) of their mass while samples bleached after heating lost an average of 4.5 ± 1.0% (n = 2). An additional set of samples was heated at 500 ^{o}C under vacuum and these samples lost 6.1 ± 0.2% (n = 2) of their mass. Samples K and V were reacted with L-

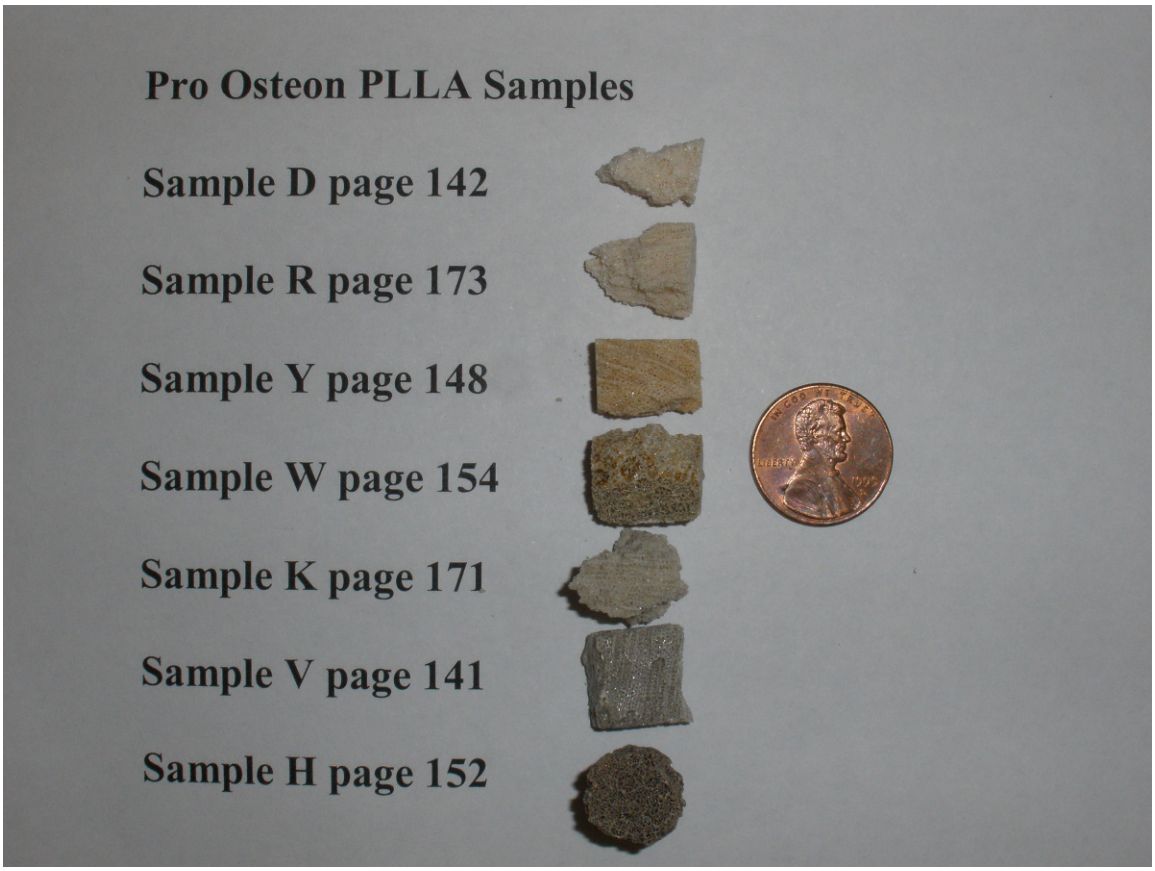

Figure 2.16. Influence of pre-reaction and reaction conditions on the color of the Pro Osteon 500R/PLLA composites. The page numbers refer to the page in my laboratory notebook on which the experimental data is recorded.

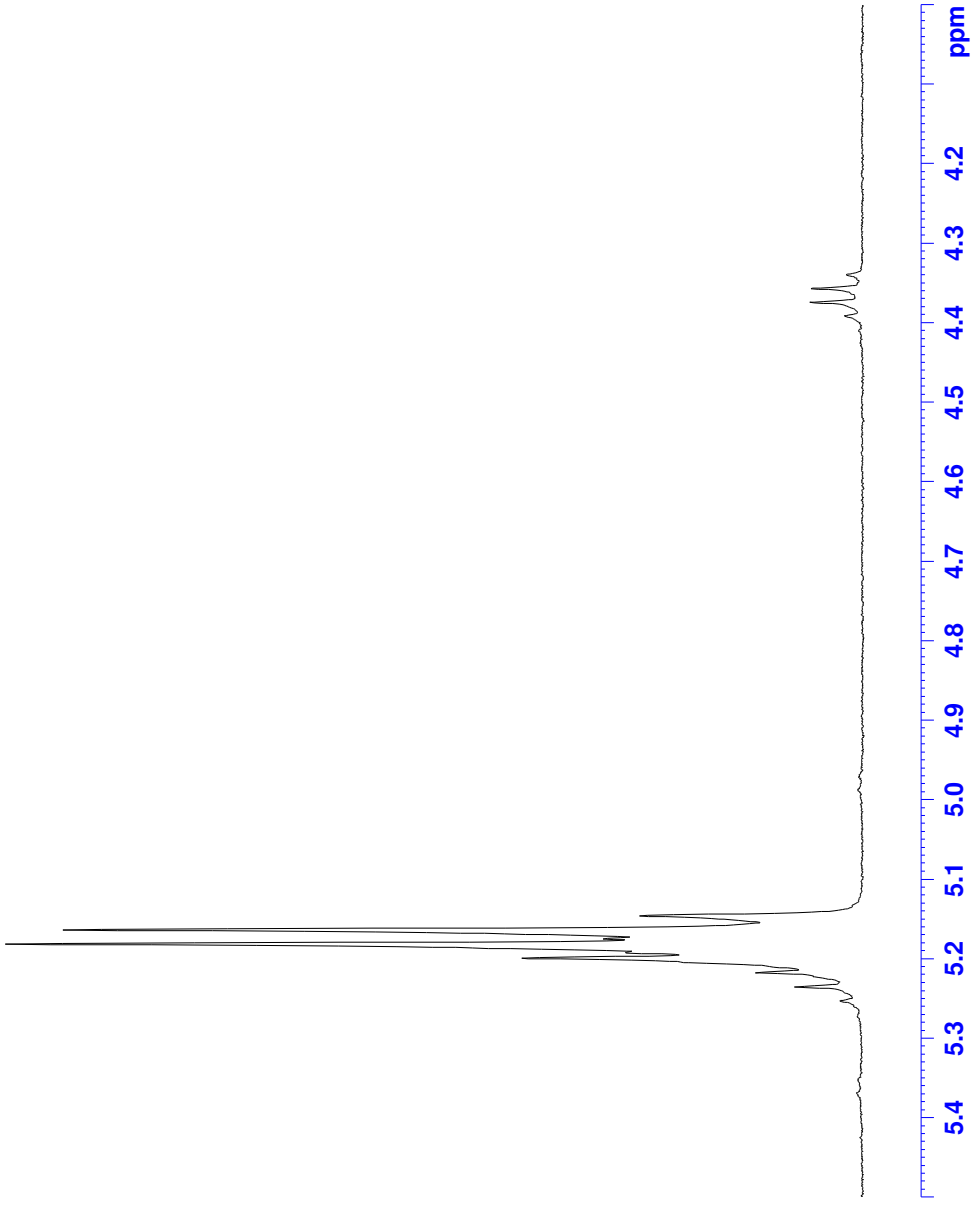

Figure 2.17. Representative ^{1}H NMR spectrum of a Pro Osteon 500R block/PLLA composite.

lactide for 6 days at 130 ^{o}C and samples W and H were reacted with L-lactide for 4 days at 160 ^{o}C. This increased polymerization temperature again resulted in yellowing of the PLLA. The percent mass gain due to PLLA for all samples that were pretreated at 500 ^{o}C was 53.1 ± 9.1% (n = 8). Polymerizations at 160 ^{o}C resulted in similar amounts of polymer in 4 days (49.9 ± 9.1%, n = 5) as did reactions done at 130 ^{o}C over 6 days, 58.4 ± 10.6% (n = 3). The average M_p of PLLA for samples pretreated at 500 ^{o}C was 6,000 ± 8,000 Da. It appears that room temperature drying is advantageous for keeping the original color of the samples, but the subsequent CVDP proceeds slowly. Although heating to 500 ^{o}C is desirable for removing the organic material and increasing the rate of the reaction, it leads to discoloration of the samples. Similarly, carrying out the CVDP at 160 ^{o}C increases the rate of the reaction, but PLLA turns yellow at this temperature.

For this set of reactions, I performed mechanical testing of the composites to determine the compressive strength and the elastic modulus. Examples of compressive stress-strain curves for several Pro Osteon/PLLA samples prepared via CVDP are shown in Figure 2.18. Strain is plotted on the x-axis and has units of percent. This is found by dividing the travel distance by the sample height and multiplying by 100. The y-axis is compressive stress with units of pressure because it is defined as the applied force divided by the cross-sectional area of the sample. Due to the high number of pre-reaction conditions and reaction temperatures, it was not possible to separate the samples into subsets based on these conditions when analyzing the data. So the samples were treated as a single data set. This data set was divided into two subsets depending on which face of the sample the cylindrical pores terminated. All mechanical testing was performed by aligning the 13 x 17 mm faces parallel to the load cell such that the mechanical properties

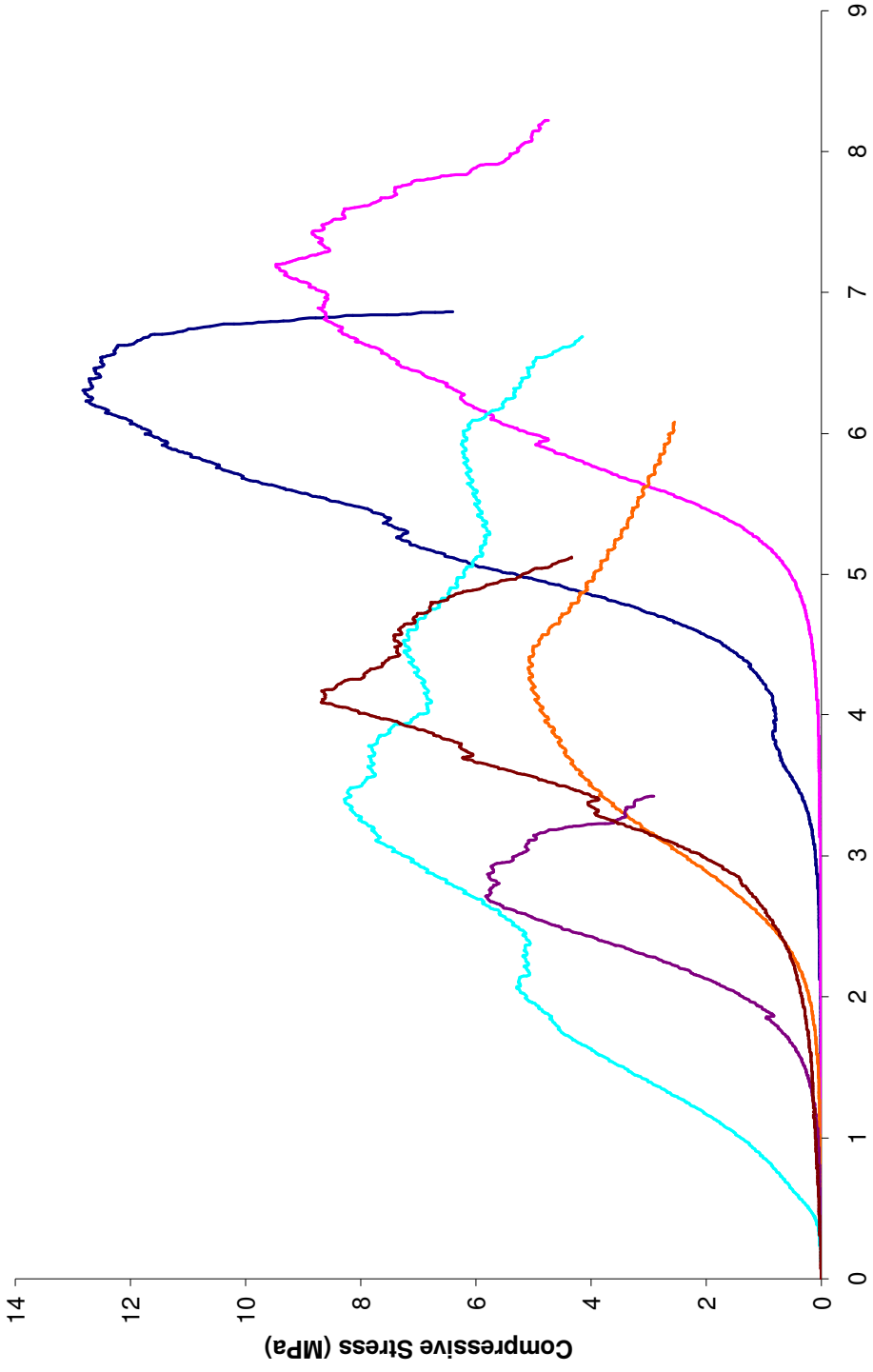

Figure 2.18. Compressive stress-strain curves for Pro Osteon/PLLA composites prepared via CVDP.

were measured along the axis between these faces. Samples containing pores terminating on a face parallel to the load cell (13 x 17 mm) were in one subset and samples with pores terminating on a face orthogonal to the load cell (14 x 17 mm and 13 x 14 mm faces) were in the second subset. These categories were necessary to account for the anisotropic nature of coral[83] and the fact not all samples were cut the same. Upon examination of the data, I saw that there is a strong correlation between the percent of the void volume filled by deposited polymer and the compressive strength (Figure 2.19). The method for calculating the percent void volume filled is shown above in equations 2.3 to 2.8. As can be seen in Figure 2.19, as the percent of the original void volume filled by polymer increases, the compressive strength of the composite also increases. Extrapolating these results to zero (an uncoated sample), the compressive strength is 3.5-4 MPa. This value is within the range of reported values for uncoated Pro Osteon 500R samples.[82] Furthermore, compressive strengths were generally higher for samples in which the cylindrical pores terminated on the face parallel to the load cell. From the best fit lines in Figure 2.19, the maximum compressive strength of the Pro Osteon 500R/PLLA composites would be 24 or 36 MPa if the pores were completely filled with PLLA. Because maintaining the interconnected porosity of the sample is also desirable, filling the macroscopic pores completely is not desirable. Filling the void volume 60 to 70 % produces a composite with a compressive strength of 20 to 25 MPa without closing the pores completely. The optimum balance between the two properties is unknown at this time and will depend greatly on the function and the location in which the composite would be used.

TB/PLLA, TB/PCLM, TB/PG, TB/PCLN composites via CVDP: Until this point

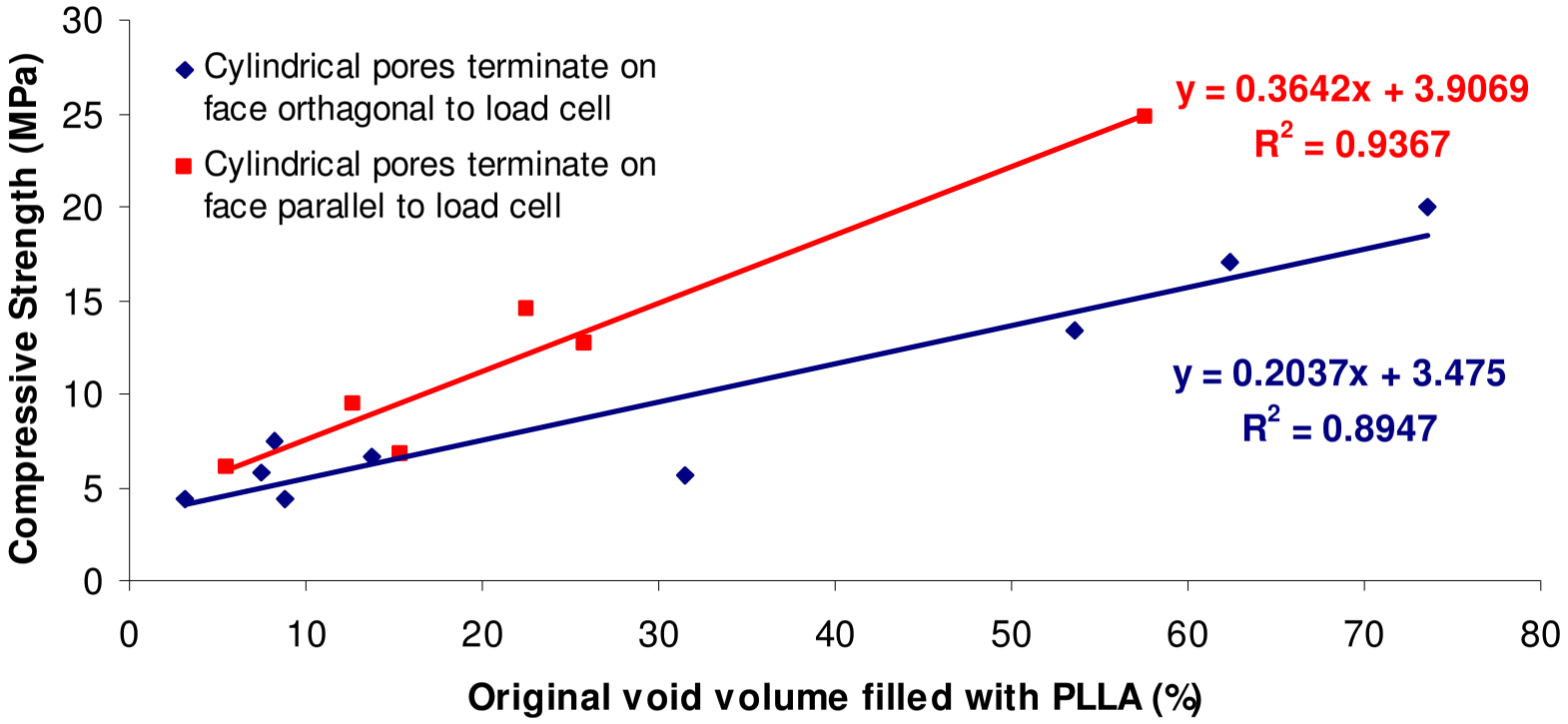

Figure 2.19. The effect of filling the void volume of Pro Osteon 500R scaffolds with PLLA via CVDP on the compressive strength of Pro Osteon 500R/PLLA composites.

in this thesis the focus has been on using porous scaffolds of marine sources that mimic the structure of trabecular bone (TB) to initiate the CVDP of L-lactide. One downside to this approach is that additional steps are often required to convert the scaffold from $CaCO_3$ to HA. During the conversion process $CaCO_3$ is converted to a CaO intermediate that is quantifiable. An alternative to using a material that mimics the structure of human trabecular bone is to use a xenograft derived from the trabecular bone of another species to initiate the polymerization of L-lactide. To this end, described below are my efforts to deproteinize and strengthen bovine trabecular bone.

Bovine trabecular bone was harvested as described in the experimental section and thermally pretreated at 600 ^{o}C in air for 24, 49, or 66.5 hr before being used to initiate the polymerization of L-lactide via CVDP. The polymerizations were performed at 130 ^{o}C for 3 or 5 days. A second set of bovine trabecular bone samples were heated at 700 ^{o}C in air for 16 hr. The CVDP of L-lactide was performed at 130 ^{o}C for 1 or 2 days using these samples. A representative ^{1}H NMR of a TB/PLLA composite is shown in Figure 2.20. Integration of the peak areas corresponding to the internal methine protons of the polymer (5.17 ppm) and the methine protons of the monomer (5.03 ppm) reveal this sample is greater than 99% polymer. SEM images of an uncoated TB sample and a TB/PLLA composite prepared via CVDP in Figure 2.21 confirm the presence of a thin even polymer layer coating the surface of the TB. Also of note, just like the coral and Pro Osteon samples, the interconnected pores are maintained after the CVDP. Table 2.4 shows the percent mass loss of the TB samples heated to 600 ^{o}C or 700 ^{o}C, the percent mass gain of the TB samples after the CVDP of L-lactide and the M_p of the resulting PLLA coating. The percent mass loss was the same for samples heated at 600 and 700

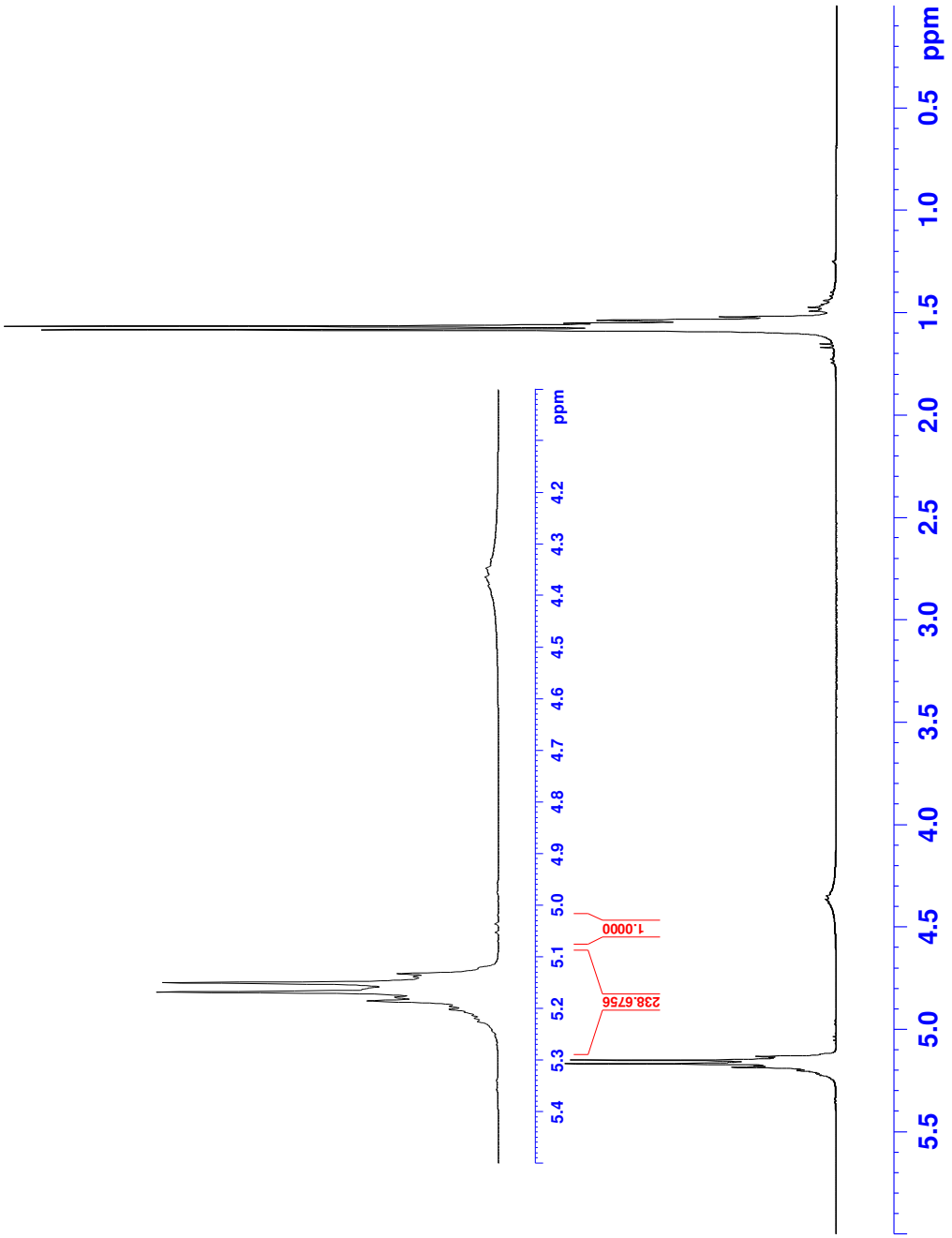

Figure 2.20. Representative ^{1}H NMR spectrum of a TB/PLLA composite prepared via CVDP.

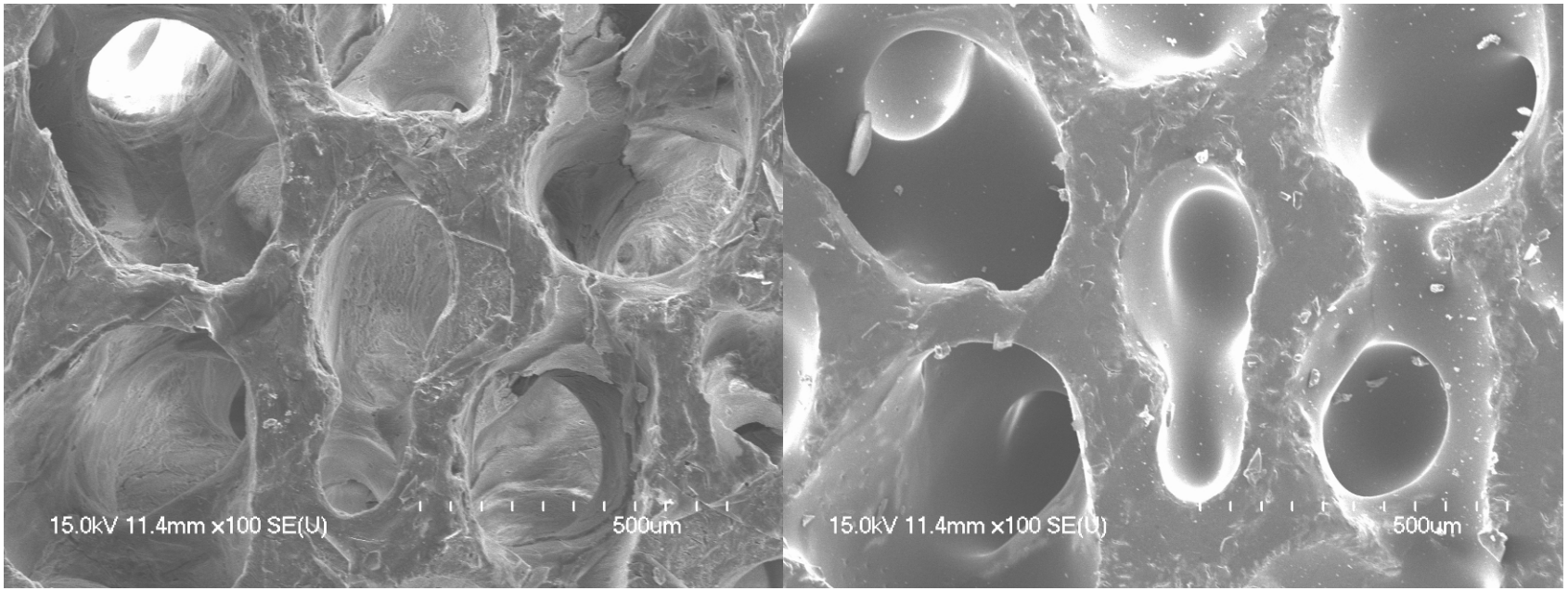

Figure 2.21. Scanning electron microscopy images of (left) uncoated bovine trabecular bone and (right) a trabecular bone/PLLA composite prepared via CVDP.

Temperature (°C)	Time heated at 600 or 700 °C (hr)	CVDP length at 130 °C (days)	TB mass loss (%)	PLLA mass gain (%)	Peak molecular weight (Da)
600	24	3	11.2 ± 2.8 (n = 4)	131 ± 74	14000 ± 7000
600	49	3	11.7 ± 4.7 (n = 4)	117 ± 45	7000 ± 5000
600	66.5	3	10.2 ± 3.2 (n = 4)	127 ± 35 (n = 8)	13000 ± 5000
600	66.5	5	8.5 ± 1.4 (n = 4)	102 ± 18 (n = 10)	14000 ± 5000
700	16	1	10.5 ± 1.0 (n = 9)	135 ± 75	
700	16	2	11.3 ± 0.6 (n = 10)	198 ± 33	11000 ± 5000

Table 2.4. TB/PLLA composite properties prepared by CVDP. The values listed for the mass loss, mass gain, and peak molecular weight are the averages with an uncertainty of one SD ($\bar{x}$ ± 1 SD).

^{o}C. It's unknown if longer heating times at 700 ^{o}C would produce additional mass loss. The percent polymer mass gained for the 600 ^{o}C samples was not significantly different based on either the heating time or the reaction time. CVDP reactions involving 700 ^{o}C samples produced percent polymer mass gains similar to the samples at 600 ^{o}C but in less time. Longer CVDP reactions involving the samples heated to 700 ^{o}C produced larger mass gains.

Besides L-lactide, HA has also been shown to initiate the ring opening polymerization of other cyclic lactones such as ε-caprolactone.[66, 67] If the nucleophilic surface of TB and other porous HA scaffolds can also be used to initiate the ring opening polymerization of L-lactide via CVDP then it seems logical that it could be used to initiate the polymerization of the other cyclic lactones as well via this method. Figure 2.22 shows a representative ^{1}H NMR spectrum of a TB/poly-ε-caprolactone (PCLN) composite prepared via CVDP. The TB was heated to 700 ^{o}C for 16 hr prior to the reaction, losing an average of 10.2 ± 0.9 % (n = 5) of its mass. CVDP was performed at 130 ^{o}C for 24 hr with an average percent mass gain of polymer of 101 ± 35 % (n = 5). A ^{1}H NMR spectrum was obtained in $CDCl_3$. Peak assignments were verified by comparison to those in the literature.[84-87] The ^{1}H NMR spectrum provides confirmation that the deposited mass is PCLN and not the monomer. The triplet at approximately 4.05 ppm is the methylene protons adjacent to the oxygen in the ester. The corresponding peak in the monomer, ε-caprolactone, would appear around 4.15 ppm if any monomer were present. When verifying the polymer/monomer composition of the composites the area of these peaks are integrated. A second triplet associated with the other methylene protons adjacent to the ester is at 2.3 ppm. The peak appearing at 3.65 ppm is due to the

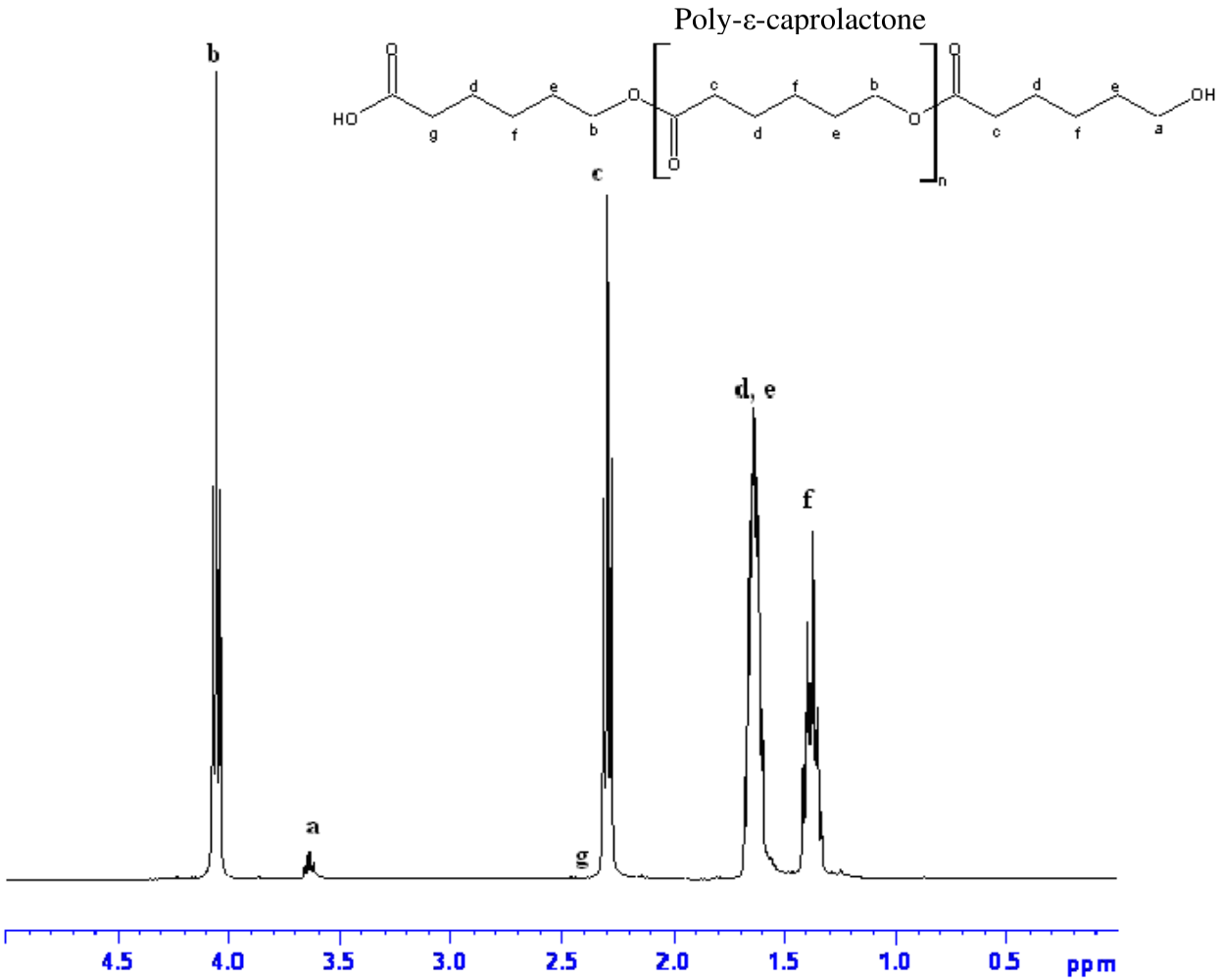

Figure 2.22. Representative ^{1}H NMR spectrum of a TB/PCLN composite prepared via CVDP.

protons on the carbon adjacent to the hydroxyl of the alcohol end group. The integrated peak intensity of this hydroxyl end group (g) relative to the internal CH_2 group next to the ester (c) can be used to estimate M_n, the number average molecular weight. Based on an integrated intensity of 1.000 for the end group (g), 84.7224 for the repeat unit (c), and a molecular weight of 114.14 g/mol for the repeat group, M_n is determined to be 5,000 Da for this sample.

TB is also capable of initiating the ROP of glycolide via CVDP. TB samples were heated at 675 ^oC for 19 hr in air losing an average of 9.2 ± 1.4 % of their mass. These samples were then used to initiate the CVDP of glycolide to polyglycolide (PG). The reaction was performed at 100 ^oC for varying lengths of time between 16 and 96 hr. Figure 2.23 shows a representative ^1H NMR spectrum of a TB/PG composite made via CVDP. The ^1H NMR spectrum was obtained in a solution of hexafluoroisopropanol (HFIP) and $CDCl_3$ in a 3 to 1 ratio (v/v). Peak assignments were confirmed with those in the literature.[88-93] The singlet at 4.89 ppm is due to the internal methylene protons of PG. The small singlet at 4.99 ppm is due to the methylene protons in glycolide. Integration of these peak areas provides information on the polymer/monomer composition of the sample. The sample shown in Figure 2.23 is 99.5% polymer. In Figure 2.24 the percent polymer mass gain is plotted versus reaction time for the CVDP of glycolide initiated by TB at 100 ^oC. Note that the percent polymer mass gain is proportional to time. The linear relationship between the reaction time and the percent mass gain indicates that the reaction is pseudo zero order. A more detailed explanation of why this and the other CVDP reactions are pseudo zero order is given in Chapter 3. From the slope of the best fit line, the rate of the CVDP of glycolide at 100 ^oC is 0.63 %/hr at 100 ^oC.

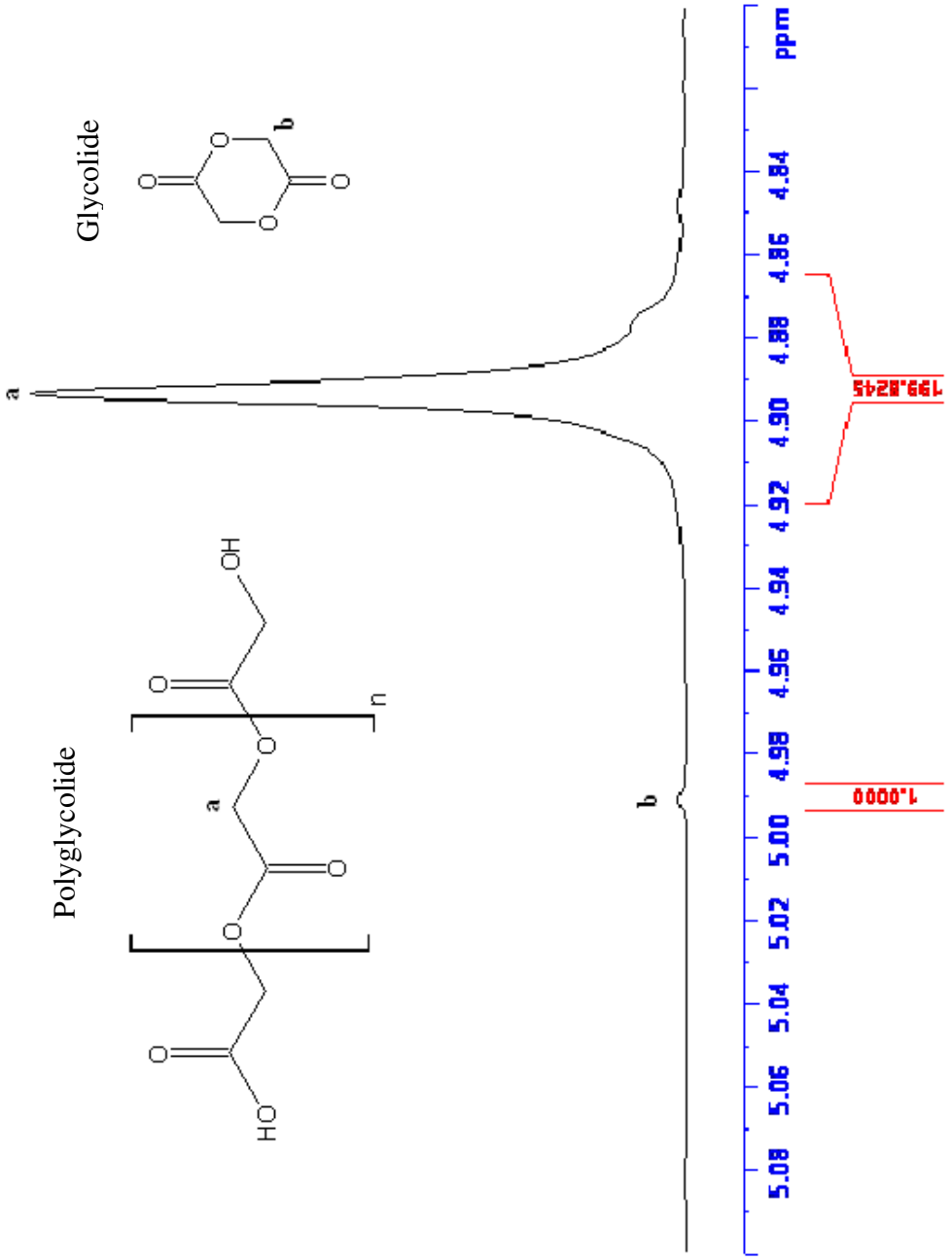

Figure 2.23. Representative ^{1}H NMR spectrum of a TB/PG composite prepared via CVDP.

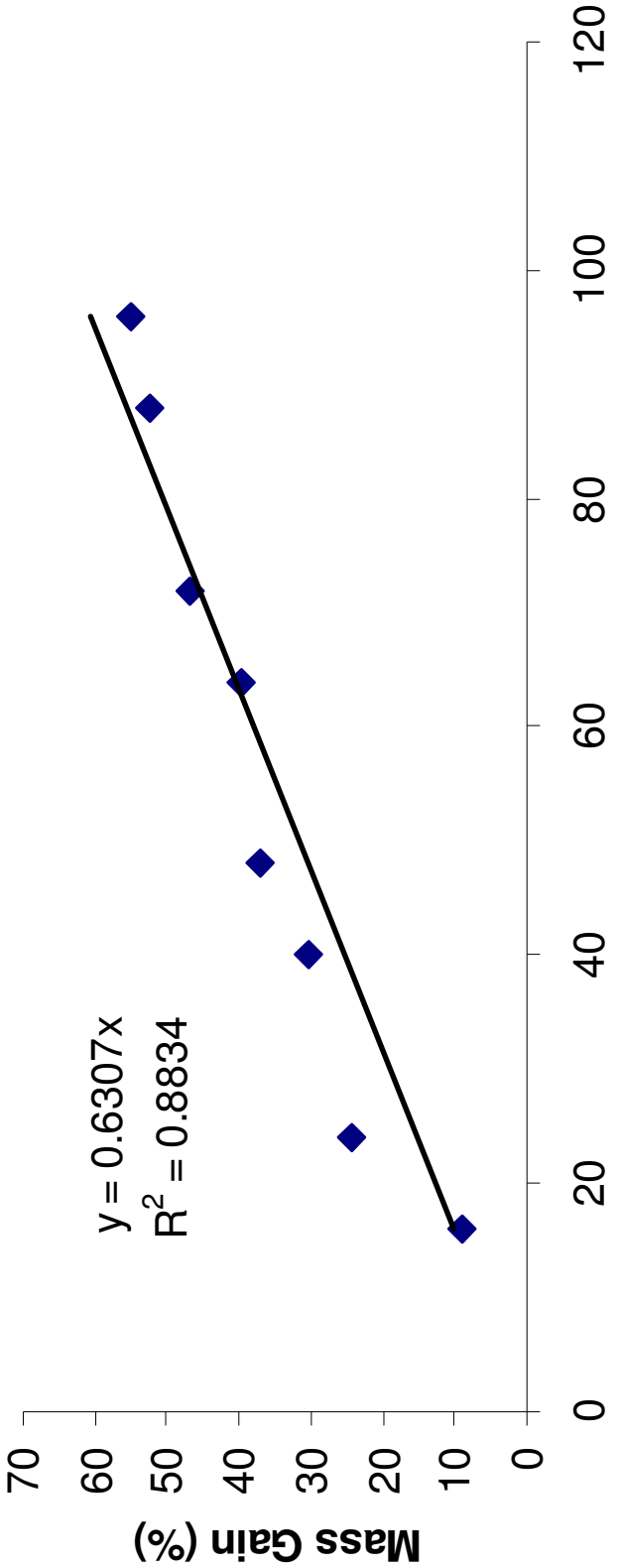

Figure 2.24. Percent of the original mass gained as the reaction time increases for the CVDP of glycolide initiated by TB at 100 °C.

Another polymer sometimes used in biodegradable medical devices is the polyamide, poly-ε-caprolactam. PCLM can be formed through the ROP of the cyclic lactam, ε-caprolactam. ε-Caprolactam has the same structure as ε-caprolactone, but with an amide functional group in place of the ester.[94] Due to this amide bond, PCLM is degraded similarly to natural polypeptides.[95] The polymers absorb 9-11% water by weight and degrades by ion-catalyzed surface and bulk hydrolysis. Hydrolysis by enzymatic catalysis can also lead to surface erosion.[96] Several attempts have been made to create composites of HA/PCLM by infusing a porous HA scaffold with ε-caprolactam and initiating the polymerization with various initiators. The ultimate goal of these studies has been to increase the mechanical strength of the HA scaffold.[97-100] But in all these cases, the surface of HA was not used to initiate the ROP of ε-caprolactam. Described below is the use of the surface of the TB to initiate the ROP of ε-caprolactam via CVDP. The ROP of ε-caprolactam initiated by the surface of anorganic bone to produce composites with a similar morphology to living bone will be discussed in Chapter 5. TB samples were heated to 675 ^{o}C for 19 hr in air and lost an average of 8.0 ± 0.6 % of their mass. These samples were then used to initiate the CVDP of ε-caprolactam. The polymerization reactions were carried out at 250 ^{o}C for varying lengths of time between 24 and 144 hr. ^{1}H NMR was used to confirm the CVDP. A representative spectrum can be seen in Figure 2.25. ^{1}H NMR spectra were obtained in a solvent mixture of trifluoroethanol (TFE) and $CDCl_3$ in a 3 to 1 ratio (v/v). Peak assignments were verified by comparison to those in the literature.[101, 102] The quartet at 3.14 ppm is due to the polymer internal methylene protons next to the nitrogen in the amide functional group. The quartet at 3.21 ppm is the monomer methylene protons next

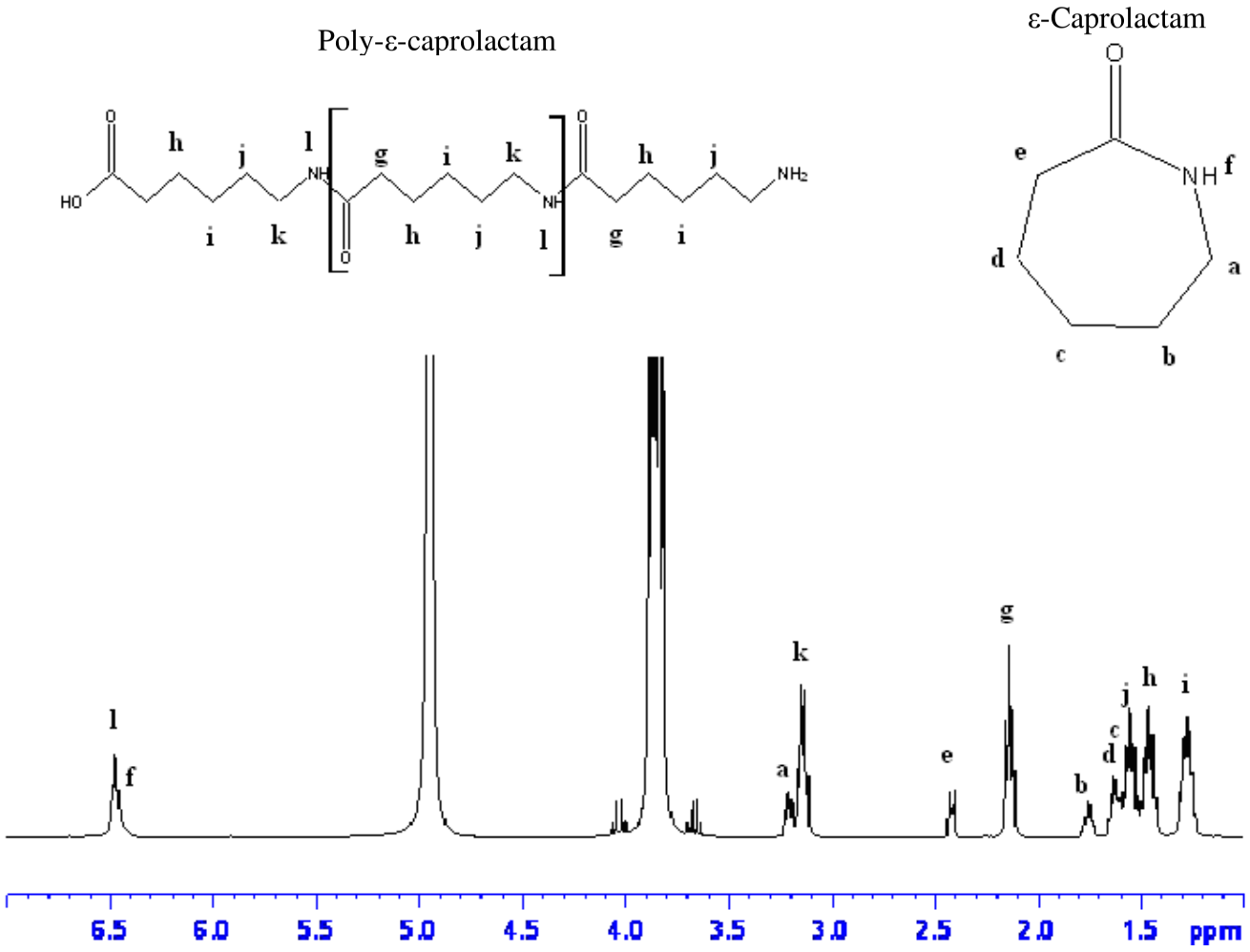

Figure 2.25. Representative ^{1}H NMR spectrum of a TB/PCLM composite prepared via CVDP.

to the nitrogen in the amide. The triplet at 2.14 ppm represents the polymer methylene protons adjacent to the other side of the amide and the triplet at 2.42 ppm is the monomer methylene protons in the same position. Integration of the area of these peaks provides the amount of polymer and monomer in the deposited material. This sample is approximately 82% polymer with the remainder being excess monomer. The series of multiplets between 1.2 and 1.8 ppm represent the remainder of the polymer internal protons and the remainder of the monomer protons not adjacent to the amide functional group. The proton attached to the nitrogen atom appears as a singlet around 6.49 ppm. The large peaks at 4.95 ppm and 3.85 ppm are due to the solvent, trifluoroethanol. For the series of CVDP reactions carried out for various lengths of time, the polymer percent mass gained is plotted versus the reaction time in Figure 2.26. As is the case for glycolide CVDP, the percent mass increase (relative to the original mass of the sample) is proportional to the reaction time indicating a pseudo zero order process. The intercept is once again set to zero because there is no polymer deposited on the TB at time t = 0 hr. The slope of the best fit line, 0.93 %/hr, is the rate of the CVDP of ε-caprolactam under these conditions.

Conclusion

In addition to initiating the ring opening polymerization of cyclic lactones and lactams from monomer melts, hydroxyapatite can be used to initiate the polymerization of these same monomers from the vapor phase. This process is particularly advantageous for coating porous scaffolds derived from biological sources, such as coral or trabecular bone, which are often used as bone grafting materials. The CVDP deposits a thin, even polymer layer on the entire of these materials while at the same time maintaining the

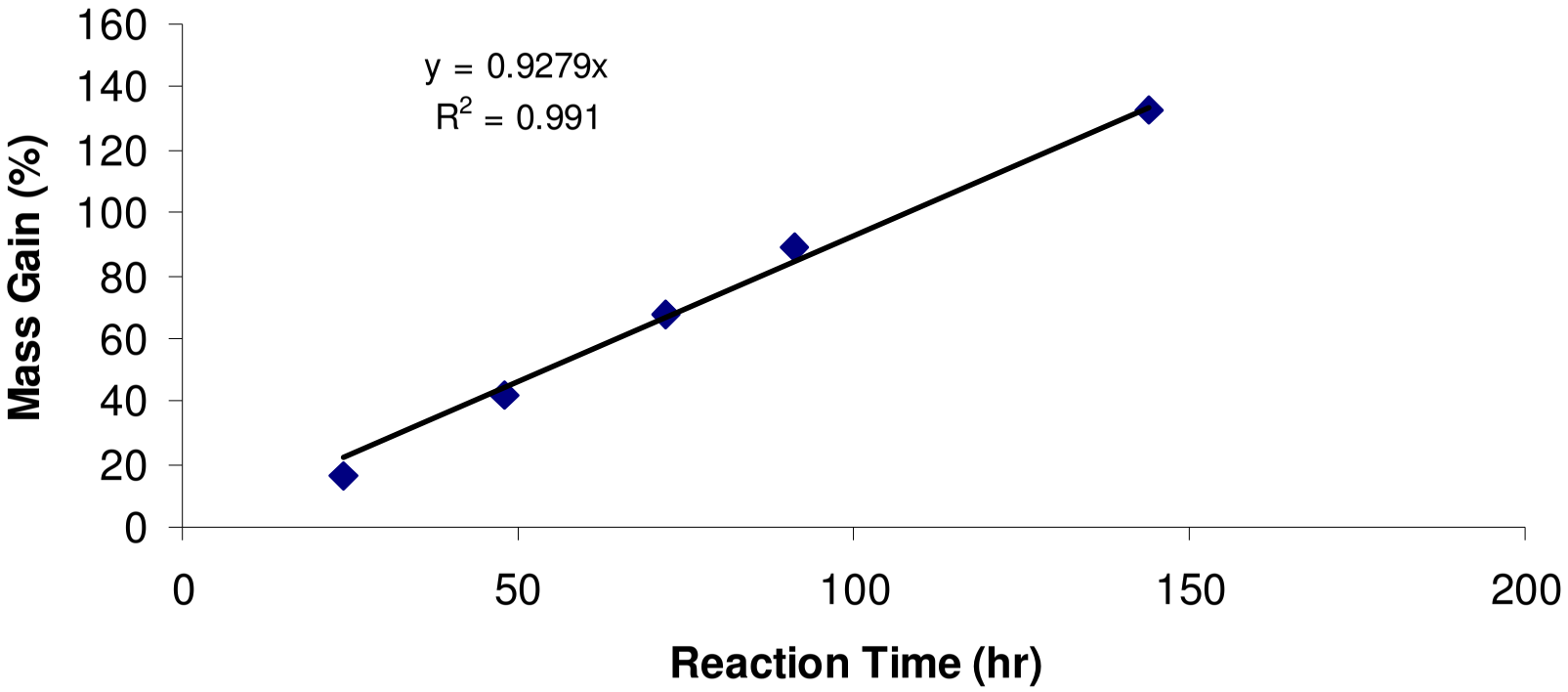

Figure 2.26. Percent polymer mass gained as the reaction time increases for the CVDP of ε-caprolactam initiated by TB at 250 °C.

interconnected porosity that is desired for osteoconductivity. The polymer layer improves the compressive strength of the brittle HA scaffold and this improvement is dependent on the extent to which the pores of the scaffold are filled. The more the pores are filled with polymer, the larger the compressive strength becomes. Because this diminishes the porosity of the sample, an optimum balance between the compressive strength and the porosity needs to be obtained to produce the best possible composite.

In addition to the biologically derived scaffolds mentioned in this chapter, future work could focus on the use of other materials of biological origin to initiate the polymerization of cyclic lactones. One such example is nacre. Although not porous like coral, nacre has layers of $CaCO_3$ plates with organic layers sandwiched in between holding them together. The remarkable mechanical properties of this material have intrigued scientists interested in synthetically duplicating the structure or using it as a bone graft material.[103-105] Figure 2.27 shows the result of an exploratory experiment conducted to investigate the plausibility of using a modified nacre sample to initiate the ROP of L-lactide. The SEM images on the top show the original structure of a cryofractured nacre bead used in jewelry. The images on the bottom show a second nacre sample in which the organic material was removed (using a Soxhlet extractor and a 80/20 v/v mixture of ethylenediamine and water) and then used to initiate the polymerization of L-lactide (the nacre bead was not converted to HA as the hydrothermal process destroys the microscopic structure, Figure 2.28). The original structure is maintained and there is a suggestion of the presence of PLLA cementing the ceramic layers together. ^{1}H NMR spectroscopy was used to confirm the presence of PLLA (Figure 2.29). A macroscopic example of how CVDP can be used to deposit polymers on irregularly shaped scaffolds is

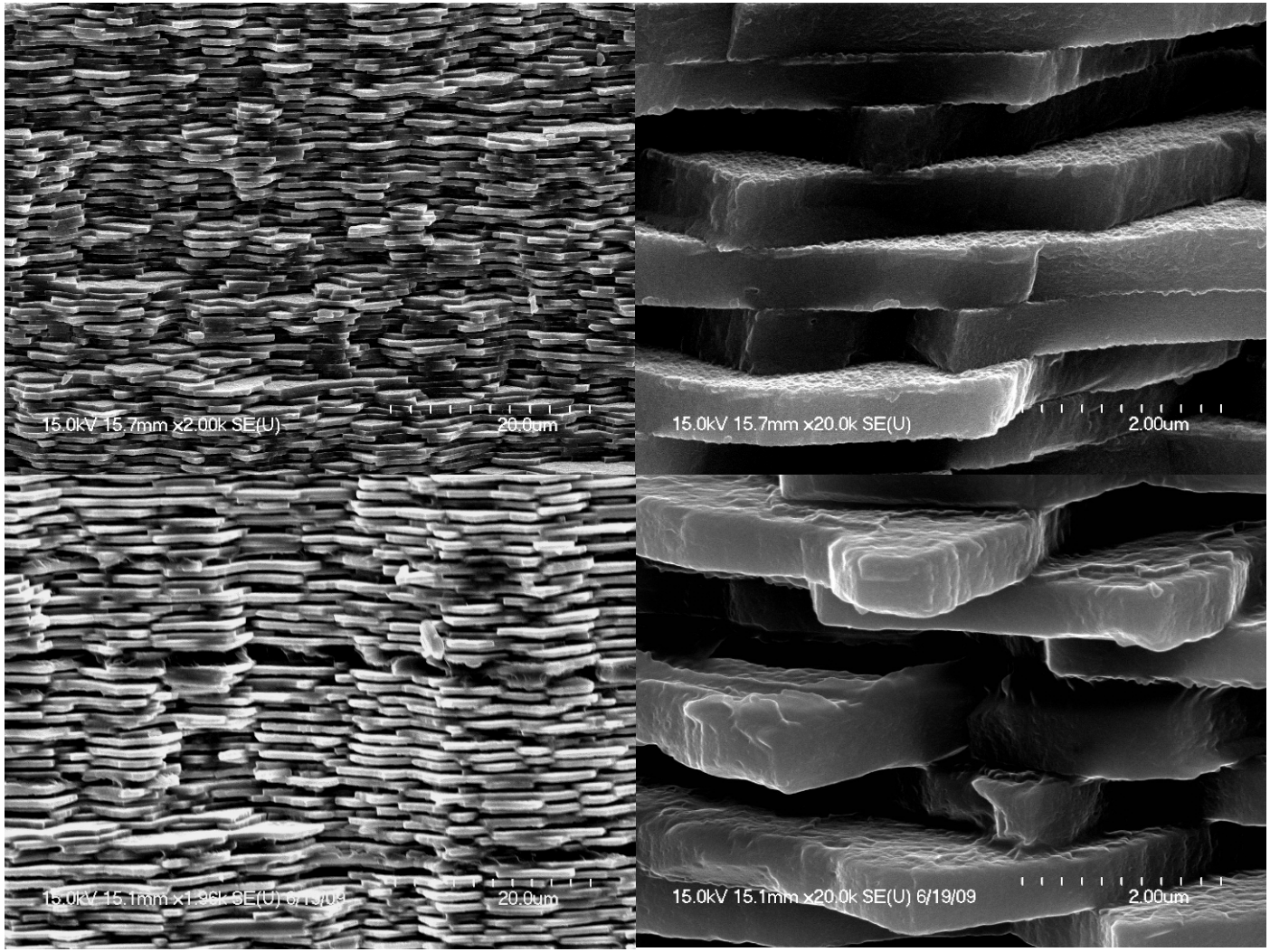

Figure 2.27. (Top) Scanning electron microscopy images of the original nacre structure and (bottom) the nacre structure after the organic material has been removed and the sample reconstituted with PLLA.

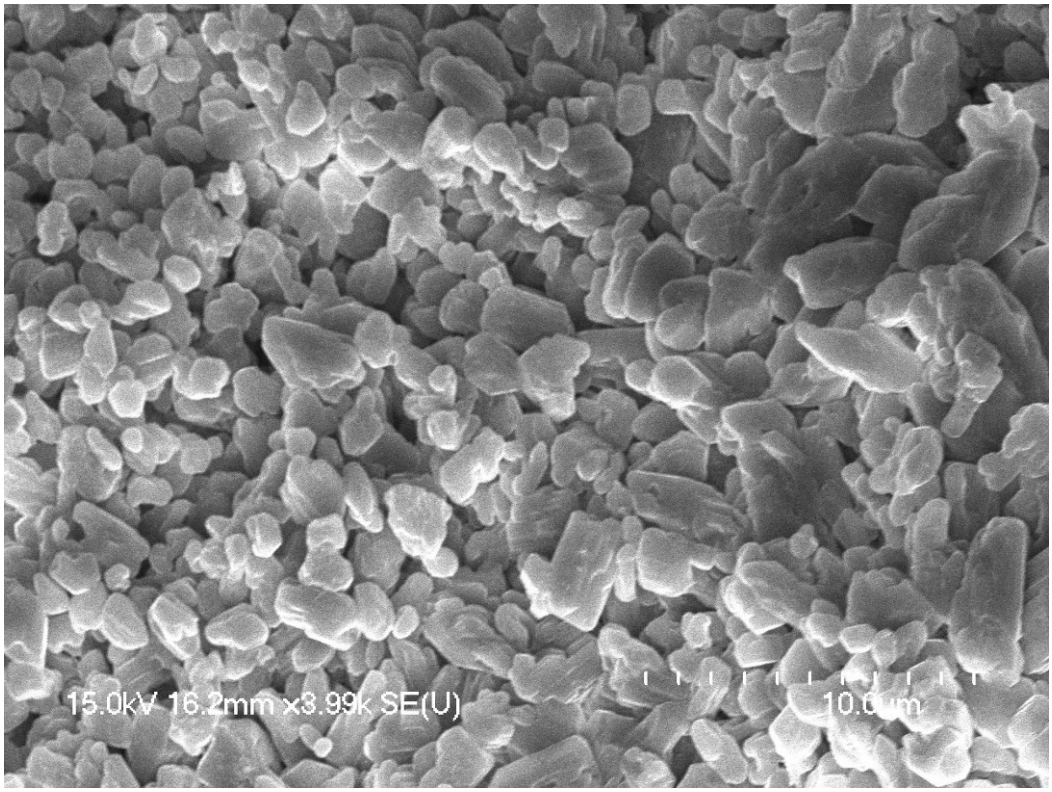

Figure 2.28. Scanning electron microscopy image of a nacre bead after it was partially converted to hydroxyapatite via the hydrothermal process. The conversion was performed at 200 ^{o}C for 5 days. In this case the microscopic structure of the nacre seen in Figure 2.27 is not conserved.

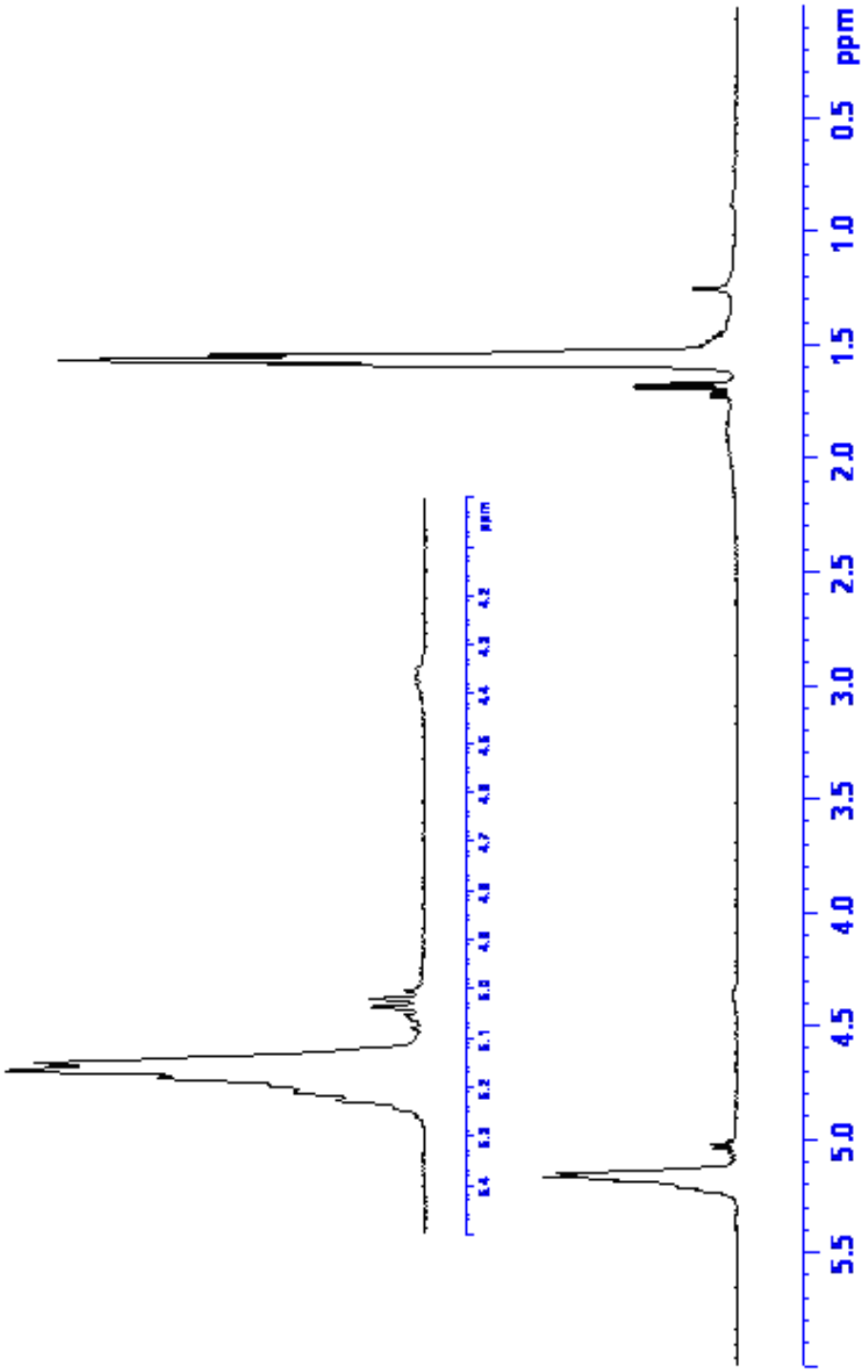

Figure 2.29. Representative ^{1}H NMR spectrum of a nacre/PLLA composite.

shown in Figure 2.30. The shell is from a young *Strombus urceus*, a gastropod from the Indo-west Pacific region. It was identified with the help of Dr. José H. Lead, director and curator at the Bailey-Matthews Shell Museum (Sanibel, FL). In the upper right and bottom images is the same shell after it has been hydrothermally converted to HA and reconstituted with PLLA by CVDP. In addition to the macroscopic structure being conserved through the hydrothermal and polymerization processes, SEM images of the cryofractured shell show that the microscopic structure of the shell is largely conserved (Figure 2.31).[106] XRD performed on the entire shell after the hydrothermal process shows that it was converted from aragonite $CaCO_3$ to HA (Figure 2.32). ^{1}H NMR spectroscopy was used to confirm the presence of PLLA (Figure 2.33). The integrated peak intensity of the methine proton from the hydroxyl end group at 4.36 ppm relative to the internal methine proton of the polymer at 5.17 ppm can be used to estimate M_n. Based on an integrated intensity of 0.1455 for the end group, 1.000 for the repeat unit, and a molecular weight of 144.06 g/mol for the repeat group, M_n is determined to be 1,100 Da for this sample. The overall structure is maintained and the color is similar to the original shell.

Finally, I would like to note that CVDP of cyclic lactones could potentially be used to fabricate hydrolyzable coatings for electronic devices.[107] A demonstration of this process is shown in Figure 2.34. A series of uncoated, patterned magnesium oxide (MgO) substrates on a silicon dioxide wafer are seen in the left SEM image. In the right image is the same substrate coated with a thin layer of PLLA via CVDP. The CVDP process enables the deposition of the polymer only on the surface that initiates the polymerization.

Figure 2.30. Images of (upper left) the shell of a young *Strombus urceus* in its original state and (upper right, bottom) the same shell after being converted to hydroxyapatite and reconstituted with PLLA via CVDP.

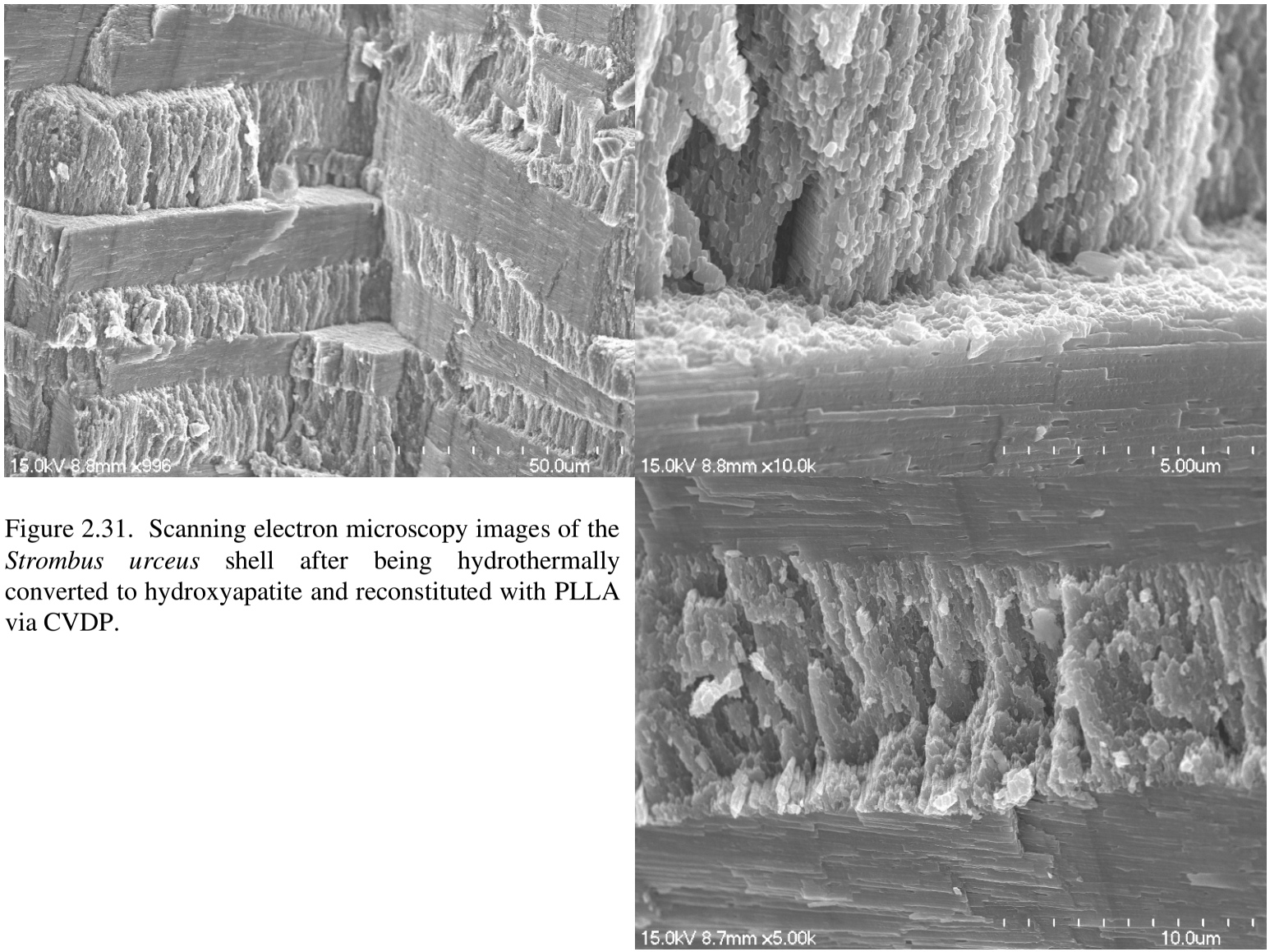

Figure 2.31. Scanning electron microscopy images of the *Strombus urceus* shell after being hydrothermally converted to hydroxyapatite and reconstituted with PLLA via CVDP.

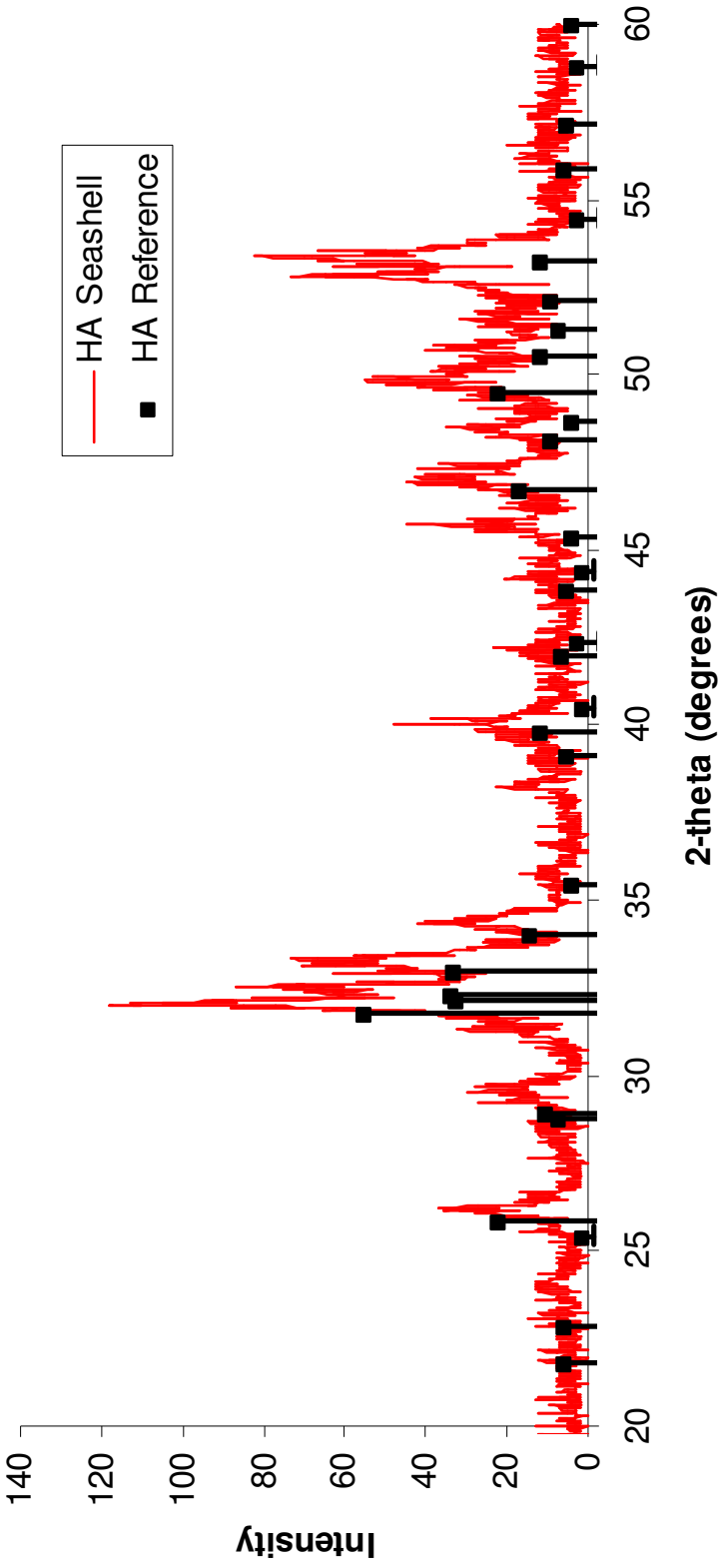

Figure 2.32. X-Ray powder diffraction pattern of the *Strombus urceus* shell after it is hydrothermally converted to HA.

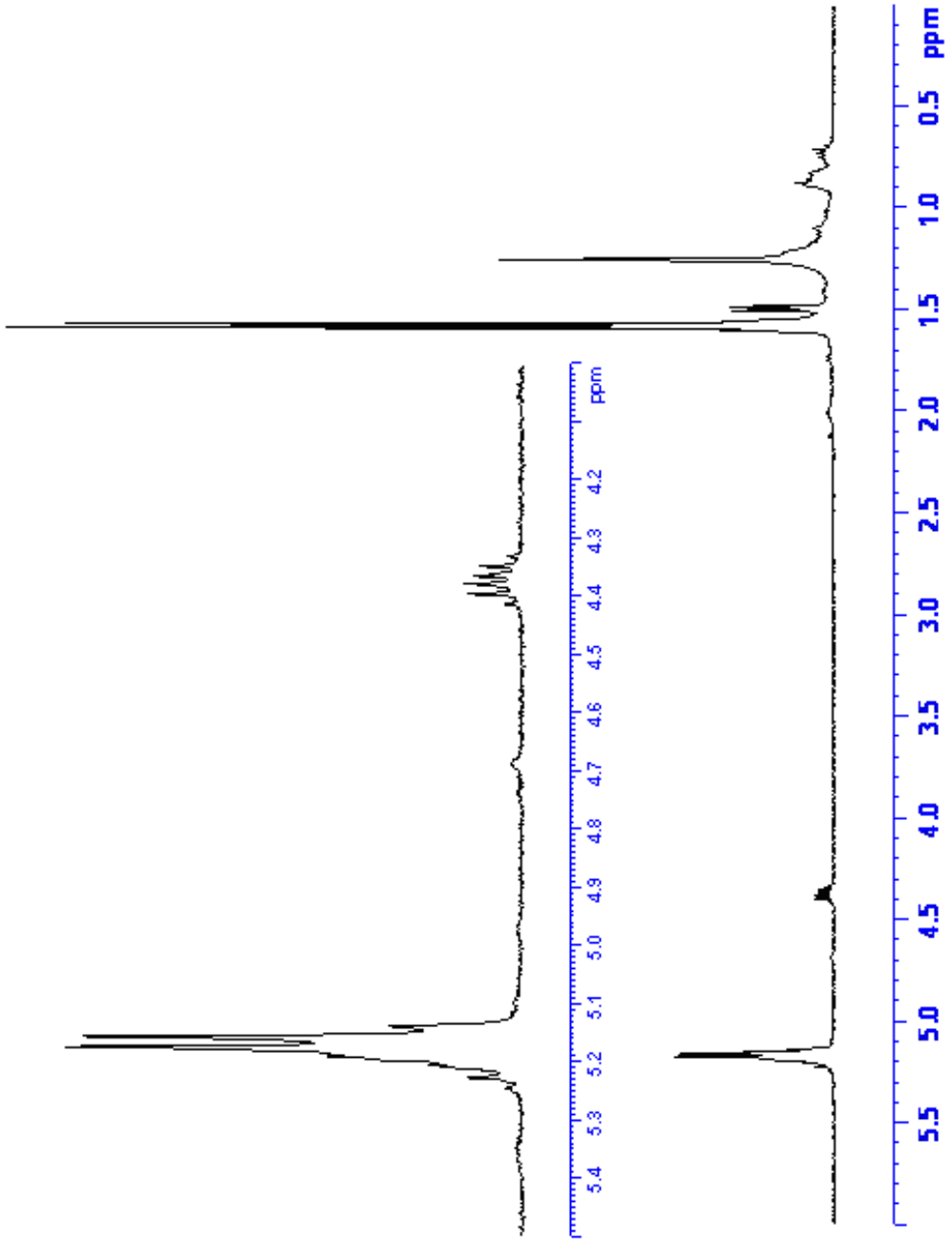

Figure 2.33. ^{1}H NMR spectrum of the *Strombus urceus* shell/PLLA composite.

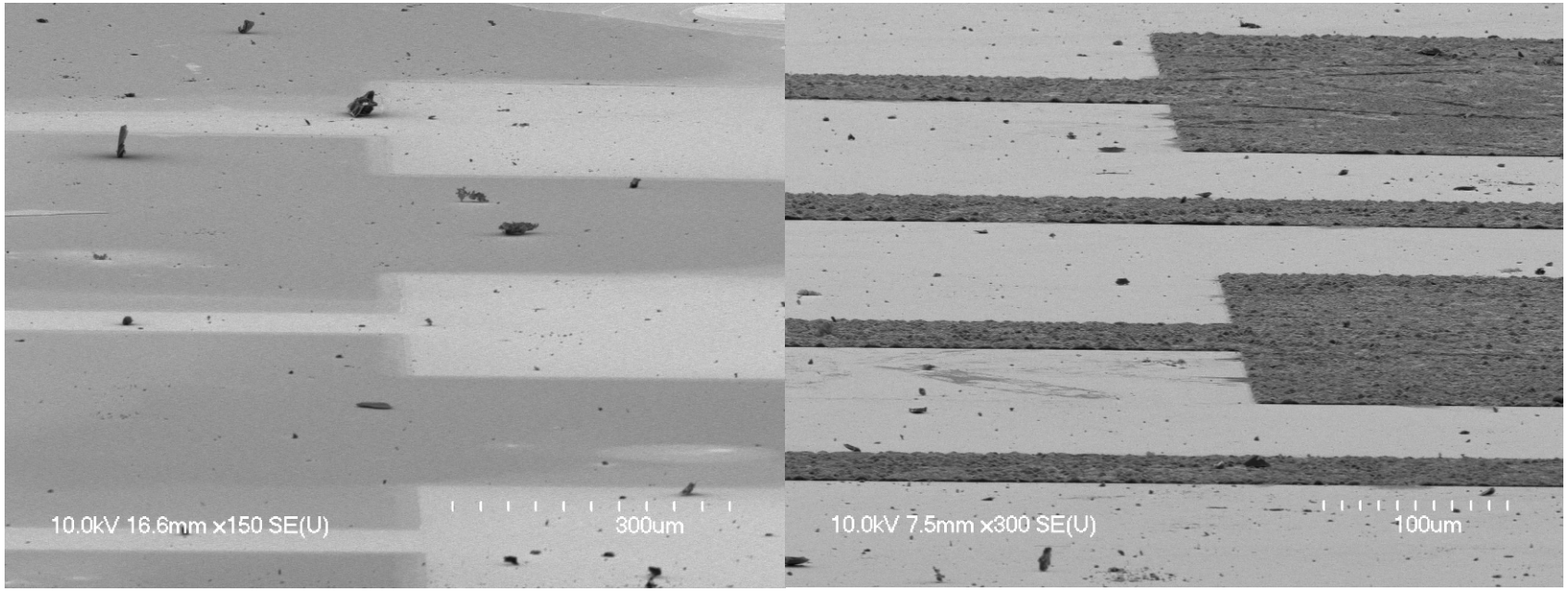

Figure 2.34. Scanning electron microscopy images of (left) patterned MgO substrates (light areas) on a silicon dioxide wafer and (right) patterned MgO substrates with a thin layer of PLLA via CVDP.

References

1. Sopyan, M.; Mel, M.; Ramesh, S.; Khalid, K.A., Porous hydroxyapatite for artificial bone applications. *Science and Technology of Advanced Materials* **2007**, 8, 116-123.

2. Karageorgiou, V.; Kaplan, D., Porosity of 3D scaffolds and osteogenesis. *Biomaterials* **2005**, 26, 5474-5491.

3. Tampieri, A.; Celotti, G.; Sprio, S.; Delcogliano, A.; Franzese, S., Porosity-graded hydroxyapatite ceramics to replace natural bone. *Biomaterials* **2001**, 22, 1365-1370.

4. Yokozeki, H.; Hayashi, T.; Nakagawa, T.; Kurosawa, H.; Shibuya, K.; Ioku, K., Influence of surface microstructure on the reaction of the active ceramics in vivo. *Journal of Materials Science: Materials in Medicine* **1998**, 9, 381-384.

5. Friess, W.; Warner, J., Biomedical applications. In *Handbook of Porous Solids*, Schuth, F.; Sing, K.S.W.; Weitkamp, J., eds.; Wiley-VCH: Weinheim, Germany, 2002.

6. Vikram, D.; Nather, A.; Khalid, K.A., Role of ceramics as bone graft substitutes. In *Bone Grafts and Bone Substitutes: Basic Science and Clinical Applications*, Nather, A., ed.; World Scientific: Hackensack, New Jersey, 2005.

7. Shirota, T.; Ohno, K.; Michi, K.I.; Tachikawa, T., An experimental study of healing around hydroxyapatite implants installed with autogenous iliac bone grafts for jaw reconstruction. *Journal of Oral and Maxillofacial Surgery* **1991**, 49, 1310–1315.

8. Benhayoune, H.; Jallot, E.; Laquerriere, P.; Balossier, G.; Bonhomme, P.; Frayssinet, P., Integration of dense HA rods into cortical bone. *Biomaterials* **2000**, 21, 235–242.

9. Shirota, T.; Kohsuke, O.; Kanako, S.; Ken-ichi, M., The effect of aging on the healing of hydroxyapatite implants. *Journal of Oral and Maxillofacial Surgery* **1993**, 51, 51–56.

10. Takeshita, F.; Iyama, S.; Ayukawa, Y.; Akedo, H.; Suetsugu, T., Study of bone formation around dense hydroxyapatite implants using light microscopy, image processing and confocal laser scanning microscopy. *Biomaterials* **1997**, 18, 317–322.

11. Andrade, J.C.T.; Camilli, J.A.; Kawachi, E.Y.; Bertran, C.A., Behavior of dense and porous hydroxyapatite implants and tissue response in rat femoral defects. *Journal of Biomedical Materials Research* **2002**, 62, 30-36.

12. Kuboki, Y.; Takita, H.; Kobayashi, D.; Tsuruga, E.; Inoue, M.; Murata, M.; Nagai, N.; Dohi, Y.; Ohgushi, H., BMP-induced osteogenesis on the surface of

hydroxyapatite with geometrically feasible and nonfeasible structures: Topology of osteogenesis. *Journal of Biomedical Materials Research* **1998**, 39, 190-199.

13. Story, B.J.; Wagner, W.R.; Gaisser, D.M.; Cook, S.D.; Rust-Dawicki, A.M., In vivo performance of a modified CSTi dental implant coating. *International Journal of Oral and Maxillofacial Implants* **1998**, 13, 749-757.

14. Hulbert, S.F.; Young, F.A.; Mathews, R.S.; Klawitter, J.J.; Talbert, C.D.; Stelling, F.H., Potential of ceramic materials as permanently implantable skeletal prostheses. *Journal of Biomedical Materials Research* **1970**, 4, 433-456.

15. Klawitter, J.J.; Hulbert, S.F., Application of porous ceramics for the attachment of load bearing internal orthopedic applications. *Journal of Biomedical Materials Research* **1971**, 5, 161-229.

16. Daculsi, G.; Passuti, N., Effect of the macroporosity for osseous substitution of calcium phosphate ceramics. *Biomaterials* **1990**, 11, 86-87.

17. Feng, B.; Jinkang, Z.; Zhen, W.; Jianxi, L.; Jiang, C.; Jian, L.; Guolin, M.; Xin, D., The effect of pore size on the tissue ingrowth and neovascularization in porous bioceramics of controlled architecture in vivo. *Biomedical Materials* **2011**, 6, 015007.

18. Simske, S.J.; Ayers, R.A.; Bateman, T.A., Porous materials for bone engineering. *Materials Science Forum* **1997**, 250, 151-182.

19. Hing, K.A.; Best, S.M.; Bonfield, W., Characterization of porous hydroxyapatite. *Journal of Materials Science: Materials in Medicine* **1999**, 10, 135-145.

20. Kühne, J.-H.; Bartl, R.; Frisch, B.; Hammer, C., Bone formation in coralline hydroxyapatite *Acta Orthopaedica Scandinavica* **1994**, 65, 246-252.

21. Eggli, P.S.; Müller, W.; Schenk, R.K., Porous hydroxyapatite and tricalcium phosphate cylinders with two different pore size ranges implanted in the cancellous bone of rabbits. A comparative histomorphometric and histologic study of bony ingrowth and implant substitution. *Clinical Orthopaedics and Related Research* **1988**, 232, 127-138.

22. Holmes, R.; Mooney, V.; Bucholz, R.; Tencer, A., A coralline hydroxyapatite bone graft substitute. *Clinical Orthopaedics and Related Research* **1984**, 188, 252-262.

23. Holmes, R.E.; Bucholz, R.W.; Mooney, V., Porous hydroxyapatite as a bone-graft substitute in metaphyseal defects. A histometric study. *Journal of Bone and Joint Surgery* **1986**, 68, 904-911.

24. Lu, J.; Flautre, B.; Anselme, K., Role of interconnections in porous bioceramics on bone re-colonization in-vitro and in-vivo. *Journal of Materials Science: Materials in Medicine* **1999,** 10, 111-120.

25. Flautre, B.; Descamps, M.; Delecourt, M., Porous HA ceramic for bone replacement: Role of the pore and interconnections: Experimental study in the rabbit. *Journal of Materials Science: Materials in Medicine* **2001,** 12, 679-682.

26. Chang, B.S.; Lee, C.K.; Youn, H.J., Osteoconduction at porous hydroxyapatite with various pore configurations. *Biomaterials* **2000,** 21, 1291-1298.

27. Hollister, S.J.; Maddox, R.D.; Taboas, J.M., Optimal design and fabrication of scaffolds to mimic tissue properties and satisfy biological constraints. *Biomaterials* **2002,** 23, 4095-4103.

28. Lecomte, A.; Gautier, H.; Bouler, J.M.; Gouvette, A.; Pegon, Y.; Daculsi, G.; Merle, C., Biphasic calcium phosphate: A comparative study of interconnected porosity in two ceramics. *Journal of Biomedical Materials Research Part B: Applied Biomaterials* **2008**, 84B, 1-6.

29. Blokhuis, T.J.; Termaat, M.F.; den Boer, F.C.; Patka, P., Properties of calcium phosphate ceramics in relation to their in vivo behavior. *Journal of Trauma: Injury, Infection, and Critical Care* **2000**, 48, 179-186.

30. Yuan, H.; Kurashina, K.; de Bruijn, J.D.; Li, Y.; de Groot, K.; Zhang, X., A preliminary study on osteoinduction of two kinds of calcium phosphate ceramics. *Biomaterials* **1999**, 20, 1799-1806.

31. Richart, O.; Descamps, M.; Liebetrau, A., Preparation and mechanical characterization of hydroxyapatite monodispersed macroporous structure. Influence of interconnection and macropores diameters. *Key Engineering Materials* **2002**, 218-220, 9-12.

32. Le Huec, J.C.; Schaeverbeke, T.; Clement, D.; Faber, J.; Le Rebeller, A., Influence of porosity on the mechanical resistance of hydroxyapatite ceramics under compressive stress. *Biomaterials* **1995,** 16, 113-118.

33. Liu, D.-M., Influence of porosity and pore size on the compressive strength of porous hydroxyapatite ceramic. *Ceramics International* **1997**, 23, 135-139.

34. Aoki, S.; Yamaguchi, S.; Nakahira, A.; Suganuma, K., Preparation of porous calcium phosphates using a ceramic foaming technique combined with a hydrothermal treatment and the cell response with incorporation of osteoblast-like cells. *Journal of the Ceramic Society of Japan* **2004**, 112, 193-199.

35. Wilson, C.E.; de Bruijn, J.D.; van Blitterswijk, C.A.; Verbout, A.J.; Dhert, W.J.A., Design and fabrication of standardized hydroxyapatite scaffolds with a defined macro-architecture by rapid prototyping for bone-tissue-engineering research. *Journal of Biomedical Materials Research Part A* **2003**, 68A, 123-132.

36. Tadic, D.; Beckmann, F.; Schwarz, K.; Epple, M., A novel method to produce hydroxyapatite objects with interconnecting porosity that avoids sintering. *Biomaterials* **2004**, 25, 3335-3340.

37. Tamai, N.; Myoui, A.; Tomita, T.; Nakase, T.; Tanaka, J.; Ochi, T.; Yoshikawa, H., Novel hydroxyapatite ceramics with an interconnective porous structure exhibit superior osteoconduction in vivo. *Journal of Biomedical Materials Research* **2002**, 59, 110-117.

38. Sepulveda, P.; Binner, J.G.; Rogero, S.O.; Higa, O.Z.; Bressiani, J.C., Production of porous hydroxyapatite by the gel-casting of foams and cytotoxic evaluation. *Journal of Biomedical Materials Research* **2000**, 50, 27-34.

39. Rejda, B.V.; Peelen, J.G.; de Groot, K., Tri-calcium phosphate as a bone substitute. *Journal of Bioengineering* **1977**, 1, 93-97.

40. Li, S.H.; De Wijn, J.R.; Layrolle, P.; De Groot, K., Synthesis of macroporous hydroxyapatite scaffolds for bone tissue engineering. *Journal of Biomedical Materials Research* **2002**, 61, 109-120.

41. Tian, J.; Tian, J., Preparation of porous hydroxyapatite. *Journal of Materials Science* **2001**, 36, 3061-3066.

42. Woyansky, J.S.; Scott, C.E.; Minnear, W.P., Processing of porous ceramics. *American Ceramic Society Bulletin* **1992**, 71, 1674-1682.

43. Ben-Nissan, B., Natural bioceramics: From coral to bone and beyond. *Current Opinion in Solid State and Materials Science* **2003**, 7, 283-288.

44. Roy, D.M.; Linnehan, S.K., Hydroxyapatite formed from coral skeletal carbonate by hydrothermal exchange. *Nature* **1974**, 247, 220-222.

45. Shors, E.C., Coralline bone graft substitutes. *Orthopedic Clinics of North America* **1999**, 30, 599-613.

46. Chiroff, R.T.; White, E.W.; Weber, K.N.; Roy, D.M., Tissue ingrowth of replamineform implants. *Journal of Biomedical Materials Research* **1975**, 9, 29-45.

47. Damien, E.; Revell, P.A., Coralline hydroxyapatite bone graft substitute: A review of experimental studies and biomedical applications. *Journal of Applied Biomaterials and Biomechanics* **2004**, 2, 65-73.

48. Holmes, R.E., Bone regeneration within a coralline hydroxyapatite implant. *Plastic and Reconstructive Surgery* **1979**, 63, 626-633.

49. Bucholz, R.W., Nonallograft osteoconductive bone graft substitutes. *Clinical Orthopaedics and Related Research* **2002**, 395, 44-52.

50. Hu, J.; Russell, J.J.; Ben-Nissan, B., Production and analysis of hydroxyapatite from Australian corals via hydrothermal process. *Journal of Materials Science Letters* **2001**, 20, 85-87.

51. Rocha, J.H.G.; Lemos, A.F.; Kannan, S.; Agathopoulos, S.; Ferreira, J.M.F., Hydroxyapatite scaffolds hydrothermally grown from aragonitic cuttlefish. *Journal of Materials Chemistry* **2005**, 15, 5007-5011.

52. Zaremba, C.M.; Morse, D.E.; Mann, S.; Hansma, P.K.; Stucky, G.D., Aragonite-hydroxyapatite conversion in gastropod (Abalone) nacre. *Chemistry of Materials* **1998**, 10, 3813-3824.

53. Gierse, H.; Donath, K., Reactions and complications after the implantation of Endobon including morphological examination of explants. *Archives of Orthopaedic and Trauma Surgery* **1999**, 119**,** 349-355.

54. Joschek, S.; Nies, B.; Krotz, R.; Göpferich, A., Chemical and physicochemical characterization of porous hydroxyapatite ceramics made of natural bone. *Biomaterials* **2000**, 21, 1645-1658.

55. Lin, F.H.; Liao, C.J.; Chen, K.S.; Sun, J.S.; Lin, C.Y., Preparation of beta TCP/HAP biphasic ceramics with natural bone structure by heating bovine cancellous bone with the addition of $(NH_4)_2HPO_4$. *Journal of Biomedical Materials Research* **2000**, 51, 157-163.

56. Mushipe, M.T.; Revell, P.A.; Shelton, J.C., Cancellous bone repair using bovine trabecular bone matrix particulates. *Biomaterials* **2002**, 23, 365-370.

57. Mushipe, M.T.; Revell, P.A.; Shelton, J.C., The effects if bovine trabecular bone matrix particulates on cortical bone repair. *Journal of Materials Science: Materials in Medicine* **2002**, 13, 99-105.

58. Rezwan, K.; Chen, Q.Z.; Blaker, J.J.; Boccaccini, A.R., Biodegradable and bioactive porous polymer/inorganic composite scaffolds for bone tissue engineering. *Biomaterials* **2006**, 27, 3413-3431.

59. Ramakrishna, S.; Mayer, J.; Wintermantel, E.; Leong, K.W., Biomedical applications of polymer-composite materials: A review. *Composites Science and Technology* **2001**, 61, 1189-1224.

60. Verheyen, C.C.P.M.; de Wijn, J.R.; van Blitterwijk, C.A.; de Groot, K., Evaluation of hydroxyapatite/poly(L-lactide) composites: Mechanical Behavior. *Journal of Biomedical Materials Research* **1992**, 26, 1277-1296.

61. Verheyen, C.C.P.M.; de Wijn, J.R.; van Blitterwijk, C.A.; de Groot, K.; Rozing, P.M., Hydroxyapatite/poly(L-lactide) composites: An animal study on push-out strengths and interface histology. *Journal of Biomedical Materials Research* **1993**, 27, 433-444.

62. Dorozhkin, S.; Ajaal, T., Toughening of porous bioceramic scaffolds by bioresorbable polymeric coatings. *Proceedings of the Institution of Mechanical Engineers, Part H: Journal of Engineering in Medicine* **2009**, 223, 459-470.

63. Peroglio, M.; Gremillard, L.; Chevalier, J.; Chazeau, L.; Gauthier, C.; Hamaide, T., Toughening of bio-ceramics scaffolds by polymer coating. *Journal of the European Ceramic Society* **2007**, 27, 2679-2685.

64. Fortin, J.B.; Lu, T.-M., *Chemical Vapor Deposition Polymerization: The Growth and Properties of Parylene Thin Films*. Kluwer Academic: Norwell, Massachusetts, 2004.

65. Wiegand, T.; Karr, J.; Steinkruger, J. D.; Hiebner, K.; Simetich, B.; Beatty, M.; Redepenning, J., Reconstruction of anorganic mammalian bone by surface-initiated polymerization of L-lactide. *Chemistry of Materials* **2008,** 20, 5016-5022.

66. Helwig, E.; Sandner, B.; Gopp, U.; Vogt, F.; Wartewig, S.; Henning, S., Ring-opening polymerization of lactones in the presence of hydroxyapatite. *Biomaterials* **2001,** 22, 2695-2702.

67. Guerra, G. D.; Cerrai, P.; Tricoli, M.; Krajewski, A.; Ravaglioli, A.; Mazzocchi, M.; Barbani, N., Composites between hydroxyapatite and poly(epsilon-caprolactone) synthesized in open system at room temperature. *Journal of Materials Science-Materials in Medicine* **2006,** 17, 69-79.

68. Fricain, J.C.; Alouf, J.; Bareille, R.; Rouais, F.; Rouvillain, J.L., Cytocompatibility study of organic matrix extracted from Caribbean coral *porites astroides*. *Biomaterials* **2002**, 23, 673-679.

69. Livingston, H.D.; Thompson, G., Trace element concentrations in some modern corals. *Limnology and Oceanography* **1971**, 16, 786-796.

70. Williams, J.B.; Irvine, J.W., Preparation of the inorganic matrix of bone. *Science* **1954**, 119, 771-772.

71. Sarin, P.; Lee, S.-J.; Apostolov, Z.D.; Kriven, W.M., Porous biphasic calcium phosphate scaffolds from cuttlefish bone. *Journal of the American Ceramic Society* **2011**, in press.

72. Nederberg, F.; Connor, E. F.; Moller, M.; Glauser, T.; Hedrick, J. L., New paradigms for organic catalysts: The first organocatalytic living polymerization. *Angewandte Chemie-International Edition* **2001,** 40, 2712-2715.

73. Kalmi, M.; Lahcini, M.; Castro, P.; Lehtonen, O.; Belfkira, A.; Leskela, M.; Repo, T., Tetrakis Sn(IV) alkoxides as novel initiators for living ring-opening polymerization of lactides. *Journal of Polymer Science Part A-Polymer Chemistry* **2004,** 42, 1901-1911.

74. Thakur, K. A. M.; Kean, R. T.; Hall, E. S.; Kolstad, J. J.; Munson, E. J., H-1 NMR spectroscopy in the analysis and characterization of poly(lactide). *International Journal of Polymer Analysis and Characterization* **1998,** 4, 379-391.

75. Espartero, J. L.; Rashkov, I.; Li, S. M.; Manolova, N.; Vert, M., NMR analysis of low molecular weight poly(lactic acid)s. *Macromolecules* **1996,** 29, 3535-3539.

76. Li, H.; Wang, C.; Bai, F.; Yue, J.; Woo, H.-G., Living ring-opening polymerization of L-lactide catalyzed by Red-Al. *Organometallics* **2004**, 23, 1411-1415.

77. Thian, E.S.; Loh, N.H.; Khor, K.A.; Tor, S.B., In vitro behavior of sintered powder injection molded Ti-6-Al-4V/HA. *Journal of Biomedical Materials Research* **2002**, 63, 79-87.

78. Gu, W.; Bousfield, D.W.; Tripp, C.P., Formation of calcium carbonate particles by direct contact of $Ca(OH)_2$ powders with supercritical CO_2. *Journal of Materials Chemistry* **2006**, 16, 3312-3317.

79. Wu, Y.-C.; Lee, T.-M.; Chiu, K.-H.; Shaw, S.-Y.; Yang, C.-Y., A comparative study of the physical and mechanical properties of three natural corals based on the criteria for bone-tissue engineering scaffolds. *Journal of Materials Science: Materials in Medicine* **2009**, 20, 1273-1280.

80. Goldstein, S.A., The mechanical properties of trabecular bone: Dependence on anatomic location and function. *Journal of Biomechanics* **1987**, 20, 1055-1061.

81. Shors, E.C., The development of coralline porous ceramic graft substitutes. In *Bone Graft Substitutes*, Laurencin, C.T., ed.; ASTM International: West Conshohocken, PA, 2003.

82. Haddock, S.M.; Debes, J.C.; Nauman, E.A.; Fong, K.E.; Arramon, Y.P.; Keaveny, T.M., Structure-function relationships for coralline hydroxyapatite bone substitute. *Journal of Biomedical Materials Research* **1999**, 47, 71-78.

83. Knackstedt, M.A.; Arns, C.H.; Senden, T.J.; Gross, K., Structure and properties of clinical coralline implants measured via 3D imaging and analysis. *Biomaterials* **2006**, 27, 2776-2786.

84. Lee, S. H.; Kim, B. S.; Kim, S. H.; Choi, S. W.; Jeong, S. I.; Kwon, I. K.; Kang, S. W.; Nikolovski, J.; Mooney, D. J.; Han, Y. K.; Kim, Y. H., Elastic biodegradable poly(glycolide-co-caprolactone) scaffold for tissue engineering. *Journal of Biomedical Materials Research Part A* **2003,** 66A, 29-37.

85. Stolt, M.; Viljanmaa, M.; Sodergard, A.; Tormala, P., Blends of poly(epsilon-caprolactone-b-lactic acid) and poly(lactic acid) for hot-melt applications. *Journal of Applied Polymer Science* **2004,** 91, 196-204.

86. Zhang, J.; Wang, L. Q.; Wang, H. J.; Tu, K. H.; Liu, L., Amphiphilic block copolymers based on methoxy poly(ethylene glycol) and either crystalline or amorphous poly(caprolactone-b-lactide): Synthesis, solid-state and aqueous solution characterizations. *Journal of Applied Polymer Science* **2007,** 105, 915-927.

87. Zhong, Z. Y.; Ankone, M. J. K.; Dijkstra, P. J.; Birg, C.; Westerhausen, M.; Feijen, J., Calcium methoxide initiated ring-opening polymerization of epsilon-caprolactone and L-lactide. *Polymer Bulletin* **2001,** 46, 51-57.

88. Zini, E.; Scandola, M.; Dobrzynski, P.; Kasperczyk, J.; Bero, M., Shape memory behavior of novel (L-lactide-glycolide-trimethylene carbonate) terpolymers. *Biomacromolecules* **2007,** 8, 3661-3667.

89. Dechy-Cabaret, O.; Martin-Vaca, B.; Bourissou, D., Controlled ring-opening polymerization of lactide and glycolide. *Chemical Reviews* **2004,** 104, 6147-6176.

90. Cai, Q.; Bei, J. Z.; Wang, S. G., Synthesis and degradation of a tri-component copolymer derived from glycolide, L-lactide, and epsilon-caprolactone. *Journal of Biomaterials Science-Polymer Edition* **2000,** 11, 273-288.

91. Dobrzynski, P.; Kasperczyk, J.; Bero, M., Application of calcium acetylacetonate to the polymerization of glycolide and copolymerization of glycolide with epsilon caprolactone and L-lactide. *Macromolecules* **1999,** 32, 4735-4737.

92. Hariharan, R.; Pinkus, A.G., Useful NMR solvent mixture for polyesters: Trifluoroacetic acid-d/chloroform-d. *Polymer Bulletin* **1993**, 30, 91-95.

93. Pinkus, A.G.; Subramanyam, R., New high-yield, one-step synthesis of polyglycolide from haloacetic acids. *Journal of Polymer Science. Polymer Chemistry Edition* **1984**, 22, 1131-1140.

94. Šebenda, J., Polymerization. In *Lactam-Based Polyamides, Volume 1: Polymerization, Structure, and Properties*, Puffr, R.; Kubánek, V., eds.; CRC Press: Boca Raton, Florida, 1991.

95. Lánská, B., Degradation and stabilization. In *Lactam-Based Polyamides, Volume 1: Polymerization, Structure, and Properties*, Puffr, R.; Kubánek, V., eds.; CRC Press: Boca Raton, Florida, 1991.

96. Coury, A.J., Chemical and biochemical degradation of polymers. In *Biomaterials Science: An Introduction to Materials in Medicine*, 2nd ed., Ratner, B.D.; Hoffman, A.S.; Schoen, F.J.; Lemons, J.E., eds.; Elsevier: San Diego, California, 2004.

97. Pezzotti, G.; Asmus, S.M.F.; Ferroni, L.P.; Miki, S., In situ polymerization into porous ceramics: A novel route to tough biomimetic materials. *Journal of Materials Science: Materials in Medicine* **2002**, 13, 783-787.

98. Nakahira, A.; Tamai, M.; Miki, S.; Pezzotti, G., Fracture behavior and biocompatibility evaluation of nylon-infiltrated porous hydroxyapatite. *Journal of Materials Science* **2002**, 37, 4425-4430.

99. Asmus, S.M.F.; Nakahira, A.; Pezzotti, G., Manufacture and bioactivity of tough hydroxyapatite/nylon hybrid composites. *Advanced Composite Materials* **2003**, 11, 255-264.

100. Liyun, Z.; Zhimin, L.; Yajun, Z., Preparation and properties of nano-hydroxyapatite modified nylon composites. *Advanced Materials Research* **2010**, 87-88, 228-232.

101. Zhang, Y.; Zhang, Q.; Cheng, K.; Xu, J., Monocarboxyl-end-grouped polycaprolactam with an adjustable molecular weight. *Journal of Applied Polymer Science* **2004**, 92, 722-727.

102. Holmes, B.S.; Moniz, W.B.; Ferguson, R.C., NMR study of nylon 66 in solution (^{1}H, ^{13}C, and ^{15}N NMR using adiabatic J cross polarization). *Macromolecules* **1982**, 15, 129-132.

103. Rubner, M., Synthetic sea shell. *Nature* **2003**, 423, 925-926.

104. Mayer, G., Rigid biological systems as models for synthetic compounds. *Science* **2005**, 310, 1144-1147.

105. Delattre, O.; Catonne, Y.; Berland, S.; Borzeix, S.; Lopez, E., Use of mother of pearl as a bone substitute – Experimental study in sheep. *European Journal of Orthopaedic Surgery and Traumatology* **1997**, 7, 143-147.

106. Kamat, S.; Su, X.; Ballarini, R.; Heuer, A.H., Structural basis for the fracture toughness of the shell of the conch *Strombus gigas*. *Nature* **2000**, 405, 1036-1040.

107. Bettinger, C.J.; Bao, Z., Organic thin film transistors fabricated on resorbable biomaterial substrates. *Advanced Materials* **2010**, 22, 651-655.

Chapter Three

Kinetic Analysis of Common Biocompatible Monomers and Polymers with Chemical Vapor Deposition Polymerization Initiated by Zinc Oxide at Various Temperatures using a Quartz Crystal Microbalance

Introduction and Background

In the preceding chapter it was established that nucleophilic surfaces of porous, biologically derived hydroxyapatite scaffolds can be used to initiate the ring opening polymerization (ROP) of common biocompatible lactones and lactams via the vapor phase. The result of this process is a biomimetic biocomposite containing a hydroxyapatite scaffold covered by a thin, even polymer film. For this process to be well-controlled, an understanding of the chemical vapor deposition polymerization (CVDP) kinetics of the reaction occurring at the surface is needed.

The two main factors that control chemical vapor deposition (CVD) processes are the thermodynamics of the reaction and the kinetics of the entire process.[1] It was demonstrated in the previous chapter that the CVDP of lactones and lactams on the surface of hydroxyapatite is thermodynamically viable. It has also been shown that various zinc salts and other metal oxides are sufficiently nucleophilic to initiate the ROP of L-lactide to poly-L-lactide (PLLA) in bulk melt polymerizations.[2-8]

The kinetics of the CVD process can be deconstructed into three major steps: the introduction of the reactant(s) into the reactor, the transport of these species to and from the surface, and the reaction that occurs at the surface. All three steps can have an effect on rate of the reaction, where the slowest step is the rate limiting step.[9-11] Choosing the

proper design of the reactor and adequate conditions inside the reactor enables one to eliminate the contributions of the first two steps and ensures that the surface reaction is the rate limiting step.

CVD methods are often described and categorized based on several different parameters: the gas flow state, activation manner, wall/substrate temperature, pressure, and temperature.[12] There are two types of gas flow systems: the open reactor and the closed reactor. In the open reactor system, the reactant gas is generated in a chamber separate from the reactor. Once the reactant is in the vapor phase, it is transported to the reactor via a carrier gas. The reactant and the carrier gas flow continuously through the reactor, entering on one side and exiting on the other. As the gaseous reactant flows through the chamber, some of the reactant diffuses to the surface of the substrate where it undergoes a reaction. The byproducts then desorb and are carried away by the carrier gas. In this system, conditions must be controlled to ensure that mass transport and diffusion of the gases to the surface are not the rate limiting step. Mass transport can be rate limiting when a boundary layer forms along the walls and substrate surface as the gas flows through the chamber. The boundary layer is a velocity gradient that develops because the velocity of the gas near the walls is zero. Its thickness varies with flow rate and is often defined by the point where the velocity of the gas near the wall or substrate reaches 99% of the velocity of the bulk gas. Thick boundary layers can slow the diffusion of the reactant gases to the substrate. A boundary layer can also form due to temperature and concentration gradients near the surface. Low pressure (a few mTorr or lower) and low temperatures can effectively minimize the boundary layer. This allows the reactant(s) to diffuse to the surface and also slows the reaction at the surface.

Conversely, the boundary layer is the thickest for high temperatures and high pressures (i.e., one atmosphere).[1, 12-15] In a closed chamber system, the precursor is loaded into the same chamber as the substrate. The chamber is then tightly sealed and the reactant gases are generated. The reaction is allowed to run to completion or until the precursor is depleted. It was traditionally used for purification of metals for chrome plating. Relative to the open reactor, the reactor for a closed system is a much simpler design that is largely free from the issues generated by the continuously flowing gas.[1, 13, 16, 17]

Reactors can also be either hot walled or cold walled. In a hot wall reactor, the entire chamber is heated to the same temperature as the substrate. While this prevents the presence of temperature and concentration gradients above the substrate, in some systems deposition can occur on the walls in addition to the surface of interest. In the cold wall reactor only the substrate is heated. In addition to this being more a more complex setup, temperature and concentration gradients may be present in a cold wall chamber.[18, 19]

The CVD process can also be categorized by the method used to generate the reactant gas. The most common method is thermal activation using either resistance heating, radio frequency (RF) heating, or infrared (IR) heating. In cases where heat can damage sensitive substrates, alternatives such as plasma-enhanced CVD (PECVD), laser-induced CVD (LCVD), and photo CVD (PCVD) can be used. All of these methods can reduce the temperature needed for deposition.[12, 20]

The temperature and pressure at which reactions are carried out can also be used to describe the CVD process. Temperatures range from ultra-high temperature (1700-1900 ^{o}C) processes to high temperature processes (above 1000 ^{o}C) and low temperature (below 300 ^{o}C) processes. Pressures range from atmospheric-pressure CVD to low

pressure CVD (less than 1 Torr) processes and ultra-high vacuum CVD (10^{-3} Torr) processes.[12, 21] As mentioned above, these conditions need to be optimized to give the best deposition and to ensure that the reaction is not limited by transport of gases to the surface.[22, 23]

The reactor design used in this chapter is a closed system. I constructed it. My system is a hot wall reactor designed to ensure even heating throughout the reactor. Additionally, it is a low temperature (less than 90 ^{o}C) and low pressure (10^{-4} Torr) system. The reactions I wished to examine were thermally activated in a straight forward manner. This reactor design enabled me to study surface initiated CVD polymerization kinetics occurring at the surface without worrying whether mass transport was rate limiting. To this end it was also necessary to design and construct my own detection system, which is described immediately below.

For the CVDP described in this chapter and other such surface polymerizations, the ideal method for monitoring the kinetics is one that measures the growth of the polymer film in real time. One such tool that offers good sensitivity and can detect small mass changes in real time, as low as 1 ng/cm^2, is a quartz crystal microbalance (QCM). QCMs have been used to monitor film deposition or molecule adsorption in a variety of conditions from vapor or solution phases,[24-27] and they have been used to monitor electrochemical and plasma polymerizations.[28-31]

The QCM relies on the piezoelectric properties of quartz crystal to gain its sensitivity. Piezoelectricity was first discovered in 1880 by Pierre and Jacques Curie.[32] When mechanical energy is applied to a piezoelectric material, an electric field is generated, allowing the transformation of the mechanical energy used to deform the

material into electrical energy.[33] The reverse process was predicted by Lippmann in 1881.[34] Applying an oscillating electric field across the thin quartz wafer induces an acoustic wave which propagates perpendicular to the surface.[35] When the crystal is twice as thick as the acoustical wavelength, a standing wave is established at a frequency called the resonant frequency, f_0. The resonant frequency for a quartz crystal wafer can be calculated based on equation 3.1,

$$f_0 = \sqrt{\frac{\mu_q}{\rho_q}} / 2t_q \tag{3.1}$$

where μ_q is the shear modulus, ρ_q is the density, and t_q is the crystal thickness.[36] These properties of the quartz crystal depend upon the angle at which the wafer is cut from a single crystal. The most common is the AT cut, which is cut at an angle 35° 15' from the Z axis. This particular cut is often chosen because its temperature dependence is essentially zero at 25 °C.[37]

If the thickness of the quartz crystal wafer changes, the resonant frequency also changes. Sauerbrey was the first to exploit this phenomenon for purposes of measuring small mass changes.[38] He made the assumption that for small mass changes, the addition of foreign mass could be treated as the addition of an equivalent mass of quartz, and therefore thickness, of the quartz crystal. Assuming the deposited material is thin, rigid and even, one can use equation 3.2 to relate the change in resonant frequency to the change in areal density.

$$\Delta f = -C_f m_f \tag{3.2}$$

In equation 3.2, Δf is the frequency shift, C_f is the mass sensitivity constant for the quartz crystal, and m_f is the areal density of the deposited film. The frequency decreases as the

areal density increases. The value of Δf is calculated by subtracting the resonant frequency of the quartz crystal from the frequency of the crystal with the deposited material.

$$\Delta f = f_c - f_0 \tag{3.3}$$

C_f is defined as

$$C_f = \frac{2 f_0^2}{\rho_q v_q} \tag{3.4}$$

where f_0 is the resonant frequency, ρ_q is the density of the quartz crystal, and v_q is the shear wave velocity in the quartz crystal. For an AT cut wafer with a 5 MHz resonant frequency, C_f is 56.6 Hz*cm^2/μg. This means that a 1 Hz change in frequency corresponds to an areal density change of 17.7 ng/cm^2. Areal density is used rather than mass because the vibrating area of the quartz crystal resonator does not extend all the way to the edge and can be hard to define. If the density of the deposited film is known, its thickness, t_f, can be calculated.

$$t_f = \frac{m_f}{\rho_f} \tag{3.5}$$

In equation 3.5, m_f is the areal density, and ρ_f is the density of the film. There are two important and advantageous features of equation 3.2. First, no calibration is needed because the mass sensitivity and resonant frequency can be calculated from the properties of the quartz crystal. Second, under the conditions stated above, the mass sensitivity is independent of the physical properties of the deposited film.[39] At greater thicknesses, equation 3.2 is no longer accurate because the elastic properties of the deposited film have an influence on the resonant frequency and can no longer be treated as an extension of the quartz crystal.[40] Lu and Lewis[41] introduced a formula to account for this. In

equation 3.6, ρ_f and ρ_q are the densities of the film and quartz respectively, v_f and v_q are the shear wave velocities in the film and quartz respectively, f_c is the resonant frequency of the film and quartz combined, f_0 is the resonant frequency of the quartz, and f_f is the resonant frequency of the freely suspended film.

$$\tan(\pi f_c / f_0) = -(\rho_f v_f / \rho_q v_q) \tan(\pi f_c / f_f) \quad (3.6)$$

It should also be noted that a well described frequency shift occurs when one or both faces of the crystal contact a liquid. This shift was first described by Kanazawa and Gordon.[42] Later, Martin et al. showed how a small mass accumulation on a crystal in a liquid environment changes the resonant frequency.[43] For applications described in this chapter, the deposited polymer is treated as a thin, rigid layer that is an even extension of the quartz crystal. Described below is the use of the QCM to study the CVDP kinetics of the ROP of L-lactide and glycolide by ZnO.

Experimental

Chemicals: Deuterated chloroform ($CDCl_3$, 99.8% D from Sigma-Aldrich, St. Louis, MO), glycolide (GL, 99.9% from Polysciences Inc., Warrington, PA), 1,1,1,3,3,3-hexafluoro-2-propanol (HFIP, 99.5%+, from Acros Organics, Geel, Belgium), and zinc oxide sputtering target (ZnO, 99.9% from Kurt J. Lesker, Clairton, PA) were used as purchased from the respective suppliers. L-Lactide (from Purac, Lincolnshire, IL) was sublimed at 90 ^oC and then transferred into a $N_{2(g)}$ atmosphere glove box for further use.

Preparation of QCM Reaction Vessel for Kinetic Analyses: All CVDP kinetics reactions were performed using a Stanford Research Systems (SRS) QCM200 Quartz Crystal Microbalance (Figure 3.1). Data was acquired using SRS QCM200 LabVIEW Data Acquisition Software Version 2.0 (SRS, Sunnyvale, CA). Data was analyzed using

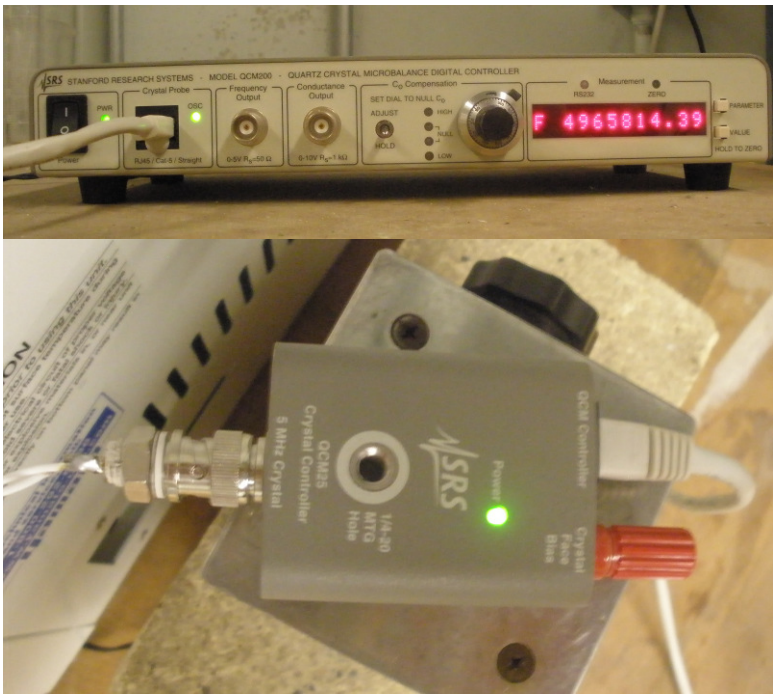

Figure 3.1. Stanford Research Systems QCM200 Quartz Crystal Microbalance controller.

Microsoft Excel. Five MHz, one inch diameter AT-cut quartz crystals with Cr/Au electrodes from SRS were used in all reactions (Figure 3.2). RF sputtering was used to deposit a thin layer of ZnO onto the side of the crystal containing the larger of the two electrodes. Deposition was performed at 100 W for 30 minutes, resulting in a 50 nm thick layer of ZnO. Sputtering was performed with equipment and assistance from Dr. Natale J. Ianno in the Department of Electrical Engineering at the University of Nebraska. A two piece CVDP reactor (Figure 3.3) was constructed from Pyrex glass. The bottom piece was constructed from a glass tube with an outer diameter (OD) of 40 mm and an inner diameter (ID) of 35 mm. Using a glass working lathe, I closed one end of the bottom piece to produce an object resembling a test tube 20 cm in length. In the reactors used to study the CVDP of glycolide, a Teflon reservoir was placed in the bottom. This reservoir was used to house the glycolide and slow its polymerization at the surface of Pyrex, which is somewhat nucleophilic. (Anecdotally, I note that soft glass was much too nucleophilic for my purposes, and although quartz was not nucleophilic enough to initiate the polymerizations of any of the cyclic lactones I examined, quartz was not used due to the practical difficulties associated with quartz "glass working".) A 40 mm (OD) and 35 mm (ID) glass tube was also used for the top of my reactor assembly. Because the diameter of the tube was large and therefore would be difficult to vacuum seal, a glass tube with an OD of 18 mm and an ID of 15 mm was attached to the top. This was achieved by narrowing the diameter of the top of the larger piece to the diameter of the smaller and joining them using the glass lathe. At this point in the process electrical feedthroughs were attached. The feedthroughs provided the electrical connection between the crystal in

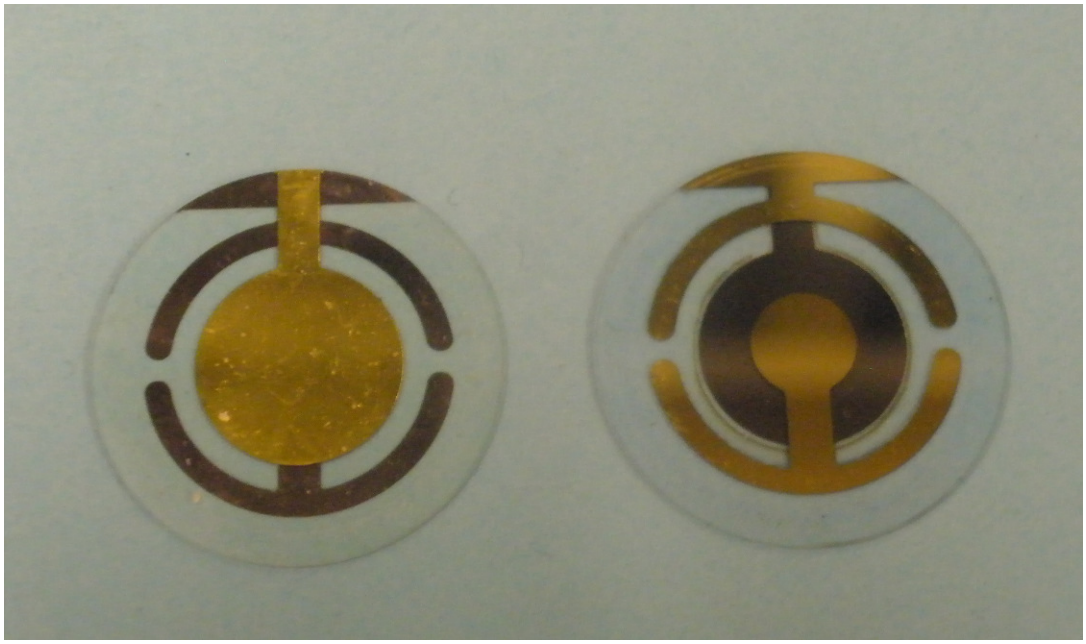

Figure 3.2. Five MHz, one inch diameter, AT-cut quartz crystal with Cr/Au electrodes from Stanford Research Systems.

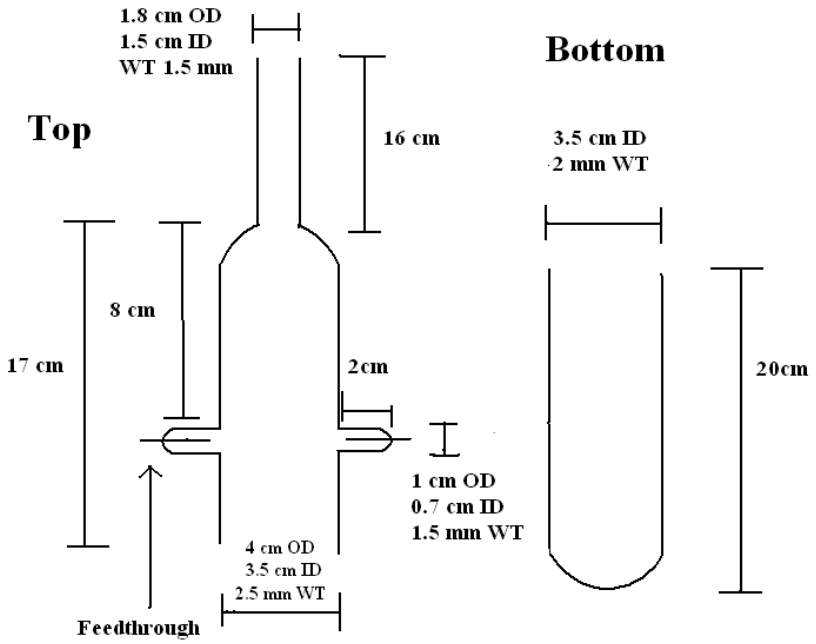

Figure 3.3. Sketch (top) and image (bottom) of the CVDP reactor.

the vacuum sealed reactor and the outside controller. They were made of either platinum or copper coated tungsten. Next the ZnO coated quartz crystal was attached to the feedthroughs. Copper wire was first attached to the feedthroughs using Kester "44" rosin core solder. At the other end, the copper wire was attached to the electrodes on the ZnO coated quartz crystal again using the same solder. The length of the copper wire was approximately 14 cm, far enough from the junction where the two reactor pieces are fused together that heating during glass working did not affect it. At this point the stability of the resonant frequency of the crystal in air was checked to ensure no damage was done when attaching the copper wire. Next the top and bottom pieces were fused together on the glass lathe. Following this step, the complete reactor was attached to a high vacuum line to check for leaks and to remove residual water from the reactor. The stability of the resonant frequency of the crystal was again checked while attached to the high vacuum line. After a minimum of 16 hours, the reactor was transferred to a $N_{2(g)}$ atmosphere glove box to be loaded with monomer. Approximately one gram of the desired monomer was added to the reactor. The exact amount was not crucial, but it was important to have excess monomer in the reactor so that its evaporation was not rate limiting. The open end of the loaded reactor was sealed with a rubber stopper and the entire assembly was removed from the glove box. The bottom of the assembly was briefly cooled in liquid N_2 before attaching the top end to a high vacuum line. The bottom was kept in the liquid N_2 while on the high vacuum line to reduce the vapor pressure of the monomer. This was necessary to prevent loss of monomer and/or its pyrolysis during the glassblowing necessary to flame seal the reactor. The reactor was sealed at a pressure of 10^{-4} Torr (Figure 3.4). The area of the reactor near the crystal was

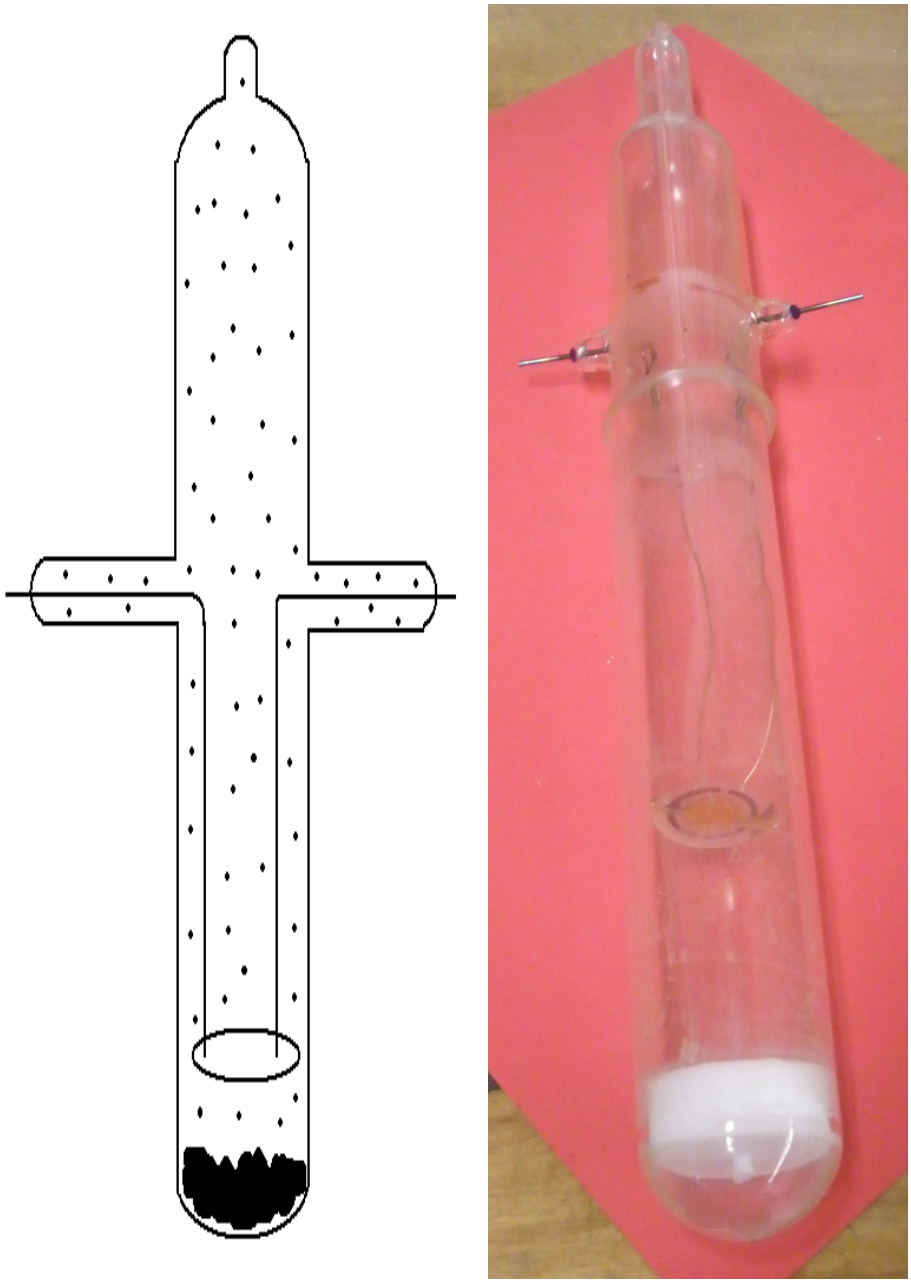

Figure 3.4. Sketch (left) and image (right) of the complete CVDP reactor.

gently heated with a heat gun to sublime any monomer away from the surface of the crystal and deposit it in the bottom of the reactor which was maintained at -196 ^{o}C in liquid N_2. The reactor was placed in a Yamato DKN402 convection oven (Santa Clara, CA). Wires attached to the outside feedthroughs were fed through a port in the side of the oven to the QCM controller (Figure 3.5).

Procedures for Kinetic Analyses: Prior to performing kinetic experiments with ZnO coated quartz crystals, I performed a control experiment on an uncoated crystal that was enclosed in a reactor containing L-lactide as described above. This control was necessary to establish that neither the quartz crystal nor the electrodes could initiate the polymerization, possibly giving erroneous or misleading results. The uncoated crystal reactor was heated to several different temperatures between 35 ^{o}C and 90 ^{o}C and held constant for two to three hours. No change in the frequency was observed. Consequently I saw no evidence that the crystal itself could initiate the polymerization of L-lactide.

After the control was complete, I was finally prepared to examine the propensity of a nucleophilic ZnO coated crystal to initiate the ring opening polymerization of L-lactide. The crystal served as a real time monitor of the mass gain due to polymer deposition, and the time dependence of this mass gain served as a real time (steady state) indicator of the reaction rate. The ZnO coated crystal was first allowed to stabilize at room temperature and then the (isothermal) temperature of the reactor and its contents was raised to 35 ^{o}C. For early reactions involving L-lactide this increase in temperature was not controlled carefully. The increase was allowed to occur as fast as the oven could make it occur. Later, in polymerizations involving glycolide, this process was controlled more carefully and the temperature was slowly raised in 5 ^{o}C increments over 3 hours.

Figure 3.5. Images of the complete reaction setup (top), the convection oven with the CVDP reactor inside (bottom left) and the CVDP reactor inside the oven (bottom right).

Although this phenomenon is not observed in L-lactide polymerizations, if the temperature was increased too quickly for the glycolide polymerizations, monomer sublimed from the reservoir and was deposited onto the crystal due to the temperature difference, thus causing instability in the resonant frequency.

For reactions involving L-lactide, the resonant frequency was given approximately one hour to stabilize after each change in temperature. The temperature was then held constant for another two to three hours. During this time the frequency and resistance were recorded. The temperature was then increased in 5 ^{o}C increments and the process was repeated until a maximum temperature of 90 ^{o}C was reached. The temperature was then decreased in 5 ^{o}C increments using the same protocol. This heating and cooling cycle was repeated until mass loading (due to polymer) on the crystal reached the critical point at which it could no longer oscillate at its resonant frequency.

For reactions involving glycolide, the temperature was increased in intervals of either three or five degrees Celsius. At high temperatures (65 to 80 ^{o}C) where the polymerization proceeded quite quickly, data was collected over five to nine hours. At each of the lower temperatures I had the luxury of collecting data over a much longer time (up to 21 hours) because the polymerization proceeded so slowly that I had few concerns about cumulating mass loading preventing the crystal from resonating. At this point the temperature was decreased in a similarly controlled fashion. The heating and cooling cycle was repeated for several times until the quartz crystal eventually stopped oscillating. Some raw data collected during the CVD polymerization of glycolide on ZnO is shown in Figure 3.6. Over the first three hours (10,800 seconds) shown in this plot, the temperature was increased from 50 to 55 ^{o}C. From three hours to 12 hours (43,200

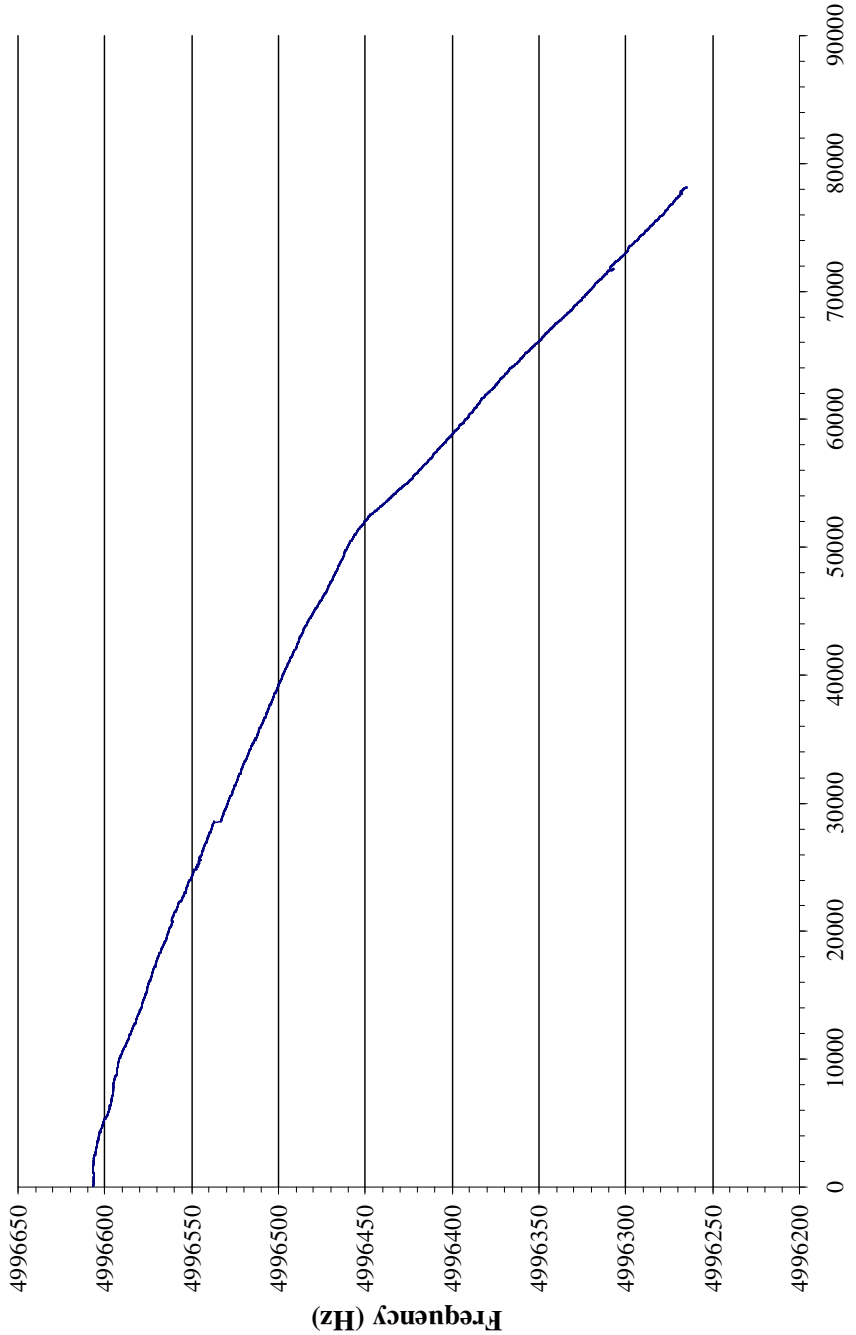

Figure 3.6. Raw data from the CVDP of L-lactide initiated by ZnO collected using SRS QCM200 LabVIEW Data Acquisition Software Version 2.0 and plotted in Microsoft Excel.

seconds) the temperature was held constant at 55 ^{o}C. The temperature increased from 55 ^{o}C to 60 ^{o}C over the period from 12 hours to 15 hours (54,000 seconds). From the 15 hour mark until the end of the experiment, the temperature was held constant at 60 ^{o}C.

Distinct changes in the slope are clearly observed in Figure 3.6. These slopes are associated with changes in the rate constants described in more detail later in this chapter. After the polymerizations were complete, the reactor was opened up and the quartz crystal was removed. The crystals from the L-lactide polymerizations were placed in $CDCl_3$. Samples from monomer reservoirs from the glycolide polymerizations were dissolved in a 3:1 v/v ratio of hexafluoroisopropanol (HFIP) and $CDCl_3$. ^{1}H NMR spectra were obtained using a Bruker (Billerica, MA) Avance 400 MHz NMR instrument. Spectral processing was done using Bruker Topspin 3.0.b.8. Peak assignments for L-lactide, glycolide, PLLA, and polyglycolide (PG) were compared to literature values.[44-54]

Results and Discussion

The ROP of lactones can be initiated by several different initiators. Examples include anionic initiators such as hydroxide, oxide, alkoxide, and amide,[55-58] and neutral initiators such as alcohols and amines.[59-61] Studies on the kinetics of homogeneously initiated ROPs have shown that they follow the rate law,

$$Rate = k[M]^{x}[I]^{y} \tag{3.7}$$

where k is the kinetic rate constant, [M] is the concentration of lactone monomer and [I] is the concentration of initiator. Both x and y are typically one. Because ROPs are living reactions, each mole of initiator that is consumed creates an equal number of moles of living polymer chains. This means the number of polymerization sites stays constant

throughout the reaction. Because $[I]^y$ is constant, the rate law in equation 3.7 can be reduced to the following,

$$Rate = k_{app}[M]^x \tag{3.8}$$

where k_{app} is equal to $k[I]^y$.[62-64] In the CVDP kinetic reactions in this chapter, the lactone monomer concentration is also constant because there is a large excess of solid monomer that maintains its vapor pressure at a constant value in the reactor. The rate law in equation 3.8 can therefore be reduced further to

$$Rate = k'_{app} \tag{3.9}$$

where k'_{app} is equal to $k[M]^x[I]^y$. Equation 3.9 can be rewritten as a differential rate law in terms of the areal density of the deposited polymer.

$$\frac{dm_{f_t}}{dt} = k'_{app} \tag{3.10}$$

Integration of equation 3.10 produces equation 3.11

$$m_f = k'_{app}t + m_{f_0} \tag{3.11}$$

where m_{f_t} is the areal density at time t and m_{f_0} is the areal density at time zero. Because the areal density of the deposited polymer at time zero is zero, equation 3.11 reduces to

$$m_f = k'_{app}t \tag{3.12}$$

This final rate law shows a pseudo zero order relationship. When m_{f_t} is plotted against reaction time, the slope of the resulting line is the pseudo zero order rate constant for the reaction at a given temperature.

Kinetic Analysis of CVDP of L-lactide initiated by ZnO: The QCM proved to be the ideal method to quickly and efficiently study the kinetics of the CVDP at various

temperatures. Recall from equation 3.2 that there is a linear relationship between the areal density of the deposited film and the frequency at which the crystal oscillates for thin, rigid, and even films. As the areal density of the film increases the resonant frequency decreases. Shown in Figure 3.7 is the dependence of areal density as a function of time for the CVDP of L-lactide at ZnO. This dependence is shown at 5 ^{o}C intervals ranging from 55 ^{o}C to 80 ^{o}C. The negative change in frequency is shown on the second y-axis on the right hand side. Two features are noteworthy in Figure 3.7. First, the areal density of the polymer increases linearly over time for each temperature. The pseudo zero order rate constant of the polymerization at each temperature can be obtained directly from the individual slopes. The rate constants for each temperature are shown in Table 3.1. Second, it is clear that the polymerization of L-lactide proceeds faster as the temperature increases.

This increase with temperature is controlled by the vapor pressure and the temperature dependence of the rate constant. The dependence of the vapor pressure on temperature is described by the Clausius-Clapeyron equation

$$P_{vap} = \beta e^{-\Delta H_{vap}/RT} \tag{3.13}$$

where P_{vap} is the vapor pressure, β is a constant, ΔH_{vap} is the enthalpy of vaporization, R is the ideal gas constant, and T is the temperature. Equation 3.13 can be converted to the linear form

$$\ln P_{vap} = \frac{-\Delta H_{vap}}{R}(\frac{1}{T}) + \beta \tag{3.14}$$

to provide a linear relationship between the natural log of the vapor pressure and the reciprocal of temperature.

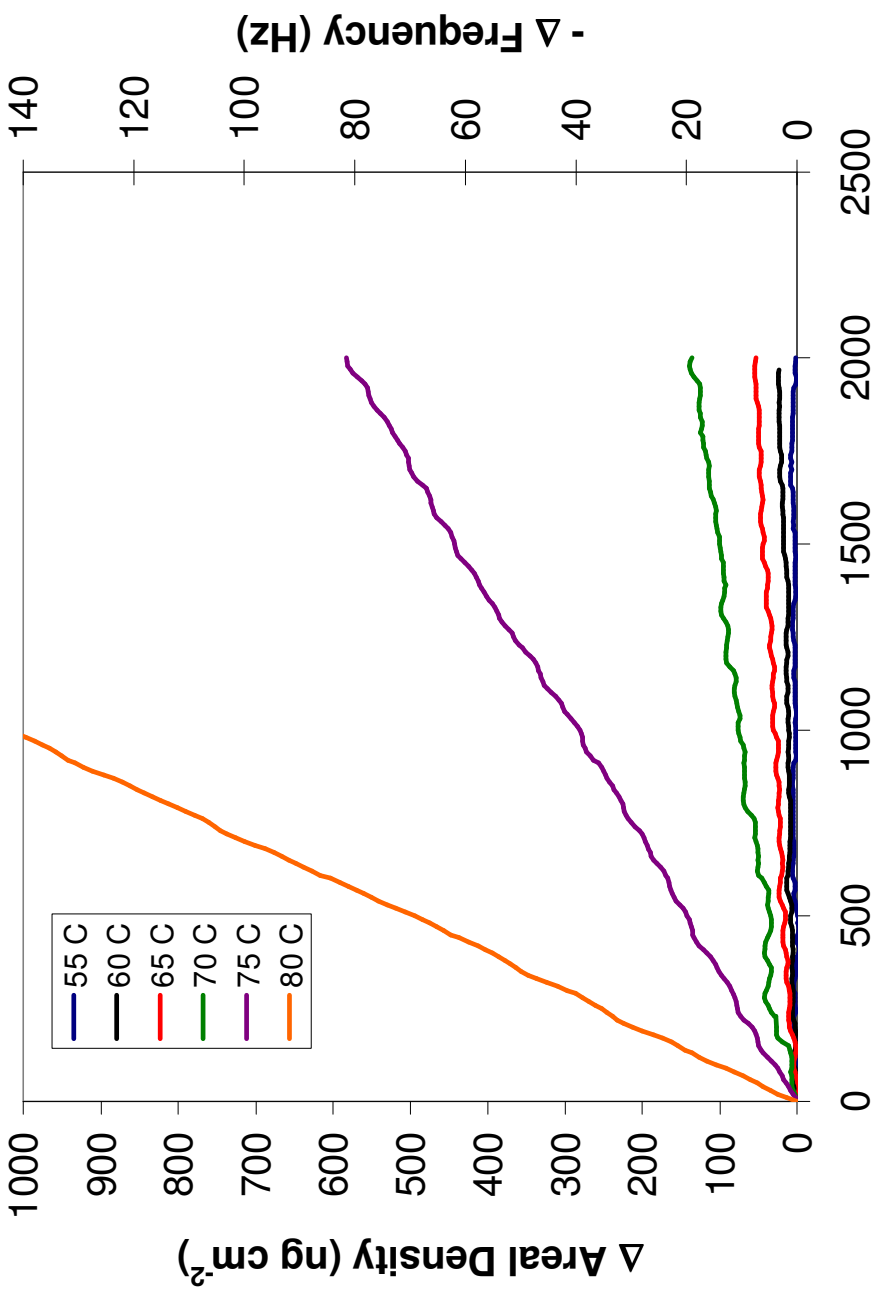

Figure 3.7. Change in areal density and negative change in frequency versus time for the CVDP of L-lactide initiated by ZnO at 55 °C, 60 °C, 65 °C, 70 °C, 75 °C, and 80 °C.

Reaction Temperature (^{o}C)	Rate Constant (ng cm^{-2} s^{-1})
55	$3.1 \times 10^{-3} \pm 1 \times 10^{-4}$
60	$1.17 \times 10^{-2} \pm 1 \times 10^{-4}$
65	$2.83 \times 10^{-2} \pm 2 \times 10^{-4}$
70	$7.00 \times 10^{-2} \pm 4 \times 10^{-4}$
75	$2.911 \times 10^{-1} \pm 3 \times 10^{-4}$
80	$1.041 \pm 1 \times 10^{-3}$

Table 3.1. Rate constants (± 1 SD) and corresponding temperatures for the CVDP of L-lactide initiated by ZnO.

As with many chemical reactions, as the temperature is increased, the number of molecules capable of overcoming the activation barrier increases. This relationship can be described by the Arrhenius equation,

$$k = Ae^{-E_a/RT} \tag{3.15}$$

where k is the rate constant, E_a is the activation energy, R is the ideal gas constant, and A is the pre-exponential factor. Equation 3.15 can be converted to the linear form

$$-\ln k = (\frac{E_a}{R})(\frac{1}{T}) - \ln A \tag{3.16}$$

to obtain a convenient linear relationship between the negative natural log of the rate constant and the reciprocal of temperature. When the negative natural log of the rate constant at each temperature is plotted versus the reciprocal of reaction temperature (Figure 3.8), a linear relationship is obtained. As the temperature of the reaction increases, so too does the reaction rate, but this rate (and rate constant) is dependent on both thermal activation and the vapor pressure, both of which exhibit the same mathematical relationship to temperature (see equations 3.14 and 3.16). Given the reported values for the vapor pressures of L-lactide[65] and glycolide,[66] ln P can be plotted versus 1/T (Figure 3.9) to give the linear relationship expected from the Clausius-Clapeyron equation. By analogy to equation 3.7, we postulated that the rate of the CVD polymerization could be described by equation 3.17,

$$Rate = kN^x P_{monomer}^y \tag{3.17}$$

where N is the number of surface nucleophiles (and the number of chain propagation sites), P is the pressure of the monomer, and x and y are 1. Similarly to equation 3.7, this

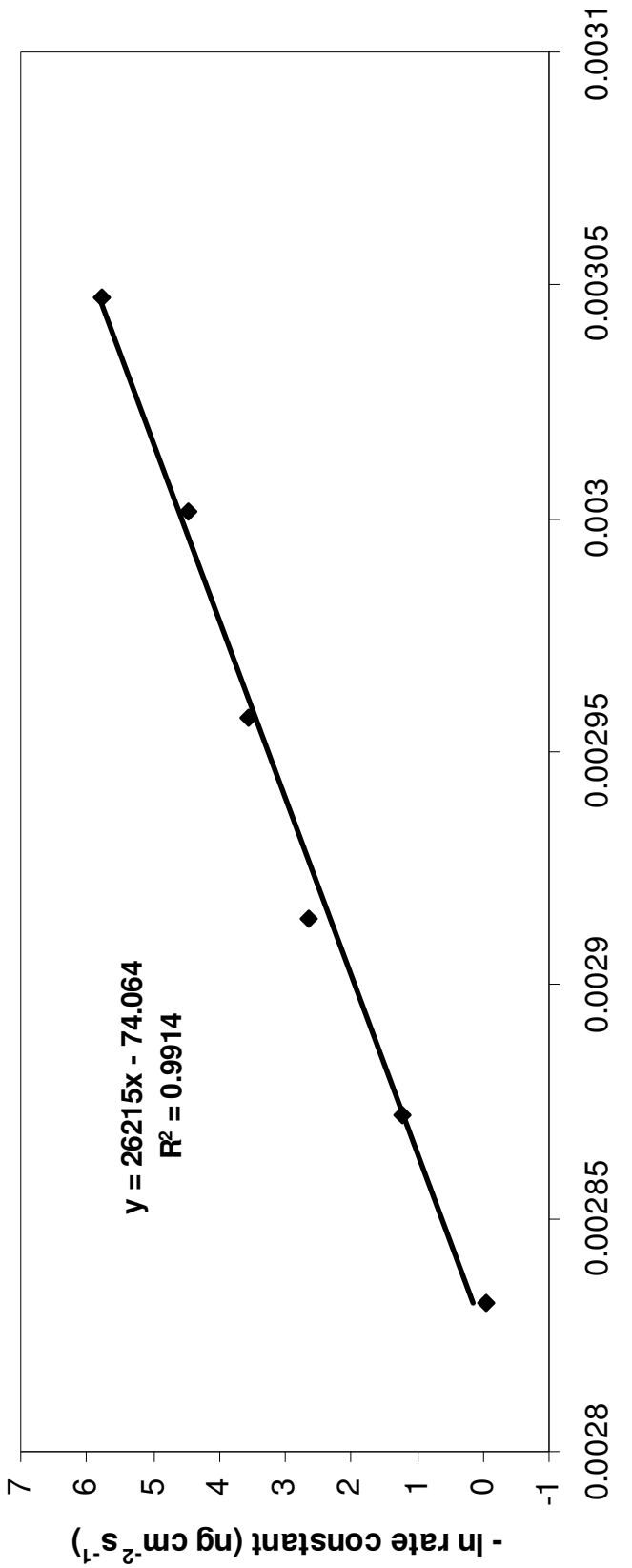

Figure 3.8. Negative natural log of the rate constant versus the reciprocal of temperature for the CVDP of L-lactide initiated by ZnO.

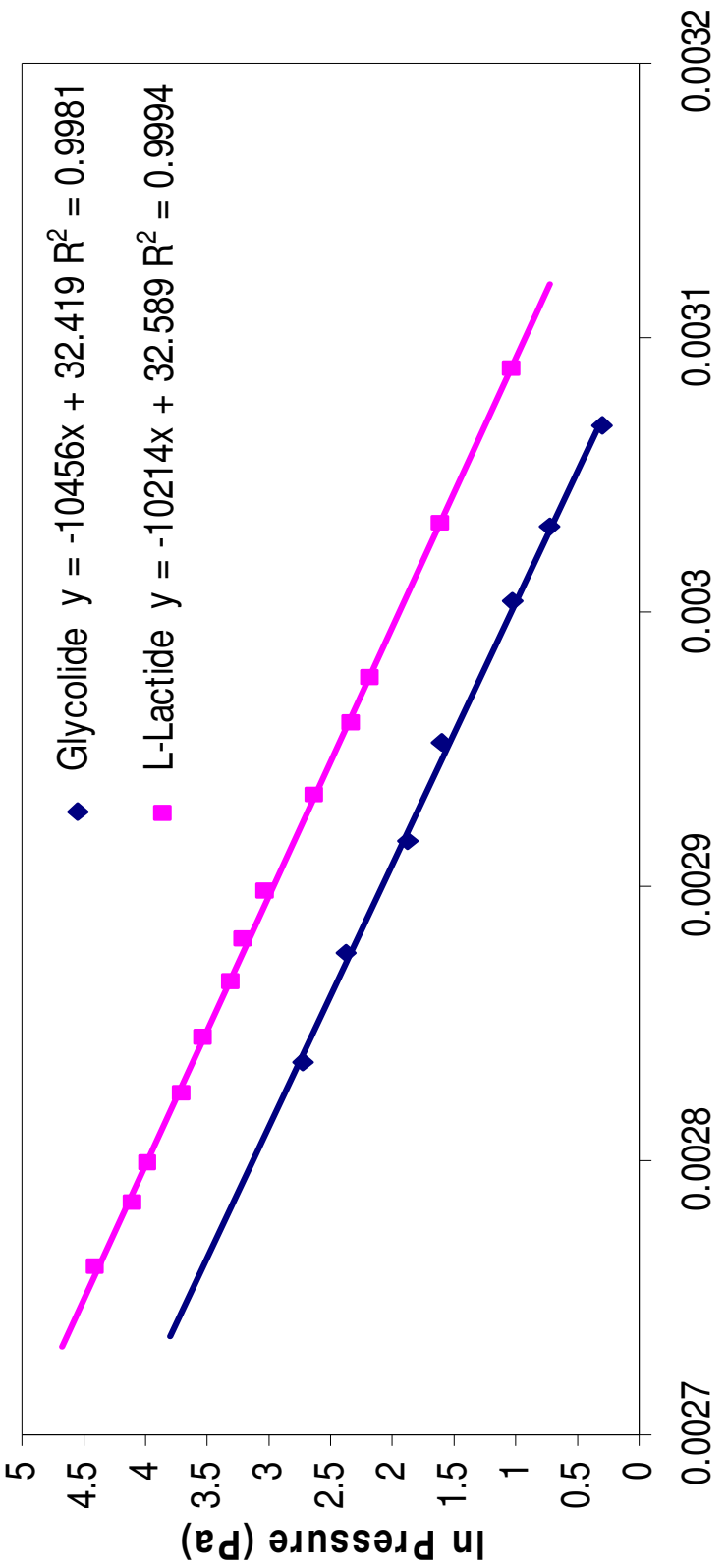

Figure 3.9. Clausius-Clapeyron plot for L-lactide and glycolide.

equation can be reduced to equation 3.9. Based on equation 3.17, $k_{app}^{'}$ in equation 3.9 can be described by equation 3.18.

$$k_{app}^{'} = k_{app} N P_{monomer} \tag{3.18}$$

By dividing $k_{app}^{'}$ in equation 3.18 by the vapor pressure of monomer, which was determined by Clausius-Clapeyron fits of experimental data (Figure 3.9) found in the literature,[65, 66] we obtained equation 3.19,

$$\frac{k_{app}^{'}}{P_{monomer}} = k_{app} N \tag{3.19}$$

which indicates that the observed reaction rates at any given temperature should be pseudo zero order. In other words the observed reaction rate should be independent of time. The negative natural log of the new rate constants, independent of vapor pressure can then be plotted versus the reciprocal of temperature to construct an Arrhenius plot (Figure 3.10). I find from this plot that the activation energy for the CVDP of L-lactide in this system is 133 ± 10 kJ/mole.

When using the Sauerbrey equation, one makes the assumption that the deposited film is thin, rigid, and evenly spread across the surface of the crystal. As the film thickness increases, the viscoelastic properties can lead to acoustic loses and have a dampening effect on the frequency at which the crystal oscillates.[40, 67, 68] This means the frequency decrease associated with the additional mass is less than it would be at smaller thicknesses. Viscoelastic dampening was not observed in the CVDP kinetics experiments described in this chapter. In fact for extremely long reaction times, it appeared that a gradual increase in the frequency change was observed as the areal density increased (Figure 3.11). Such a response is inconsistent with equation 3.18. To investigate this

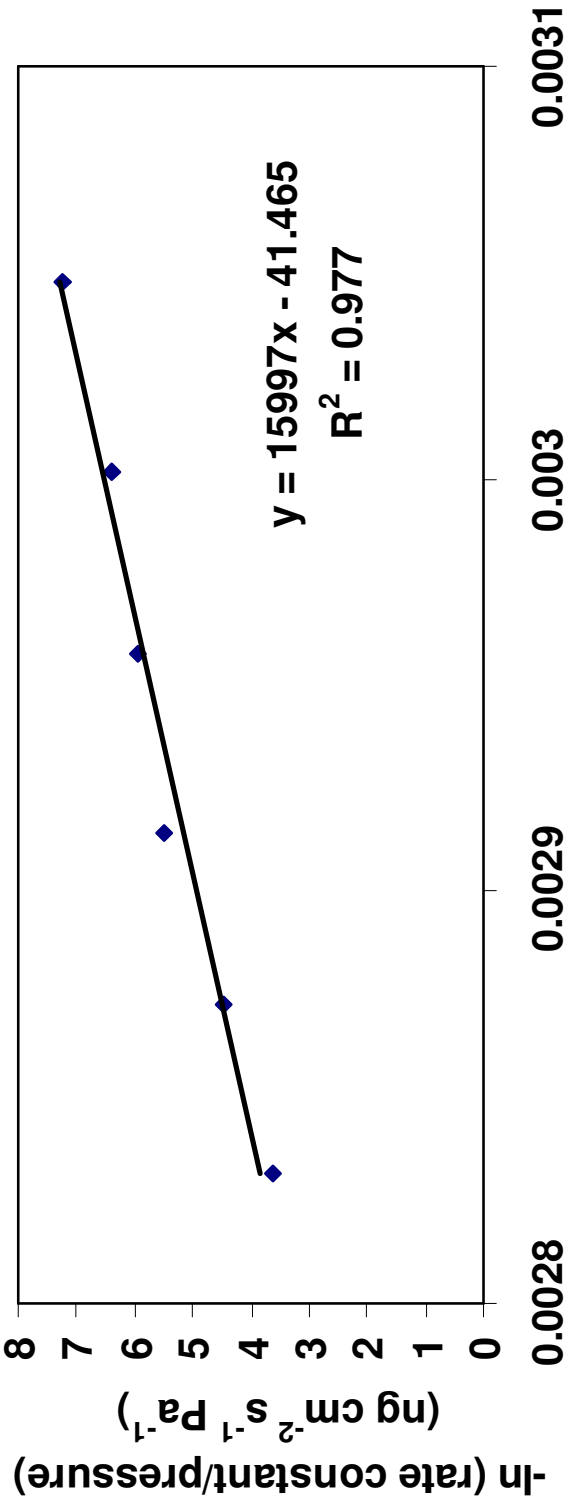

Figure 3.10. Arrhenius plot for CVDP of L-lactide initiated by ZnO.

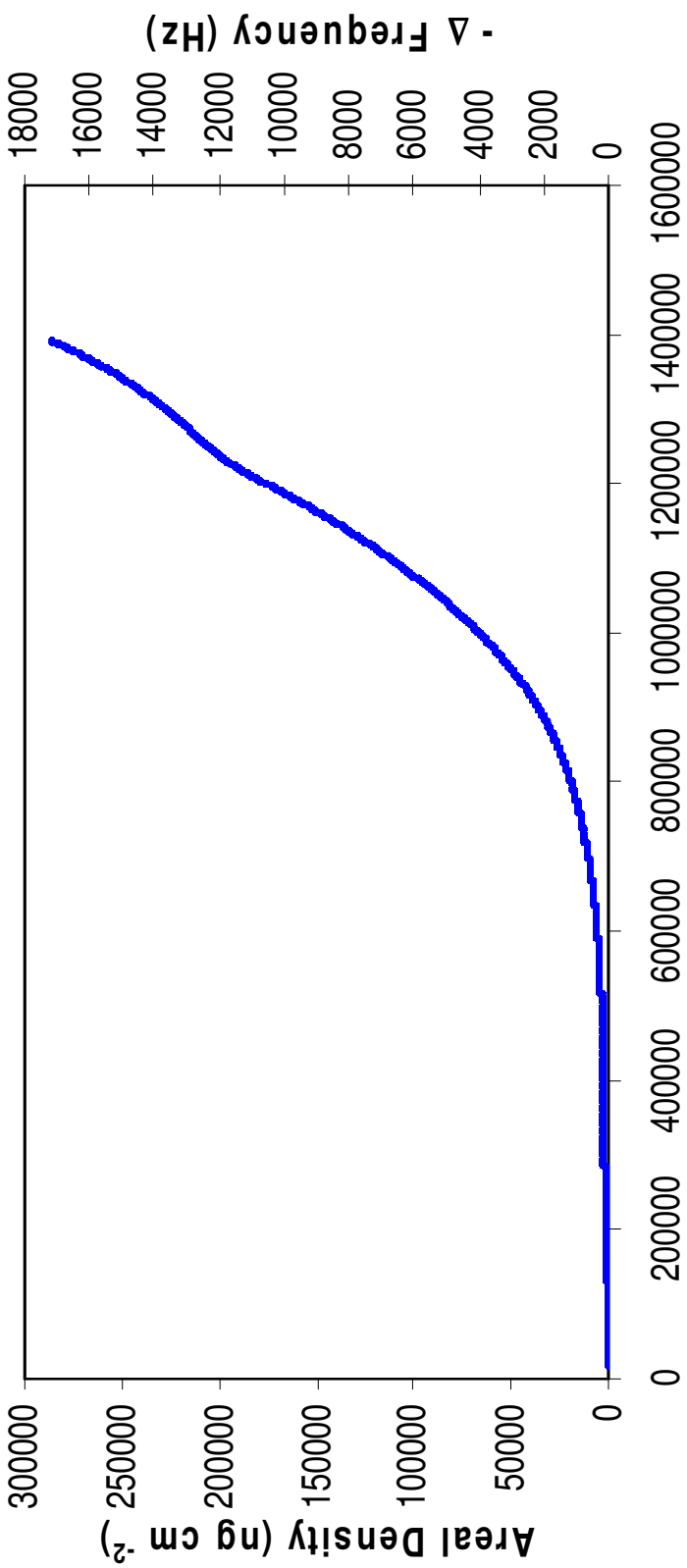

Figure 3.11. Areal density of deposited film over time for CVDP of L-lactide initiated by ZnO at 65 °C.

unusual behavior, I conducted a relatively simple but time consuming experiment in which the CVDP was carried out for a very long time at a constant temperature. The reaction in Figure 3.11 is the CVDP of L-lactide initiated by ZnO at a constant temperature of 65 ^{o}C over a period of 1,400,000 seconds (389 hours or 16 days). For this isothermal reaction, the polymerization rate is expected to be linear over time. For short reaction times and small areal density values, less than 600,000 seconds (167 hours or 7 days), the areal density increase is linear as expected. At later times, however, a progressively increasing deviation from the linear response of short times is observed. So the question becomes, what is causing this increase? The initiator, ZnO, was present in the beginning at a fixed amount, and since the CVDP is a living polymerization one mole of initiator can only produce one mole of polymer chain. Furthermore, because the temperature was constant, monomer was present in the vapor phase at a constant pressure. It is unclear whether the cause of this increase in the deposition rate is due to an increase in the areal density or the longer reaction times. One plausible explanation that occurred to us was that the PLLA degraded over the course of the reaction to produce additional initiation sites. In bulk, melt processes, thermal degradation is known to occur through random chain scission and unzipping depolymerization reactions.[69] Chain scission can happen by hydrolysis,[70] oxidative degradation, *cis*-elimination, intramolecular and intermolecular transesterification, and homolysis.[71-73] The main products generated are cyclic oligomers[72, 74, 75] and linear oligomers.[76] Additionally, it has been shown that recombination reactions occur.[77-79] Other factors that have been shown to effect thermal degradation include residual catalysts,[80, 81] residual monomers, oligomers[82] and other impurities.[69, 83] Degradation of PLLA and other polyesters leads to

a decrease in molecular weight.[78] The ^{1}H NMR spectra of the polymer coating on the quartz crystal offers strong support for this theory (Figure 3.12). The ^{1}H NMR spectrum in Figure 3.12 was obtained by dissolving PLLA from the QCM monitored CVDP in $CDCl_3$. The portion of the spectra shown contains the methine protons of PLLA. The quartet at 4.36 ppm is attributed to the hydroxyl end group of the polymer. The methine quartet of the carboxylate end group overlaps with the internal methines quartet producing a broad set of peaks from 5.28 to 5.10 ppm. There is present a quartet at 5.045 ppm, due to the methine proton of the monomer.[44-48] Integration of the internal methines quartet and the hydroxyl end methine quartet reveals an approximate 2:1 ratio of internal methines to hydroxyl end methine. This small ratio indicates that the polymer is low molecular weight. In fact, the deposition is best described as a low molecular weight oligomer. If the deposited PLLA was high molecular weight polymer, the end group quartet would be small compared to the internal methines quartet. To avoid the increasing deposition rate issue associated with thermal degradation of the polymer, all L-lactide CVDPs described previously in this chapter were conducted at small areal densities (below 11 $\mu g/cm^2$) and at short reaction times (less than 4 days).

Kinetic Analysis of CVDP of glycolide initiated by ZnO: The same QCM setup and method can be used to study the CVDP of glycolide initiated by ZnO. Figure 3.13 shows the rate of polymerization of glycolide to polyglycolide for seven different temperatures between 35 ^oC and 55 ^oC. The primary y-axis is areal density and the secondary y-axis is negative change in frequency and both are plotted against time. Again, as was the case with the CVDP of L-lactide (Figure 3.7), there are two distinct features that are notable. At all seven temperatures the areal density increases linearly

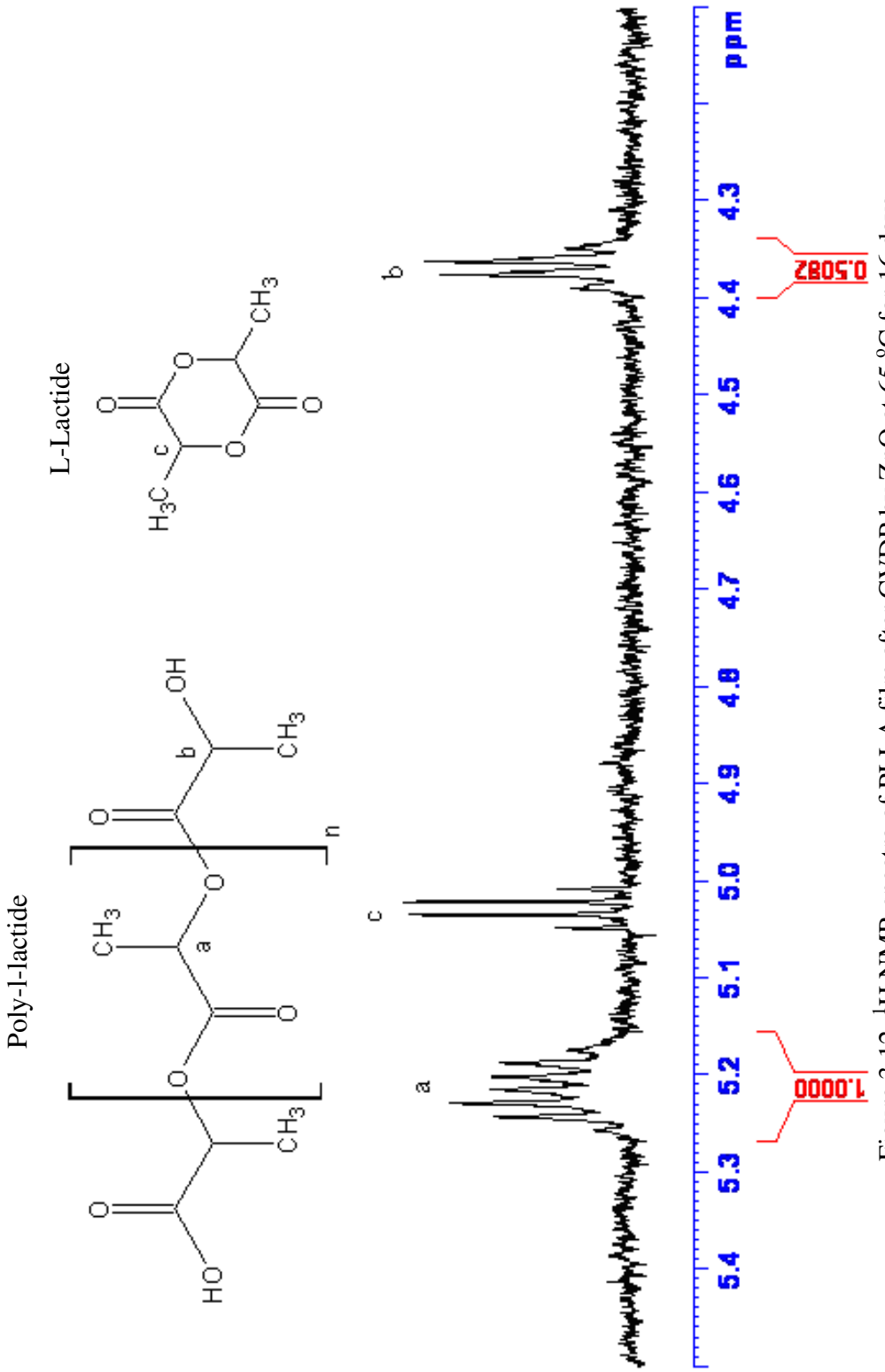

Figure 3.12. ^{1}H NMR spectra of PLLA film after CVDP by ZnO at 65 ^{o}C for 16 days.

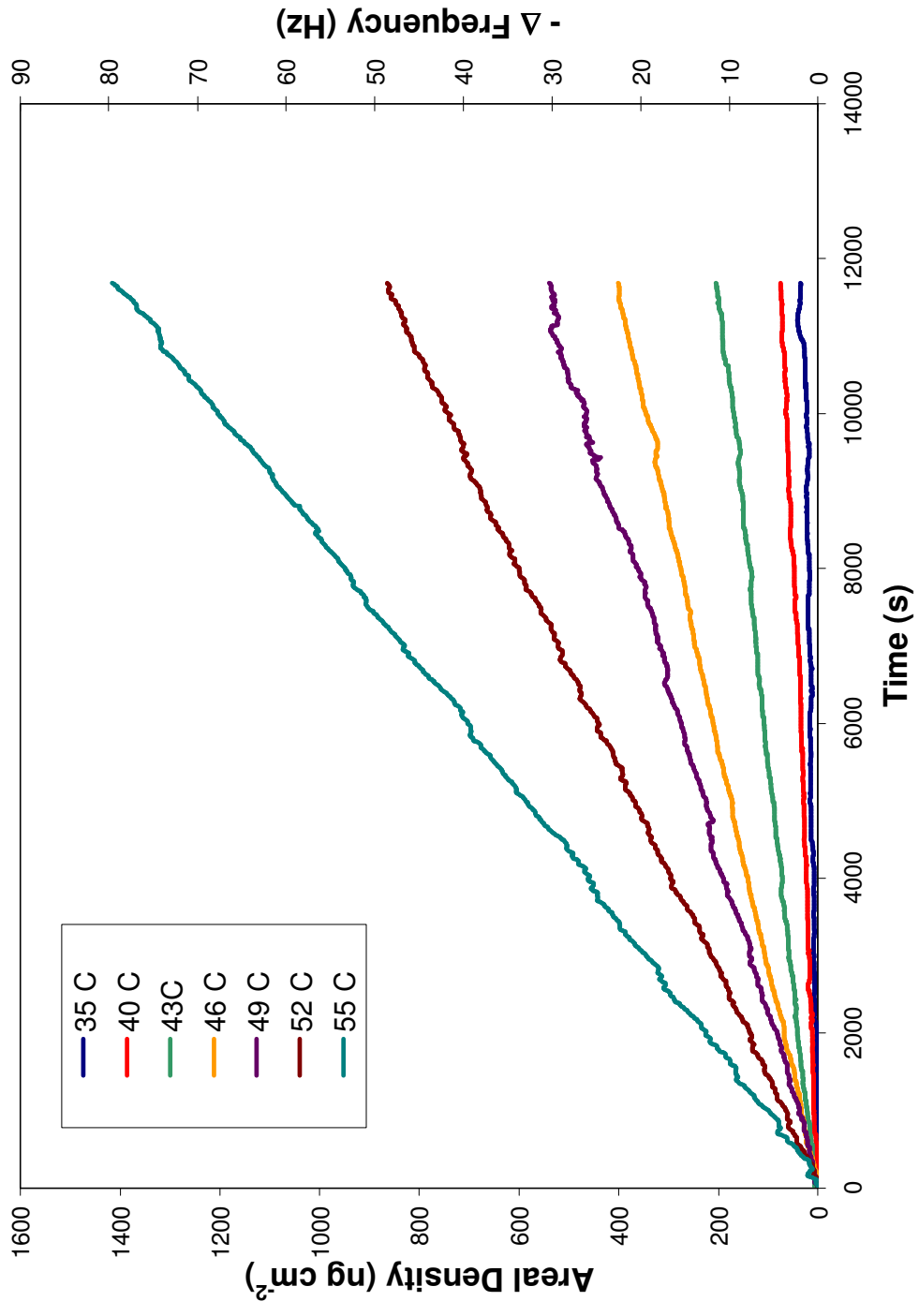

Figure 3.13. Change in areal density and negative change in frequency versus time for the CVDP of glycolide initiated by ZnO at 35 °C, 40 °C, 43 °C, 46 °C, 49 °C, 52 °C and 55 °C.

with time. Again, this indicates that the reaction is pseudo zero order. Also, as the temperature is increased, the rate of polymerization increases. The slope of each individual trend is the overall rate of the reaction which includes contributions from the temperature dependent pressure in the reaction vessel, and the temperature dependent heterogeneous rate constant. These rates are listed in Table 3.2. When compared to the rates for the CVDP of L-lactide, one can see that the CVDP of glycolide proceeds at much faster rates. The increased rates were anticipated from reading the literature and explain my main reason for choosing a lower temperature range. When comparing the rates at 55 ^{o}C, one can see that the rate of the glycolide polymerization is 38.5 times as fast as the L-lactide polymerization. The glycolide polymerization rate at 35 ^{o}C is only slightly slower than the L-lactide polymerization rate at 55 ^{o}C (2.52 x 10^{-3} ng cm^{-2} s^{-1} compared to 3.1 x 10^{-3} ng cm^{-2} s^{-1}). This is in agreement with melt polymerization results in the literature.[50, 84] The negative natural log of the rate constant can be plotted versus the reciprocal of temperature (Figure 3.14). This plot shows a linear relationship. But as with L-lactide, this rate is due to both the vapor pressure and thermal activation. The dependence of the vapor pressure can be removed by dividing the rate constant by the vapor pressure of glycolide. Vapor pressure values were obtained from the literature[66] and used to construct Figure 3.9. The negative natural log of the rate constant divided by the pressure was plotted versus the reciprocal of temperature (Figure 3.15). This Arrhenius plot again shows a linear relationship and the slope is E_a/R. More specifically, I find the activation energy of this process to be 79 ± 11 kJ/mole.

The glycolide CVDP reactions described above were all performed at small areal densities, less than 12 μg/cm^2, and short reaction times, less than six days. at very long

Temperature (^{o}C)	Rate Constant (ng cm^{-2} s^{-1})
35	$2.52 \times 10^{-3} \pm 1 \times 10^{-5}$
40	$6.14 \times 10^{-3} \pm 1 \times 10^{-5}$
43	$1.738 \times 10^{-2} \pm 2 \times 10^{-5}$
46	$3.463 \times 10^{-2} \pm 1 \times 10^{-5}$
49	$4.663 \times 10^{-2} \pm 4 \times 10^{-5}$
52	$7.439 \times 10^{-2} \pm 3 \times 10^{-5}$
55	$1.1916 \times 10^{-1} \pm 5 \times 10^{-5}$

Table 3.2. Rate constants (± 1 SD) and corresponding temperatures for the CVDP of glycolide initiated by ZnO.

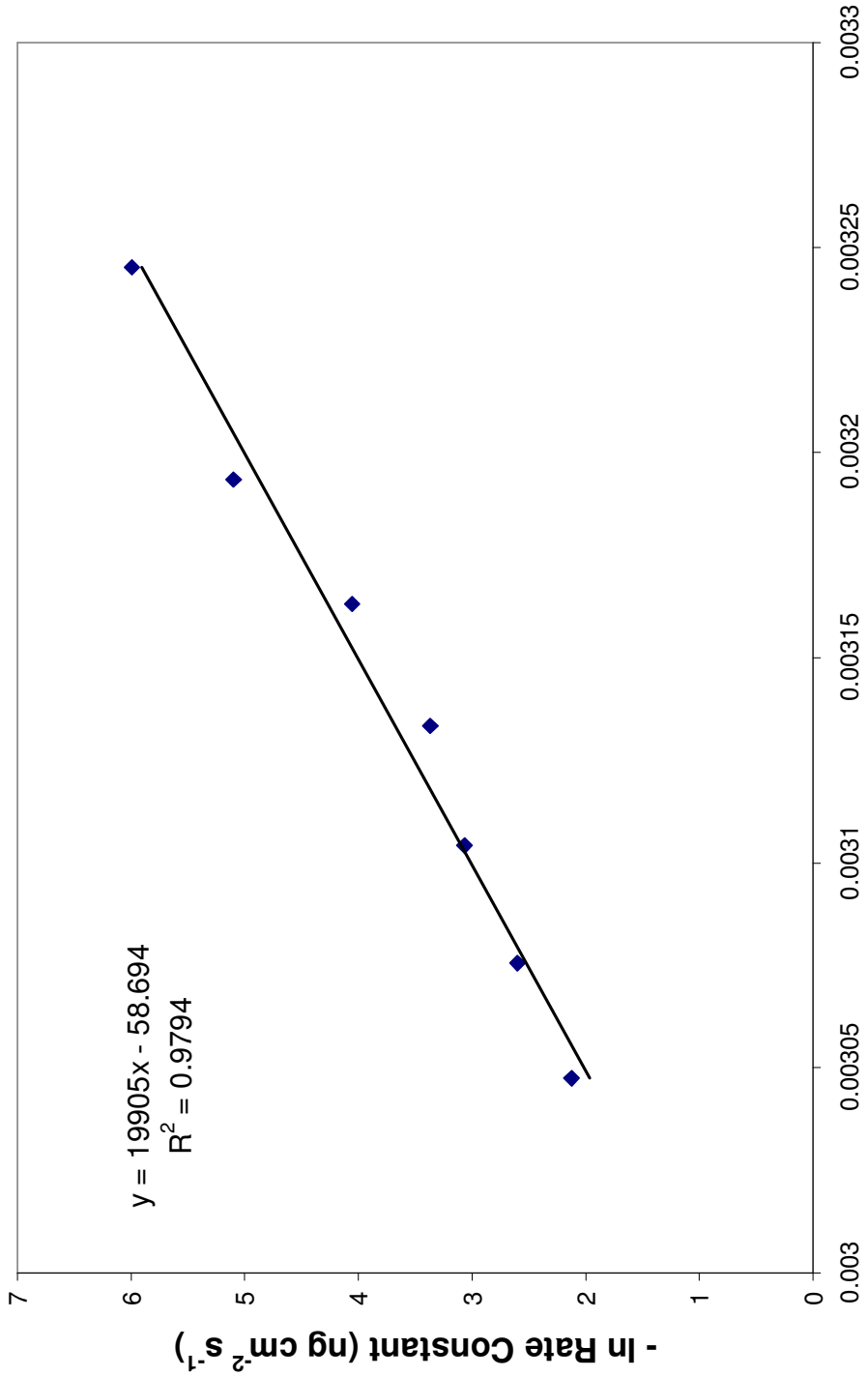

Figure 3.14. Negative natural log of rate constant versus the reciprocal of temperature for the CVDP of glycolide initiated by ZnO.

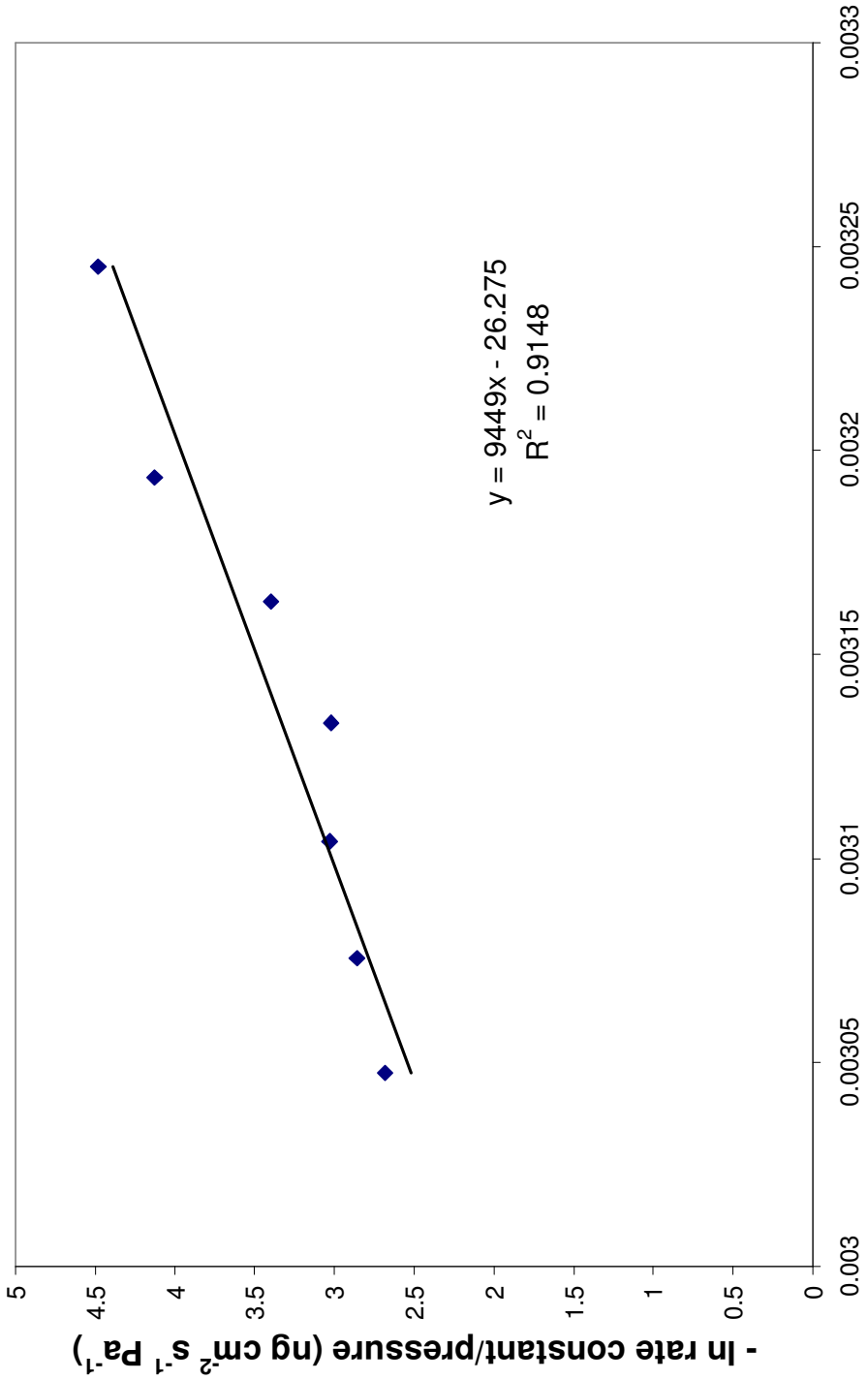

Figure 3.15. Arrhenius plot for the CVDP of glycolide initiated by ZnO.

times an increase in the rate of polymerization was also seen for the polymerization of glycolide. This increase was expected because of the similar structures of glycolide and L-lactide. It is likely that the increase in rate of each process is caused by the same factor, probably the thermal degradation of the polymer.[85] Unexpectedly at even longer reaction times, the glycolide polymerizations slowed and eventually stopped propagating. Upon examination of the Pyrex glass reactor it was noticed that it was no longer clear but slightly hazy. It appeared the Pyrex reaction vessel had polymerized the glycolide. Examination of what was supposed to be excess monomer in the bottom of the reactor confirmed the existence of polymer. The first confirmation was that the material was not soluble in $CDCl_3$, but it did dissolve in HFIP. Polyglycolide is known to be insoluble in most solvents, unless they are highly fluorinated.[53] In addition the ^1H NMR showed the glycolide had been converted to polyglycolide (Figure 3.16). The ^1H NMR was run in a solvent mixture of HFIP and $CDCl_3$ (3:1 ratio v/v) and referenced to the solvent singlet at 7.27 ppm. In Figure 3.16a, a reference sample of glycolide monomer shows a singlet peak at 4.97 ppm. This singlet can be attributed to the methylene protons of glycolide. In Figure 3.16b, a sample of the material from the reactor also shows a singlet peak, but it appeared at 4.86 ppm. No peak is observed at 4.97 ppm that could be attributed to monomer. This peak at 4.86 ppm is the internal methylene protons of polyglycolide. Figure 3.16c is a spectrum of the reactor material spiked with glycolide monomer as a reference. It is clear that at long reaction times the CVDP at the glass surface consumes the vast majority of monomer, thus reducing the glycolide vapor pressure causing the reaction to slow (and ultimately stop) because it is rate limited by mass transfer of glycolide to the surface of the crystal.

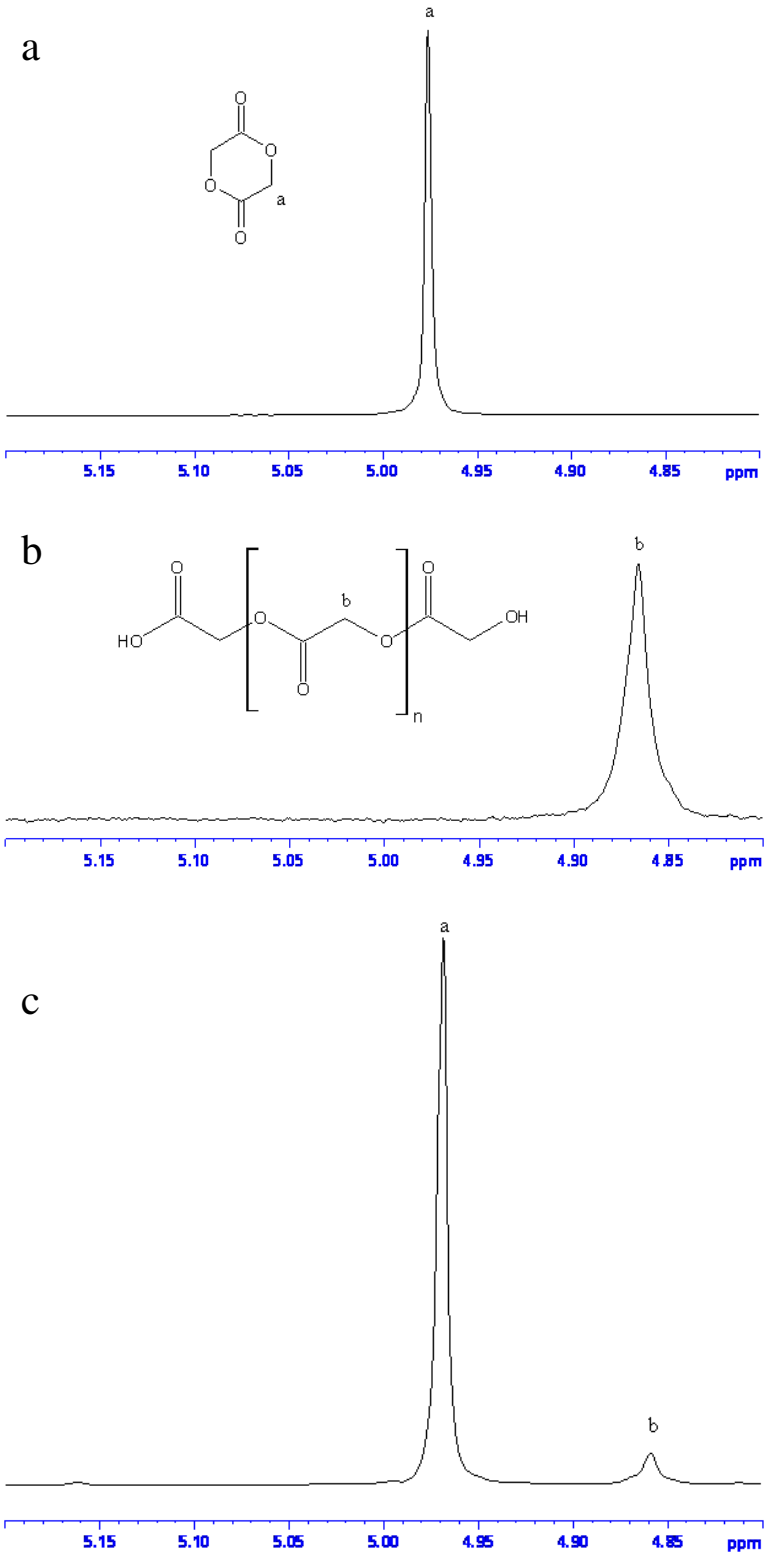

Figure 3.16. ^{1}H NMR spectra of (a) glycolide, (b) material from the CVDP reactor and (c) glycolide and reactor material.

Conclusion

The QCM proves to be an ideal method for studying the CVDP of L-lactide and glycolide at small areal densities and short reaction times. The polymerization of both monomers is pseudo zero order and the reaction rate increases as the temperature is increased. The rate at a given temperature is dependent on both thermal activation and vapor pressure of the monomer. The activation energies for the CVDP of L-lactide and glycolide were found to be 133 kJ/mole and 79 kJ/mole respectively. In future work this method could be applied to the study of the CVDP of other monomers common in biomedical applications such as the lactones ε-caprolactone and p-dioxanone, and lactams such as ε- caprolactam. Different initiators could also be investigated, particularly hydroxyapatite which was shown in the previous chapter to initiate the CVDP of lactones and lactams and is a common component of many biocomposites due to it being the mineral component of bone.

References

1. Pierson, H.O., *Handbook of Chemical Vapor Deposition: Principles, Technology and Applications*. 2nd ed.; William Andrew/Noyes: Norwich, New York, 1999.

2. Kricheldorf, H.R.; Kreiser-Saunders, I.; Damrau, D.-O., Resorbable initiators for polymerization of lactones. *Macromolecular Symposia* **1999**, 144, 269-276.

3. Kricheldorf, H.R.; Serra, A., Polylactones 6. Influence of various metal salts on the optical purity of poly(L-lactide). *Polymer Bulletin* **1985**, 14, 497-502.

4. Kricheldorf, H.R.; Damrau, D.-O., Polylactones 37. Polymerizations of L-lactide initiated with Zn(II) L-lactate and other resorbable Zn salts. *Macromolecular Chemistry and Physics* **1997**, 198, 1753-1766.

5. Bero, M.; Kasperczyk, J.; Jedlinsk, Z., Coordination polymerization of lactides, 1. Structure determination of obtained polymers. *Makromolekulare Chemie* **1990**, 191, 2287-2296.

6. Dittrich, V.W.; Schulz, R.C., Kinetik und Mechanismus der ringöffnenden polymerization von L-lactid. *Angewandte Makromolekulare Chemie* **1971**, 15, 109-126.

7. Chabot, F.; Vert, M.; Chapelle, S.; Granger, P., Configurational structures of lactic acid stereocopolymers as determined by ^{13}C-{^{1}H} N.M.R. *Polymer* **1983**, 24, 53-59.

8. Kricheldorf, H.R.; Boettcher, C., Polylactones XXV. Polymerizations of racemic- and meso-D,L-lactide with Zn, Pb, Sb, and Bi salts – stereochemical aspects. *Journal of Macromolecular Science. Pure and Applied Chemistry* **1993**, 30, 441-448.

9. Blanquet, E.; Schuster, F., Chemical vapor deposition: Principles and applications. In *Vapor Surface Treatments*. Galerie, A., Ed.; John Wiley and Sons: Hoboken, New Jersey, 2010; p 139-161.

10. Fortin, J.B.; Lu, T.-M., *Chemical Vapor Deposition Polymerization: The Growth and Properties of Parylene Thin Films*; Kluwer Academic: Norwell, Massachusetts, 2004; p 42.

11. Pattanaik, A.K.; Sarin, V.K., Basic principles of CVD thermodynamics and kinetics. In *Chemical Vapor Deposition*. Park, J.-H.; Sudarshan, T.S., Eds.; ASM International: Materials Park, Ohio, 2001; p 33-34.

12. Xu, Y.; Yan, X.-T., *Chemical Vapour Deposition: An Integrated Engineering Design for Advanced Materials*; Springer: London, 2010.

13. Sherman, A., *Chemical Vapor Deposition for Microelectronics: Principles, Technology, and Applications*; Noyes: Park Ridge, New Jersey, 1987.

14. Dobkin, D.M.; Zuraw, M.K., *Principles of Chemical Vapor Deposition: What's Going on Inside the Reactor*; Kluwer Academic: Dordrecht, The Netherlands, 2003.

15. van de Ven, J.; Rutten, G.M.J.; Raaijmakers, M.J.; Giling, L.J., Gas phase depletion and flow dynamics in horizontal MOCVD reactors. *Journal of Crystal Growth* **1986**, 76, 352-372.

16. Retzloff, D.G., Chemical vapor deposition. In *Encyclopedia of Chemical Processing Volume 1*. Sunggyu, L., Ed.; Taylor and Francis Group: New York, 2006; 441-448.

17. Paorici, C.; Attolini, G., Interface kinetics and the vapour phase mass transport in closed tube CdS:I_2-System. *Kristall und Technik* **1979**, 14, 645-651.

18. Choy, K.L., Chemical vapour deposition of coatings. *Progress in Materials Science* **2003**, 48, 57-170.

19. Hitchman, M.L., A consideration of the effect of the thermal boundary layer on CVD growth rates. *Journal of Crystal Growth* **1980**, 48, 394-402.

20. Jones, A.C.; Hitchman, M.L., Overview of chemical vapour deposition. In *Chemical Vapour Deposition: Precursors, Processes and Applications*. Jones, A.C.; Hitchman, M.L., Eds.; Royal Society of Chemistry: Cambridge, United Kingdom, 2009.

21. Kern, W.; Schnable, G.L., Low-pressure chemical vapor deposition for very large-scale integration processing – A review. *IEEE Transactions on Electron Devices* **1979**, 26, 647-657.

22. van Sark, W.G.J.H.M.; de Croon, M.H.J.M.; Janssen, G.; Giling, L.J., Analytical models for growth by metal organic vapour phase epitaxy: II. Influence of temperature gradient. *Semiconductor Science and Technology* **1990**, 5, 36-44.

23. Vrentas, J.S.; Vrentas, C.M., Transport effects in low-pressure chemical vapor deposition reactors. *Chemical Engineering Series* **1988**, 43, 1437-1445.

24. Wain, K.S.; Sen, A.; Kim, S.H., Growth of polystyrene films via gas-phase polymerization with $[Pd(CH_3CN)_4][BF_4]_2$ thin film catalyst. *Journal of Polymer Science: Part A: Polymer Chemistry* **2005**, 43, 1930-1934.

25. Rabek, J.F.; Linden, L.A.; Adamczak, E.; Sanetra, J.; Starzyk, F.; Pielichowski, J., Polymerization of thin pyrrole films on poly(ethylene oxide) – $FeCl_3$ coordination complex. *Materials Science Forum* **1995**, 191, 225-234.

26. Russell, S.P.; Weinkauf, D.H., Vapor sorption in plasma polymerized vinyl acetate and methyl methacrylate thin films. *Polymer* **2001**, 42, 2827-2836.

27. Aubert, J.H., Solubility of carbon dioxide in polymers by the quartz crystal microbalance technique. *Journal of Supercritical Fluids* **1998**, 11, 163-172.

28. Kurosawa, S.; Hirokawa, T.; Kashima, K.; Aizawa, H.; Han, D.-S.; Yoshimi, T.; Okada, Y.; Yase, K.; Miyake, J.; Yoshimoto, M.; Hilborn, J., Detection of deposition rate of plasma-polymerized films by quartz crystal microbalance. *Journal of Thin Solid Films* **2000**, 374, 262-267.

29. Niwa, M.; Date, M.; Higashi, N., In situ photopolymerization of methacrylic acid at a self-assembled xanthate monolayer surface on gold. Formation of poly(methacrylic acid) brushes and their interaction with cytochrome c. *Macromolecules* **1996**, 29, 3681-3685.

30. Kvarnström, C.; Bilger, R.; Ivaska, A.; Heinze, J., An electrochemical quartz crystal microbalance study on polymerization of oligo-p-phenylenes. *Electrochimica Acta* **1998**, 43, 355-366.

31. Winther-Jensen, B.; Chen, J.; West, K.; Wallace, G., Vapor phase polymerization of pyrrole and thiophene using iron(III) sulfonates as oxidizing agents. *Macromolecules* **2004**, 37, 5930-5935.

32. Curie, P.; Curie, J., Développement, par pression, de l'électricité polaire dans les cristaux hémièdres à faces inclines. *Comptes Rendus* **1880**, 91, 294-295.

33. Arnau, A.; Soares, D., Fundamentals of piezoelectricity. In *Piezoelectric Transducers and Applications*. 2nd ed. Arnau, A., ed.; Springer: Berlin, Germany, 2008.

34. Lippmann, G., Principe de conservation de l'électricité. *Annales de Physique et de Chimie, 5a Serie* **1881**, 24, 145-178.

35. O'Sullivan, C.K.; Guibault, G.G., Commercial quartz crystal microbalances – theory and applications. *Biosensors and Bioelectronics* **1999**, 14, 663-670.

36. Gamry Instruments, *Basics of a Quartz Crystal Microbalance*. http://www.gamry.com/App_Notes/Basics_of_QCM.pdf. Accessed June 25,2011.

37. Smith, A.L., The quartz crystal microbalance. In *Handbook of Thermal Analysis and Calorimetry, Volume 5: Recent Advances, Techniques and Applications*. Brown, M.E.; Gallagher, P.K., eds.; Elsevier: Amsterdam, The Netherlands, 2008.

38. Sauerbrey, G., Verwendung von schwingquarzen zur wägung dünner schichten und zur mikrowägung. *Zeitschrift für Physik* **1959**, *155*, 206-222.

39. Lu, C. Theory and Practice of the Quartz Crystal Microbalance. In *Applications of Piezoelectric Quartz Crystal Microbalances*. Lu, C., Czanderna, A.W., eds.; Elsevier: Amsterdam, The Netherlands, 1984.

40. Lucklum, R.; Behling, C.; Hauptmann, P., Gravimetric and non-gravimetric chemical quartz resonators. *Sensors and Actuators B* **2000**, 65, 277-283.

41. Lu, C.-S.; Lewis, O., Investigation of film-thickness determination by oscillating quartz resonators with large mass load. *Journal of Applied Physics* **1972**, 43, 4385-4390.

42. Kanazawa, K.K.; Gordon, J.G., Frequency of a quartz microbalance in contact with liquid. *Analytical Chemistry* **1985**, 57, 1770-1771.

43. Martin, S.J.; Granstaff, V.E.; Frye, G.C., Characterization of a quartz crystal microbalance with simultaneous mass and liquid loading. *Analytical Chemistry* **1991**, 63, 2272-2281.

44. Nederberg, F.; Connor, E. F.; Moller, M.; Glauser, T.; Hedrick, J. L., New paradigms for organic catalysts: The first organocatalytic living polymerization. *Angewandte Chemie-International Edition* **2001,** 40, 2712-2715.

45. Kalmi, M.; Lahcini, M.; Castro, P.; Lehtonen, O.; Belfkira, A.; Leskela, M.; Repo, T., Tetrakis Sn(IV) alkoxides as novel initiators for living ring-opening polymerization of lactides. *Journal of Polymer Science Part A-Polymer Chemistry* **2004,** 42, 1901-1911.

46. Thakur, K. A. M.; Kean, R. T.; Hall, E. S.; Kolstad, J. J.; Munson, E. J., H-1 NMR spectroscopy in the analysis and characterization of poly(lactide). *International Journal of Polymer Analysis and Characterization* **1998,** 4, 379-391.

47. Espartero, J. L.; Rashkov, I.; Li, S. M.; Manolova, N.; Vert, M., NMR analysis of low molecular weight poly(lactic acid)s. *Macromolecules* **1996,** 29, 3535-3539.

48. Li, H.; Wang, C.; Bai, F.; Yue, J.; Woo, H.-G., Living ring-opening polymerization of L-lactide catalyzed by Red-Al. *Organometallics* **2004**, 23, 1411-1415.

49. Zini, E.; Scandola, M.; Dobrzynski, P.; Kasperczyk, J.; Bero, M., Shape memory behavior of novel (L-lactide-glycolide-trimethylene carbonate) terpolymers. *Biomacromolecules* **2007,** 8, 3661-3667.

50. Dechy-Cabaret, O.; Martin-Vaca, B.; Bourissou, D., Controlled ring-opening polymerization of lactide and glycolide. *Chemical Reviews* **2004,** 104, 6147-6176.

51. Cai, Q.; Bei, J. Z.; Wang, S. G., Synthesis and degradation of a tri-component copolymer derived from glycolide, L-lactide, and epsilon-caprolactone. *Journal of Biomaterials Science-Polymer Edition* **2000,** 11, 273-288.

52. Dobrzynski, P.; Kasperczyk, J.; Bero, M., Application of calcium acetylacetonate to the polymerization of glycolide and copolymerization of glycolide with epsilon caprolactone and L-lactide. *Macromolecules* **1999,** 32, 4735-4737.

53. Hariharan, R.; Pinkus, A.G., Useful NMR solvent mixture for polyesters: Trifluoroacetic acid-d/chloroform-d. *Polymer Bulletin* **1993**, 30, 91-95.

54. Pinkus, A.G.; Subramanyam, R., New high-yield, one-step synthesis of polyglycolide from haloacetic acids. *Journal of Polymer Science. Polymer Chemistry Edition* **1984**, 22, 1131-1140.

55. Chisholm, M. H.; Eilerts, N. W.; Huffman, J. C.; Iyer, S. S.; Pacold, M.; Phomphrai, K., Molecular design of single-site metal alkoxide catalyst precursors for ring-opening polymerization reactions leading to polyoxygenates. 1. Polylactide formation by achiral and chiral magnesium and zinc alkoxides, (eta(3)-L)MOR, where L = trispyrazolyl- and trisindazolylborate ligands. *Journal of the American Chemical Society* **2000,** 122, 11845-11854.

56. Chisholm, M. H.; Gallucci, J.; Phomphrai, K., Coordination chemistry and reactivity of monomeric alkoxides and amides of magnesium and zinc supported by the diiminato ligand CH(CMeNC6H3-2,6-Pr-i(2))(2). A comparative study. *Inorganic Chemistry* **2002,** 41, 2785-2794.

57. Kricheldorf, H. R.; Boettcher, C., Polylactones. 27. Anionic-polymerization of L-lactide - Variation of end groups and synthesis of block-copolymers with poly(ethylene oxide). *Makromolekulare Chemie-Macromolecular Symposia* **1993,** 73, 47-64.

58. Kricheldorf, H. R.; Berl, M.; Scharnagl, N., Poly(lactones). 9. Polymerization mechanism of metal alkoxide initiated polymerizations of lactide and various lactones. *Macromolecules* **1988,** 21, 286-293.

59. Albertsson, A.-C.; Varma, K.I., Recent developments in ring opening polymerization of lactones for biomedical applications. *Biomacromolecules* **2003,** 4.

60. Westerhausen, M.; Schneiderbauer, S.; Kneifel, Alexander N.; Söltl, Y.; Mayer, P.; Nöth, H.; Zhong, Z.; Dijkstra, Pieter J.; Feijen, J., Organocalcium compounds with catalytic activity for the ring-opening polymerization of lactones. *European Journal of Inorganic Chemistry* **2003,** 2003, 3432-3439.

61. Schwach, G.; Coudane, J.; Engel, R.; Vert, M., Ring opening polymerization of D,L-lactide in the presence of zinc metal and zinc lactate. *Polymer International* **1998,** 46, 177-182.

62. Penczek, S.; Duda, A., Kinetics and mechanisms in anionic ring-opening polymerization. *Makromolekulare Chemie-Macromolecular Symposia* **1993,** 67, 15-42.

63. Ouhadi, T.; Hamitou, A.; Jerome, R.; Teyssie, P., Soluble bimetallic μ-oxoalkoxides. 8. Structure and kinetic behavior of the catalytic species in unsubstituted lactone ring-opening polymerization. *Macromolecules* **1976,** 9, 927-931.

64. Miola-Delaite, C.; Hamaide, T.; Spitz, R., Anionic coordinated polymerization of epsilon-caprolactone with aluminum, zirconium and some rare earths alkoxides as initiators in the presence of alcohols. *Macromolecular Chemistry and Physics* **1999,** 200, 1771-1778.

65. Emel'yanenko, V.N.; Verevkin, S.P.; Pimerzin, A.A., The thermodynamic properties of DL- and L-lactides. *Russian Journal of Physical Chemistry A* **2009**, 83, 2013-2021.

66. Emel'yanenko, V.N.; Verevkin, S.P.; Stepurko, E.N.; Roganov, G.N.; Georgieva, M.K., Thermodynamic properties of glycolic acid and glycolide. *Russian Journal of Physical Chemistry A* **2010**, 84, 1301-1308.

67. Lucklum, R.; Soares, D.; Kanazawa, K., Models for resonant sensors. In *Piezoelectric Transducers and Applications*, 2nd ed. Arnau, A., ed.; Springer: Berlin, Germany, 2008.

68. Jiménez, Y.; Otero, M.; Arnau, A., QCM data analysis and interpretation. In *Piezoelectric Transducers and Applications*, 2nd ed. Arnau, A., ed.; Springer: Berlin, Germany, 2008.

69. Nishida, H., Thermal degradation. In *Poly(lactic acid): Synthesis, Structures, Properties, Processing, and Applications*. Auras, R.; Lim, L.-T.; Selke, S.E.M.; Tsuji, H., eds.; John Wiley and Sons: Hoboken, New Jersey, 2010.

70. Hakkarainen, M.; Karlsson, S.; Albertsson, A.-C., Influence of low molecular weight lactic acid derivatives on degradability of polylactide. *Journal of Applied Polymer Science* **2000**, 76, 228-239.

71. McNeill, I.C.; Leiper, H.A., Degradation studies of some polyesters and polycarbonates – 1. Polylactide: General features of the degradation under programmed heating conditions. *Polymer Degradation and Stability* **1985**, 11, 267-285.

72. McNeill, I.C.; Leiper, H.A., Degradation studies of some polyesters and polycarbonates – 2. Polylactide: Degradation under isothermal conditions, thermal degradation mechanism and photolysis of the polymer. *Polymer Degradation and Stability* **1985**, 11, 309-326.

73. Tsuji, H.; Fukui, I.; Daimon, H.; Fujie, K., Poly(L-lactide) XI. Lactide formation by thermal depolymerisation of poly(L-lactide) in a closed system. *Polymer Degradation and Stability* **2003**, 81, 501-509.

74. Garozzo, D.; Giuffrida, M.; Montaudo, G., Primary thermal decomposition processes in aliphatic polyesters investigated by chemical ionization mass spectrometry. *Macromolecules* **1986**, 19, 1643-1649.

75. Kopinke, F.-D.; Remmler, M.; Mackenzie, K.; Möder, M.; Wachsen, O., Thermal decomposition of biodegradable polyesters – II. Poly(lactic acid). *Polymer Degradation and Stability* **1996**, 53, 329-342.

76. Lüderwald, I., Thermal degradation of polyesters in the mass spectrometer. In *Developments in Polymer Degradation, Volume 2*. Grassie, N., ed.; Applied Science Publishers: London, United Kingdom, 1979.

77. Wachsen, O.; Platkowski, K.; Reichert, K.H., Thermal degradation of poly-L-lactide – studies on kinetics, modeling and melt stabilisation. *Polymer Degradation and Stability* **1997**, 57, 87-94.

78. Yu, H.; Huang, N.; Wang, C.; Tang, Z., Modeling of poly(L-lactide) thermal degradation: Theoretical prediction of molecular weight and polydispersity index. *Journal of Applied Polymer Science* **2003**, 88, 2557-2562.

79. Wachsen, O.; Reichert, K.H.; Krüger, R.P; Much, H.; Schulz, G., Thermal decomposition of biodegradable polyesters – III. Studies on the mechanisms of thermal degradation of oligo-L-lactide using SEC, LACCC and MALDI-TOF-MS. *Polymer Degradation and Stability* **1997**, 55, 225-231.

80. Abe, H.; Takahashi, N.; Kim, K.J.; Mochizuki, M.; Doi, Y., Thermal degradation processes of end-capped poly(L-lactide)s in the presence and absence of residual zinc catalyst. *Biomacromolecules* **2004**, 5, 1606-1614.

81. Motoyama, T.; Tsukegi, T.; Shirai, Y.; Nishida, H.; Endo, T., Effects of MgO catalyst on depolymerization of poly-L-lactic acid to L,L-lactide. *Polymer Degradation and Stability* **2007**, 92, 1350-1358.

82. Jamshidi, K.; Hyon, S.-H.; Ikada, Y., Thermal characterization of polylactides. *Polymer* **1988**, 29, 2229-2234.

83. Garlotta, D., A literature review of poly(lactic acid). *Journal of Polymers and the Environment* **2001**, 9, 63-84.

84. Yin, M.; Baker, G.L., Preparation and characterization of substituted polylactides. *Macromolecules* **1999**, 32, 7711-7718.

85. McNeill, I.C.; Leiper, H.A., Degradation studies of some polyesters and polycarbonates: 3 – Polyglycolide. *Polymer Degradation and Stability* **1985**, 12, 373-385.

Chapter Four

Preparation and Characterization of a Demineralized Bone Matrix Simulant (DBMS) Prepared from Composites of Anorganic Bovine Bone and Polylactones or Polylactams

Introduction and Background

The previous two chapters have focused on the chemical vapor deposition polymerization (CVDP) of various polylactones and polylactams initiated by the surface of a porous ceramic scaffold, usually hydroxyapatite, and the kinetics of this reaction. This process was shown to retain the porosity of the original scaffold and create a mechanically strong composite that could potentially be used as a bone graft material. The focus in this chapter will shift to the preparation of a different type of porous scaffold that could potentially be used for the same purpose. The scaffolds in this chapter will be prepared by the ultimate removal of the inorganic material from anorganic bone/polymer composites, leaving a porous polymer scaffold with a structure similar to demineralized bone matrix (DBM).

Bone grafting is a common reconstructive orthopedic procedure in which large defects (e.g. non-union in the bone due to fractures, tumors, or other diseases) are repaired through implantation of various natural and manufactured biocompatible materials. As stated in Chapter 1, the current gold standard for such procedures is autogenous bone, due to its osteogenic, osteoconductive, and osteoinductive properties, plus the lack of disease transmission or immunogenicity. The most important problem with autogenous bone is its limited supply. Other concerns include variable quality, operation time and blood loss, increased morbidity, chronic donor site pain, and increased cost.[1-3] Some of these obstacles can be overcome through the use of bone allografts,

which still provide an osteoconductive matrix but have limited osteoinductive properties. The disadvantages of using allografts include the possibility of disease transmission, complications at the host-donor junction, slow replacement times, lack of osteogenesis, and limited osteoinduction in preserved samples.[2, 4] Fresh allografts are rarely used because the speed at which the grafting transfer must be completed leaves no time for sterilization or disease testing. Additionally, allografts often evoke an intense immune response. Freeze drying and deep freezing are the most widely used techniques for the preservation of allografts. Deep freezing at temperatures below -60 ^{o}C decreases the immunogenicity of the allograft while maintaining the mechanical properties. Freeze drying has the same effect on the immunogenicity but alters the mechanical properties.[5] In countries where power shortages in hospitals are common, preservation is an important issue.[2, 6, 7]

DBM is a type of processed allograft that was developed, in part, as a solution to the above problems.[6] It was first used by Nicholas Senn in 1889 in the treatment of bone cavities.[8] DBM is prepared by the removal of the mineral phase of the bone, hydroxyapatite (HA). This can be accomplished by using acids such as hydrochloric acid (HCl) to solublize the mineral phase or by using chemicals such as ethylenediamine tetraacetic acid (EDTA) that dissolve HA by chelating its calcium ions. The organic matrix that is left behind consists of noncollagenous proteins, bone growth factors, and collagen.[6, 9, 10] Although both methods successfully demineralize the bone, different noncollagenous proteins are left behind.[9, 11, 12] The resulting organic matrix is osteoconductive and osteoinductive but has virtually no structural strength.[6, 13] Consequently, DBM is often used in powder or putty form. The osteoinductive

properties of DBM where first recognized by Urist in 1965.[14] Since then it has been discovered that the osteoinductivity is due primarily to low molecular weight glycoproteins including bone morphogenic proteins (BMPs).[15] The complex mechanism by which DBM stimulates new bone growth is dependent on many factors, including extent of demineralization, particle size, donor related effects, preparation of the matrix, and degradation of the matrix during demineralization.[10, 16, 17] Due to these many variables, the clinical outcome is often difficult to predict.

Synthetic materials made from biodegradable polymers, ceramics, and metals are increasingly being used in bone graft procedures. While synthetic materials may lessen the threat of certain forms of rejection, the development of biomaterials with desirable chemical, physical, and mechanical properties is challenging. To overcome these problems, researchers have developed a variety of new materials that are biomimetic and bioinspired, attempting to copy the blueprint provided by nature.[18-22] In previous work, anorganic bovine bone was reconstituted using the inorganic portion, HA, to initiate the polymerization of L-lactide. The resulting product exhibited macroscopic and microscopic morphologies similar to the original bone.[23] I describe below a process to remove the HA template from these composites to produce DBM simulants (DBMS) comprised of various polylactones and polylactams. The resulting porous scaffold has microscopic morphologies similar to that of DBM. Furthermore, the demineralized bone matrix simulants described below maintain their original macroscopic shape and structure after demineralization and can exhibit improved mechanical properties over DBM.

Experimental

Chemicals: Ammonium hydroxide (NH_4OH, 28-30% from VWR, Radnor, PA), deuterated chloroform ($CDCl_3$, 99.8% D from Sigma-Aldrich, St. Louis, MO), disodium ethylenediamine tetraacetic acid (Na_2EDTA, 99% from Fisher, Waltham, MA), ε-caprolactam (99%+ from Acros Organics, Geel, Belgium), ε-caprolactone (99% from Acros Organics), ethylenediamine (99% from Sigma Aldrich), hydrochloric acid (HCl, from Fisher), polystyrene (PolyCAL^{TM} gel permeation chromatography (GPC) standards from Viscotek, Worchestershire, U.K.), tetrahydrofuran (THF, HPLC grade from Sigma Aldrich), and 2,2,2-trifluoroethanol (TFE, ≥ 99% from Sigma Aldrich) were used as purchased from their respective suppliers. L-Lactide (from Purac, Lincolnshire, IL) was sublimed at 90 ^{o}C and then transferred into a $N_{2(g)}$ atmosphere glove box for further use. Anorganic cortical bone was obtained from bovine femur donated by Premium Protein Products (Lincoln, NE).

Preparation of anorganic bone (AB)/poly-L-lactide (PLLA), AB/poly-ε-caprolactone (PCLN), AB/poly-ε-caprolactam (PCLM) composites: A band saw was used to remove the distal and proximal ends of the bovine femurs and to cut them into 1.5 to 2 cm thick sections along their length. Cylindrical plugs of cortical bone, with a diameter of 6 mm and a length between 12 and 20 mm, were machined in the longitudinal direction from the diaphyseal section of the bovine femur using a 6 mm diameter dowel tool (Figure 4.1). A Soxhlet extractor was then used to remove the majority of the organic material. The solvent mixture used for the extraction was 80% ethylenediamine and 20% deionized water (v/v).[24] The solvent was observed to reflux at 119 ^{o}C. The samples were extracted for a minimum of 48 hr. Fresh solvent was cycled through approximately every 10 min. After the extraction period, the solvent mixture

Figure 4.1. Cylindrical cortical bone plugs cut using an end mill and 6 mm dowel tool.

was replaced with deionized water. The Soxhlet extraction of the bone cylinders with water was continued until the water was neutral pH. The water was replaced 3-4 times during this process. At this stage the bone cylinders, which were greatly whitened, were removed and allowed to dry at room temperature in air. Samples were then activated by being heated at either 600 ^{o}C for 96 hr or 700 ^{o}C for 16 hr in air. They were then placed in a vacuum desiccator, cooled to room temperature under vacuum, and transferred to a $N_{2(g)}$ atmosphere glove box for later use.

To begin the polymerization, an anorganic bone plug was placed in a Pyrex glass tube that was approximately 9.5 mm in diameter. For reactions run with L-lactide and ε-caprolactone, the plugs were placed in a ¼" diameter Teflon sleeve that made sample removal from the reaction vessel easier upon completion of the reaction. An excess of L-lactide, ε-caprolactone, or ε-caprolactam was added to the tube. Enough monomer was added to ensure that the sample was completely covered. The tubes were sealed with a short section of tygon tubing that was closed with a hose clamp. They were then removed from the $N_{2(g)}$ glove box and attached to a rotary vane rough pump. The samples were maintained under a vacuum for 10 min before the bottom was dipped in liquid N_2 and the vacuum was maintained for an additional 5 min. The tubes were then sealed at a reduced pressure (~30 mTorr) after placing a slight constriction near the midsection. L-Lactide and ε-caprolactone reactions were placed in a convection oven at 130 ^{o}C. Upon melting, the monomer infused into the pores of the anorganic bone, where the ring opening polymerization (ROP) was initiated by the surface of the HA.[23] After 3 days, the samples were inverted so excess monomer could drain away from the sample. The constriction kept the sample from sliding to the other end of the tube (Figure 4.2).

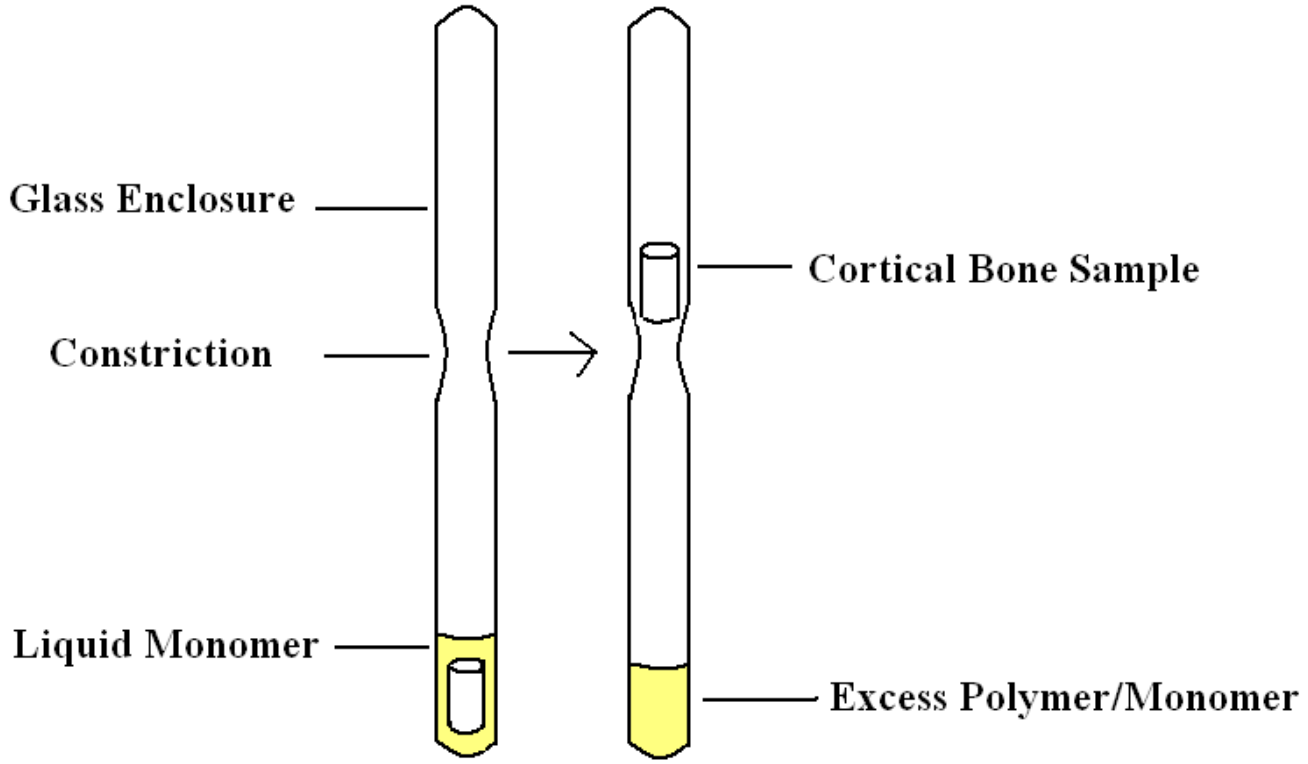

Figure 4.2. Method used to create AB/polymer composites. The AB plug is first immersed in the liquid monomer for several days. At this point it is inverted and excess monomer is allowed to drain to the bottom while the constriction keeps the sample from doing the same.

The reaction was allowed to proceed for an additional 3-4 days. ε-Caprolactam samples were placed in a convection oven at 250 ^{o}C. They were immersed for 4 days, then inverted, and allowed to react an additional 4 days. After this time, the reaction vessels were removed from the oven and allowed to cool to room temperature. Samples were then removed from the reaction vessels and excess polymer on the outside of the cylinder was removed using a Colchester-Clausing lathe. A rotation speed of 800 rpm was used to machine the samples into cylinders with a height to diameter ratio of 2:1, typically 11 mm x 5.5 mm.

Preparation of DBMS from AB/PLLA, PLCN, PLCM composites: The HA was then removed from the composites prepared as described above. Samples were extracted in either a 0.6 M HCl or 0.5 M EDTA solution. The EDTA was dissolved by adding ammonium hydroxide and then adjusting the pH to 7 using concentrated HCl. Samples were placed in 40 ml of the HCl or EDTA solution for 7 days. The solutions were replaced every 2 days. Following their extraction, samples were placed into deionized water to remove any remaining HCl or EDTA. Samples were then stored in water or allowed to air dry.

X-Ray powder diffraction (XRD) was performed using a Rigaku (Tokyo, Japan) D-Max/B Horizontal Q/2Q X-Ray diffractometer (Nebraska Center for Materials and Nanoscience (NCMN), University of Nebraska-Lincoln (UNL)). X-Rays were produced by a 2 kW copper target with K_{α} of λ = 154.4 pm. The acquired diffraction patterns were referenced to standards from the International Centre for Diffraction Data. Scanning electron microscopy (SEM) was performed using a Hitachi (Tokyo, Japan) S4700 Field-Emission microscope (Morrison Microscopy Core Research Facility, UNL). Mechanical

properties of the DBMS were measured using a single-axis Instron 5967 electromechanical machine with a 30 kN load cell (Department of Chemistry, UNL). Instrument control, data acquisition, and data processing were performed using Blue Hill version 2.23 software (Norwood, MA). For mechanical testing, the samples were machined into rods between 1.0 – 1.2 cm in length and 0.5 – 0.6 cm in diameter. The specimens were then subjected to compression testing using a 1.0 mm/min crosshead speed. Molecular weights were estimated using a Viscotek VE 2001 GPC (Department of Chemistry, UNL). All samples are referenced to polystyrene standards. THF was used for the mobile phase at a flow rate of 1 ml/min. Detection was accomplished with a Viscotek VE 3580 refractive index detector. ^{1}H NMR spectra were obtained using a Bruker (Billerica, MA) 300 MHZ or 400 MHz Bruker DRX Avance spectrometer (Research Instrumentation Facility (RIF), UNL). Spectral processing was done using Bruker Topspin 3.0.b.8. PLLA and PCLN samples were dissolved in $CDCl_3$ and all chemical shifts were reported in ppm referenced to the solvent peak, which was assigned a value of 7.27 ppm. PLCM samples were dissolved in a solution containing a 3:1 ratio (v/v) of trifluoroethanol and $CDCl_3$. Again, all chemical shifts were referenced to the $CDCl_3$ peak at 7.27 ppm. Chemical shifts for PLLA,[25-29] PLCN,[30-33] and PCLM[34, 35] were verified by comparison to values reported previously in the literature.

Results and Discussion

The organic material in bone is the primary source of undesirable immune response when used as a bone graft.[36] The removal of this organic material produces a porous inorganic template that has the same structure as the original bone. This material is known as anorganic bone.[37] The mineral phase is hydroxyapatite (HA,

$Ca_{10}(PO_4)_6(OH)_2$) that is highly substituted, with carbonate (CO_3^{-2}) ions often replacing phosphate (PO_4^{-3}) or hydroxyl (OH^-) ions, fluoride (F^-) and chloride (Cl^-) ions replacing OH^- ions, and various metal ions such as magnesium (Mg^{2+}), sodium (Na^+), potassium (K^+), or strontium (Sr^{2+}) replacing calcium (Ca^{2+}) ions.[38] Previous work has shown that when the anorganic bone template is heated under vacuum in the presence of L-lactide, the liquid monomer infuses the pores left behind by the removal of the organic material and the ring opening polymerization is initiated by the nucleophilic surface of the HA. The resulting ceramic/polymer composite has a structure that is similar to the original bone.[23] This process can be applied to other similar monomers such as ε-caprolactone, glycolide, p-dioxanone, or ε-caprolactam to produce similar composites.

If the polymer infuses the pores left behind by the organic material, then removing the inorganic portion of the composite should produce a porous polymer scaffold that has a structure similar to DBM. Figure 4.3 shows SEM images of cryofractured PCLN DBMS and PCLM DBMS samples prepared by removing the HA from AB/polymer composites as was described in the experimental section. Removal of the HA leaves behind a highly porous polymer scaffold that is similar to the microscopic structure of DBM.[39, 40] Similar to the porous scaffolds described in the previous chapters, this porous polymer DBMS could potentially provide a suitable osteoconductive scaffold for bone growth, allowing diffusion of nutrients, waste removal, and a place for bone cells to proliferate.[40-43] One major difference between the DBMS described in this chapter and actual DBM is the DBMS retains its original shape after the removal of HA. DBM contracts significantly upon drying and therefore is often used as powders, chips or in gel form in conjunction with other grafting materials.[6] Figure 4.4 shows an example of

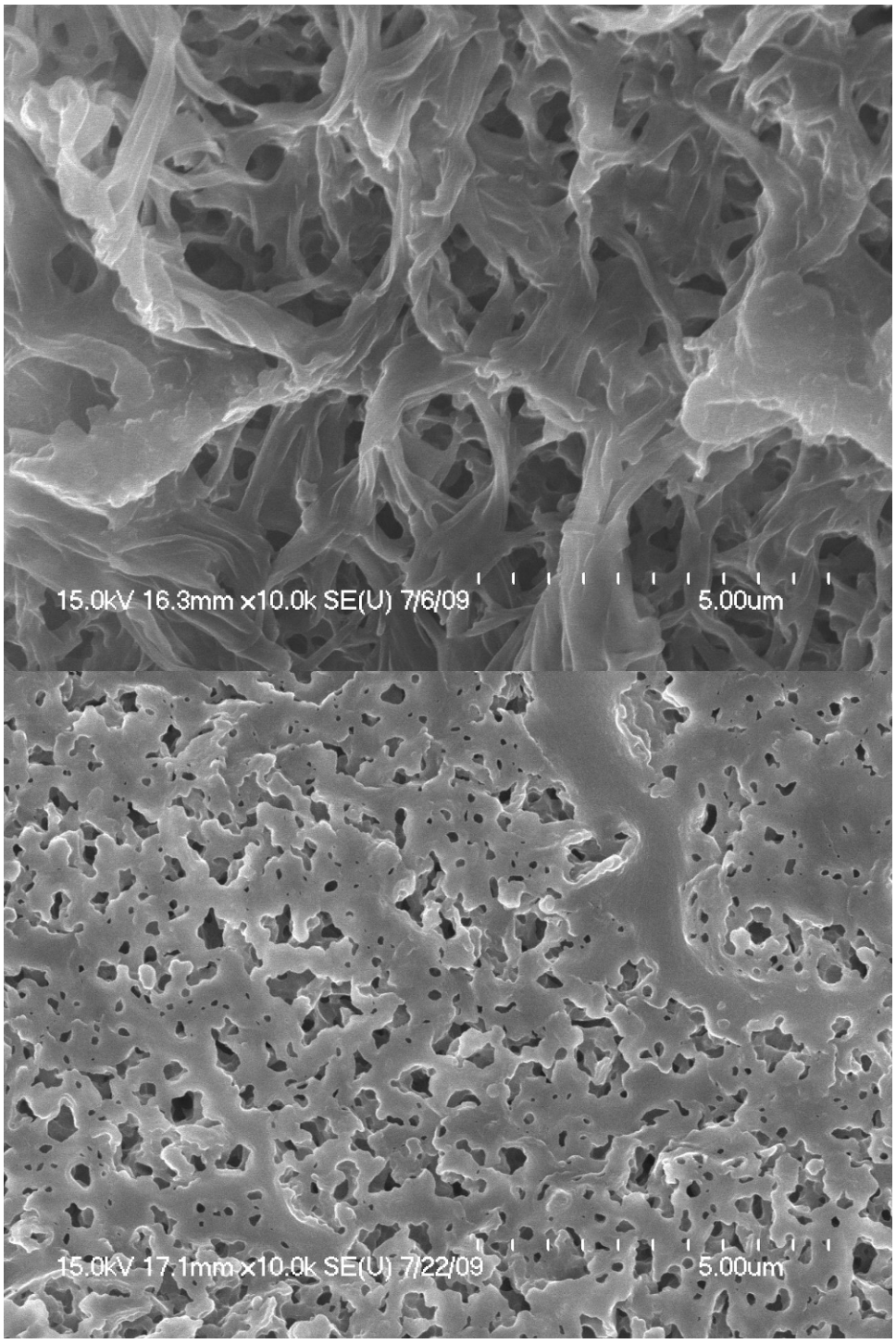

Figure 4.3. SEM images of (top) PCLN DBMS and (bottom) PCLM DBMS.

Figure 4.4. DBMS created from a diaphyseal section of bovine femur that was converted to anorganic bone, reconstituted with poly-ε-caprolactone, and had the HA removed via extraction in 0.6 M HCl.

this remarkable feature of the DBMS. The object in Figure 4.4 began as a section of a bovine femur. It was first converted to anorganic bone and then used to initiate the ROP of ε-caprolactone. The HA was removed with 0.6 M HCl. As one can see, after the removal of the HA, the macroscopic morphology of the section of the femur was retained despite removing nearly 75% of the original composite's mass. If the sample was allowed to dry, small cracks were observed, but this was avoidable by storing the sample in water. For smaller samples, cracking was not observed upon drying.

For samples extracted in HCl and EDTA for the same length of time, those extracted in acid showed a higher percent mass loss. Table 4.1 lists the average percent mass loss for PLCN DBMS, PLCM DBMS, and PLLA DBMS prepared either by HCl or EDTA extraction. All extractions were carried out for 7 days. All acid extracted samples had a mass loss of around 70%. As indicated by XRD analysis (Figure 4.5), this process resulted in the complete removal of the HA. The samples extracted in EDTA had a wider range of mass losses, from 24% for PLLA DBMS to 52% for PLCM DBMS. This clearly indicates that not all of the HA was removed after 7 days. In all cases, the EDTA extracted samples had smaller mass losses then their acid extracted counterparts. This observation is consistent with observations from early experiments in which EDTA was used as an alternative to acid extraction for DBM.[44, 45] XRD confirmed the complete removal of the HA in the acid extracted samples and the partial removal in the EDTA samples. Figure 4.5 shows the XRD patterns for an AB/PCLN composite before demineralization, a PCLN DBMS prepared by demineralization with 0.6 M HCl for 7 days, and a PCLN DBMS prepared by demineralization with 0.5 M EDTA for 7 days. The composite pattern, confirmed with a reference pattern from the database, was

Material	Mass Loss (%)	
	HCl	EDTA
PCLN (n = 5,5)	72 ± 3	33 ± 4
PCLM (n = 5,4)	73 ± 4	52 ± 5
PLLA (n = 5,5)	71 ± 4	24 ± 10

Table 4.1. Percent mass loss of PCLN DBMS, PCLM DBMS, and PLLA DBMS prepared by HCl and EDTA extraction for 7 days. Mass loss values are reported as the average with an uncertainty of one standard deviation ($\bar{x}$ ± 1 SD).

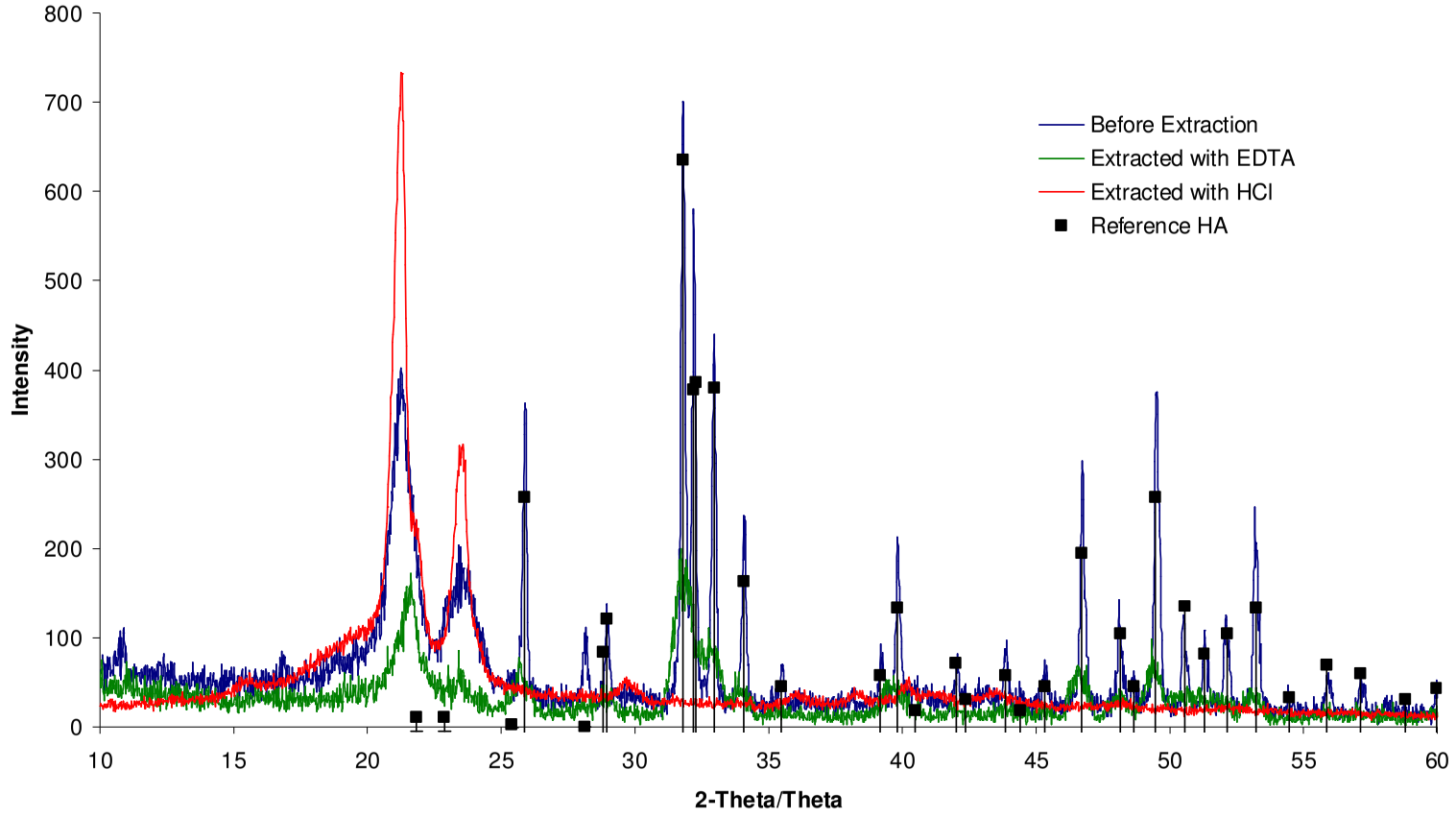

Figure 4.5. XRD patterns for AB/PCLN composite and PCLN DBMS prepared by HCl and EDTA extraction for 7days.

consistent with that of hydroxyapatite with the addition of two broad peaks. The broad peaks at 21.3^{o} and 23.6^{o} can be attributed to the PCLN. When this pattern was compared to the pattern for the acid prepared PCLN DBMS, the HA peaks were absent, leaving only the PCLN peaks. The pattern for the PCLN DBMS demineralized with EDTA still displayed both the HA pattern and the PCLN pattern, but the intensity of the HA peaks was greatly diminished.

It's clear from the above results that 7 days was sufficient time to remove all of the HA using acid extraction. Not clear from the data was the rate at which the demineralization was occurring and whether 7 days exceeded the minimum amount of time needed to completely demineralize the sample. The kinetics of the demineralization process of bone has been studied by several investigators. The kinetics of the process can be described using the classic shrinking core reaction model. In this model, there is a distinct reaction front that separates the demineralized area from the mineralized portion of the bone.[46-51] In other words, the demineralization occurs starting on the outside of the sample and slowly works its way to the center. The acid concentration and temperature of the solution have an effect on the demineralization rate, where increases in concentration and temperature produce faster demineralization rates.[52]

Figure 4.6 shows the percent mass loss over time for a set of AB/PCLN composites. Each sample was machined into cylinders that were 11 mm in height and 5.5 mm in diameter. They were demineralized using 0.6 M HCl at room temperature. This plot indicates that under these conditions the demineralization gave a good fit to a zero order reaction for which the mass of the composite decreases by approximately 1.3 %/hr. The demineralization continued at this rate until the mass loss approaches 75%, at which

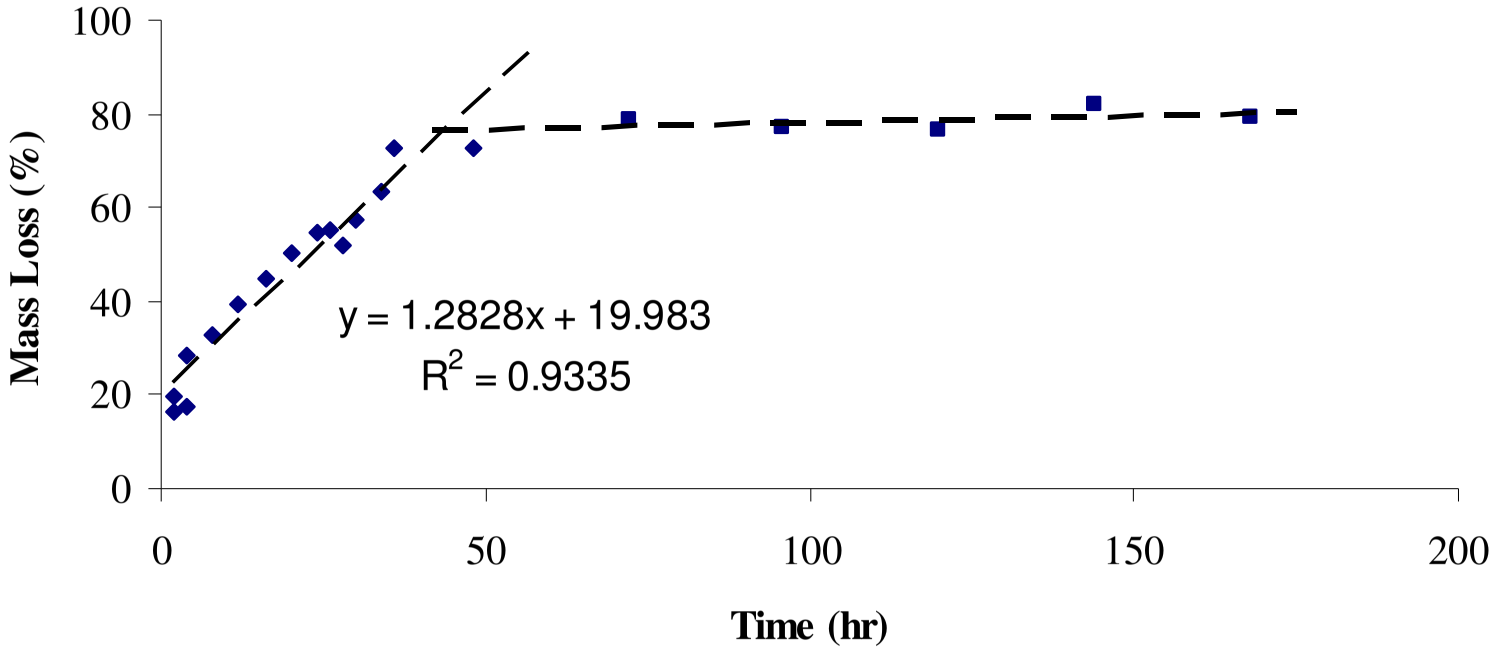

Figure 4.6. Percent mass loss over time for AB/PCLN composites demineralized with 0.6 M HCl at room temperature.

point nearly all of the HA had been removed. This occurred within the first 48 hours of demineralization. Figure 4.6 serves as an example that the demineralization process could potentially be controlled, allowing one to make samples with varying amounts of HA remaining in the core of the sample. The benefits of having a porous outside and solid core are not yet known, but one can envision that having a porous osteoconductive outer layer and a solid core to improve the mechanical properties could be advantageous. Furthermore, it has been demonstrated in DBM that a residual calcium level of 2 % had the highest osteoinductivity.[16]

Compressive stress-strain curves were obtained for PCLN DBMS, PCLM DBMS, and PLLA DBMS samples. The compressive strength and elastic modulus were determined for samples that were demineralized in both HCl and EDTA for 7 days. As noted above, a portion of the HA remained in the EDTA extracted samples. Additionally, both dry and wet samples were tested. Dry samples were allowed to dry in air. Wet samples were stored in water until being tested. Figure 4.7 displays the stress-strain plot from the compression testing of the PCLM DBMS samples. The x-axis is the compressive strain in units of travel distance over sample height. Compressive stress is plotted on the y-axis with units of pressure because its definition is the applied force divided by the sample's cross-sectional area. A more complete explanation of the mechanical properties is given in Chapter 5. Table 4.2 displays the compressive strength and elastic modulus values for all the samples tested. In general, the EDTA extracted samples had higher compressive strength values than their acid extracted counterparts. This was expected due to the incomplete demineralization of these samples. Also, the wet samples exhibited lower compressive strengths than the dry samples, except for the

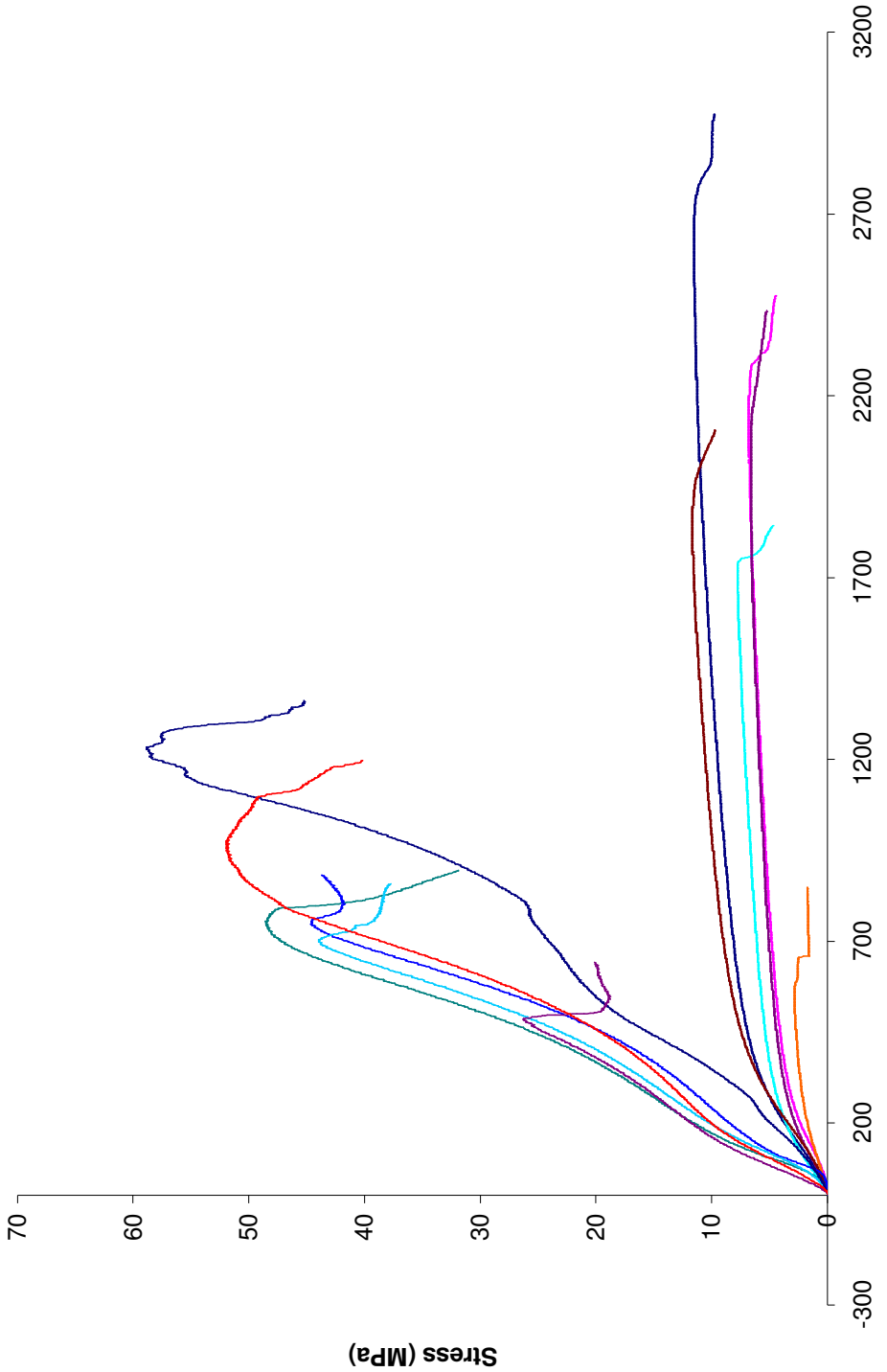

Figure 4.7. Compressive stress-strain curves for PCLM DBMS samples prepared by demineralization with HCl and EDTA.

Material	HCl Extracted Samples				EDTA Extracted Samples			
	Dry Samples		Wet Samples		Dry Samples		Wet Samples	
	Compressive Strength (MPa)	Elastic Modulus (MPa)	Compressive Strength (MPa)	Elastic Modulus (MPa)	Compressive Strength (MPa)	Elastic Modulus (MPa)	Compressive Strength (MPa)	Elastic Modulus (MPa)
PCLN	10 ± 2	300 ± 30	3 ± 2	200 ± 200	55 ± 8	1300 ± 400	12 ± 5	600 ± 600
PCLM	8 ± 3	180 ± 50	1 ± 1	60 ± 10	46 ± 11	1140 ± 90	22 ± 2	300 ± 100
PLLA	3 ± 1	500 ± 900	5 ± 3	300 ± 200	9 ± 4	1500 ± 800	23 ± 14	1100 ± 700

Table 4.2. Mechanical Properties for PLCN, PLCM, and PLLA DBMS samples prepared by extraction in 0.6 M HCl and 0.5 M EDTA. The values reported are the averages with an uncertainty of one standard deviation ($\bar{x}$ ± 1 SD).

PLLA DBMS. Between the three different DBMS types, the dry PLLA DBMS was significantly weaker than the PCLN and PCLM DBMS samples. For the wet samples, the compressive strength of PLLA DBMS was not significantly different from the other materials. For comparative purposes, Lin et al. reported the compressive strength of DBM in phosphate buffer saline (PBS) to be 4.1 ± 0.42 kPa, and heparin crosslinked DBM (also in PBS) had a compressive strength of 31.4 ± 3.1 kPa.[40] Additional values for the compressive strength of DBM have been reported by Zhao et al.[53] The extent to which the mechanical properties can be controlled by manipulating the degree of demineralization remains to be investigated. As mentioned above, it could be advantageous to have a porous outer layer to improve osteoconductivity and a solid core to provide greater mechanical strength.

The demineralization process also has an effect on the polymer composition and molecular weight. Before demineralization, the AB/polymer composites contain a small amount of monomer. The ^{1}H NMR spectra for AB/PCLN (Figure 4.8), AB/PLLA (Figure 4.9), and AB/PCLM (Figure 4.10) composites all show small amounts of monomer remaining after the polymerization was terminated. The sample in Figure 4.8 contained 98.6% PCLN. This was determined by integrating the areas of the triplet at 4.05 ppm, which represents the internal methylene protons adjacent the oxygen in the ester of the polymer, and the triplet at 4.15 ppm, which represents the same protons in the monomer. The sample in Figure 4.9 contained 96.8% PLLA. This was determined by integrating the areas of the quartet at 5.15 ppm, which represents the internal methine protons of the polymer, and the quartet at 5.05 ppm which represents the same protons in the monomer. The sample in Figure 4.10 contained 85.9% PCLM. This was determined

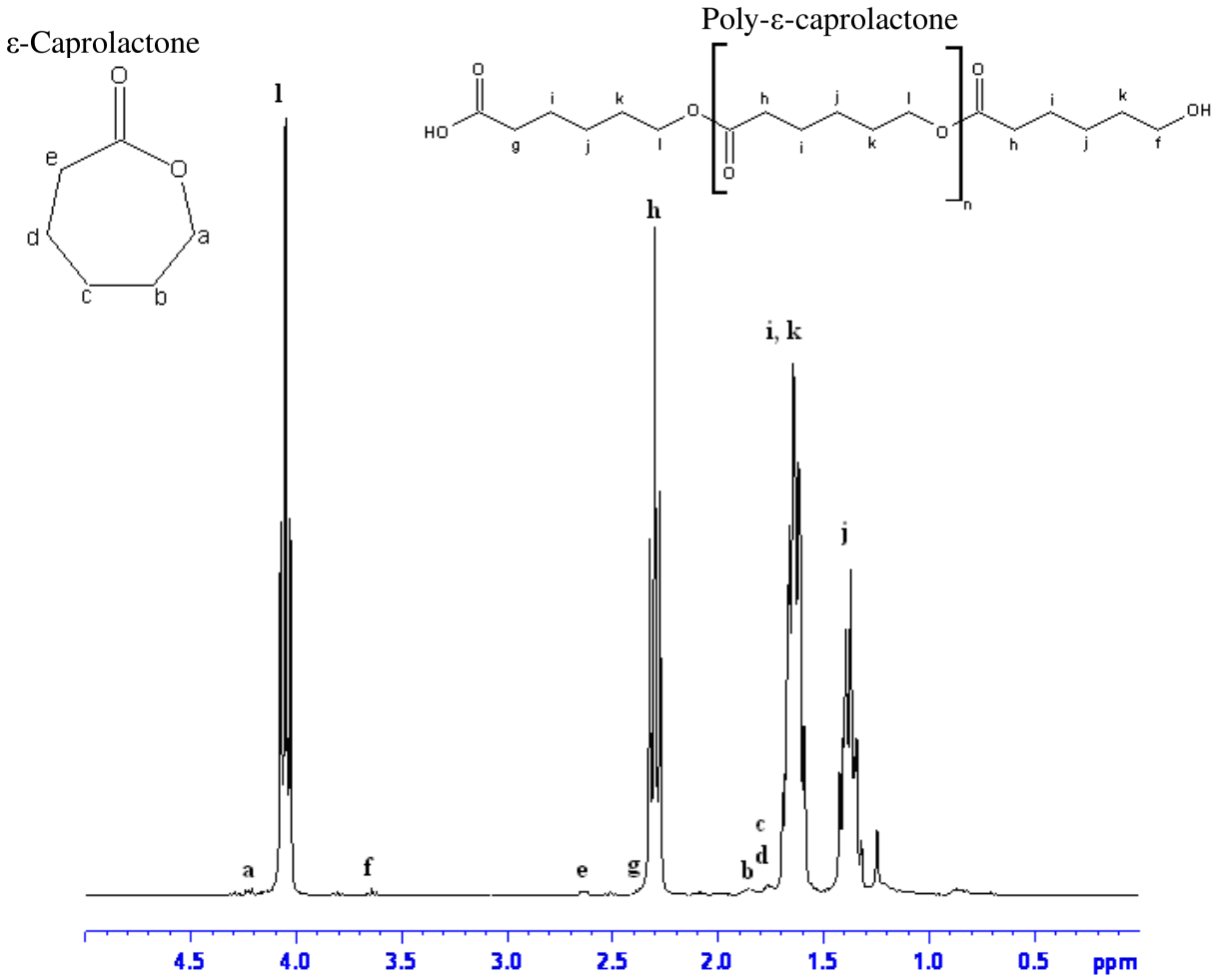

Figure 4.8. ^{1}H NMR spectrum of AB/PCLN composite before demineralization. Small amounts of ε-caprolactone are still present.

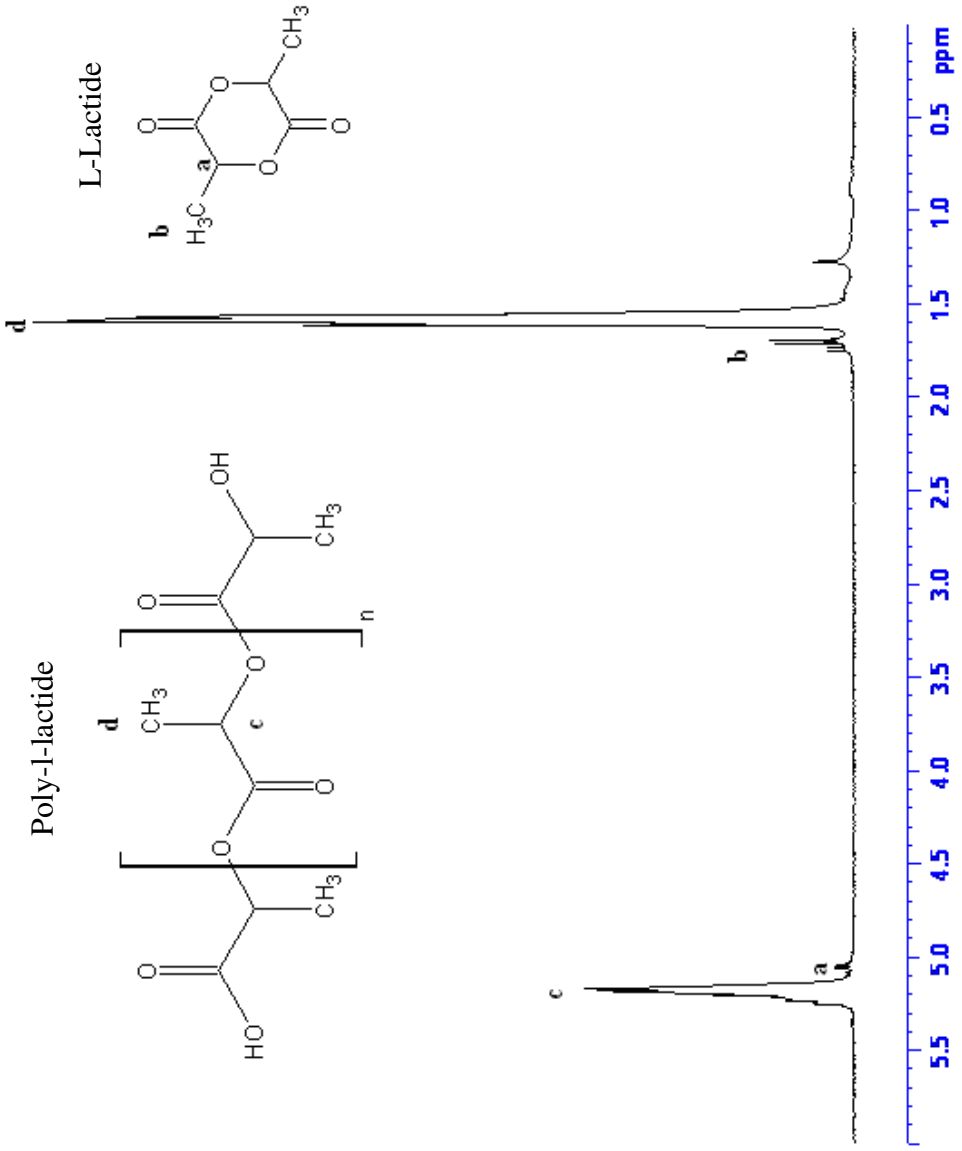

Figure 4.9. ^{1}H NMR spectrum of an AB/PLLA composite before demineralization. Small amounts of L-lactide are still present.

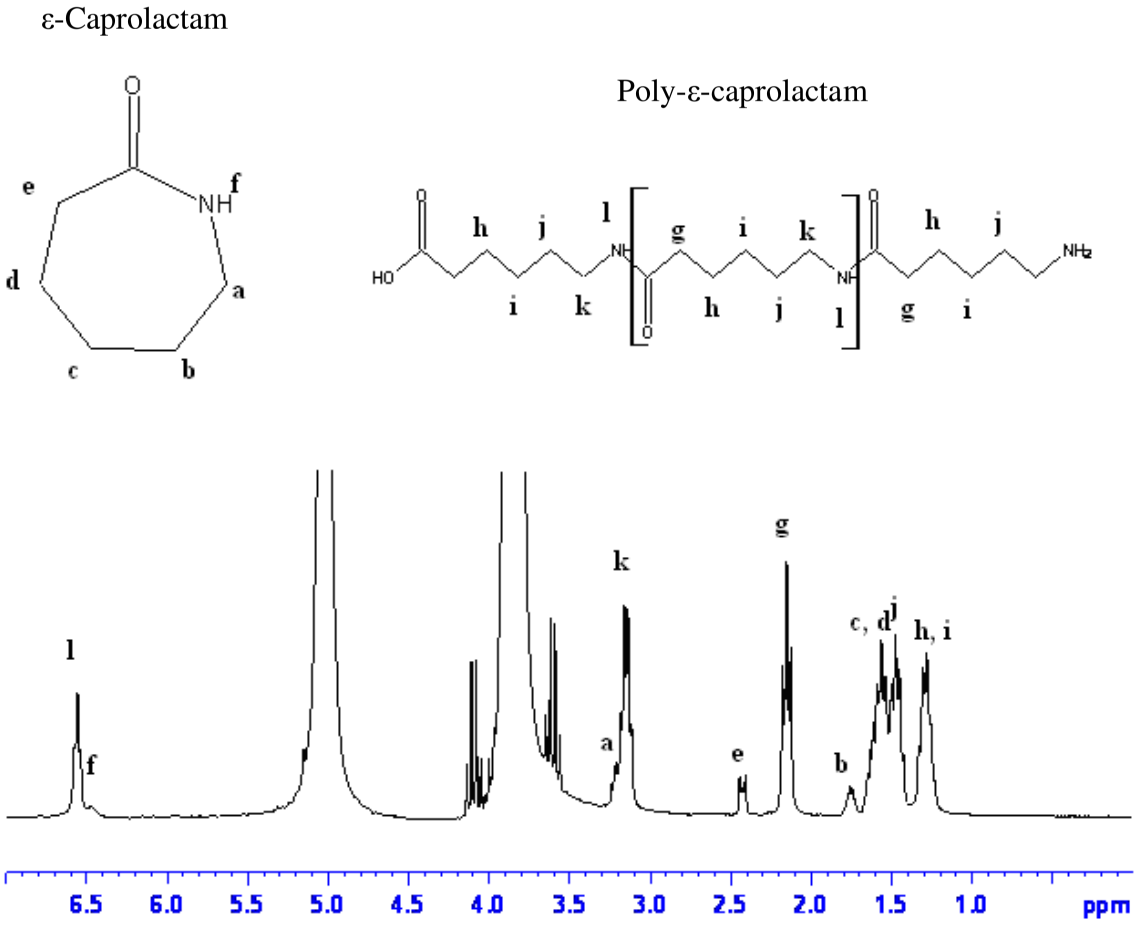

Figure 4.10. ^{1}H NMR spectrum of an AB/PCLM composite before demineralization. Small amounts of ε-caprolactam are still present.

by integrating the areas of the triplet at 4.15 ppm, which represents the internal methylene protons adjacent the carbon in the amide functional group of the polymer, and the triplet at 4.45 ppm which represents the same protons in the monomer. The two large peaks in the PLCM spectrum are due to the solvent, trifluoroethanol. When Figures 4.8 – 4.10 are compared to ^{1}H NMR spectra for PCLN DBMS (Figure 4.11), PLLA DBMS (Figure 4.12), and PLCM DBMS (Figure 4.13) after being extracted with HCl, one can see that the monomer peaks are now absent from the samples. The same is observed after samples are extracted using EDTA.

The extraction process also decreased the molecular weight of the polymers. Table 4.3 displays the peak molecular weights (M_p) of AB/PCLN and AB/PLLA composites before demineralization and after demineralization. The M_p decreased in all four groups by approximately 60%. Degradation of PLLA, PCLN, PCLM, and other polyesters and polyamides is due to hydrolysis of the ester and amide linkages. This occurs randomly along the backbone of the polymer as well as at the chain ends.[54-56] The rate of the degradation is also dependent on the pH of the solution.[57, 58] Makino et al. showed that PLLA degrades the slowest at pH 5.0. The degradation rate increases as the solution is made more acidic or more alkaline.[59, 60] The rate is also influenced by the M_n and the presence of oligomers and monomer due to the autocatalysis of the hydrolytic degradation of polyesters which produces carboxylic acid end groups.[61-64] It is unclear at this time what role these various processes play in the hydrolysis of the DBMS samples.

The hydrolytic degradation of polylactones and polylactams can release acidic products that can lead to a decrease in the pH of the surrounding tissue.[65] The degradation mechanism is regarded to be bulk erosion, as indicated by the large

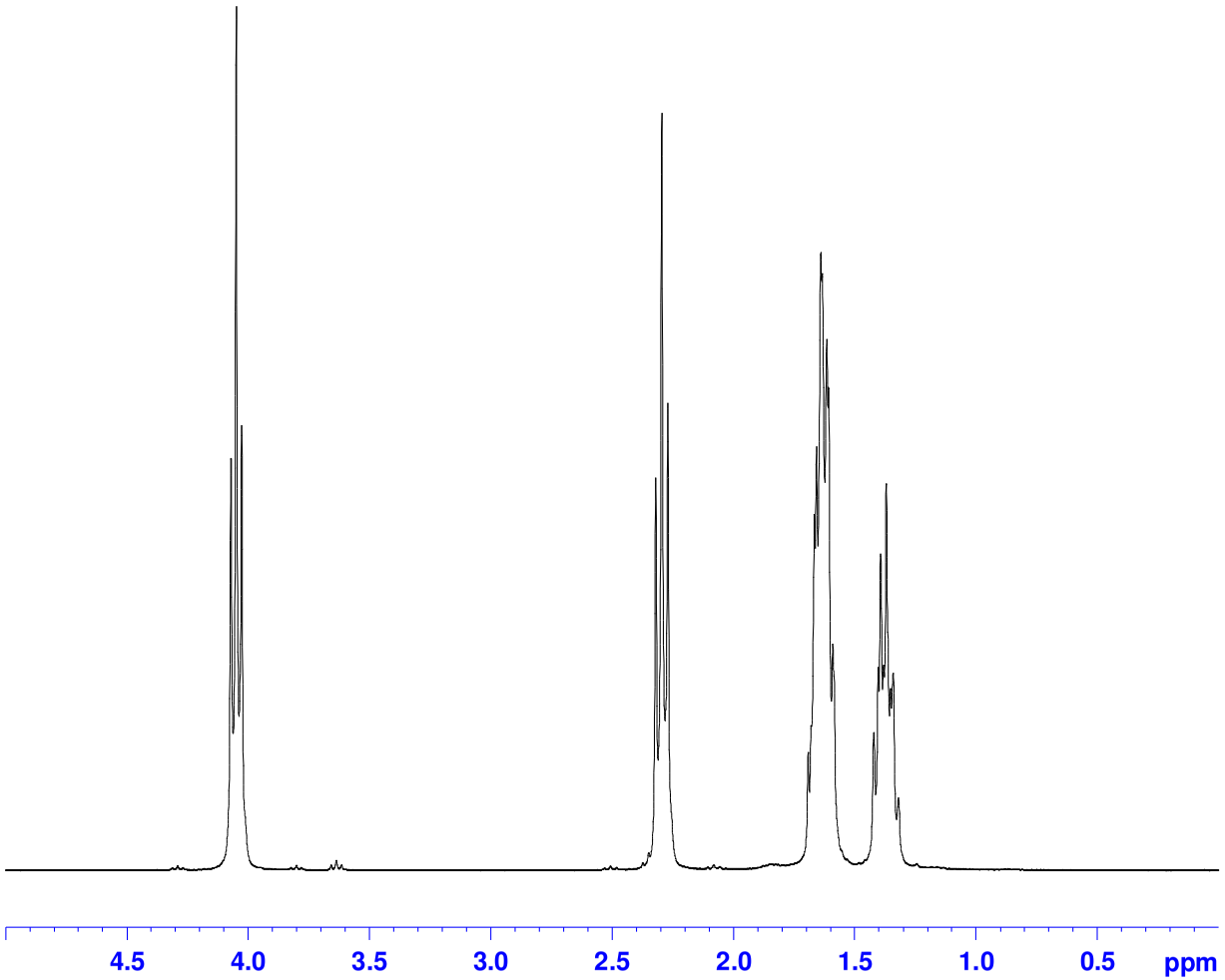

Figure 4.11. ^{1}H NMR spectrum of a PCLN DBMS sample after being extracted with HCl. The monomer peaks are no longer present.

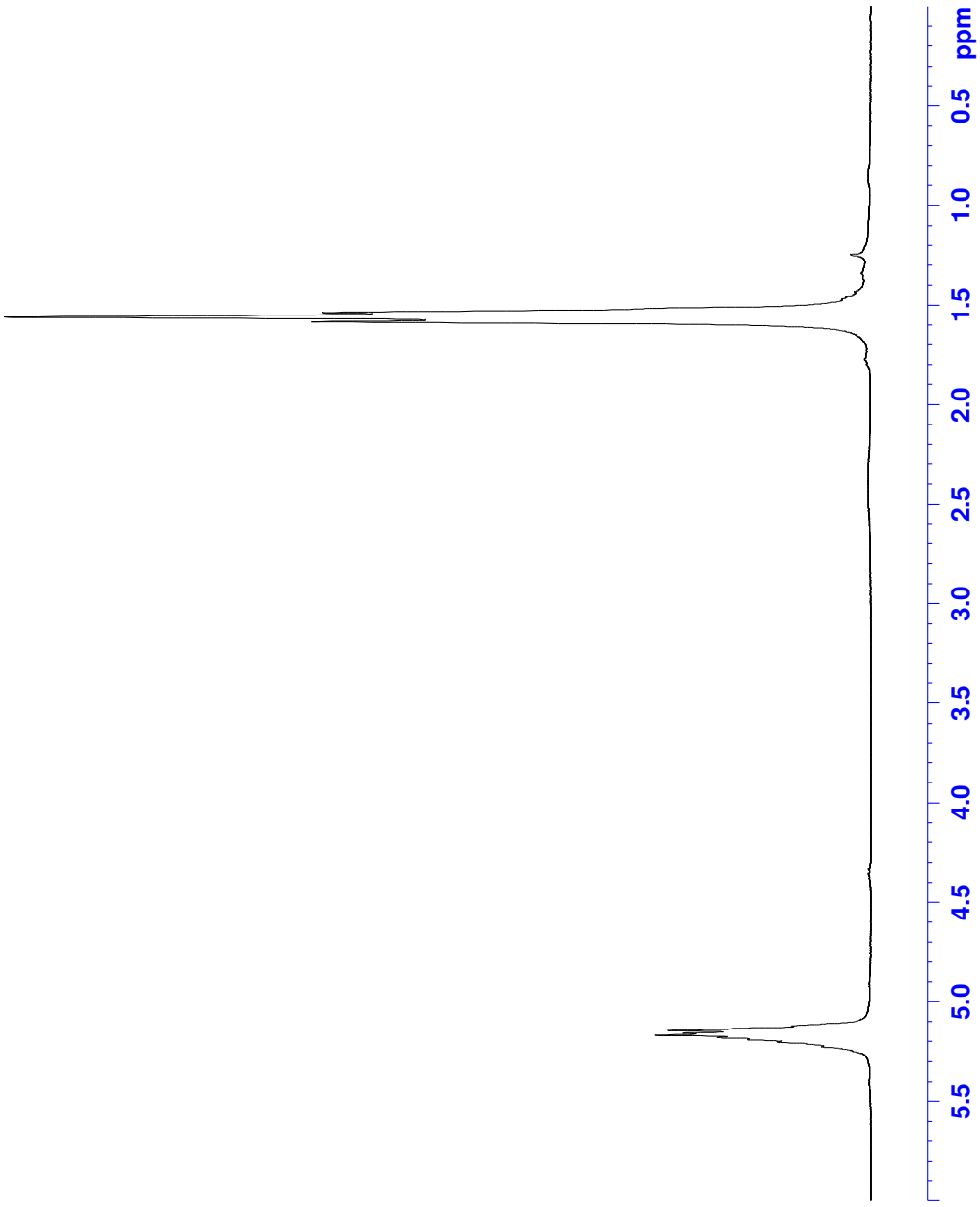

Figure 4.12. ^{1}H NMR spectrum of a PLLA DBMS sample after demineralization with HCl. The monomer peaks are no longer present.

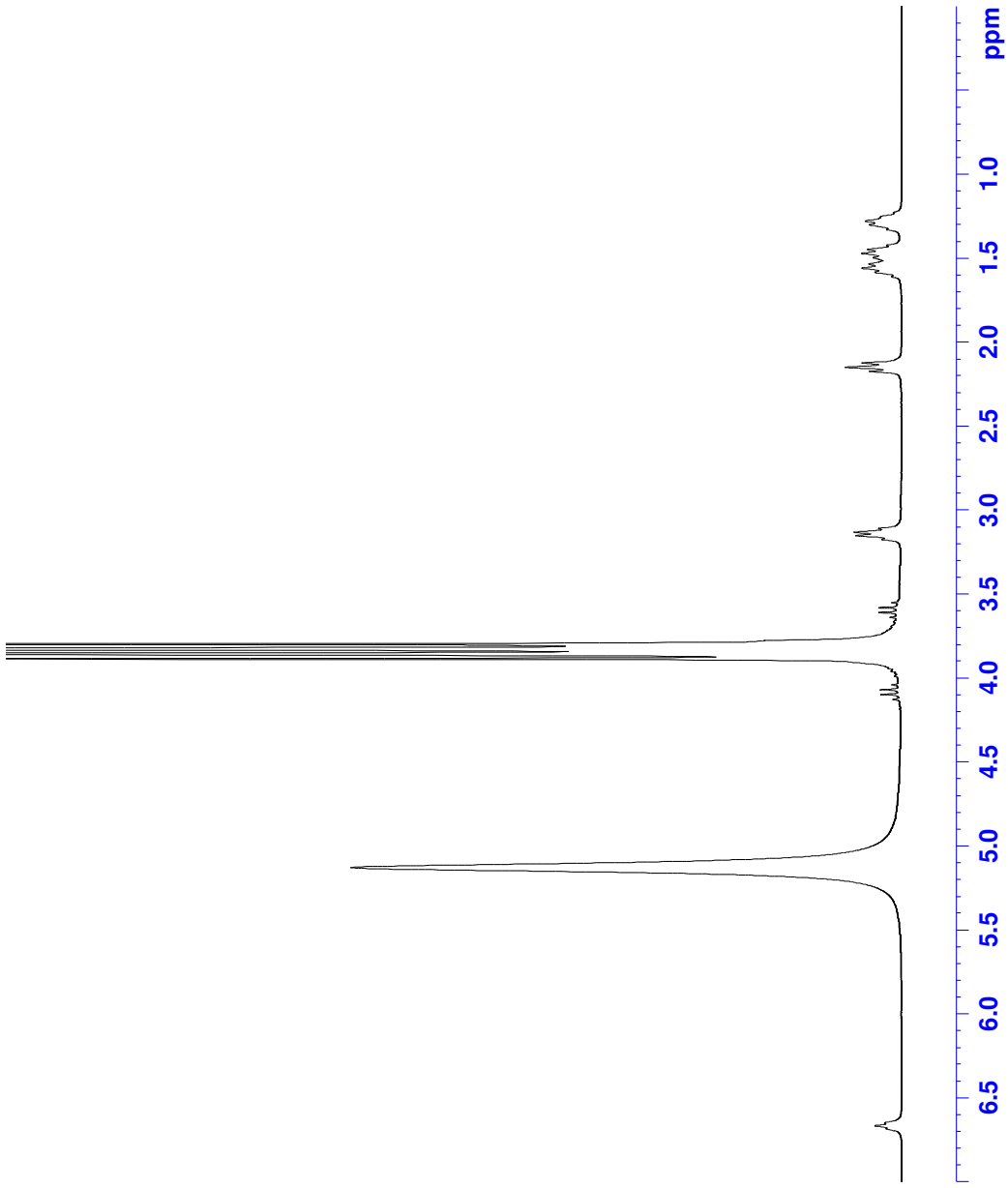

Figure 4.13. ^{1}H NMR spectrum of a PLCM DBMS sample after demineralization with HCl. The monomer peaks are no longer present.

Material	Peak Molecular Weight (kDa)					
	HCl			EDTA		
	Before	After	Difference	Before	After	Difference
PCLN	40 ± 23	17 ± 5	-57%	54 ± 18	21 ± 9	-62%
PLLA	21 ± 8	8 ± 3	-60%	23 ± 11	11 ± 3	-55%

Table 4.3. Peak molecular weight of AB/PCLN and AB/PLLA composites before and after demineralization with HCl or EDTA. The values reported are the averages with an uncertainty of one standard deviation ($\bar{x} \pm 1$ SD).

molecular weight decrease that precedes the release of the monomer.[66] This release can lead to local acidosis if there is a large mass of the polymer in a concentrated form, such as a solid pin.[67] One recent study reported that local inflammatory reactions and intraosseous cysts in the bone where bioresorbable polymer implants are placed.[68] These issues generally do not effect highly porous scaffolds that have a low polymer mass per unit volume and in general;[67] the buffering capacity of biological fluids is thought to compensate for the acidic products of the degradation and the movement of these fluids dilutes and diffuses the products away from the implant site.[65, 69, 70] Other environmental factors can affect the degradation and the build up of degradation products, such as fluid flow[71] and degree of loading.[72] The polymer composition and physical properties also play a role in the degradation rate.[72, 73]

Conclusion

Even though efforts to produce a synthetic, biomimetic substrate similar to DBM are in their early stages, the present DBMS produced using anorganic bone as a scaffold exhibited a porous microscopic matrix similar to that of collagen in the original bone. Despite losing nearly 75% of its mass during the removal of its inorganic framework, the DBMS maintained its original structure and exhibited mechanical properties that exceeded those of DBM. Future investigations could more thoroughly explore the extent of demineralization and the conditions that will produce a product that has good mechanical properties and osteoconductivity. The use of other monomers such as glycolide could also be pursued. Combining the DBMS with bone morphogenetic proteins (BMPs) and other growth factors could be investigated to determine if the osteoinductive ability of the DBMS can be improved.[74-76] Such studies could be done in

conjunction with *in vivo* resorption studies to evaluate the biological performance of the DBMS.[77]

References

1) Doll, B.; Aleef, M.; Hollinger, J.O., Overview of fracture repair. In *Musculoskeletal Tissue Regeneration: Biological Materials and Methods*, Pietrzak, W.S., ed.; Humana Press: Totowa, New Jersey, **2008**.

2) Goel, S.C.; Tuli, S.M. Use of decalbone in healing of osseous cystic defects. In *Bone Grafts, Derivatives and Substitutes*, Urist, M.R., O'Conner, B.T., Burwell, R.G., eds.; Butterworth-Heinemann: Oxford, England, **1994**.

3) Drosos, G.I.; Kazakos, K.I.; Kouzoumpasis, P.; Verettas, D.-A., Safety and efficacy of commercially available demineralised bone matrix preparations: A critical review of clinical studies. *Injury: International Journal of the Care of the Injured* **2007**, 38S4, S13-S21.

4) Goldberg, V.M., Biology of bone allograft and clinical applications. In *Musculoskeletal Tissue Regeneration: Biological Materials and Methods*, Pietrzak, W.S., ed.; Humana Press: Totowa, New Jersey, **2008**.

5) Poynton, A.R.; Lane, J.M., Review of the state of the art: Allograft-based systems for use as bone graft substitutes. In *Bone Graft Substitutes*, Laurencin, C.T., ed.; ASTM International: West Conshohocken, Pennsylvania, **2003**.

6) Sutherland, D.; Bostrom, M., Grafts and bone graft substitutes. In *Bone Regeneration and Repair: Biology and Clinical Applications*, Lieberman, J.R., Friedlaender, G.E., eds.; Humana Press: Totowa, New Jersey, **2005**.

7) Joyce, M.J.; Joyce, D.M., Musculoskeletal allograft tissue banking and safety. In *Bone Graft Substitutes*, Laurencin, C.T., ed.; ASTM International: West Conshohocken, Pennsylvania, **2003**.

8) Senn, N., On the healing of aseptic bone cavities by implantation of antiseptic decalcified bone. *American Journal of the Medical Sciences* **1889**, 98, 219-240.

9) Walsh, W.R.; Christiansen, D.L., Demineralized bone matrix as a template for mineral-organic composites. *Biomaterials* **1995**, 16, 1363-1371.

10) Wolfinbarger Jr., L.; Eisenlohr, L.M.; Ruth, K., Demineralized bone matrix: Maximizing new bone formation for successful bone implantation. In *Musculoskeletal Tissue Regeneration: Biological Materials and Methods*; Pietrzak, W.S., Ed.; Humana Press: Totowa, New Jersey, **2008**.

11) Scott, J.E.; Kyffin, T.W., Demineralization in organic solvents by alkylammonium salts of ethylenediaminetetra-acetic acid. *Biochemical Journal* **1978**, 169, 697-701.

12) Cook, S.F.; Ezra-Cohn, H.E., A comparison of methods for decalcifying bone. *Journal of Histochemistry and Cytochemistry* **1962**, 10, 560-563.

13) Urist, M.R.; Silverman, B.F.; Buring, K.; Dubuc, F.L.; Rosenberg, J.M., The bone induction principle. *Clinical Orthopaedics and Related Research* **1967**, 53, 243-283.

14) Urist, M.R., Bone: Formation by autoinduction. *Science* **1965**, 150, 893-899.

15) Mizutani, H.; Urist, M.R., The nature of bone morphogenetic protein (BMP) fractions derived from bovine bone matrix gelatin. *Clinical Orthopaedics and Related Research* **1982**, 171, 213-223.

16) Zhang, M.; Powers Jr., R.M.; Wolfinbarger Jr., L., Effect(s) of the demineralization process on the osteoinductivity of demineralized bone matrix. *Journal of Periodontology* **1997**, 68, 1085-1092.

17) Russell, J.L.; Block, J.E., Clinical utility of demineralized bone matrix for osseous defects, arthrodesis and reconstruction: Impact of processing techniques and study methodology. *Orthopaedics* **1999**, 22, 524-531.

18) Janeway, P.A., Bioceramics: Materials that mimic mother nature. *American Ceramic Society Bulletin* **2006**, 85, 26-30.

19) Ben-Nissan, B., Biomimetics and bioceramics. In *Learning from Nature How to Design New Implantable Biomaterials: From Biomineralization Fundamentals to Biomimetic Materials and Processing Routes*, Reis, R.L., Weiner, S., eds.; Kluwer Academic: Dordrecht, The Netherlands, **2004**.

20) Oyen, M.L., The materials science of bone: Lessons from nature for biomimetic materials synthesis. *MRS Bulletin* **2008**, 33, 49-55.

21) Ben-Nissan, B., Natural bioceramics: From coral to bone and beyond. *Current Opinion in Solid State and Materials Science* **2003**, 7, 283-288.

22) Green, D.; Walsh, D.; Mann, S.; Oreffo, R.O.C., The potential of biomimesis in bone tissue engineering: Lessons from the design and synthesis of invertebrate skeletons. *Bone* **2002**, 30, 810-815.

23) Wiegand, T.; Karr, J.; Steinkruger, J. D.; Hiebner, K.; Simetich, B.; Beatty, M.; Redepenning, J., Reconstruction of anorganic mammalian bone by surface-initiated polymerization of L-lactide. *Chemistry of Materials* **2008,** 20, 5016-5022.

24) Williams, J.B.; Irvine, J.W., Preparation of the inorganic matrix of bone. *Science* **1954**, 119, 771-772.

25) Nederberg, F.; Connor, E. F.; Moller, M.; Glauser, T.; Hedrick, J. L., New paradigms for organic catalysts: The first organocatalytic living polymerization. *Angewandte Chemie-International Edition* **2001,** 40, 2712-2715.

26) Kalmi, M.; Lahcini, M.; Castro, P.; Lehtonen, O.; Belfkira, A.; Leskela, M.; Repo, T., Tetrakis Sn(IV) alkoxides as novel initiators for living ring-opening polymerization of lactides. *Journal of Polymer Science Part A-Polymer Chemistry* **2004,** 42, 1901-1911.

27) Thakur, K. A. M.; Kean, R. T.; Hall, E. S.; Kolstad, J. J.; Munson, E. J., H-1 NMR spectroscopy in the analysis and characterization of poly(lactide). *International Journal of Polymer Analysis and Characterization* **1998,** 4, 379-391.

28) Espartero, J. L.; Rashkov, I.; Li, S. M.; Manolova, N.; Vert, M., NMR analysis of low molecular weight poly(lactic acid)s. *Macromolecules* **1996,** 29, 3535-3539.

29) Li, H.; Wang, C.; Bai, F.; Yue, J.; Woo, H.-G., Living ring-opening polymerization of L-lactide catalyzed by Red-Al. *Organometallics* **2004**, 23, 1411-1415.

30) Lee, S. H.; Kim, B. S.; Kim, S. H.; Choi, S. W.; Jeong, S. I.; Kwon, I. K.; Kang, S. W.; Nikolovski, J.; Mooney, D. J.; Han, Y. K.; Kim, Y. H., Elastic biodegradable poly(glycolide-co-caprolactone) scaffold for tissue engineering. *Journal of Biomedical Materials Research Part A* **2003,** 66A, 29-37.

31) Stolt, M.; Viljanmaa, M.; Sodergard, A.; Tormala, P., Blends of poly(epsilon-caprolactone-b-lactic acid) and poly(lactic acid) for hot-melt applications. *Journal of Applied Polymer Science* **2004,** 91, 196-204.

32) , J.; Wang, L. Q.; Wang, H. J.; Tu, K. H.; Liu, L., Amphiphilic block copolymers based on methoxy poly(ethylene glycol) and either crystalline or amorphous poly(caprolactone-b-lactide): Synthesis, solid-state and aqueous solution characterizations. *Journal of Applied Polymer Science* **2007,** 105, 915-927.

33) Zhong, Z. Y.; Ankone, M. J. K.; Dijkstra, P. J.; Birg, C.; Westerhausen, M.; Feijen, J., Calcium methoxide initiated ring-opening polymerization of epsilon-caprolactone and L-lactide. *Polymer Bulletin* **2001,** 46, 51-57.

34) Zhang, Y.; Zhang, Q.; Cheng, K.; Xu, J., Monocarboxyl-end-grouped polycaprolactam with an adjustable molecular weight. *Journal of Applied Polymer Science* **2004**, 92, 722-727.

35) Holmes, B.S.; Moniz, W.B.; Ferguson, R.C., NMR study of nylon 66 in solution (^{1}H, ^{13}C, and ^{15}N NMR using adiabatic J cross polarization). *Macromolecules* **1982**, 15, 129-132.

36) Bach, F. H., Xenotransplantation: Problems and prospects. *Annual Review of Medicine* **1998**, 49, 301-310.

37) ASTM F1581-99, Standard specification for composition of anorganic bone for surgical implants. In *Book of Standards*; American Society for the Testing of Materials: West Conshohocken, Pennsylvania, 2007; Vol.13.01.

38) Elliott, J.C., *Structure and Chemistry of the Apatites and Other Calcium Orthophosphates*. Elsevier: Amsterdam, The Netherlands, 1994.

39) Mauney, J.R.; Blumberg, J.; Pirun, M.; Volloch, V.; Vunjak-Novakovic, G.; Kaplan, D.L., Osteogenic differentiation of human bone marrow stromal cells on partially demineralized bone scaffolds in vitro. *Tissue Engineering* **2004**, 10, 81-92.

40) Lin, H.; Zhao, Y.; Sun, W.; Chen, B.; Zhang, J.; Zhao, W.; Xiao, Z.; Dai, J., The effect of crosslinking heparin to demineralized bone matrix on mechanical strength and specific binding to human bone morphogenetic protein-2. *Biomaterials* **2008**, 29, 1189-1197.

41) Cornell, C.N.; Lane, J.M., Current understanding of osteoconduction in bone regeneration. *Clinical Orthopaedics and Related Research* **1998**, 355, S267-S273.

42) Sopyan, I.; Mel, M.; Ramesh, S.; Khalid, K.A., Porous hydroxyapatite for artificial bone applications. *Science and Technology of Advanced Materials* **2007**, 8, 116-123.

43) Liu, W.; Zhang, W.; Cao, Y., Bone and cartilage reconstruction. In *Principles of Tissue Engineering*; Lanza, R., Langer, R., Vacanti, J., eds.; Elsevier: San Diego, CA, **2007**.

44) Sreebny, L.M.; Nikiforuk, G., Demineralization of hard tissues by organic chelating agents. *Science* **1951**, 113, 560.

45) Belanger, L.F.; Copp, D.H.; Morton, M.A., Demineralization with EDTA by constant replacement. *Anatomical Record* **1965**, 153, 41-47.

46) Lewandrowski, K.-U.; Tomford, W.W.; Michaud, N.A.; Schomacker, K.T.; Deutsch, T.F., An electron microscopic study on the process of acid demineralization of cortical bone. *Calcified Tissue International* **1997**, 61, 294-297.

47) Kiviranta, I.; Tammi, M.; Lappalainen, R.; Kuusela, T.; Helminen, H.J., The rate of calcium extraction during EDTA decalcification from thin bone slices as assessed with atomic absorption spectrophotometry. *Histochemistry and Cell Biology* **1980**, 68, 119-127.

48) Eggert, F.M.; Germain, J.P., Rapid demineralization in acidic buffers. *Histochemistry and Cell Biology* **1979**, 59, 215-224.

49) Makarewicz, P.J.; Harasta, L.; Webb, S.L., Kinetics of acid diffusion and demineralization of bone. *Journal of Photographic Science* **1980**, 22, 148-159.

50) Lewandrowski, K.-U.; Venugopalan, V.; Tomford, W.W.; Schomacker, K.T.; Mankin, H.J.; Deutsch, T.F., Kinetics of cortical bone demineralization: Controlled demineralization – a new method for modifying cortical bone allografts. *Journal of Biomaterials Research* **1996**, 31, 365-372.

51) Birkedal-Hansen, H., Kinetics of acid demineralization in histologic technique. *Journal of Histochemistry and Cytochemistry* **1974**, 22, 434-441.

52) Castro-Cesena, A.B.; Novitskaya, E.E.; Chen, P.-Y.; Hirata, G.A.; McKittrick, J., Kinetic studies of bone demineralization at different HCl concentrations and temperatures. *Materials Science and Engineering: C* **2011**, 31, 523-530.

53) Zhao, Y.; Chen, B.; Lin, H.; Sun, W.; Zhao, W.; Zhang, J.; Dai, J., The bone-derived collagen containing mineralized matrix for the loading of collagen-binding bone morphogenetic protein-2. *Journal of Biomedical Materials Research Part A* **2009**, 88A, 725-734.

54) Henton, D.E.; Gruber, P.; Lunt, J.; Randall, J., Polylactic acid technology. In *Natural Fibers, Biopolymers and Biocomposites*, Mohanty, A.K.; Misra, M.; Drzal, L.T., Eds.; CRC Press: Boca Raton, FL, **2005**.

55) Shih, C., A graphical method for the determination of the mode of hydrolysis of biodegradable polymers. *Pharmaceutical Research* **1995**, 12, 2036-2040.

56) Shih, C., Chain-end scission in acid catalyzed hydrolysis of poly(D,L-lactide) in solution. *Journal of Controlled Release* **1995**, 34, 9-15.

57) Tsuji, H.; Nakahara, K., Poly(L-lactide). IX. Hydrolysis in acid media. *Journal of Applied Polymer Science* **2002**, 86, 186-194.

58) Li, S.; McCarthy, S., Further investigations on the hydrolytic degradation of poly(DL-lactide). *Biomaterials* **1999**, 20, 35-44.

59) Makino, K.; Arakawa, M.; Kondo, T., Preparation and in vitro degradation properties of polylactide microcapsules. *Chemical and Pharmaceutical Bulletin* **1985**, 33, 1195-1201.

60) Makino, K.; Ohshima, H.; Kondo, T., Mechanism of hydrolytic degradation of poly(L-lactide) microcapsules: Effects of pH, ionic strength and buffer concentration. *Journal of Microencapsulation* **1986**, 3, 203-212.

61) Joziasse, C.A.P.; Grijpma, D.W.; Bergsma, J.E.; Cordewener, F.W.; Bos, R.R.M.; Pennings, A.J., The influence of morphology on the (hydrolytic degradation of as-polymerized and hot-drawn poly(L-lactide)). *Colloid Polymer Science* **1998**, 276, 968-975.

62) Mauduit, J.; Perouse, E.; Vert, M., Hydrolytic degradation of films prepared from blends of high and low molecular weight poly(DL-lactic acid). *Journal of Biomedical Materials Research* **1996**, 30, 201-207.

63) Hyon, S.; Jamshidi, K.; Ikada, Y., Effects of residual monomer on the degradation of DL-lactide polymer. *Polymer International* **1998**, 46, 196-202.

64) Lam, C.X.F.; Savalani, M.M.; Teoh, S.-H.; Hutmacher, D.W., Dynamics of in vitro polymer degradation of polycaprolactone-based scaffolds: Accelerated versus simulated physiological conditions. *Biomedical Materials* **2008**, 3, 34108-34123.

65) Boyan, B.D.; McMillan, J.; Lohmann, C.H.; Ranly, D.M.; Schwartz, Z., Bone graft substitutes: Basic information for successful clinical use with special focus on synthetic graft substitutes. In *Bone Graft Substitutes*, Laurencin, C.T., ed.; ASTM International: West Conshohocken, Pennsylvania, 2003.

66) Gombotz, W.R.; Pettit, D.K., Biodegradable polymers for protein and peptide drug delivery. *Bioconjugate Chemistry* **1995**, 6, 332-351.

67) Wong, W.H.; Mooney, D., Synthesis and properties of biodegradable polymers used as synthetic matrices for tissue engineering. In *Synthetic Biodegradable Polymer Scaffolds*, Atala, A.; Mooney, D.; Vacanti, J.P.; Langer, R., eds.; Birkhäuser: Boston, Massachusetts, 1997.

68) Bostman, O.M.; Pihlajamaki, H.K., Adverse tissue reaction to bioabsorbable fixation devices. *Clinical Orthopaedics and Related Research* **2000**, 371, 216-227.

69) Vasenius, J.; Majola, A.; Miettinen, E.-L.; Törmälä, P.; Rokkanen, P., Do intramedullary rods of self-reinforced poly-L-lactide or poly-DL/L-lactide cause lactic acid acidosis in rabbits? *Clinical Materials* **1992**, 10, 213-218.

70) Pihlajamäki, H.; Böstman, O.; Tynninen, O.; Laitinen, O., Long-term tissue response to bioabsorbable poly-L-lactide and metallic screws: An experimental study. *Bone* **2006**, 39, 932-937.

71) Agrawal, C.M.; McKinney, J.S.; Lanctot, D.; Athanasiou, K.A., Effects of fluid flow on the in vitro degradation kinetics of biodegradable scaffolds for tissue engineering. *Biomaterials* **2000**, 21, 2443-2452.

72) Lu, L.; Peter, S.J.; Lyman, M.D.; Lai, H.L.; Leite, S.M.; Tamada, J.A.; Uyama, S.; Vacanti, J.P.; Langer, R.; Mikos, A.G., In vitro and in vivo degradation of porous poly(DL-lactic-co-glycolic acid) foams. *Biomaterials* **2000**, 21, 1837-1845.

73) Lu, L.; Peter, S.J.; Lyman, M.D.; Lai, H.L.; Leite, S.M.; Tamada, J.A.; Vacanti, J.P.; Langer, R.; Mikos, A.G., In vitro degradation of porous poly(L-lactic acid) foams. *Biomaterials* **2000**, 21, 1595-1605.

74) Yu, N.Y.C.; Schindeler, A.; Little, D.G.; Ruys, A.J., Biodegradable poly(α-hydroxy acid) polymer scaffolds for bone tissue engineering. *Journal of Biomedical Materials Research Part B: Applied Biomaterials* **2010**, 93B, 285-295.

75) Yang, X.B.; Whitaker, M.J.; Sebald, W.; Clarke, N.; Howdle, S.M.; Shakesheff, K.M.; Oreffo, R.O., Human osteoprogenitor bone formation using encapsulated bone morphogenetic protein 2 in porous polymer scaffolds. *Tissue Engineering* **2004**, 10, 1037-1045.

76) Howard, D.; Partridge, K.; Yang, X.; Clarke, N.M.P.; Okubo, Y.; Bessho, K.; Howdle, S.M.; Shakesheff, K.M.; Oreffo, R.O.C., Immunoselection and adenoviral genetic modulation of human osteoprogenitors: In vivo bone formation on PLA scaffold. *Biochemical and Biophysical Research Communications* **2002**, 299, 208-215.

77) Nagura, I.; Fujioka, H.; Kokubu, T.; Makino, T.; Sumi, Y.; Kurosaka, M., Repair of osteochondral defects with a new porous synthetic polymer scaffold. *Journal of Bone and Joint Surgery – British Volume* **2007**, 89-B, 258-264.

Chapter Five

Preparation and Characterization of Anorganic Bone (AB)/Poly-ε-Caprolactam (PCLM) Biocomposites

Introduction and Background

Previous work in Professor Redepenning's research group has focused on using the nucleophilic surface of hydroxyapatite (HA) to initiate the ring opening polymerization (ROP) of lactones, specifically L-lactide. Composites of anorganic bone (AB), the inorganic framework left behind when the organic material is removed from bone, and poly-L-lactide produced using this process exhibited microscopic morphologies and mechanical properties similar to the living bone.[1-3] Since the first AB/PLLA composites were developed, several additional lactones have been polymerized using the surface of HA. These include glycolide, ε-caprolactone, and p-dioxanone. ε-Caprolactam is structurally similar to ε-caprolactone, with an amide group taking the place of the ester group (Figure 5.1). Due to this structural similarity, it was hypothesized that HA would be capable of initiating the ROP of ε-caprolactam. This chapter describes efforts to prepare an AB/PCLM composite with a microscopic morphology and mechanical properties similar to living bone.

ε-Caprolactam is a cyclic amide containing six carbons and one nitrogen atom within a ring (Figure 5.1).[4] It is the precursor to the polymer nylon 6. There are two common ways to initiate the ROP of ε-caprolactam. The first is hydrolysis at temperatures above 250 ^{o}C. Linear polymer chains can be formed through polycondensation, but the more common route is through polyaddition. The equilibrium of this reaction results in a 90% conversion to the polymer.[5, 6] It is also possible to

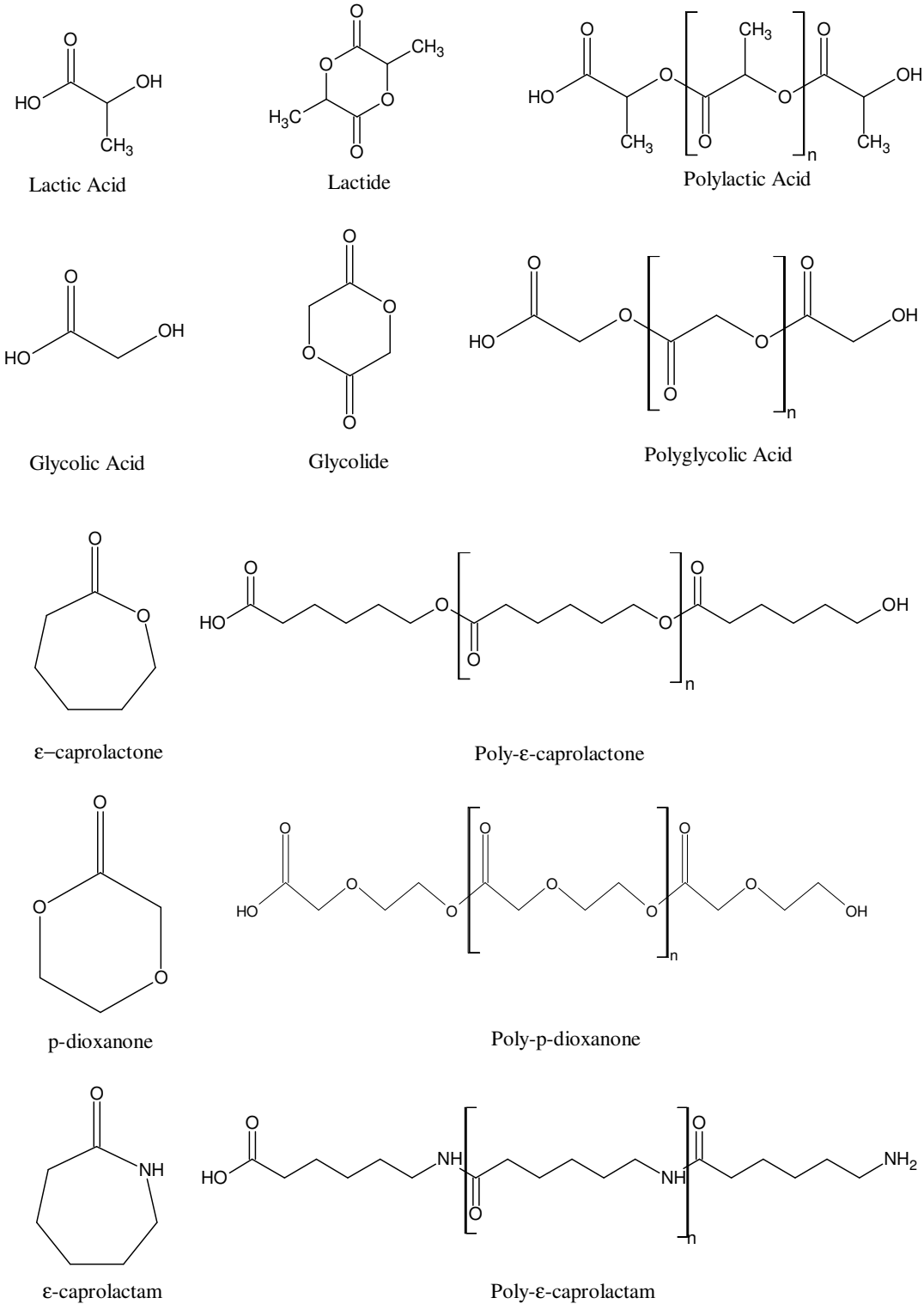

Figure 5.1. Structures of common bioresorbable polymers and their respective monomers that have been polymerized using the surface of hydroxyapatite.

polymerize ε-caprolactam by anionic polymerization. This can be carried out at temperatures around 150 ^{o}C in the presence of a strong base.[7-9] In addition to these common industrial techniques, ε-caprolactam has also been polymerized using metal oxides as a catalyst,[10, 11] alkali metal hydroxides, and carbonates or bicarbonates.[12]

Nylon has often been used as surgical suture in biomedical applications. Two examples are Ethilon™ and Nurolon™.[13] Recently, several attempts have been made to create composites of HA/PCLM by infusing a porous HA scaffold with ε-caprolactam and initiating the polymerization with various initiators. The ultimate goal of these studies has been to increase the mechanical strength of the HA scaffold.[14-17] In all these previous cases, the surface of HA was not used to initiate the ROP of ε-caprolactam, as is described in this chapter.

Due to the amide bond, nylon and other polyamides are degraded similar to natural polypeptides.[18] They absorb 9-11% water by weight and degrade by ion-catalyzed surface and bulk hydrolysis. Hydrolysis by enzymatic catalysis is also possible and leads to surface erosion.[19] Longer chain polyamides (polydodecanamide) are more stable than shorter chain polymers. In one study nylon 6,6 lost 25% of its tensile strength after 89 days and 83% after 276 days in dogs.[20, 21]

In addition to safety and biocompatibility, the efficacy and performance of the bone graft substitute must be evaluated.[22] The mechanical properties of a material are certainly relevant to its efficacy. An ideal bone graft substitute should have mechanical properties similar to that of the bone it is replacing so that the substitute can withstand the stress and strain of its environment. If these properties are too dissimilar the implant may fail mechanically or issues at the bone-implant interface may arise that could affect the

ability of new bone to grow into the implant.[23-25] In this chapter, a discussion of the compression and torsional properties of the AB/PCLM composites will be provided in addition to details concerning their preparation.

Static mechanics deals with the influence of forces on the form of a body at rest or when there is equilibrium between forces. For the purposes of performing mechanical characterizations, these forces are generally categorized as compressive, tensile, or shear force. These forces are defined by the direction and effect of the force on the body. A compressive force is applied towards the surface of the material and results in shortening and fattening of the sample. A tensile force is applied away from the surface, resulting in stretching and elongation of the sample. A shear force is applied perpendicular to the surface, causing a change in shape to the sample (Figure 5.2). Force is measured in newtons. One newton is the force needed to accelerate a 1 kg mass at a rate of 1 m/sec^2. A load cell is used to record the applied force, and sample dimensions are indicated by the load application system. The resulting load-displacement curve gives the total deformation in the direction of the applied force. These forces are normalized so that samples of different shapes and size can be compared. The force and deformation are normalized by dividing by the dimensions of the sample to give stress and strain, which form the stress-strain curve. Stress (σ) is the resistance of the material to the force acting upon it. It is defined as shown below,

$$\sigma = F/A \tag{5.1}$$

where F is the force and A is the cross sectional area over which the force acts. For a cylindrical sample, equation 5.1 becomes

$$\sigma = \frac{F}{\pi r^2} \tag{5.2}$$

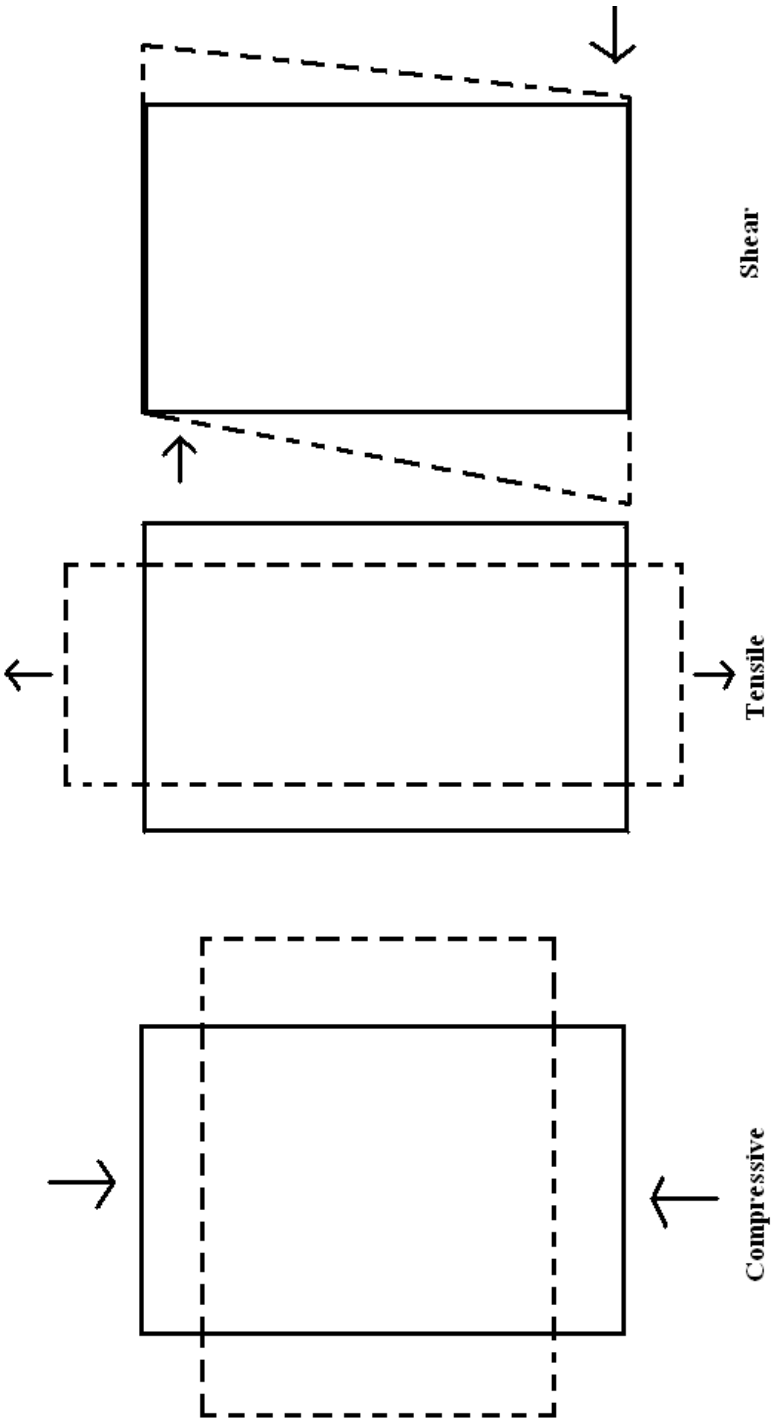

Figure 5.2. Three basic types of force: compressive, tensile, and shear. The symbol (—) represents the original shape and (- - -) represents the shape after the force is applied.

where r is the radius of the cylinder. In a stress-strain plot, stress is plotted on the y-axis and has units of pressure (Pa = N/m^2). Strain (ε) is defined as the geometric change in a material in response to the applied force. When the sample is compressed, its dimensions change as it is deformed. Strain is defined as

$$\varepsilon = \Delta h/h \tag{5.3}$$

where Δh is the change in the height, or the distance the load cell has traveled, and h is the height of the sample (Figure 5.3). Strain is dimensionless and is plotted on the x-axis in a stress-strain curve. Ceramic-polymer composites like the AB/PCLM composite described in this chapter are usually treated as brittle materials rather than flexible materials. A simulated stress-strain plot for a brittle material is shown in Figure 5.4. The linear region of the stress-strain curve is the elastic region. In this region, deformation is not permanent and the sample will return to its original shape if the load is removed. Beyond this region, permanent deformation occurs. The slope is known as the elastic modulus (E), which is a measure of a materials resistance to deformation. Brittle samples typically have higher moduli than flexible materials. At the apex of the curve, catastrophic failure occurs in brittle materials. This is the point when the maximum stress a sample can withstand is exceeded and the material fails. For this to occur the force applied on the sample (F_D) must exceed the critical force (F_C), where the critical force is defined as[26-29]

$$F_C = \frac{(Elastic\ Modulus)(Cross\ Sectional\ Area)^2}{(Sample\ Height)^2} \tag{5.4}$$

For cylindrical samples this can be rewritten as

$$F_C = \frac{E\,\pi^2\,r^4}{h^2} \tag{5.5}$$

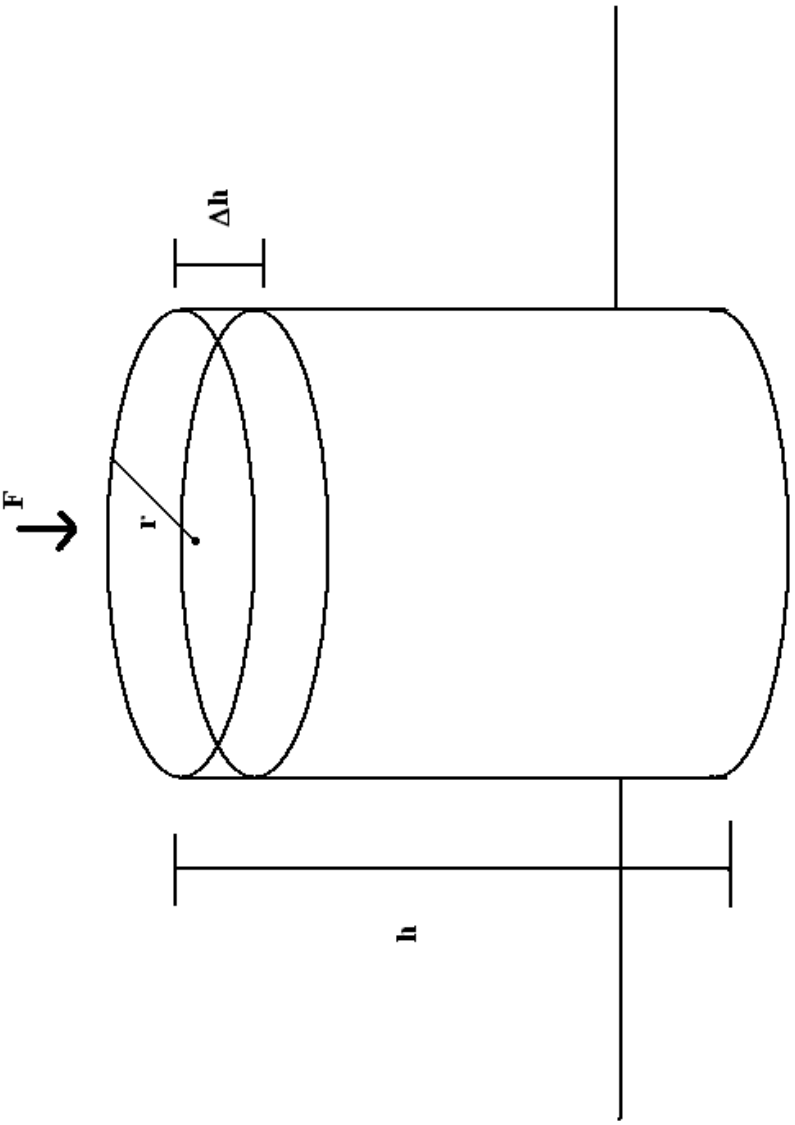

Figure 5.3. Diagram of compressive force being applied to a cylindrical sample of radius (r) and height (h) resulting in a change in the sample height (Δh).

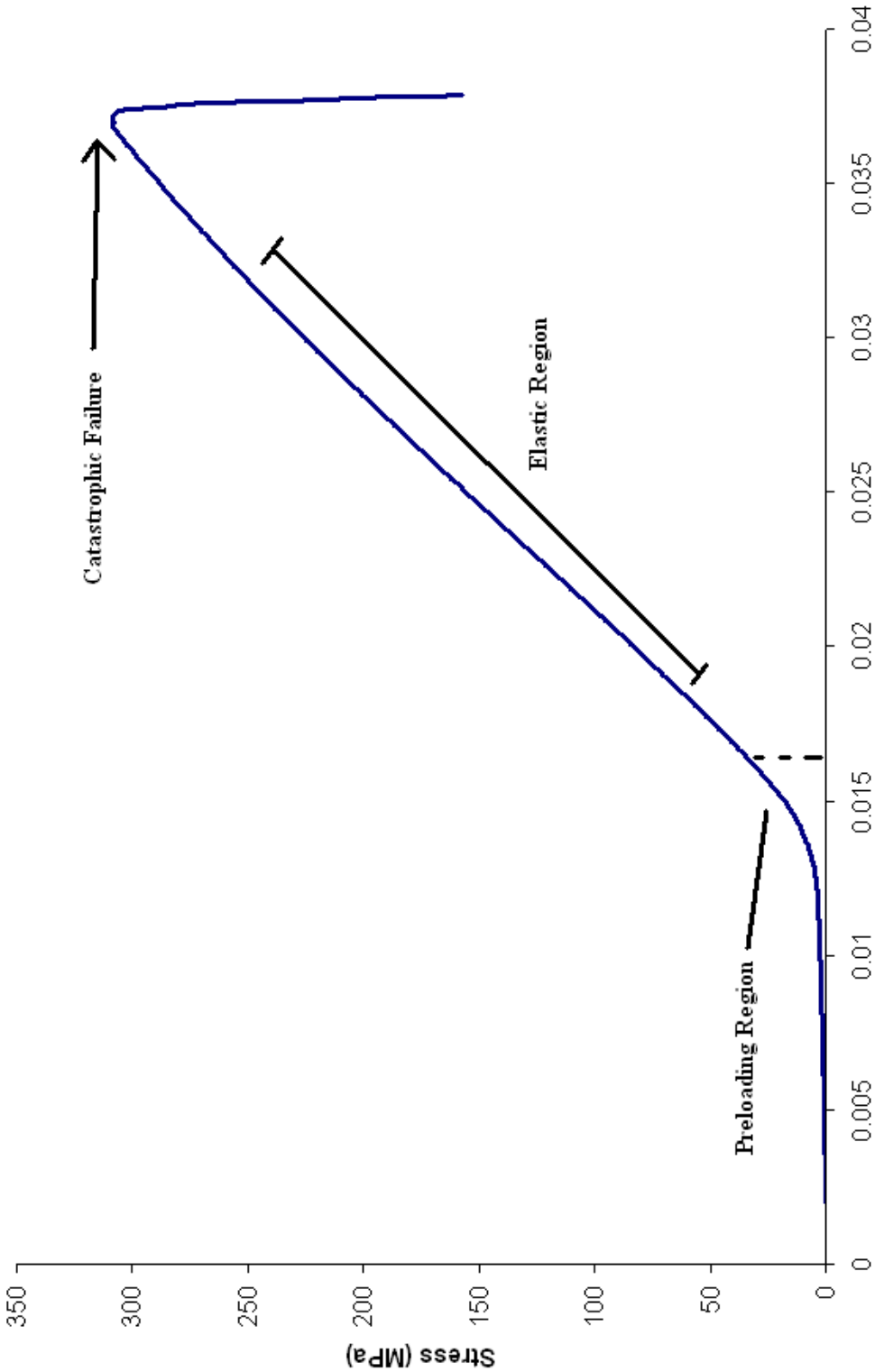

Figure 5.4. Simulated compressive stress-strain curve for a brittle material.

For purposes of later comparing the properties of the AB/PCLM composites, the compressive strength of wet human femoral bone is 167 MPa and the elastic modulus is 17.2 GPa.[30, 31] Bovine femoral bone is reported to exhibit a compressive strength as high as 240-295 MPa and a elastic modulus of 21.9-31.4 GPa.[32] Other reports list its compressive strength as 144 MPa and its modulus as 8.52 GPa.[1, 31]

In addition to being subjected to compressive forces, composites in certain applications, such as screws or pins, can be subjected to torsional forces. Torsion is defined as the twisting of an object due to an applied torque (force). For solid cylinder samples, such as the AB/PCLM composites described in this chapter, torsion stress-strain plots can be constructed similar to the ones constructed for compression testing. For the measurements performed in this chapter, one end of the cylindrical rod was held fixed in a static jaw and the other was attached to a drive motor to twist the sample. A load cell measured the applied torque. The applied torque produces shearing stresses perpendicular to the axis of the cylinder. For this experimental setup the shear stress (τ) on the outside of the cylinder is defined as

$$\tau = \frac{T\,r}{J} \tag{5.6}$$

where T is the torque in Nm, r is the radius of the cylinder, and J is the polar moment of inertia. The term J is a measure of the material's ability to resist torsion,[26] as defined by

$$J = \frac{\pi r^4}{2} = \frac{\pi d^4}{32} \tag{5.7}$$

where d is the diameter of the cylinder. The shear strain (γ), also known as the shear angle, is dependent on the angle of twist (φ), the radius, and the length (L) of the sample (Figure 5.5).

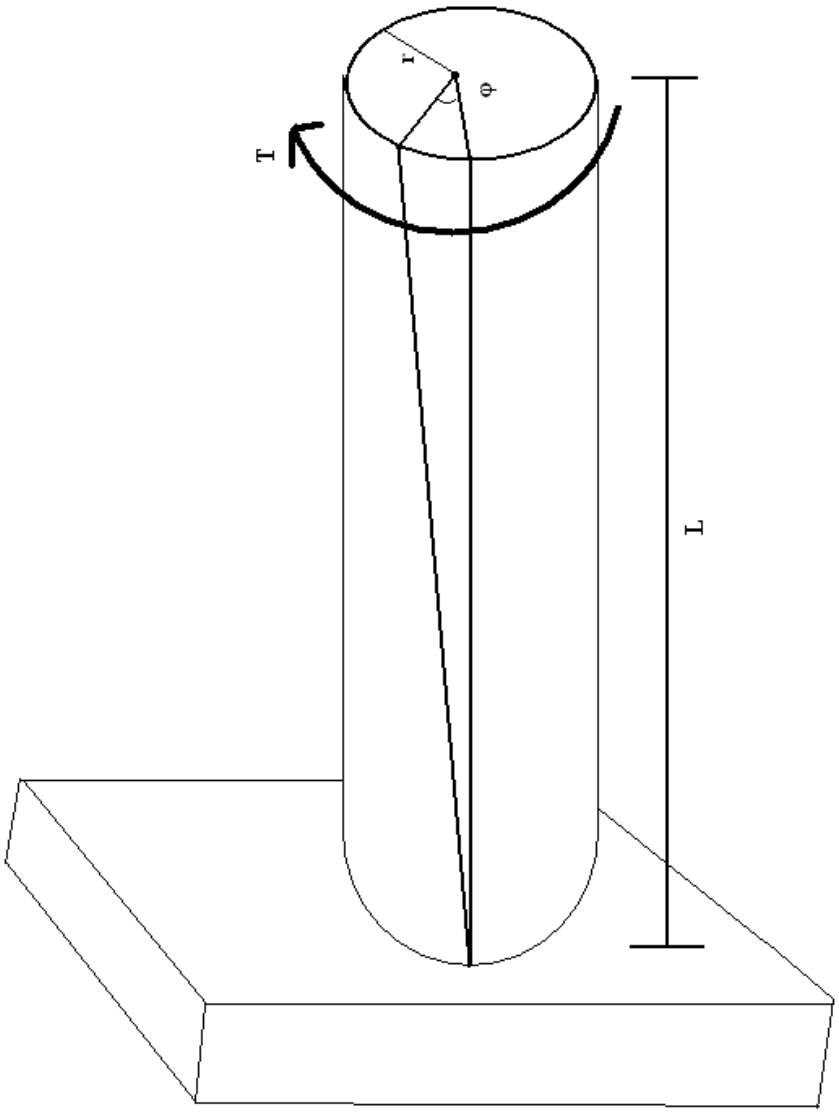

Figure 5.5. Diagram of torque (T) being applied to a cylindrical sample of radius (r) and length (L) and the angle of twist (φ).

$$\gamma = \frac{\varphi r}{L} \tag{5.8}$$

Shear strain can be related to the shear stress through the shear modulus (G), also known as the modulus of rigidity.

$$\gamma = \frac{\tau}{G} \tag{5.9}$$

The modulus of rigidity is a measure of the stiffness of the sample, where stiffer or more brittle samples have higher moduli. Determination of G is one parameter of interest in torsion measurements. Calculation of G can be accomplished by first substituting equation 5.8 into 5.9 to give equation 5.10.

$$\frac{\varphi r}{L} = \frac{\tau}{G} \tag{5.10}$$

Next, equation 5.6 can be substituted into equation 5.10 to give equation 5.11.

$$\frac{\varphi r}{L} = \frac{T r}{J G} \tag{5.11}$$

Equation 5.11 can be rearranged to equation 5.12.

$$T = \frac{G J \varphi}{L} \tag{5.12}$$

The modulus of rigidity can be calculated from the slope when T, in units of Nm, is plotted versus φ, in units of radians. The slope of the linear region can then be multiplied by the sample length and divided by J to yield G in units of Pa.[33, 34] A simulation of such a plot is shown in Figure 5.6. Again, as in the compressive strength plot, the linear region is known as the elastic region. Deformation is not permanent in this region. At the apex of the curve, catastrophic failure occurs in brittle materials. This is the point when the

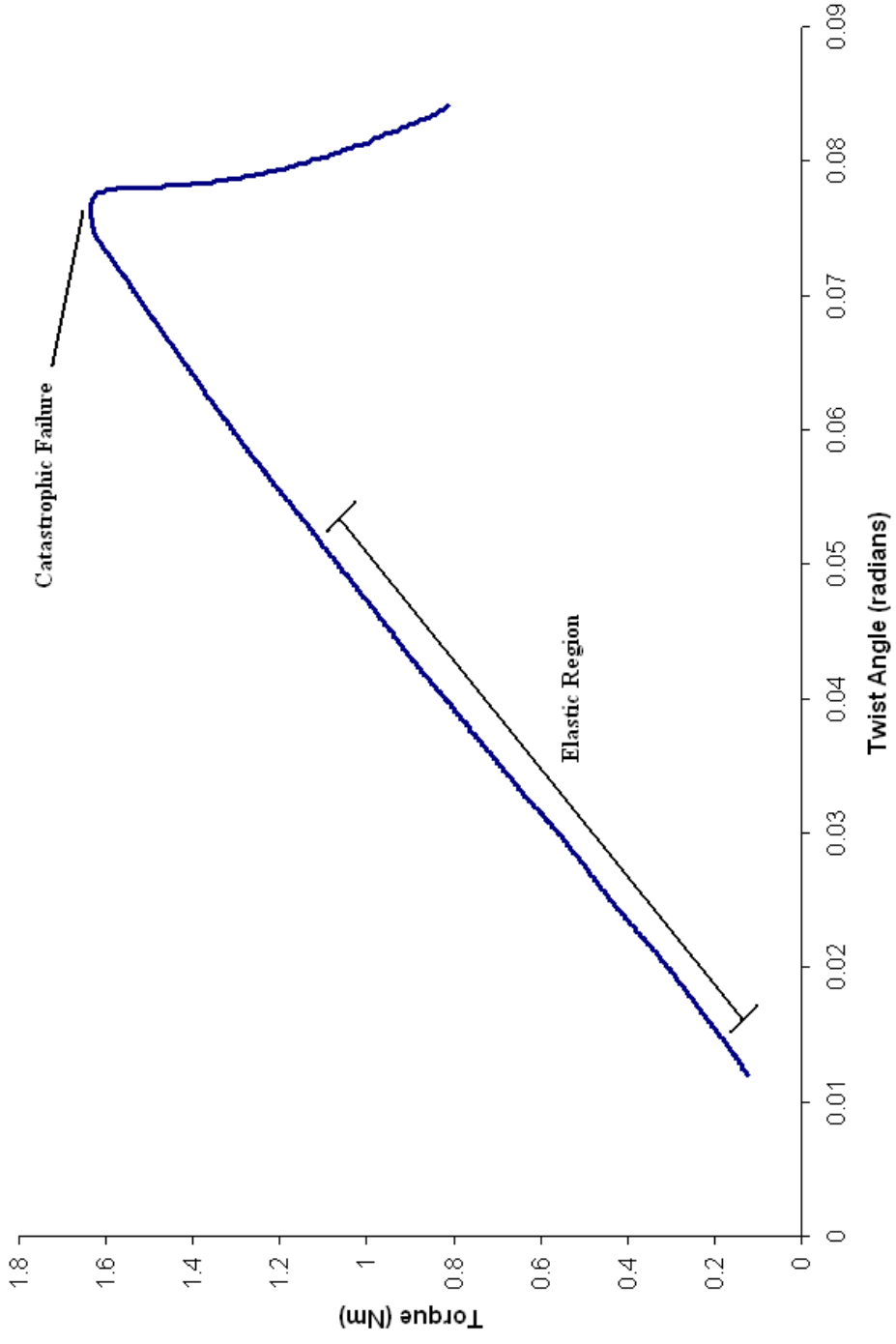

Figure 5.6. Simulation of a torsional torque versus angle plot for a brittle material.

maximum torque a sample can withstand is exceeded and the material fails. Alternatively, stress can be plotted against strain, using equation 5.6 to calculate the stress and equation 5.13 to calculate the strain.

$$\tau = \frac{\varphi r}{L} \tag{5.13}$$

The slope of the linear region of this plot is equal to G in units of Pa.

For purposes of later comparison to the torsional data of the AB/PCLM samples, wet human femoral bone has a torsional strength of 53-71 MPa and a torsional modulus of 3.1 to 3.7 GPa. Wet bovine femoral bone is reported to exhibit a torsional strength of 62-76 MPa, but a modulus was not listed.[32] The broad range of mechanical properties for bone found in the literature can be attributed to a variety of factors. These factors include *in vivo* factors such as age, sex, species, function, and composition and *in vitro* factors such as embalming or fixation, boiling and autoclaving, storage, drying and freeze drying, sterilization, and testing procedure.[35]

Experimental

Chemicals: Deuterated chloroform ($CDCl_3$, 99.8% D from Sigma-Aldrich, St. Louis, MO), ε-caprolactam (99%+ from Acros Organics, Geel, Belgium), ethylenediamine (99% from Sigma Aldrich), and nylon 6 (from Sigma Aldrich), 2,2,2-trifluoroethanol (TFE, ≥ 99% from Sigma Aldrich) were used as purchased from their respective suppliers. Anorganic cortical bone was derived from bovine femur donated by Premium Protein Products (Lincoln, NE).

Preparation of anorganic cortical bone: A band saw was used to remove the distal and proximal ends of the bovine femurs and to cut them into 1.5 to 2 cm thick sections along their longitude. Cylindrical plugs of cortical bone, with a diameter of 6 mm and a

length between 12 and 20 mm, were machined in the longitudinal direction from the diaphyseal section of the bovine femur using a 6 mm diameter dowel tool. A Soxhlet extractor was then used to remove the majority of the organic material. The solvent mixture used for the extraction was 80% ethylenediamine and 20% deionized water (v/v).[36] The solvent was observed to reflux at 119 ^{o}C. The samples were extracted for a minimum of 48 hr. Fresh solvent cycled through approximately every 10 min. After the extraction period, the solvent mixture was replaced with deionized water. The Soxhlet extraction of the bone cylinders with water was continued until the water was neutral pH. The water was replaced 3-4 times during this process. At this stage the bone cylinders which were greatly whitened were removed and allowed to dry at room temperature in air.

Preparation of AB/PCLM composites: Extracted rods of anorganic bone were then activated by heating in air at either 600 ^{o}C for 96 hr or 700 ^{o}C for 16 hr in air. Activated samples were then placed in a vacuum desiccator and cooled to room temperature under vacuum, where upon they were transferred to a $N_{2(g)}$ atmosphere glove box for later use. The preparation of the desired AB/PCLM composite was initiated by placing an anorganic bone plug in a Pyrex glass tube that was approximately 9.5 mm in diameter. Excess of ε-caprolactam was added to the tube so that the sample was covered. The tubes were sealed with a short section of tygon tubing that was closed with a hose clamp. They were then removed from the $N_{2(g)}$ glove box and attached to a rotary vane rough pump. The samples were maintained under a vacuum for 10 min before the bottom was dipped in liquid N_2 and the vacuum was maintained for an additional 5 min. The tubes were then sealed at a reduced pressure (~30 mTorr) after placing a slight

constriction near the midsection. The polymerizations were carried out by placing the sealed reaction vessel and its contents in a convection oven at one of three temperatures: 200 ^{o}C, 250 ^{o}C, or 300 ^{o}C. At 200 ^{o}C, reaction times varied from 5 to 12 days. At 250 ^{o}C, reaction times varied from 4 to 17 days with the most common length being 7 or 8 days. At 300 ^{o}C, reaction times varied from 32 hr to 168 hr with the most common lengths being 32 or 48 hr. Samples were all immersed for a period of time and then the reaction vessels were inverted to drain the excess monomer/polymer to the other end of the reaction tube. At the end of the preselected reaction period, the reaction vessels were removed from the oven and allowed to cool to room temperature. Samples were then removed from the reaction vessels and excess polymer on the outside of the cylinder was removed using a Colchester-Clausing lathe. A rotation speed of 800 rpm was used to machine the samples into cylinders with a height to diameter ratio of 2:1, typically 11 mm x 5.5 mm. Samples used for torsional strength determination were machined into cylinders with a recess cut out of the center. The resulting device resembled a dumbbell (Figure 5.7). The recess was the weakest portion of the sample; hence its dimensions were used in determining the material's properties.

Compressive strengths of the AB/PCLM composites were measured using a single-axis Instron 5967 electromechanical machine with a 30 kN load cell (Department of Chemistry, University of Nebraska-Lincoln (UNL)). Instrument control, data acquisition, and data processing were performed using Blue Hill version 2.23 software (Norwood, MA). Specimens were subjected to compression testing using a 1.0 mm/min crosshead speed. Torsional strengths were measured using an Instron MT1 fitted with a 200 in-lb torque load cell (College of Dentistry, Department of Chemistry, UNL).

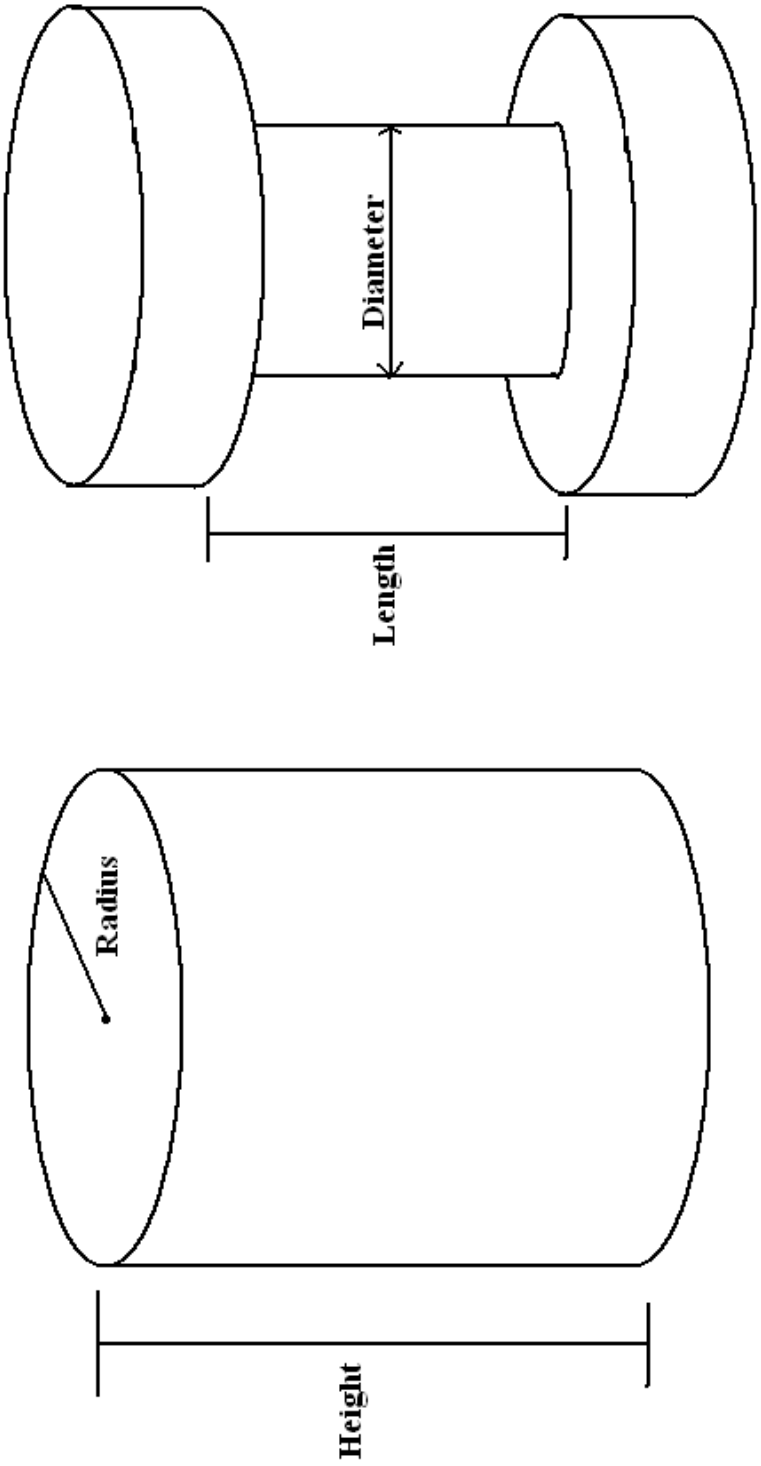

Figure 5.7. Representative diagram of samples used for (left) compressive and (right) torsional testing.

Instrument control, data processing, and data acquisition were performed using Partner version 8.4d software (Norwood, MA). Specimens were subjected to torsional testing using a 0.5 rev/min turn rate. Scanning electron microscopy (SEM) was performed using a Hitachi (Tokyo, Japan) S4700 Field-Emission microscope (Morrison Microscopy Core Facility, UNL). ^{1}H NMR spectra were obtained using a Bruker (Billerica, MA) 300 MHz or 400 MHz Bruker DRX Avance spectrometer (Research Instrumentation Facility (RIF), UNL). Spectral processing was done using Bruker Topspin 3.0.b.8. AB/PLCM samples were dissolved in a solution containing a 3:1 ratio (v/v) of trifluoroethanol and $CDCl_3$. All chemical shifts are referenced to the $CDCl_3$ peak at 7.27 ppm. Chemical shifts for PCLM were verified by comparison to values reported previously in the literature.[37, 38]

Results and Discussion

The specific goal of this chapter of my thesis was to successfully initiate the polymerization of ε-caprolactam of anorganic bone to produce a composite relevant to the repair or reconstruction of extremity trauma or craniofacial injuries. To begin with, it was necessary to determined if hydroxyapatite could even be used to polymerize ε-caprolactam to poly-ε-caprolactam, in a manner similar to that described previously to polymerize various lactones.[1-3, 39, 40] Powdered HA and ε-caprolactam were combined in a 1:1 mass ratio in a glass tube and sealed under a reduced pressure. The tube was placed in a convection oven at 185 ^{o}C. Once the monomer melted, the resulting suspension exhibited low viscosity, but by 65 hr it was so viscous that little flow was observed upon tilting the reaction vessel. This observation was a strong and positive indicator that the desired polymerization was possible. Next ^{1}H NMR spectroscopy was performed on ε-caprolactam (Figure 5.8) and nylon 6 (Figure 5.9) to identify and assign the peaks. In

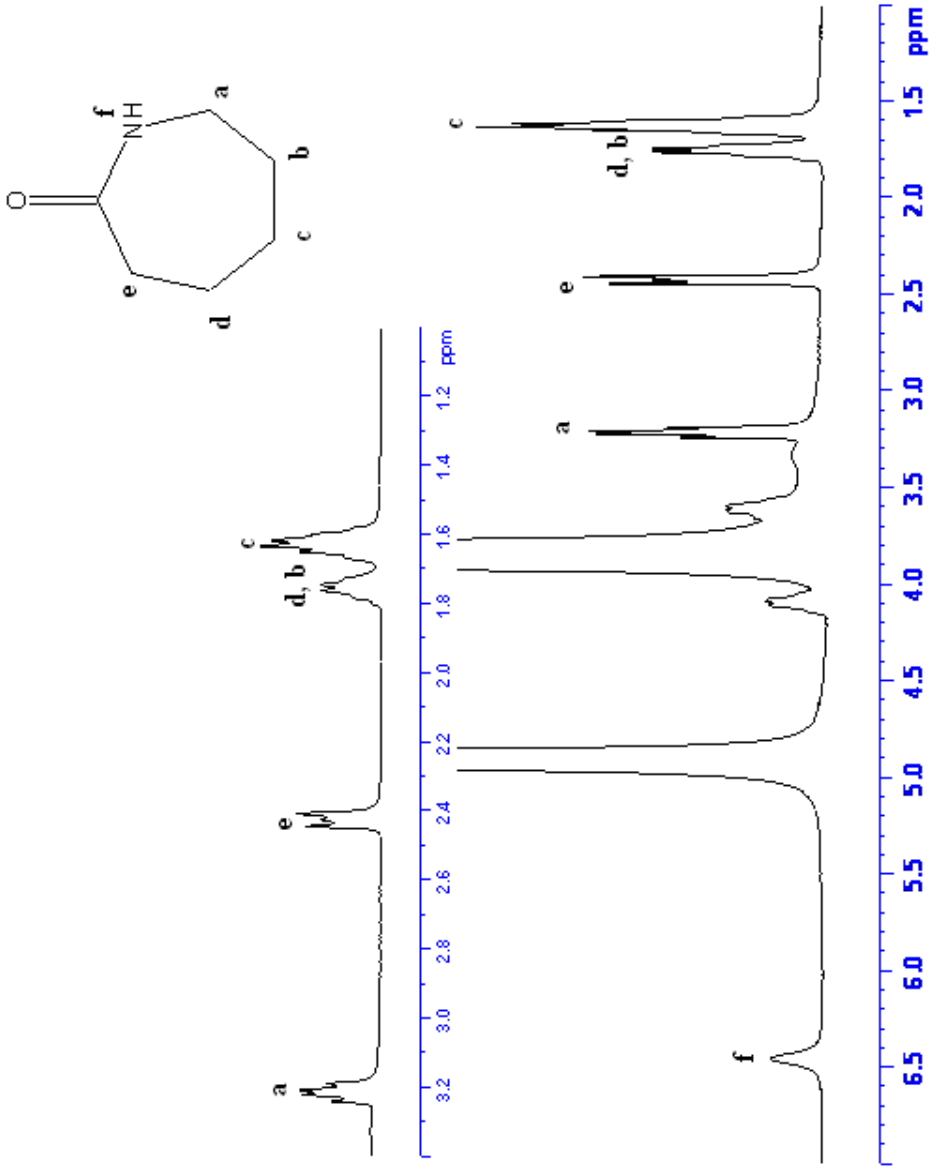

Figure 5.8. ^{1}H NMR spectrum of ε-caprolactam.

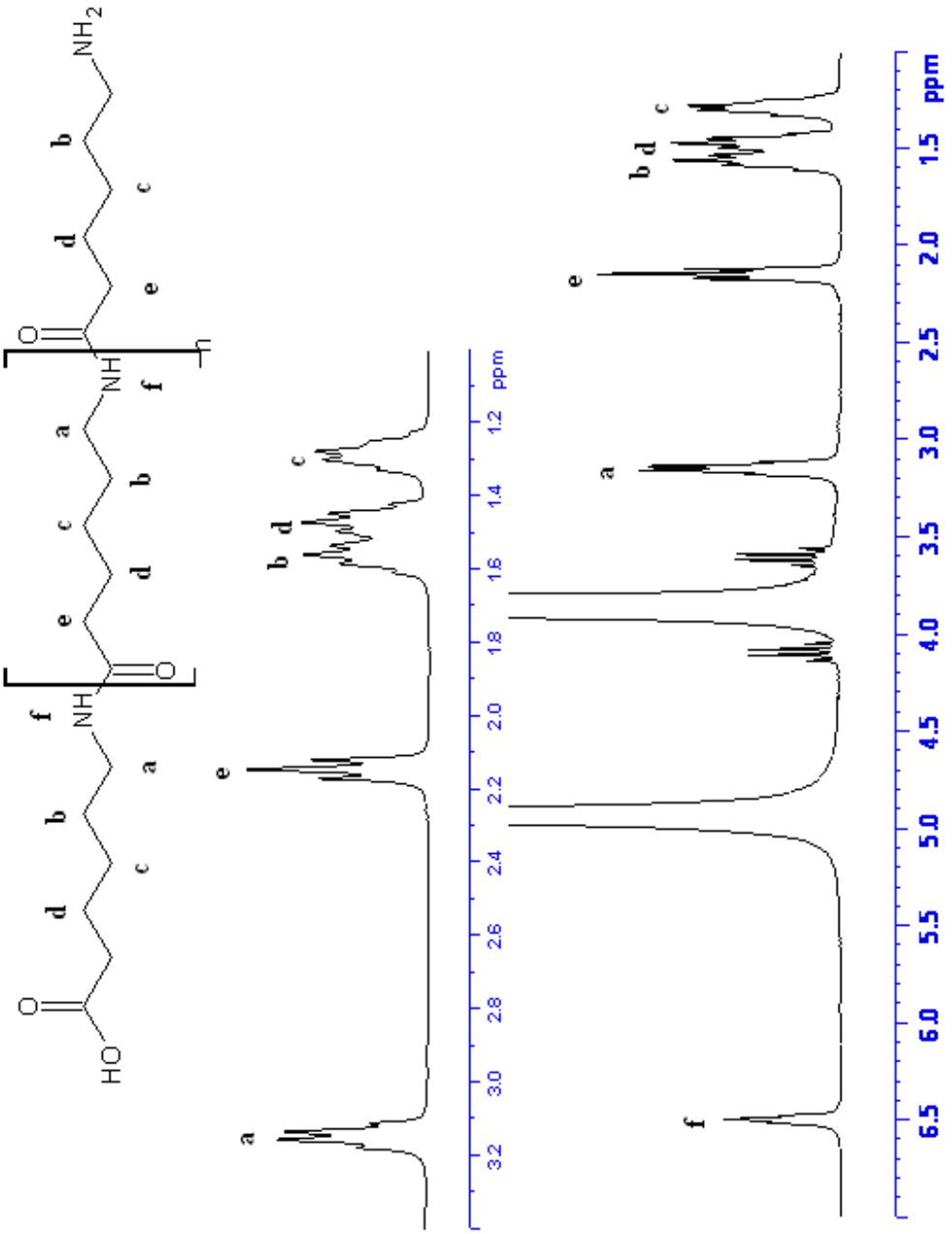

Figure 5.9. ^{1}H NMR spectrum of nylon 6.

Figure 5.8, the quartet at 3.21 ppm is due to the methylene protons next to the nitrogen in the amide. The triplet at 2.42 ppm is due to the methylene protons adjacent to the carbon involved in the amide group. The proton attached to the nitrogen appears as a singlet at 6.49 ppm. The multiplets between 1.5 and 1.8 ppm are the remainder of the protons in the lactam ring. The two large peaks between 3.5 and 5 ppm are due to the solvent, trifluoroethanol. In Figure 5.9, the quartet at 3.15 ppm is due to the internal methylene protons adjacent to the nitrogen in nylon 6. The triplet at 2.15 ppm is due to the internal methylene protons adjacent the carbon involved in the amide group. The proton attached to the nitrogen appears at 6.45 ppm. The multiplets from 1.1 to 1.7 ppm are associated with the remaining internal protons of nylon 6. Again the two large peaks are due to the solvent.

The next reaction temperature chosen was 200 ^{o}C. Although the powder HA reaction had proceeded relatively quickly at 185 ^{o}C, I wished to increase the reaction rate even further. Samples were heated to 700 ^{o}C for 16 hr to activate them prior to their use as polymerization initiators. During this process, the samples lost 14 ± 2% (n = 10) of their mass. One set was reacted for 5 days total. At the end of this period of time the samples gained 26 ± 7% of their mass, but this additional mass was only 35 ± 8% polymer. The percent polymer was determined from the ^{1}H NMR spectrum (Figure 5.10). The area of the peaks at 2.42 and 2.15 ppm, due to the methylene protons adjacent the carbon in the amide group for the monomer and polymer, were integrated. The integrated area of the polymer peak was divided by the total area and multiplied by 100. These peaks were chosen because they had the greatest separation in the spectrum and were resolved from other responses due to other protons in the system. In addition to

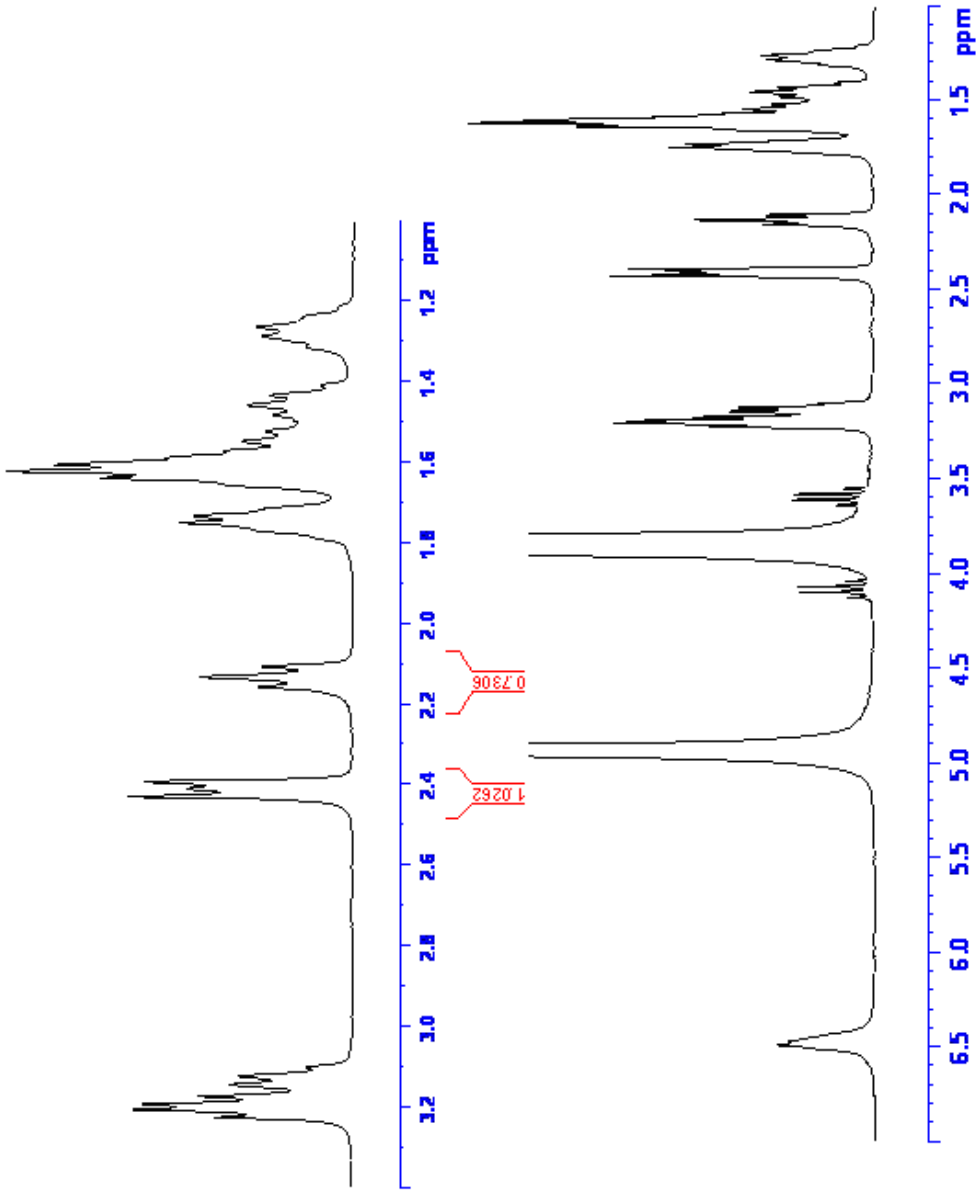

Figure 5.10. ^{1}H NMR spectrum of an AB/PCLM composite prepared at 200 ^{o}C for 5 days.

being 65% monomer, these samples proved to be extremely brittle and fragile. Another set of samples were reacted for 12 days total. These samples lost 9.1 ± 0.4% (n = 10) of their mass when heated to 700 ^{o}C for 16 hr. At the end of a 12 day reaction period, a mass gain of 31 ± 5% was observed. ^{1}H NMR spectroscopy was performed on one of the samples and revealed it was only 31.4% polymer. It was concluded that 200 ^{o}C was not a desirable reaction temperature, and hopefully not optimal.

Next 300 ^{o}C was chosen as the reaction temperature. Anorganic bone samples were activated at 700 ^{o}C for 16 hr and lost 9.5 ± 0.5 % (n = 16) of their mass. The reaction time at this temperature was either 48 hr or 32 hr. At the end of the preselected reaction periods, the two sets gained similar amounts of mass, 36 ± 3% (n = 6) for 48 hr samples and 37 ± 4 % (n = 10) for 32 hr samples. ^{1}H NMR spectroscopy was performed on one sample from each set and it was shown that the 48 hr sample was 87.8% polymer and the 32 hr sample was 80.5%. These samples were also observed to turn yellow at 300 ^{o}C. This discoloration was not observed for reactions performed at 200 ^{o}C where the polymer was white. To determine the optimum reaction time at 300 ^{o}C, I performed a series of reactions for varying lengths of time between 32 and 168 hr. The results of these reactions can be seen in Table 5.1. Once again the samples were activated at 700 ^{o}C for 16 hr. During this time they lost 9.4 ± 0.8% of their mass, which is consistent with results reported immediately above. From this series of reactions it appears that under these conditions the percent polymer of the resulting composite reaches a maximum around 50-60 hr before beginning to decline. A set of samples were prepared for compression testing based on these results. The samples were heated at 700 ^{o}C for 16 hr and lost 10 ± 1% (n = 6) of their mass. After a 48 hr reaction period the samples gained

Sample	Reaction Time (hr)	Mass Gain (%)	Organic Material that was Polymer (%)
53	32	36.9	80.2
54	32	34.3	66.7
55	36	36.8	84.1
56	36	40.7	74.3
57	40	44.8	88.0
58	40	41.9	83.3
59	44	33.4	77.9
60	44	43.2	83.9
61	48	46.1	92.8
62	48	44.4	92.2
63	52	32.8	89.7
64	56	31.9	90.4
65	60	44.9	91.6
66	72	31.0	80.8
67	72	31.7	81.8
68	96	35.2	80.4
69	120	27.2	76.2
70	144	26.8	75.8
71	168	31.6	74.4

Table 5.1. Results from the polymerization of ε-caprolactam initiated by anorganic bone at 300 ^{o}C for varying lengths of time.

42 ± 6% of their initial mass and of that mass, 85 ± 3% was PCLM based on ^{1}H NMR integrations (Figure 5.11). The compressive strength of the samples was found to be 184 ± 55 MPa and the elastic modulus was 9.7 ± 1.3 GPa. This compares favorably to the values listed earlier for human femoral bone,[30, 31] and within the broad range of values for bovine femoral bone.[32] This value is also comparable to the values of AB/poly-L-lactide (PLLA) composites prepared under similar conditions.[3] The AB/PLLA composites were first activated by sintering the bone in air for 16 hr at either 700 ^{o}C or 675 ^{o}C. Prepared previously, the activated anorganic bone was then reacted with L-lactide at 130 ^{o}C under reduced pressure until the reaction was deemed complete. The resulting composites have compressive strengths of 194 ± 26 MPa and 212 ± 62 MPa, and elastic moduli of 8.85 ± 0.49 GPa and 13.2 ± 1.7 GPa, respectively.[3]

Because discoloration of the PCLM from white to yellow was an issue at 300 ^{o}C, the reaction temperature was lowered to 250 ^{o}C. The samples were again activated at 700 ^{o}C for 16 hr and lost 10.2 ± 0.9% of their mass during this period. A series of reactions were run for periods ranging from 4 to 15 days, to determine the adequate reaction time. The results are shown in Table 5.2. The percent mass gain due to polymer, as determined by ^{1}H NMR (Figure 5.12), was found to increase until 8 days after which it remained fairly constant. Because the deposited mass of organic material was only 59-77% polymer, an effort was made to increase this percentage. The samples were machined into cylinders for later use in compressive strength testing and to remove excess polymer. They were then reheated for 4 days under reduced pressure at 250 ^{o}C. The result was an increase in the percent polymer present in the composite (Figure 5.13). This increase was partly due to further conversion of the monomer into the polymer, and partly to removal

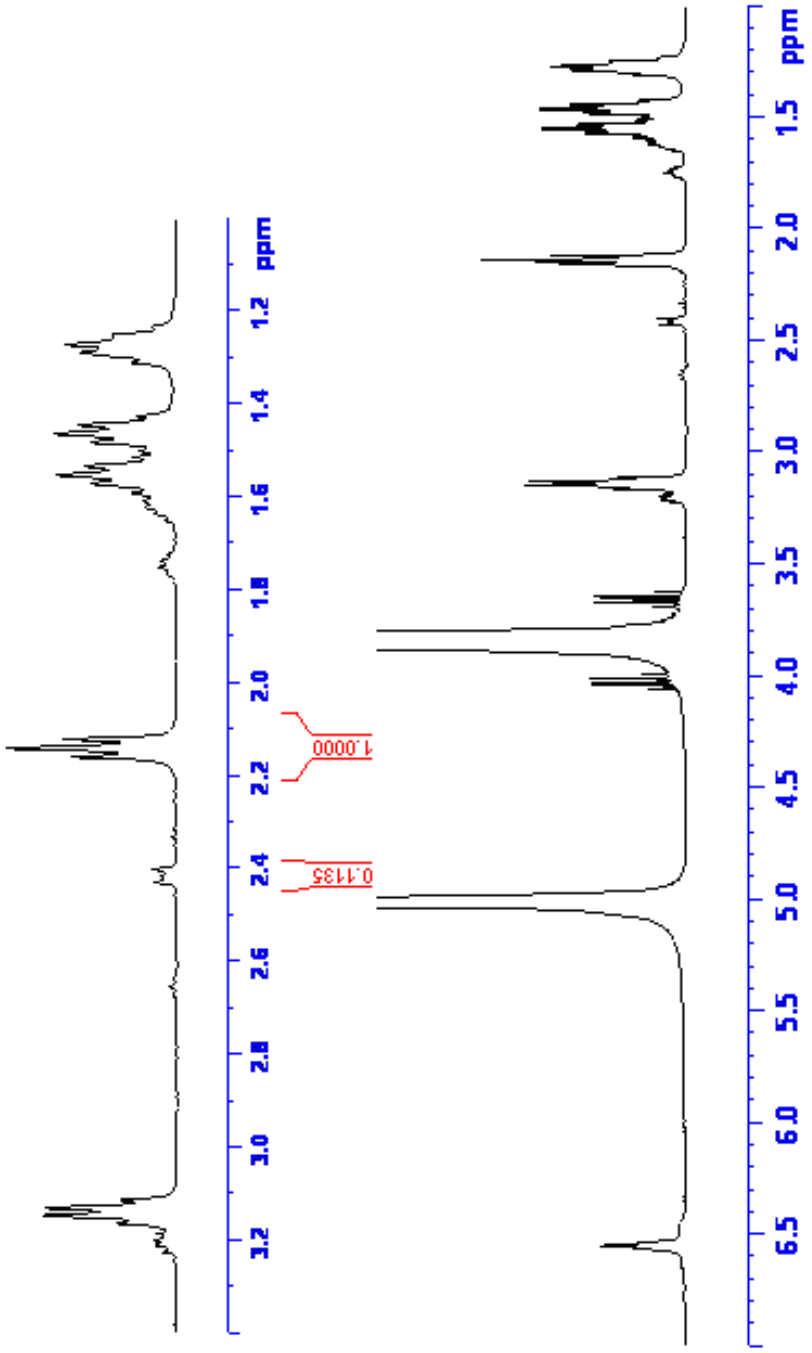

Figure 5.11. ^{1}H NMR spectrum of AB/PCLM composite prepared at 300 ^{o}C for 48 hrs.

Sample	Reaction Time (d)	Volume (cm^3)	(%) Organic Material that was Polymer	Density (g/cm^3)	Mass Loss after Reheating (%)	Void Volume (%)	(%) Reheated Organic Material that was Polymer	Reheated Density (g/cm^3)	Compressive Strength (MPa)	Modulus (GPa)
78	4	0.064	59.6	1.77	2.76	4.5	98.1	1.72	41.1	2.10
79	5	0.148	62.4	1.98	1.26	2.3	96.6	1.95	94.4	4.52
80	6	0.128	65.3	2.02	2.23	4.2	96.5	1.98	97.3	5.16
81	7	0.162	67.7	2.01	2.34	4.3	92.6	1.96	124.5	5.40
82	8	0.211	77.1	2.11	0.47	0.9	90.7	2.10	167.6	6.82
83	9	0.270	75.8	1.98	0.47	0.9	98.8	1.97	213.2	7.07
84	10	0.238	69.8	2.14	1.52	3.0	99.5	2.10	133.9	7.14
85	11	0.227	71.6	2.12	0.60	1.2	98.3	2.10		
86	12	0.173	73.8	2.10	0.83	1.6	92.7	2.08	128.25	5.67
87	15	0.200	68.1	2.02	0.84	1.6	97.4	2.00	159.0	6.36

Table 5.2. Results from the polymerization of ε-caprolactam initiated by anorganic bone at 250 ^{o}C for varying lengths of time and the mechanical properties of the resulting composites.

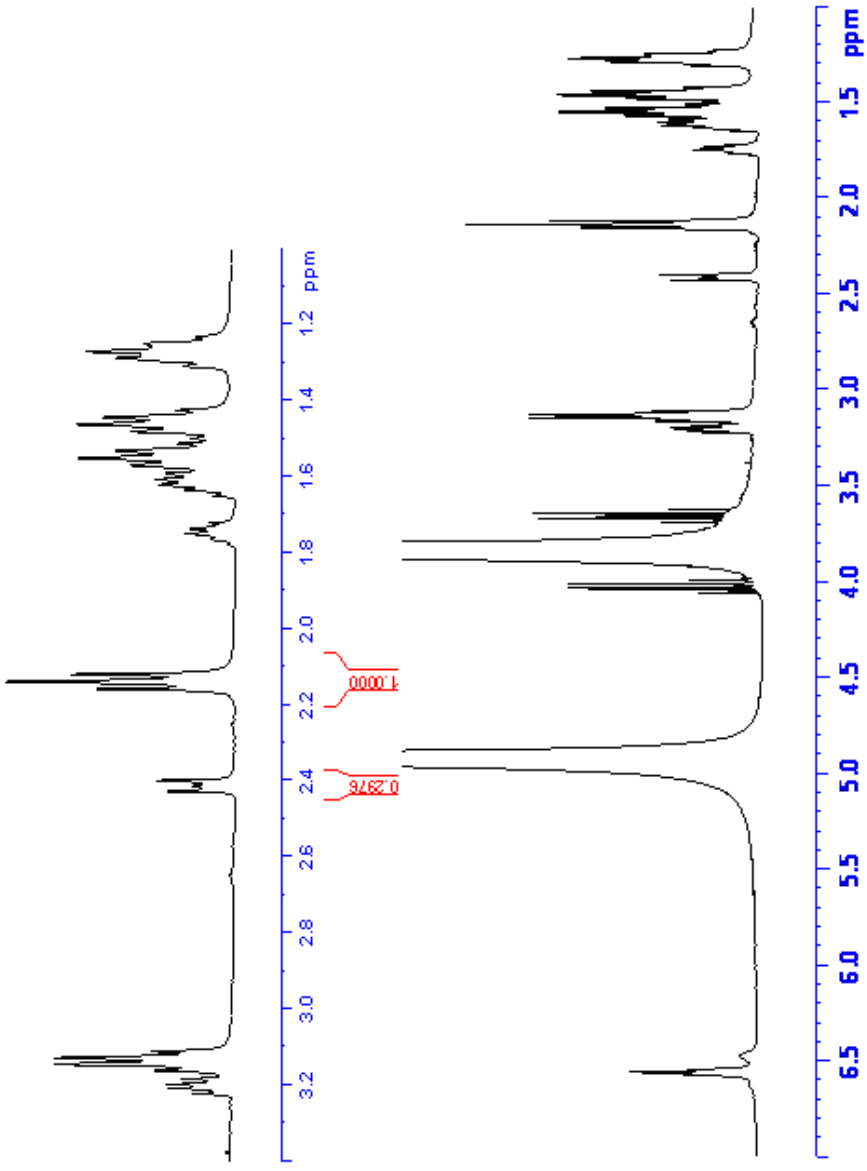

Figure 5.12. ^{1}H NMR spectrum of AB/PCLM composite prepared at 250 ^{o}C for 8 days. The percent of the mass gain that is polymer is 77.07 % for this particular sample.

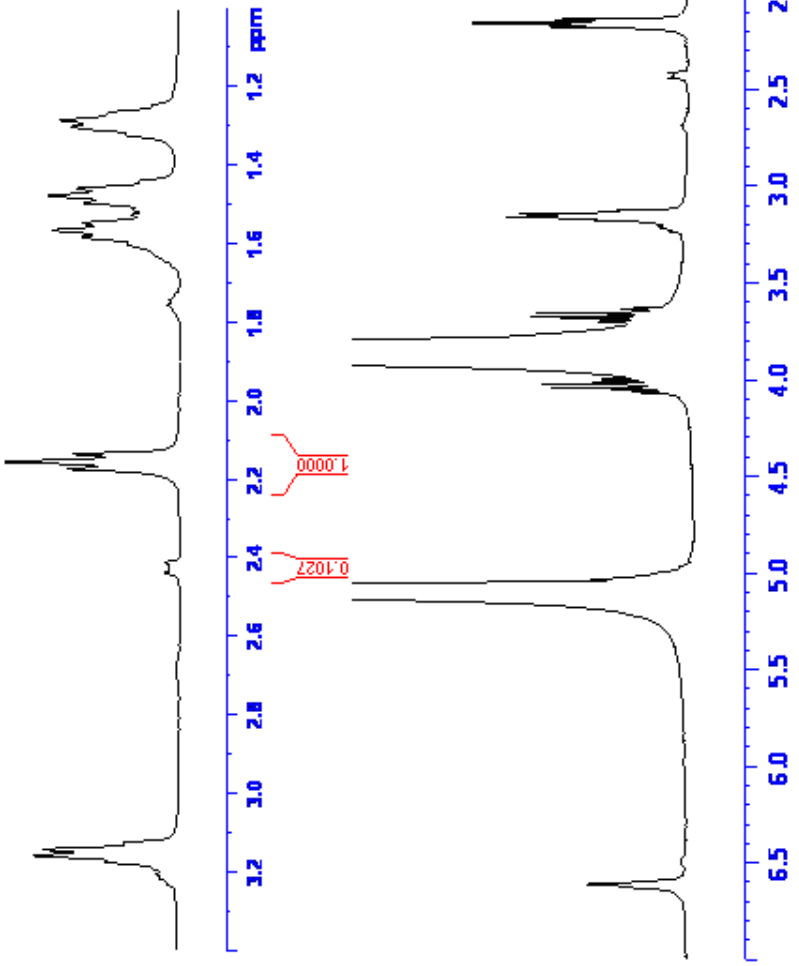

Figure 5.13. ^{1}H NMR spectrum of the AB/PCLM composite from Figure 5.12 reheated under vacuum for 4 days at 250 °C. The percent of the mass due to polymer is now 90.69%.

of excess monomer. The loss of excess monomer was first confirmed when I observed material deposited on the reaction vessel walls after reheating the samples. As can be seen in Table 5.2, a mass loss was observed for all samples. The mass loss was higher for the samples that had a higher percentage of monomer originally present. The compressive strength and elastic modulus values are also listed in Table 5.2. No value is listed for sample 85 because it broke after reheating. For the composites listed in Table 5.2, the compressive strength was plotted versus the volume of the sample (Figure 5.14). This plot showed a linear relationship with a high degree of correlation. Such a result is unexpected because compressive strength is an intrinsic property of a material, and therefore should not vary with its composite. Results in the literature suggest strain rate has an affect on the observed compressive strength of bone.[41, 42] Strain rate ($\dot{\varepsilon}$) is defined as

$$\dot{\varepsilon} = \frac{\nu}{l_o} \tag{5.14}$$

where ν is the speed of deformation and l_o is the original length of the sample. The literature results are at best inconclusive, and often contradictory. It is noteworthy that my results are not highly correlated with strain rate. For the composites listed in Table 5.2, it is presently unclear what the relationship is between compressive strength and sample volume. Dr. Mark Beatty, Professor of Dentistry at the University of Nebraska Medical School, has postulated that the mineral distribution and the content might not be proportional for each cylinder size. With bone, as it becomes larger and therefore supports more weight (or other force), the thickness of the outer annulus increases, the bone is often denser (corresponding to increased HA content), and the crystalline microstructure changes to accommodate greater compressive loads. With this in mind, a

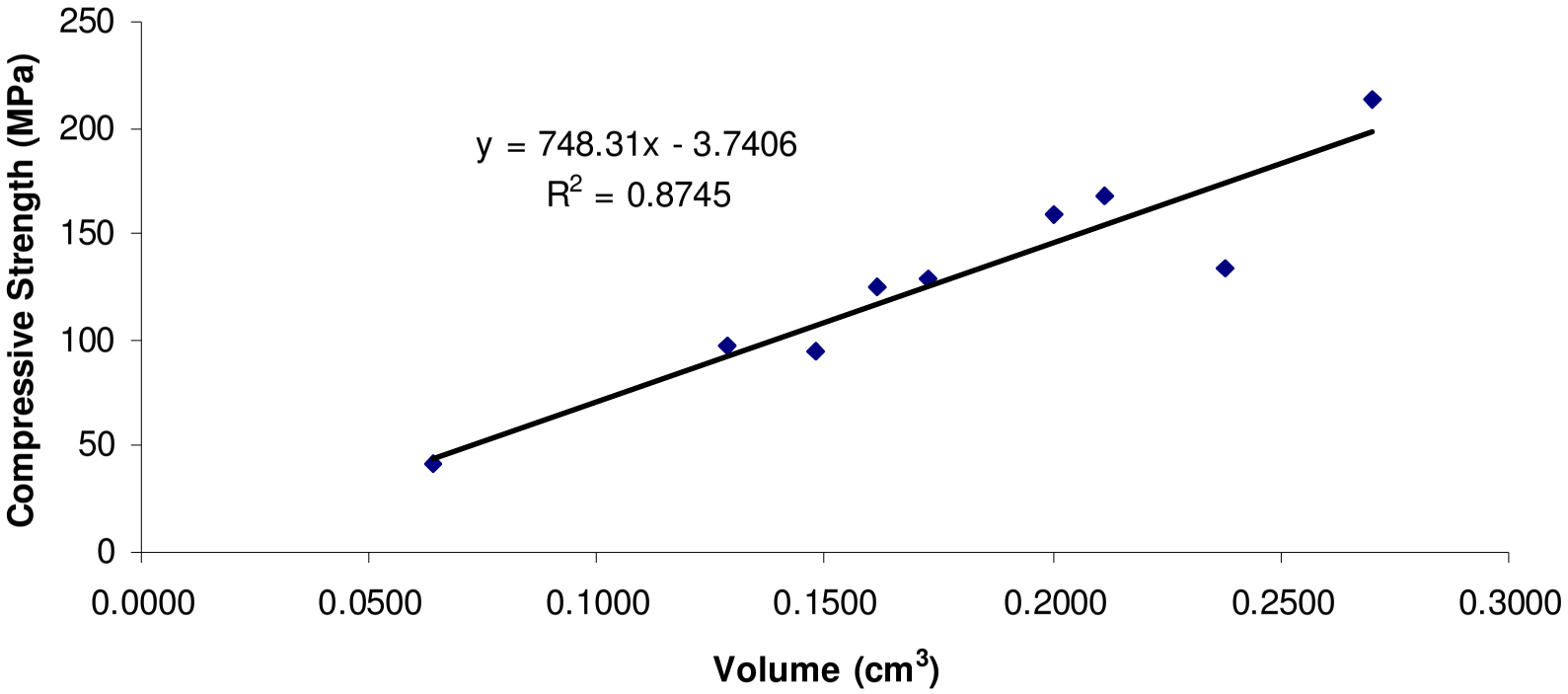

Figure 5.14. Compressive strength plotted versus the volume for AB/PCLM prepared at 250 ^{o}C and reheated for 4 days.

larger cylinder producing a higher strength may be coincidental - it's not the cylinder volume that causes the increased strength (even though the two are correlated), but the quality and quantity of bone (or HA phase in this case) present in the rods, which is also correlated with volume.

Additional AB/PCLM composites were prepared in the same manner as described above for torsion measurements. Samples were heated in air at 700 ^{o}C for 16 hr and reacted at 250 ^{o}C for a total of 8 days. The torsion plots, torque versus twist angle, for each sample is shown in Figure 5.15. The peak torque, peak stress and modulus of rigidity of each sample are shown in Table 5.3. The average peak torque for all 11 samples is 0.23 ± 0.11 Nm, the peak stress is 15.5 ± 6.4 MPa, and the average modulus of rigidity is 3.1 ± 1.4 GPa. The three samples that exhibited the lowest peak stresses and moduli (178, 179, and 184) broke at the junction of the large and small diameter. The remaining samples exhibited a typical break pattern for brittle samples. Brittle samples typically break along planes perpendicular to the direction in which tension is a maximum, for example at 45^{o} to the shaft axis (Figure 5.16).[33] The average peak torque for the 8 samples that did not show an anomalous fracture pattern was 0.28 ± 0.07 Nm, the peak stress was 18.7 ± 3.8 MPa, and the average modulus of rigidity was 3.9 ± 0.5 GPa. The modulus compares favorable to that of human femoral bone, but the peak stress is about a third of the value.

Finally, different pre-reaction activating conditions were used to prepare a large set of samples. These samples were sintered in air at 600 ^{o}C for 4 days. These samples lost an average of 8.6 ± 0.8% (n = 16) of their mass during the activation. Polymerizations were performed at 250 ^{o}C for varying lengths of time between 5 and 17

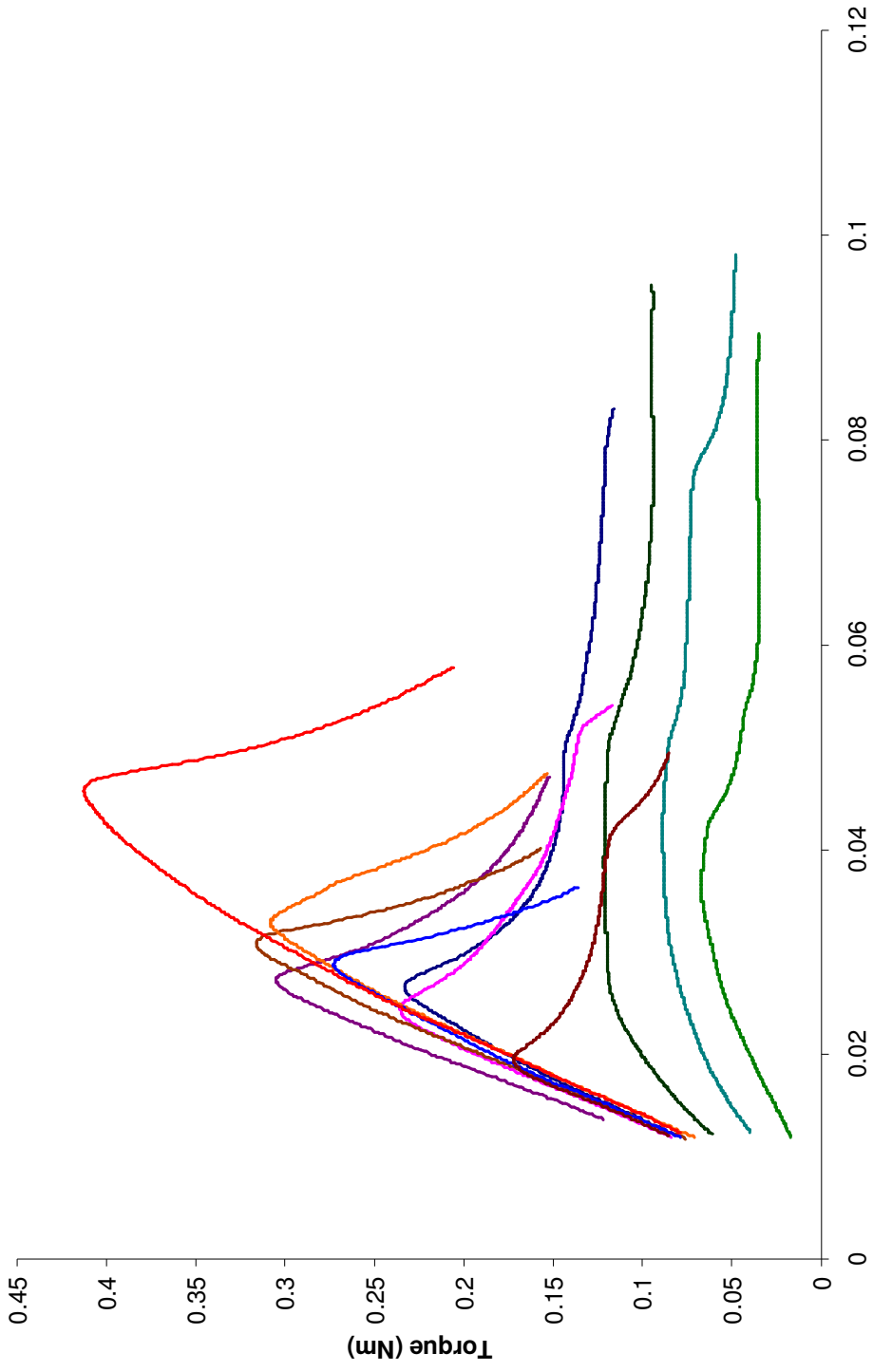

Figure 5.15. Torque versus twist angle curves for AB/PCLM composites.

Sample	Length (mm)	Radius (mm)	Peak Torque (Nm)	Peak Stress (MPa)	Modulus of Rigidity (GPa)
176	10.44	2.075	0.233	16.60	4.42
177	8.00	1.98	0.236	19.36	4.51
178	7.51	2.07	0.067	4.81	0.77
179	7.52	2.00	0.089	7.08	1.25
180	7.41	2.10	0.305	20.97	3.69
181	8.81	2.165	0.316	19.82	3.54
182	10.02	2.23	0.308	17.68	3.30
183	11.35	2.165	0.273	17.13	4.37
184	6.76	2.045	0.122	9.08	1.39
191	10.51	2.17	0.413	25.73	3.86
192	6.93	2.06	0.172	12.53	3.19

Table 5.3. Torsional properties of AB/PCLM composites.

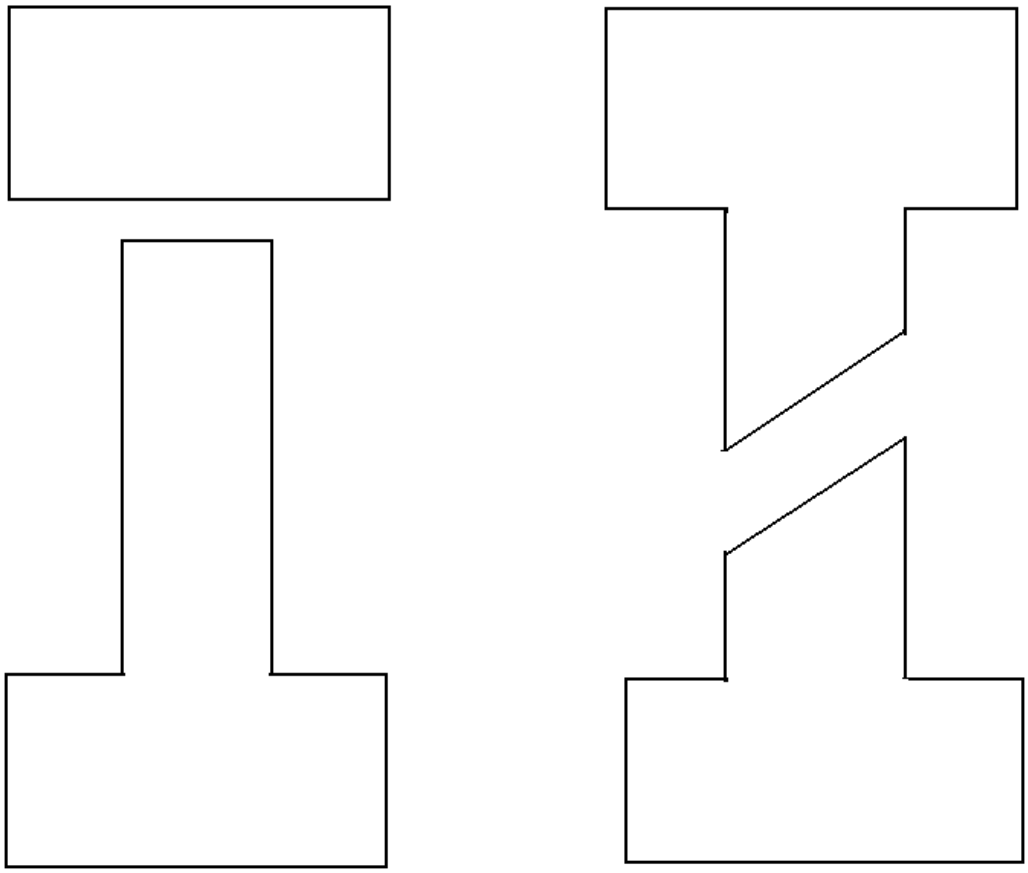

Figure 5.16. (Left) AB/PCLM composites with low peak stresses and moduli broke at the junction of the large and small diameter of the dumbbell. (Right) The remaining samples broke in a manner typical of brittle materials.

days. The reaction time was varied because the new activation conditions were expected to influence the relative rates. As can be seen from the data found in Table 5.4, for this set of samples differences in final composite properties, percent mass gain, percentage of the mass gain that is polymer, and the compressive strength, were not correlated with the reaction time. Figure 5.17 shows a scanning electron microscopy image of a sample prepared using these conditions. The composite was polished sequentially with 1200 grit wet sandpaper, 3 μm alumina polishing powder, and 0.5 μm alumina polishing powder. The sample was then cleaned of any residual alumina by brief ultrasonic cleaning in water. The dark areas seen in Figure 5.17 are the PCLM and the lighter areas are the HA. As with previously prepared samples in Professor Redepenning's group,[1-3] the microscopic morphology of the original bone is conserved. The PCLM fills the Haversian canals and the lacunae. The infusion and filling of the pores occurred during the reaction when liquid ε-caprolactam filled the pores and reacted at the surface of the HA. It is also noteworthy that these samples show a seamless transition between the inorganic and polymer phases, which is indicative of a strong electrostatic interaction between the anionic polymer charges and a cationic inorganic surface.

The reaction time, percent mass gain, percentage of the mass gain that is polymer, compressive strength, and elastic modulus for the AB/PCLM samples is shown in Table 5.4. The stress strain curves are shown in Figure 5.18. The average mass gain was 54.0 ± 10.3%, the average percentage of the mass gain due to polymer was 88 ± 4%, the average compressive strength was 215 ± 37 MPa, and the average elastic modulus was 6.9 ± 0.6 GPa. The compressive strength was slightly higher than for the samples

Sample	Reaction Time (d)	Mass Gain (%)	(%) Organic Material that was Polymer	Compressive Strength (MPa)	Elastic Modulus (GPa)
94	5	52.1	88.9	222.3	7.07
95	5	55.3	83.5	230.0	7.33
88	7	85.4	91.4	185.0	7.16
89	7	49.8	86.4	226.9	6.50
90	7	49.3	86.0	167.8	5.82
91	7	49.1	83.7	162.4	7.55
92	7	50.0	89.9	239.3	7.75
93	7	51.8	96.5	263.4	6.77
96	8	51.4	83.7	270.7	6.90
97	8	50.6	91.4	194.0	6.37
98	11	61.0	83.1	224.6	7.11
99	11	66.6	90.6	221.7	6.46
100	14	55.6	91.3	169.0	5.79
101	14	51.6	87.9	159.5	7.01
102	17	41.2	88.5	252.4	7.59
103	17	43.2	89.7	250.0	7.28

Table 5.4. Physical Properties for AB/PCLM composites prepared by sintering at 600 ^{o}C for 4 days and reacting at 250 ^{o}C for varying lengths of time.

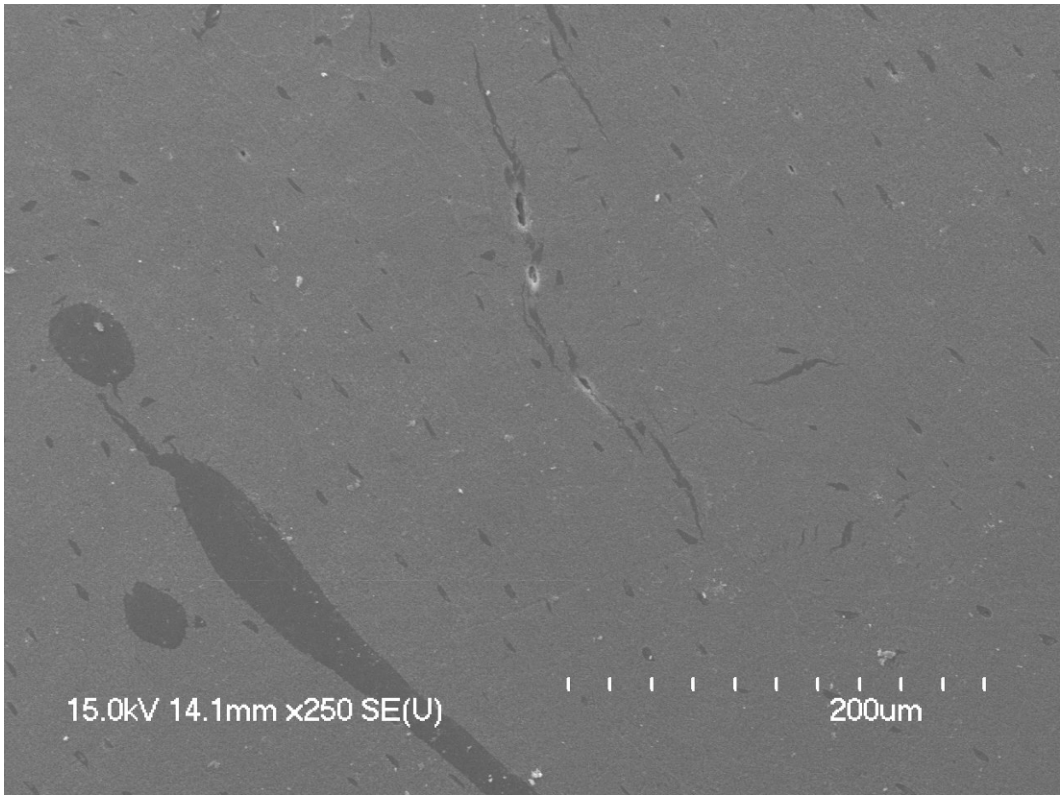

Figure 5.17. SEM image of an AB/PCLM composite.

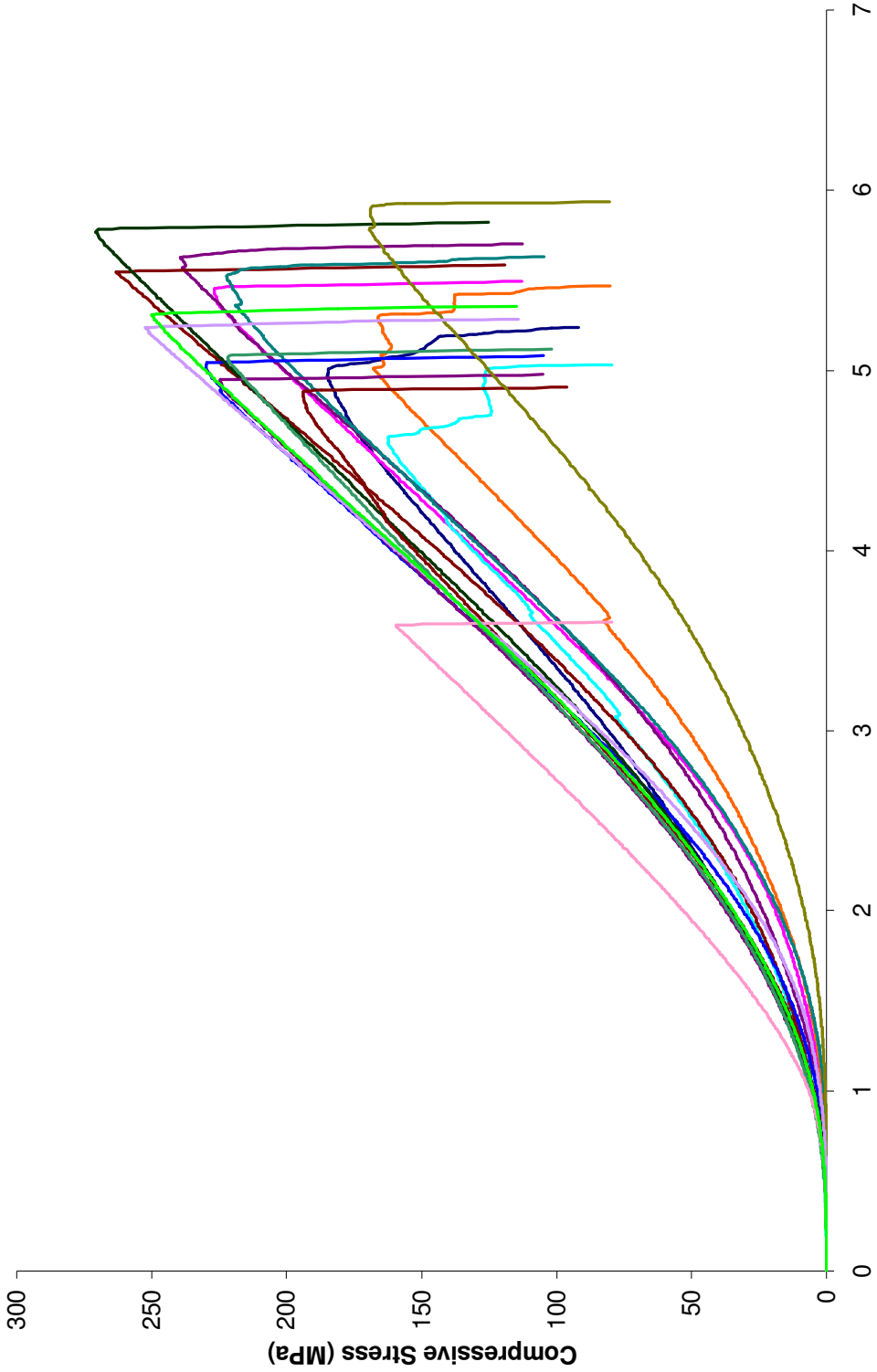

Figure 5.18. Compressive stress-strain curves for AB/PCLM composites.

prepared at 300 ^{o}C for 48 hr but not statistically different at the 95% confidence level. The modulus was lower and statistically different than the value obtained for those same samples. When comparing to previously prepared AB/PLLA composites,[1] the compressive strength was not statistically different at the 95% confidence level, but the modulus was statistically different. My compressive strength of 215 ± 37 MPa compared favorably with the compressive strength of 167 MPa reported for human femoral bone.[31] My result was higher than the value for human femoral bone at the 99.95% confidence level.

Conclusion

Like previous reactions involving lactones, anorganic bone proved capable of initiating the ROP of ε-caprolactam. The resulting AB/PCLM composite had a microscopic morphology similar to that of the original bone. The mechanical properties are comparable to those of human femoral bone. The compressive strength and modulus of rigidity met or exceeded the reported values for human bone, while the elastic modulus and peak torsional stress of my materials were slightly lower. It is noteworthy that the high compressive strength and lower modulus of my samples should result in improved toughness (defined as the integrated area under the stress-strain curve). The improved toughness and longer resorption times could prove to be beneficial in certain load bearing applications where durability is a high priority. The mechanical properties were also similar to those reported previously for AB/PLLA composites prepared in a similar fashion.

References

1) Wiegand, T.; Karr, J.; Steinkruger, J. D.; Hiebner, K.; Simetich, B.; Beatty, M.; Redepenning, J., Reconstruction of anorganic mammalian bone by surface-initiated polymerization of L-lactide. *Chemistry of Materials* **2008,** 20, 5016-5022.

2) Karr, J.J., Preparation and Characterization of Ceramic/Polymer Biomaterials, Ph.D. dissertation, University of Nebraska, Lincoln, Nebraska, 2007.

3) Wiegand, T.E., Resorbable Polymer-Hydroxyapatite Composites for Bone Trauma Treatment: Synthesis and Properties, Ph.D. dissertation, University of Nebraska, Lincoln, Nebraska, 2011.

4) Puffr, R., Lactams. In *Lactam–Based Polyamides Volume 1: Polymerization, Structure, and Properties*, Puffr, R.; Kubánek, V., eds.; CRC Press: Boca Raton, Florida, 1991.

5) Ritz, J.; Fuchs, H.; Kieczka, H.; Moran, W.C., Caprolactam. In *Ullmann's Encyclopedia of Industrial Chemistry*; Wiley-VCH: Weinheim, Germany, 2002.

6) Braun, D.; Cherdron, H.; Rehahn, M.; Ritter, H.; Voit, B., Synthesis of macromolecules by chain growth polymerization. In *Polymer Synthesis: Theory and Practice – Fundamentals, Methods, Experiments*, 4th ed.; Springer: Berlin, Germany, 2005.

7) Šebenda, J., Polymerization. In *Lactam–Based Polyamides Volume 1: Polymerization, Structure, and Properties*, Puffr, R.; Kubánek, V., eds.; CRC Press: Boca Raton, Florida, 1991.

8) Rusu, G.; Rusu, E., Anionic nylon 6/zinc composite materials: Evaluation of the thermal and mechanical behavior. *International Journal of Polymer Analysis and Characterization* **2010**, 15, 509-523.

9) Wichterle, O.; Šebenda, J.; Králíček, J., The anionic polymerization of caprolactam. *Fortschritte der Hochpolymeren-Forschung (Advances in Polymer Science)* **1961**, 2, 578-595.

10) Gorbunova, Y.V.; Deyev, Y.S.; Ryabov, Y.A., Capro- and dodecalactam polymerizations catalyzed by d-metal oxides: TiO_2, ZrO_2 and ZnO. *Polymer Science U.S.S.R.* **1981**, 23, 907-915.

11) Mohrschladt, R.; Hildebrandt, V., Use of Heterogeneous Catalysts in Methods for the Production of Polyamides. US Patent 6590064, 2003.

12) Saunders, J., The alkali-catalyzed polymerization of caprolactam. *Journal of Polymer Science* **1958**, 30, 479-492.

13) Shi, D., *Introduction to Biomaterials*; Tsinghua University Press: Beijing, China, 2006.

14) Pezzotti, G.; Asmus, S.M.F.; Ferroni, L.P.; Miki, S., In situ polymerization into porous ceramics: A novel route to tough biomimetic materials. *Journal of Materials Science: Materials in Medicine* **2002**, 13, 783-787.

15) Nakahira, A.; Tamai, M.; Miki, S.; Pezzotti, G., Fracture behavior and biocompatibility evaluation of nylon-infiltrated porous hydroxyapatite. *Journal of Materials Science* **2002**, 37, 4425-4430.

16) Asmus, S.M.F.; Nakahira, A.; Pezzotti, G., Manufacture and bioactivity of tough hydroxyapatite/nylon hybrid composites. *Advanced Composite Materials* **2003**, 11, 255-264.

17) Liyun, Z.; Zhimin, L.; Yajun, Z., Preparation and properties of nano-hydroxyapatite modified nylon composites. *Advanced Materials Research* **2010**, 87-88, 228-232.

18) Lánská, B., Degradation and stabilization. In *Lactam-Based Polyamides, Volume 1: Polymerization, Structure, and Properties*, Puffr, R.; Kubánek, V., eds.; CRC Press: Boca Raton, Florida, 1991.

19) Zaikov, G.E., Quantitative aspects of polymer degradation in the living body. *Journal of Macromolecular Science, Part C: Polymer Reviews* **1985**, 25, 551-597.

20) Kopecek, J.; Ulbrich, K., Biodegradation of biomedical polymers. *Progress in Polymer Science* **1983**, 9, 1-58.

21) Coury, A.J., Chemical and biochemical degradation of polymers. In *Biomaterials Science: An Introduction to Materials in Medicine*, 2nd ed., Ratner, B.D.; Hoffman, A.S.; Schoen, F.J.; Lemons, J.E., eds.; Elsevier: San Diego, California, 2004.

22) Long, M.; Talac, R.; Yaszemski, M.J., Issues involving standards development for synthetic material bone graft substitutes. In *Bone Graft Substitutes*, Laurencin, C.T., ed.; ASTM International: West Conshohocken, Pennsylvania, 2003.

23) Bradley, G.W.; McKenna, G.B.; Dunn, H.K.; Daniels, A.U.; Statton, W.O., Effects of flexural rigidity of plates on bone healing. *Journal of Bone and Joint Surgery* **1979**, 61-A, 866-872.

24) Terjesen, T.; Apalset, K., The influence of different degrees of stiffness of fixation plates on experimental bone healing. *Journal of Orthopaedic Research* **1988**, 6, 293-299.

25) Daniels, A.U.; Chang, M.K.O.; Andriano, K.P.; Heller, J., Mechanical properties of biodegradable polymers and composites proposed for internal fixation of bone. *Journal of Applied Biomaterials* **1990**, 1, 57-78.

26) An, Y.H.; Barfield, W.R.; Draughn, R.A., Basic concepts of mechanical property measurement and bone biomechanics. In *Mechanical Testing of Bone and the Bone-Implant Interface*, An, Y.H.; Draughn, R.A., eds.; CRC Press: Boca Raton, Florida, 2000.

27) Osswald, T.A.; Menges, G., *Materials Science of Polymers for Engineers*, 2nd ed.; Hanser Gardner Publications: Munich, Germany, 2003.

28) Brown, R., *Handbook of Polymer Testing: Physical Methods of Plastics Engineering*, 1st ed.; Marcel Dekker: New York, New York, 1999.

29) Nielsen, L.E.; Landhl, R.F., *Mechanical Properties of Polymers and Composites*, 2nd ed.; Marcel Dekker: New York, New York, 1993.

30) Park, J.B., *Biomaterials Science and Engineering*, 1st ed.; Springer: New York, New York, 1984.

31) Yamada, H.; Evans, F.G., *Strength of Biological Materials*; Williams and Wilkins: Baltimore, Maryland, 1970.

32) An, Y.H.; Mechanical properties of bone. In *Mechanical Testing of Bone and the Bone-Implant Interface*, An, Y.H.; Draughn, R.A., eds.; CRC Press: Boca Raton, Florida, 2000.

33) Beer, F.P.; Johnston Jr., E.R.; DeWolf, J.T. *Mechanics of Materials*, 3rd ed.; McGraw-Hill: New York, New York, 2001.

34) Gramoll, K., *Mechanics* (eBook). https://ecourses.ou.edu/cgi-bin/ebook.cgi?doc=&topic=me&chap_sec=02.0, Accessed July 21, 2011.

35) Zioupos, P.; Smith, C.W.; An, Y.H., Factors affecting mechanical properties of bone. In *Mechanical Testing of Bone and the Bone-Implant Interface*, An, Y.H.; Draughn, R.A., eds.; CRC Press: Boca Raton, Florida, 2000.

36) Williams, J.B.; Irvine, J.W., Preparation of the inorganic matrix of bone. *Science* **1954**, 119, 771-772.

37) Zhang, Y.; Zhang, Q.; Cheng, K.; Xu, J., Monocarboxyl-end-grouped polycaprolactam with an adjustable molecular weight. *Journal of Applied Polymer Science* **2004**, 92, 722-727.

38) Holmes, B.S.; Moniz, W.B.; Ferguson, R.C., NMR study of nylon 66 in solution (^{1}H, ^{13}C, and ^{15}N NMR using adiabatic J cross polarization). *Macromolecules* **1982**, 15, 129-132.

39) Helwig, E.; Sandner, B.; Gopp, U.; Vogt, F.; Wartewig, S.; Henning, S., Ring-opening polymerization of lactones in the presence of hydroxyapatite. *Biomaterials* **2001,** 22, 2695-2702.

40) Guerra, G. D.; Cerrai, P.; Tricoli, M.; Krajewski, A.; Ravaglioli, A.; Mazzocchi, M.; Barbani, N., Composites between hydroxyapatite and poly(epsilon-caprolactone) synthesized in open system at room temperature. *Journal of Materials Science-Materials in Medicine* **2006,** 17, 69-79.

41) Carter, D.R.; Hayes, W.C., Bone compressive strength: The influence of density and strain rate. *Science* **1976**, 194, 1174-1176.

42) Hansen, U.; Zioupos, P.; Simpson, R.; Currey, J.D.; Hynd, D., The effect of strain rate on the mechanical properties of human cortical bone. *Journal of Biomechanical Engineering* **2008**, 130, 011011-1-011011-8.

Chapter Six

Preliminary *in vitro* Biocompatibility Studies for Anorganic Bone/Bioresorbable Polymer Composites

Modern research involving the synthesis of new biomaterials is generally complement by feedback from some form of biological system. This feedback often begins by examining a variety of performance parameters obtained from *in vitro* cell cultures. Subsequent studies often involve evaluating the performance in animal models, which can range from subcutaneous implantation of the material in mice to full-scale double blind studies in humans.

Biological and medical feedback regarding the performance of new biomaterials often necessitates multi-investigator collaborative research efforts in which research teams rely on each other's complementary expertise. The preliminary results described in this chapter are no exception. The experimental procedures for conducting cell cultures described in this chapter were originally supplied by Dr. Paul Wooley, director of research at Orthopaedic Research Institute at Via Christi Hospital in Wichita, KS. Wooley's contribution was part of his contribution to the funded research proposal that supported my thesis research. Dr. Wooley is a Co-PI on the proposal. The experimental procedures were then carried out by Wooley's group, primarily by Dr. Haiying Yu and Zheng Song at Wichita State University and Via Christ Hospital. Yu and Song also wrote a first draft concerning their results and forwarded them to Professor Wooley, who vetted the results and forwarded them to Professor Redepenning who provided them to me. In this chapter I have lightly edited the wording provided by Wooley's group and inserted the resulting text at appropriate spots around which I have supplied scientific

context and background information. The intent of this exercise was for me to gain experience providing a first draft of a collaborative manuscript involving the collaborative research effort focused on the materials I prepared. Chapter 6 of this thesis serves as my initial contribution to this writing process.

Introduction and Background

As mentioned in Chapter 1, biocompatibility is one of several properties that are important when creating a material that could potentially be used as a bone graft. Ideally the material should not be cytotoxic, meaning it should not be toxic to the cells in the surrounding tissue, and should not produce a prolonged, chronic inflammatory response known as an undesirable foreign body response (FBR). A FBR occurs when the host body perceives the implanted material as foreign and attempts to eliminate it or isolate it from the surrounding tissue. This response can lead to a number of issues including fibrosis, bone resorption, implant degradation, increased infection rates, delayed healing, pain, and device failure.[1]

The general response following implantation of a biomaterial into the body consists of several stages. These stages are blood-material interactions, provisional matrix formation, acute inflammation, chronic inflammation, granulation tissue development, foreign body reaction, and fibrous capsule development. Immediately upon implantation, protein adsorption occurs on the biomaterial surface and a blood clot subsequently forms at the tissue/material interface. The clot serves as the initial provisional matrix that provides structural, biochemical, and cellular components necessary for wound healing.

Following deposition of the provisional matrix, acute and chronic inflammation of the site occurs. Such an inflammatory response can be beneficial if it is not excessive. Acute inflammation is characterized by the exudation of fluid and proteins and the emigration of leukocytes. Neutrophils are the first leukocytes to arrive at the wound site. Additionally, mast cells degranulate and release histamine, interleukin-4 (IL-4), and interleukin-13 (IL-13) as well as adsorb fibrinogen. Chronic inflammation follows the acute inflammation stage. It can be identified by the presence of monocytes, lymphocytes and macrophages. They are attracted to the wound site by chemokines and other chemoattractants. The role of these cells is to phagocytose microorganisms and other foreign material. Due to the size disparity, biomaterials are generally not phagocytosed, but cells do attach to the material. Because the cells cannot engulf the material, "frustrated phagocytosis" occurs, where the leukocytes release products in an attempt to degrade the biomaterial.[2,3] During the inflammatory stage, macrophages also play a role in the recruitment of other macrophages and regulation of the immune response to the implant. The release of platelet-derived growth factor (PDGF), tumor necrosis factor (TNF-α), IL-6, granulocyte-colony stimulating factor (G-CSF), and granulocyte macrophage colony stimulating factor (GM-CSF) call more macrophages to the wound site. Additional mediators such as IL-1, IL-6, IL-12, and IL-15 can stimulate or mediators such as transforming growth factor (TGF-β), IL-10, and prostaglandin E2 (PGE_2) can inhibit lymphocyte function. For biocompatible materials, the inflammatory response usually does not last longer than a couple of weeks.[3-5]

Macrophages also release cytokines to attract fibroblasts and stimulate angiogenesis. Fibroblasts are necessary for the production of granulation tissue and the

synthesis of the extracellular matrix and collagen in an attempt to close the wound. The continual presence of an implant inhibits the normal healing process. Instead of entering the remodeling phase, the foreign body response can occur. This is characterized by the encapsulation of the foreign object by macrophages and foreign body giant cells (FBGC), which result from macrophage fusion.[2,3] Encapsulation occurs around all implants, but if it releases low molecular weight components or debris, moves, or causes pressure on the surrounding tissue the fibrous capsule will grow in size. The surface properties of the implant play a role in the capsule formation. Cells are capable of penetrating porous implants and a small capsule forms that is incorporated into the implant. If the material biodegrades rapidly, no capsule is observed. In permanent non biodegradable implants a small fibrous capsule is observed throughout the life of the implant. Solid implants are associated with larger capsules.[6]

Both *in vitro* and *in vivo* methods can be employed when studying cell viability and other related cellular functions. *In vitro* cell culture models are less complex, provide a simplified, cost-effective and focused analysis, while utilizing fewer animals and allowing higher throughput. The downside of *in vitro* models is that they can be overly simplistic, only looking at a limited number of cells and their responses, while being silent regarding cellular signaling that can only be observed *in vivo*.[1] Additionally for ethical reasons, beginning with *in vitro* testing can help to limit adverse reactions of implanted, untested biomaterials in animals.

In this chapter, two *in vitro* experiments were used to quantify cell viability and other related cellular functions. The 3-(4,5-Dimethylthiazol-2-yl)-2,5-diphenyltetrazolium bromide (methylthiazol tetrazolium) assay (MTT assay) was used to

determine cell viability and real-time reverse transcriptase polymerase chain reactions (RT-rt-PCR) was used to determine gene expression. Qualitative morphological evaluations were done using scanning electron microscopy (SEM).

The MTT assay is a colorimetric assay that measures cell metabolic function, which serves as an indication of cell viability during culture proliferation on the composite. The assay detects the activity of the mitochondrial enzyme, succinate dehyrogenase in complex II. This enzyme plays a role in oxidative phosphorylation and the tricarboxylic acid cycle.[7-11] If a material is cytotoxic, the activity of this enzyme is impaired. When MTT is added to the culture, it is reduced to the purple-colored formazan. The absorbance can be quantified at a certain wavelength (between 500 and 600 nm) using a spectrophotometer.[12]

RT-rt-PCR can be used to quantify gene expression by a cell. It simultaneously amplifies and quantifies the targeted sequence within the DNA molecule. The first step requires creating a complementary DNA (cDNA) copy of the messenger RNA (mRNA) using a reverse transcriptase. Amplification of the short DNA sequences is achieved using a pair of primers, approximately 20 nucleotides in length, that are complementary to the sequence on each strand of the DNA. They are extended by a DNA polymerase so that a copy is made of the designated sequence. The same primers are used again to make another copy of the original DNA and also the short copy that was made in the first iteration. This process is repeated and leads to exponential amplification. The temperature must be raised between each round to separate the DNA, so a thermo-stable DNA polymerase must be used. This cycling is usually continued for 30-40 rounds. In traditional PCR, the reaction products are then analyzed by agarose gel electrophoresis.[13]

In real time PCR, a fluorescent dye is used that binds to double stranded DNA but not to single-stranded DNA. The fluorescence intensity increases as the amount of DNA increases and can be measured and quantified after each cycle. The fluorescence of the target gene is often normalized to an internal standard.[13, 14] The internal standard is typically a housekeeping gene that is present in all cell types because they are necessary for cell survival. These include glyceraldehyde-3-phosphate dehydrogenase (G3PDH), albumin, actins, tubulins, cyclophilin, 18S rRNA, or 28S rRNA.[15, 16]

Several researchers have studied the biocompatibility of HA/bioresorbable polymer composites both *in vitro* and *in vivo*. Previous *in vitro* studies conducted using HA/PLLA composites have demonstrated good cell viability and function, especially compared to pure PLLA materials.[17-20] *In vivo* studies have demonstrated little undesirable inflammatory response to HA/PLLA composite implants. In addition, bony ingrowth into the implant has been observed.[21, 22]

Experimental

Chemicals: Deuterated chloroform ($CDCl_3$, 99.8% D from Sigma-Aldrich, St. Louis, MO), ε-caprolactam (99%+ from Acros Organics, Geel, Belgium), ε-caprolactone (99% from Acros Organics), ethylenediamine (99% from Sigma Aldrich), polystyrene (PolyCAL™ gel permeation chromatography (GPC) standards from Viscotek, Worchestershire, U.K.), tetrahydrofuran (THF, HPLC grade from Sigma Aldrich), and 2,2,2-trifluoroethanol (TFE, ≥ 99% from Sigma Aldrich) were used as purchased from their respective suppliers. Anorganic cortical bone was derived from bovine femur donated by Premium Protein Products (Lincoln, NE).

Preparation of anorganic bone (AB)/bioresorbable polymer composite samples: A band saw was used to remove the distal and proximal ends of the bovine femurs and to cut them into 1.5 to 2 cm thick sections along their longitude. Cylindrical plugs of cortical bone, with a diameter of 6 mm and a length between 12 and 20 mm, were machined in the longitudinal direction from the diaphyseal section of the bovine femur using a 6 mm diameter dowel tool (Figure 4.1). A Soxhlet extractor was then used to remove the majority of the organic material. The solvent mixture used for the extraction was 80% ethylenediamine and 20% deionized water (v/v).[24] The solvent was observed to reflux at 119 ^{o}C. The samples were extracted for a minimum of 48 hr. Fresh solvent cycled through approximately every 10 min. After the extraction period, the solvent mixture was replaced with deionized water. The Soxhlet extraction of the bone cylinders with water was continued until the water was neutral pH. The water was replaced 3-4 times during this process. At this stage the bone cylinders which were greatly whitened were removed and allowed to dry at room temperature in air. Samples used to initiate the polymerization of ε-caprolactone were then activated by being heated at 700 ^{o}C for 16 hr in air. Samples used to initiate the polymerization of ε-caprolactam were activated by being heated at 600 ^{o}C for 96 hr in air. They were then placed in a vacuum desiccator, cooled to room temperature under vacuum, and transferred to a $N_{2(g)}$ atmosphere glove box for later use.

To begin the polymerization, an anorganic bone plug was placed in a Pyrex glass tube that was approximately 9.5 mm in diameter. An excess of ε-caprolactone or ε-caprolactam was added to the tube. Enough monomer was added to ensure that the sample was completely covered. The tubes were sealed with a short section of tygon

tubing that was closed with a hose clamp. They were then removed from the $N_{2(g)}$ glove box and attached to a rotary vane rough pump. The samples were maintained under a vacuum for 10 min before the bottom was dipped in liquid N_2 and the vacuum was maintained for an additional 5 min. The tubes were then sealed at a reduced pressure (~30 mTorr) after placing a slight constriction near the midsection. ε-Caprolactone reactions were placed in a convection oven at 130 ^{o}C. Upon melting, the monomer infused into the pores of the anorganic bone where the ring opening polymerization (ROP) was initiated by the surface of the HA.[23] After 3 days the samples were inverted so excess monomer could drain away from the sample. The constriction kept the sample from sliding to the other end of the tube. The reaction was allowed to proceed for an additional 3-4 days. ε-Caprolactam samples were placed in a convection oven at 250 ^{o}C. They were immersed for 4 days, then inverted, and allowed to react an additional 4-5 days. After this time, the reaction vessels were removed from the oven and allowed to cool to room temperature.

AB/PCLN composites had a peak molecular weight (M_p) of 71,000 ± 11,000 Da and were 94.0 ± 2.6% polymer as determined by ^{1}H NMR (Figure 6.1). This was determined by integrating the areas of the triplet at 4.05 ppm, which corresponds to the internal methylene protons adjacent the oxygen in the ester of the polymer, and the triplet at 4.15 ppm which corresponds to the same protons in the monomer. AB/PCLM composites were 84.5 ± 3.5% polymer, also determined by ^{1}H NMR (Figure 6.2). This was determined by integrating the areas of the triplet at 4.15 ppm, associated with the internal methylene protons adjacent the carbon in the amide functional group of the

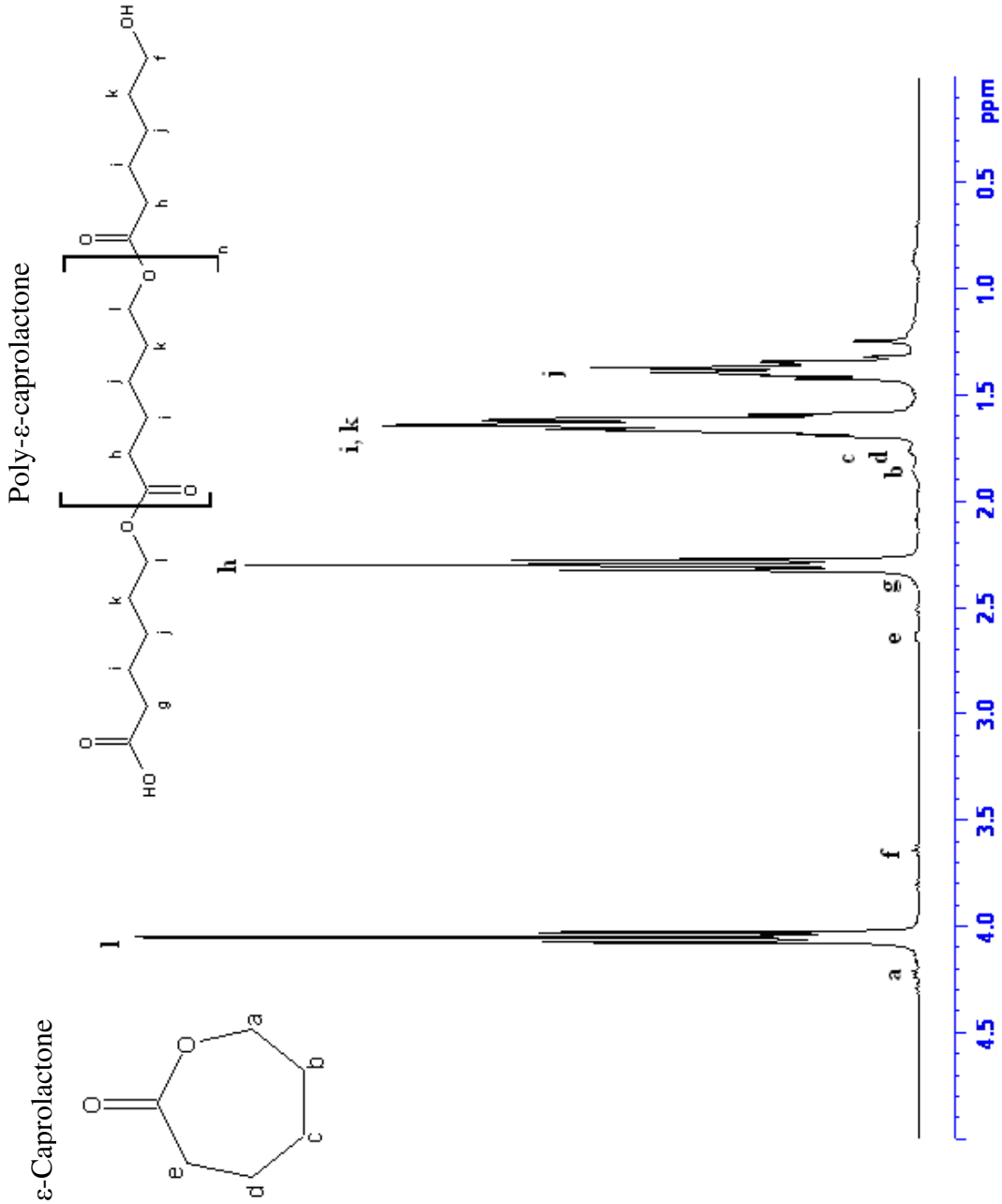

Figure 6.1. Representative ^{1}H NMR spectrum of AB/PCLN composite prepared for cell culture studies.

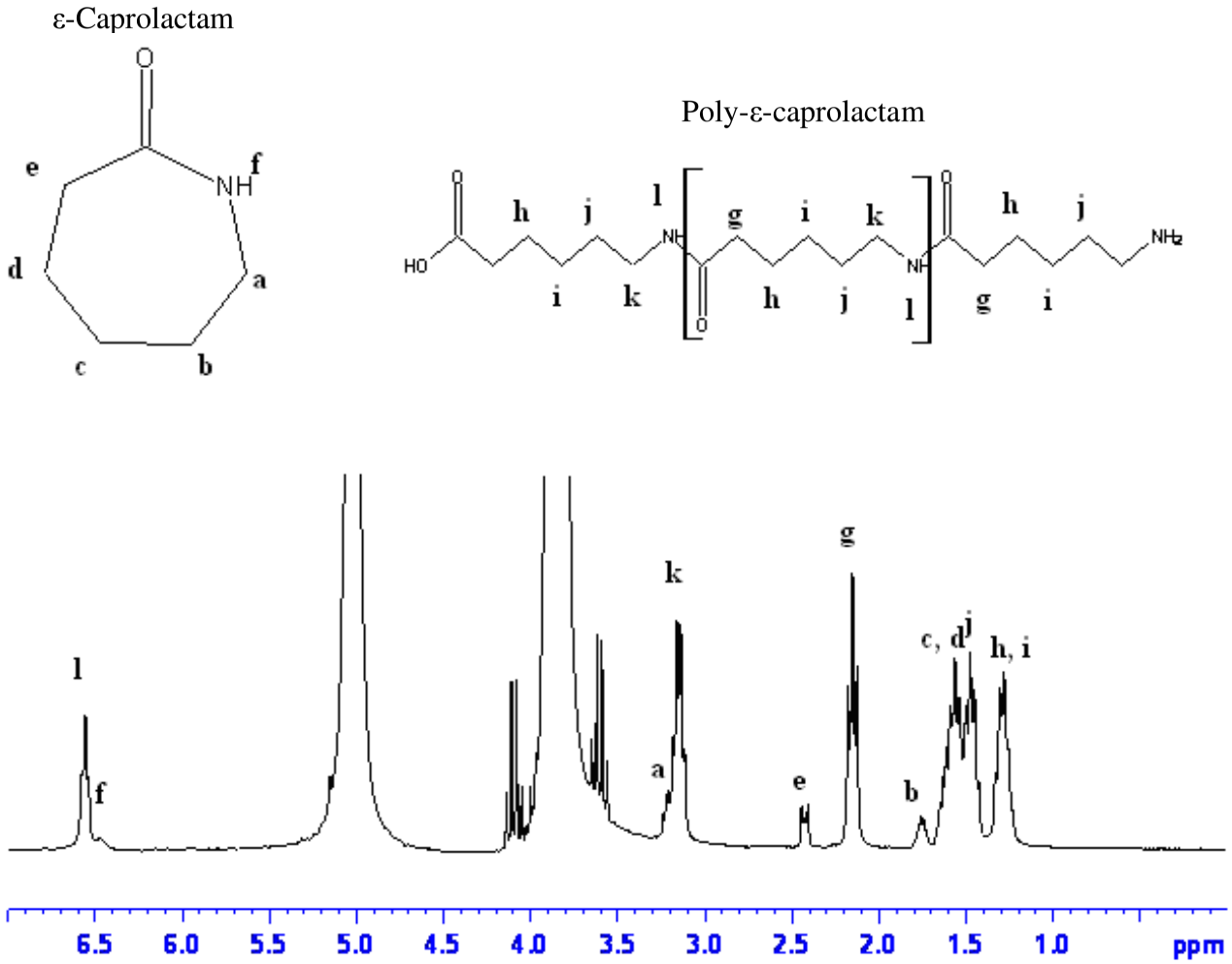

Figure 6.2. Representative ^{1}H NMR spectrum of AB/PCLM composite prepared for cell culture studies.

polymer, and the triplet at 4.45 ppm associated with the same protons in the monomer. The two large peaks in the spectrum are due to the solvent, trifluoroethanol.

Excess polymer on the outside of the cylinder was removed using a Colchester-Clausing lathe. A rotation speed of 800 rpm was used to machine the outside diameter of the cylinders to 6.0 mm. A parting tool was used to section the cylinder into 1.0 mm thick discs. The discs were then polished on the lather at a rotation speed of 400 rpm. The composites were polished sequentially with 1200 grit wet sandpaper, 3 μm alumina polishing powder, and 0.5 μm alumina polishing powder. The sample was then cleaned of any residual alumina by brief ultrasonic cleaning in water. This process produced discs that had a relatively smooth surface, free of tooling marks. Figure 6.3 shows SEM images of the polished composites. The microscopic morphology of the original bone is conserved. Additional composites of AB/PLLA and AB/polydioxanone (PDX) were prepared for the cell culture experiments by Troy Wiegand.[24]

Scanning electron microscopy (SEM) was performed using a Hitachi (Tokyo, Japan) S4700 Field- Emission microscope (Morrison Microscopy Core Facility, University of Nebraska-Lincoln (UNL)). Molecular weights of AB/poly-ε-caprolactone (PCLN) samples were estimated using a Viscotek VE 2001 GPC (Department of Chemistry, UNL). All samples are referenced to polystyrene standards. THF was used for the mobile phase at a flow rate of 1 ml/min. Detection was accomplished with a Viscotek VE 3580 refractive index detector. ^{1}H NMR spectra were obtained using a Bruker (Billerica, MA) 300 MHZ or 400 MHz Bruker DRX Avance spectrometer instrument (Research Instrumentation Facility (RIF), UNL). Spectral processing was done using

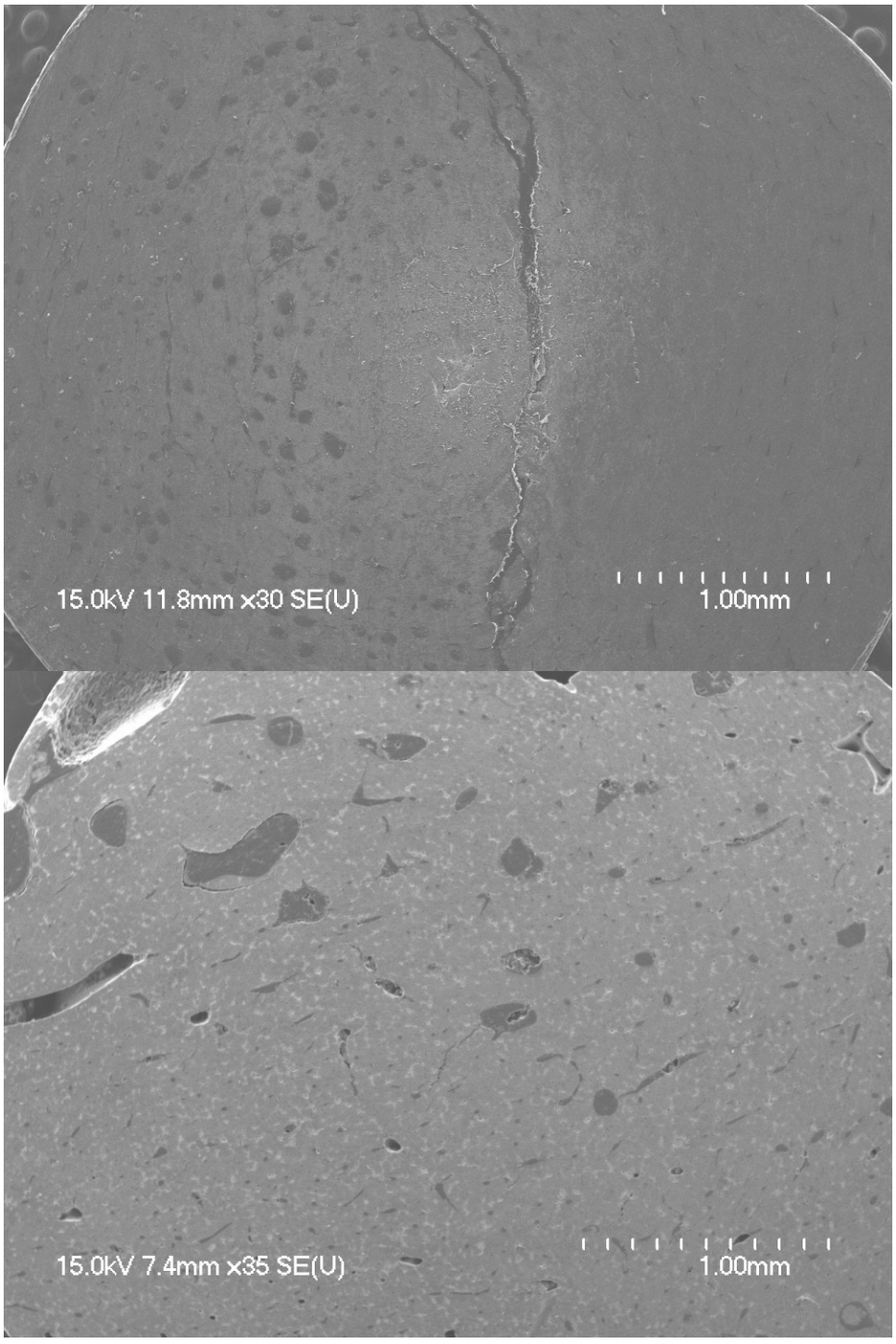

Figure 6.3. Representative SEM images of (top) AB/PCLN composite and (bottom) AB/PCLM composite for cell culture studies.

Bruker Topspin 3.0.b.8. PCLN samples were dissolved in $CDCl_3$ and all chemical shifts were reported in ppm referenced to the solvent peak, which was assigned a value of 7.27 ppm. PLCM samples were dissolved in a solution containing a 3:1 (v/v) ratio of trifluoroethanol and $CDCl_3$. All chemical shifts were referenced to the $CDCl_3$ peak at 7.27 ppm. Chemical shifts for PLCN[25-28] and PCLM[29, 30] were verified by comparison to values reported previously in the literature.

Cell Cultures: All cell culture studies were performed by Dr. Haiying Yu and Zheng Song at the Orthopaedic Research Institute at Via Christi Hospital in Wichita, KS. In addition to the four experimental composites, cell viability and gene expression of the cells was assessed on standard polystyrene (PS) tissue culture plates for comparison purposes. Prior to seeding all samples were sterilized with a 70% ethanol solution and allowed to air dry in a biological hood overnight. The cell lines chosen for these experiments were Raw264.7, a monocyte-macrophage cell line, and NIH.3T3, a fibroblast cell line. These lines were chosen because monocytes-macrophages are present at the site of the implant and are involved in chronic inflammation and FBR. Fibroblasts are known to attach to the surfaces of implanted materials and are involved in wound healing.[1-3, 31] A total of 4×10^3/10 µl/sample Raw264.7 or 1×10^4/10 µl/sample NIH/3T3 cells were seeded onto each sample examined. The cells were cultured at 37 ^oC for 7 days under a 5% CO_2 atmosphere in a complete media consisting of Dulbecco's Modified Eagle's Medium supplemented with 10% fetal bovine serum (FBS), 2 mM glutamine, 100 U/ml penicillin, and 100 mg/ml streptomycin.

MTT assay: Cell viability of both the Raw264.7 and NIH/3T3 cells, and therefore the cytotoxicity of the composites was determined using the MTT assay. After 7 days of

culture, 0.5 mg/ml MTT was added to the samples and incubated for 6 hrs at 37 ^{o}C under a 5% CO_2 atmosphere. The cells were lysed in 10% sodium dodecyl sulfate (SDS). The absorbance of the purple color due to the formazan that formed during cell metabolism was measured at 509 nm using spectrophotometry. The absorbance reading of the composites was compared to the reading for the PS standard.

RNA isolation and RT-rt-PCR: The inflammatory response invoked by the composites was measured using RT-rt-PCR. This was done by determining the gene expression of the inflammation-associated genes interleukin-1 β (IL-1 β) and tumor necrosis factor-α (TNF-α) by the Raw264.7 cells. Macrophages play an important role in the inflammatory response and also wound healing around the implant. The recruitment of other macrophages and fibroblasts as well as the regulation of the inflammatory response are achieved by the production of cytokines, including those listed above.[3-5, 32] After 7 days of culture, the cells were harvested and the RNA was extracted using TRIzol® reagent. A reverse transcription kit was used to make cDNA. SYBR Green-based RT-rt-PCR analysis was performed using a StepOnePlus Realtime PCR System (Applied Biosystems, USA). Thermal cycling conditions used were 95 ^{o}C for 10 min followed by 40 cycles of 95 ^{o}C for 15 s and 60 ^{o}C for 1 min. The amplification primers sequence for each gene is listed in Table 6.1. Gene expression was determined from the average cycle threshold (Ct) of three measurements and normalized to the gene expression of 18s RNA, the internal standard. This ratio is shown in equation 6.1.

$$Ratio = \frac{(2^{\Delta Ct})_{composite}}{(2^{\Delta Ct})_{18s\ RNA}} \tag{6.1}$$

SEM of cell seeded composites: Qualitative determination of cell viability was assessed using SEM. The morphology of the cells as well as the topography of the

Gene	Forward and reverse primers
TNF-α	5’- CTGGGACAGTGACCTGGACT
	3’- GCACCTCAGGGAAGAGTCTG
IL-1β	5’- GGGCCTCAAAGGAAAGAATC
	3’- TACCAGTTGGGGAACTCTGC
18sRNA	5’- CGGCTACCACATCCAAGGAA
	3’- GCTGGAATTACCGCGGCT

Table 6.1. DNA sequence of amplification primers used for RT-rt-PCR.

composites was observed. In addition to the composites seeded with the Raw264.7 and NIH/3T3 cells, composites that were subjected to the same treatment minus the seeding were also evaluated using SEM. This was done to determine if there were any environmental effects on the topography of the composites when compared to the seeded samples. Samples underwent a fixation procedure to preserve the cells for SEM observation. The fixation was affected by placing the samples in 2% glutaraldehyde for 1 hr, followed by rinsing them in 0.1 M sodium cacodylate buffer. The samples were then placed in 1% osmium tetroxide in 0.1 M sodium cacodylate buffer for 2 hr. Dehydration was achieved using a series of ethanol solutions that increased in ethanol composition (50, 70, 90, 100%) for 2-5 min in each solution. The fixation was completed by exposing the cells to hexamethyl disilazane (HMDS) for 10 min. The fixed cells were then air dried, mounted, and sputter coated with gold prior to placing in the SEM.

Results and Discussion

One of the first steps in evaluating the biocompatibility of a potential biomaterial is to determine the cytotoxicity of the material using *in vitro* testing. The AB/bioresorbable polymer composites were seeded with the Raw264.7 macrophage and NIH/3T3 fibroblast cell lines and MTT assay was used to determine cell viability based on the activity of the mitochondrial enzyme succinate dehydrogenase in complex II as described above. Macrophage and fibroblast cell lines were chosen because they play an important role in the inflammation and wound healing around an implant. The results of the MTT assay are shown in Figure 6.4. The cell viability was the highest on the PS culture plate (the control group). Among the AB/bioresorbable polymer composites, AB/PCLN showed the highest viability followed by the AB/PLLA composites.

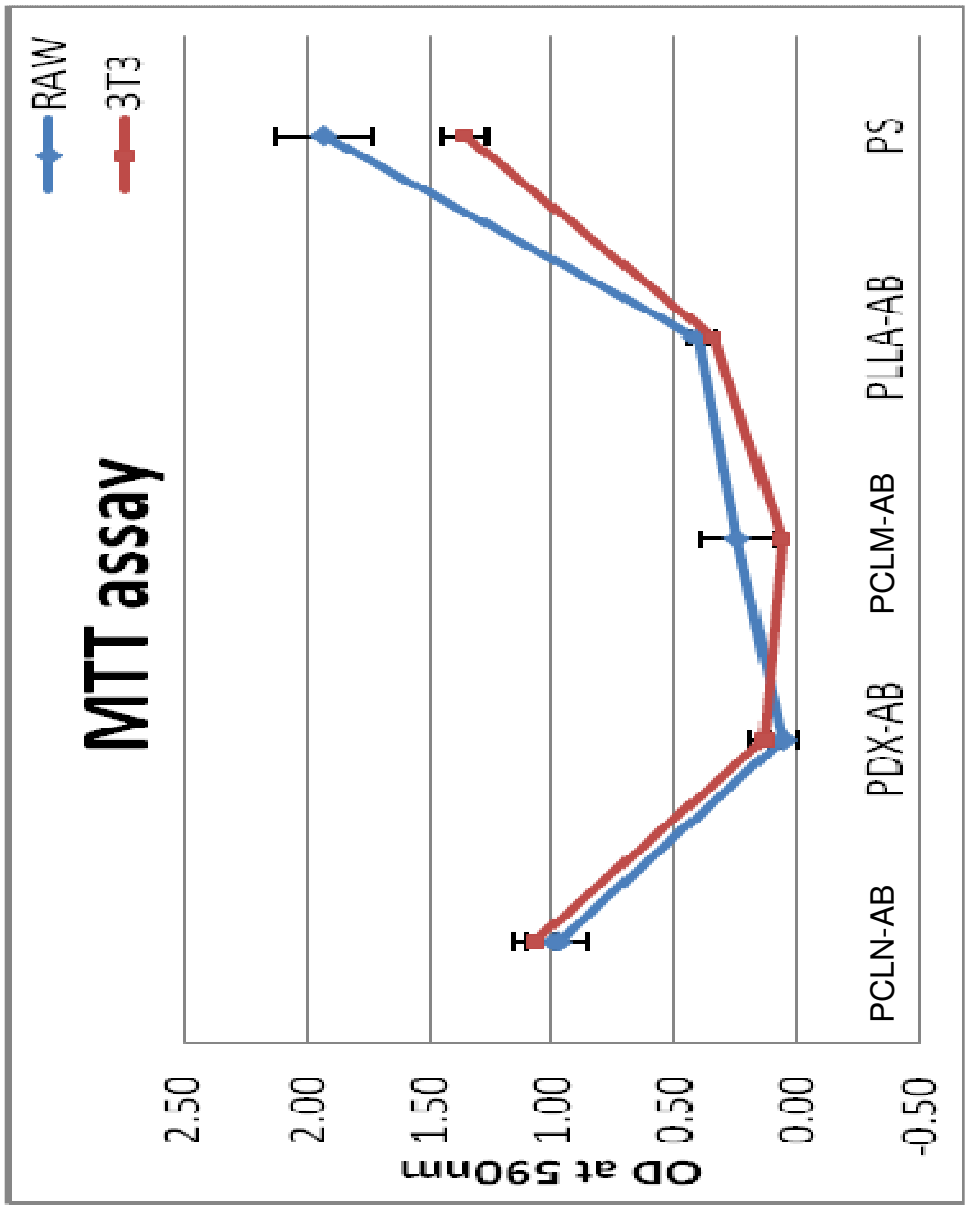

Figure 6.4. MTT assay results for the AB/bioresorbable composites (PCLN-AB, PDX-AB, PCLM-AB, and PLLA-AB) and a PS control. Error bars represent ± 1 standard deviation (SD).

AB/PCLM and AB/PDX displayed much lower readings in the MTT assay. This is evidence of low cell viability on these composites, but there is a possibility that the low viability on AB/PCLM may be due to poor cell adhesion and loss of cells during the seeding process. The viability of both cell lines appeared similar for each composite. This indicated that the materials were consistent in their cytotoxicity effect on both cell lines. SEM images provided confirmation of the cell growth on the materials. Figure 6.5 shows the SEM images of AB/PCLN composites after being cultured for 7 days with the Raw264.7 and NIH/3T3 cells. The cells maintained their original morphology, spherical for the Raw264.7 cells[33] and spindle-like for the NIH/3T3 cells.[34] Additionally, they covered over 90% of the surface. In contrast, the cells cultured for the same length on time on the AB/PCLM composites were not evenly distributed and mostly located at the edges of the sample (Figure 6.6). This experiment will ultimately be repeated because it was quite surprising. The cells still maintained their morphology. Preliminary results from soaking the samples in the cell culture medium and comparing them to the original samples did not show any clear pathways of degradation on this time scale.

My composites were also tested to determine if they would elicit an inflammatory response. Macrophages play many roles during wound healing and one of them is to initiate and mediate the inflammatory response. This is done through the production of various cytokines, including IL-1β and TNF-α. RT-rt-PCR can be used to quantify *in vitro* the generation of these cytokines by the Raw264.7 cell line. The results of the PCR analysis are shown in Figure 6.7. AB/PDX composites were not tested because of the extremely low cell counts and an adequate amount of RNA could not be extracted. All the composites and the PS control stimulated the production of IL-1β and TNF-α. In

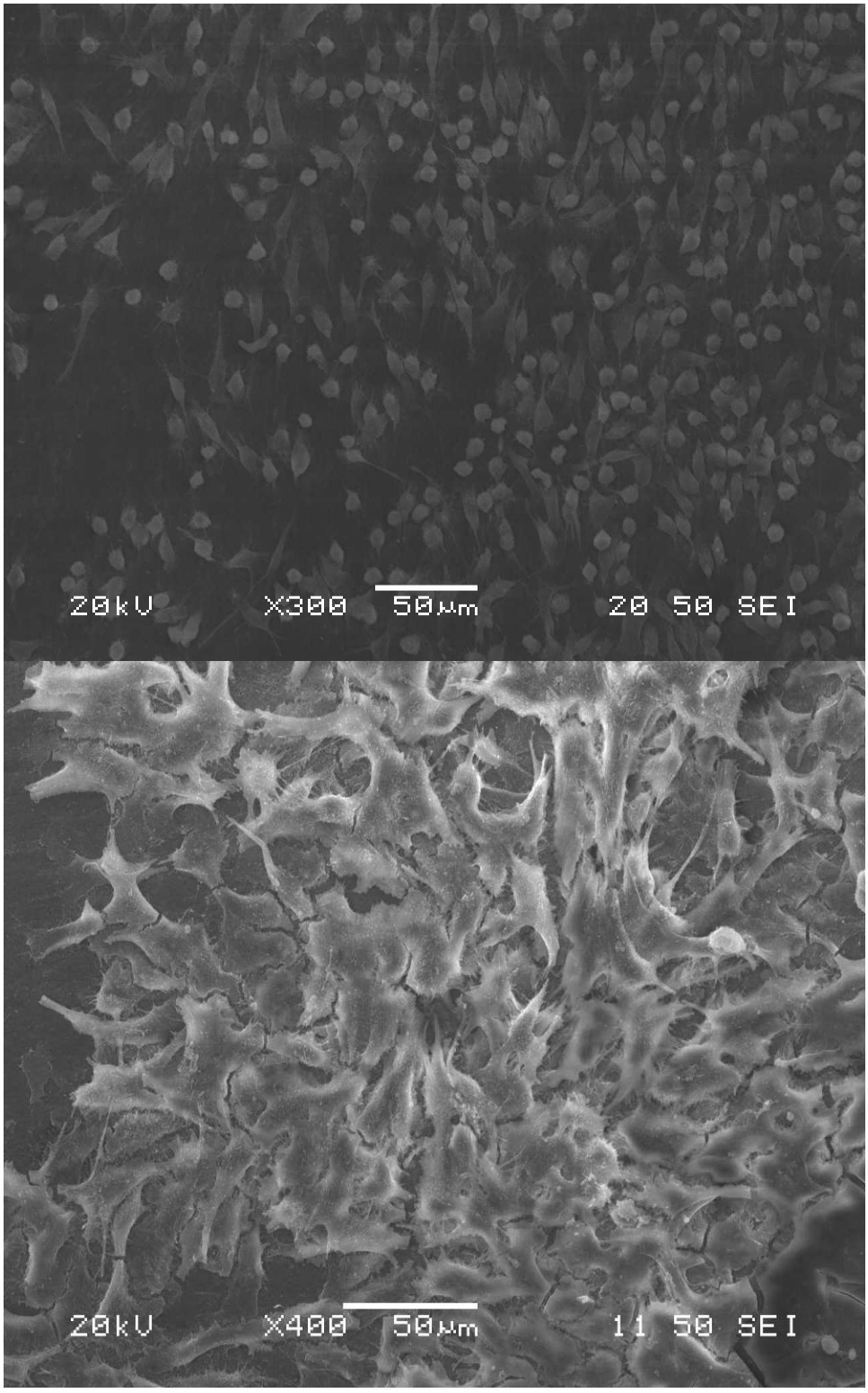

Figure 6.5. SEM images of (top) Raw264.7 macrophage cells and (bottom) NIH/3T3 fibroblast cells on an AB/PCLN composite.

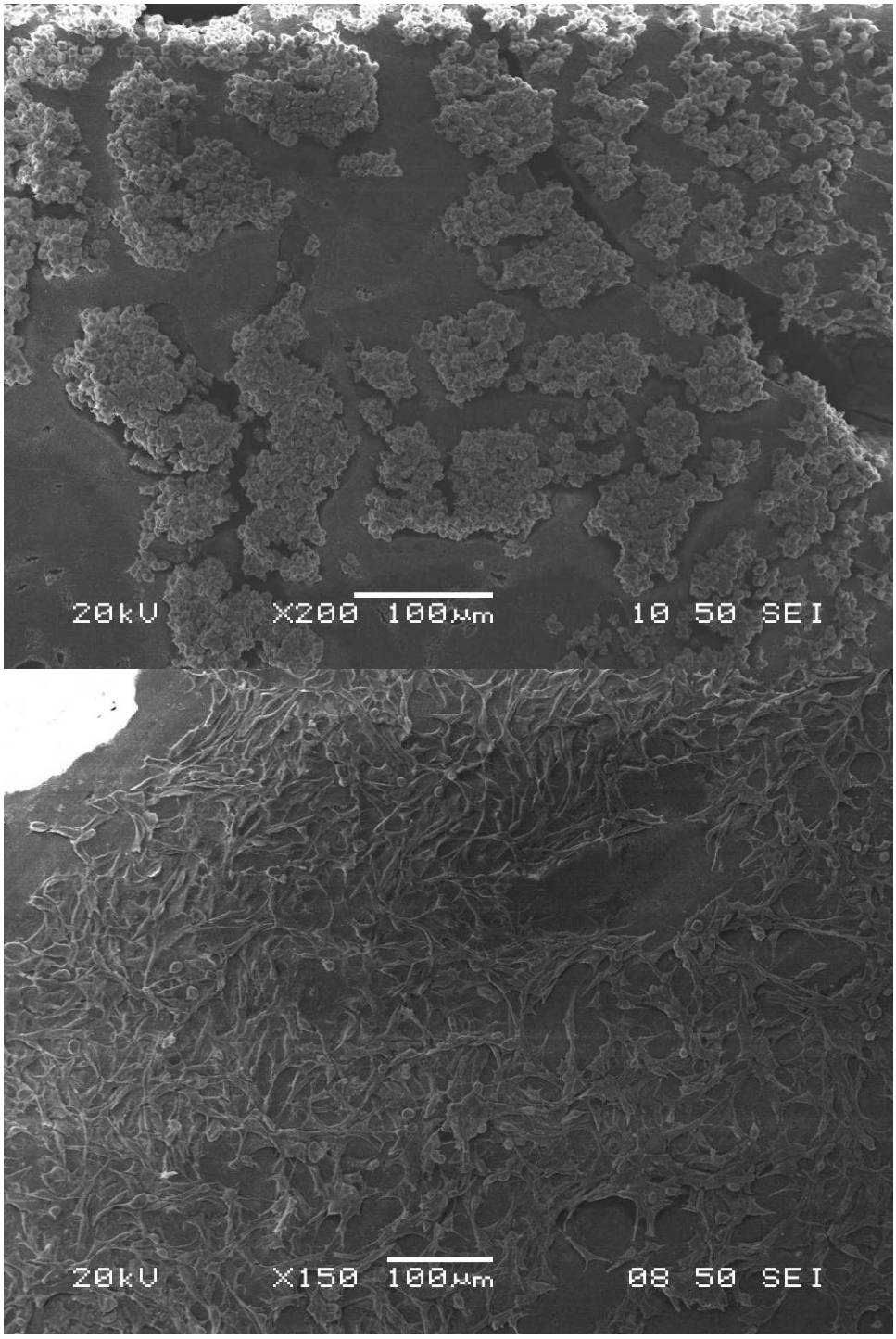

Figure 6.6. SEM images of (top) Raw 264.7 macrophage and (bottom) NIH/3T3 fibroblast cells on an AB/PCLM composite.

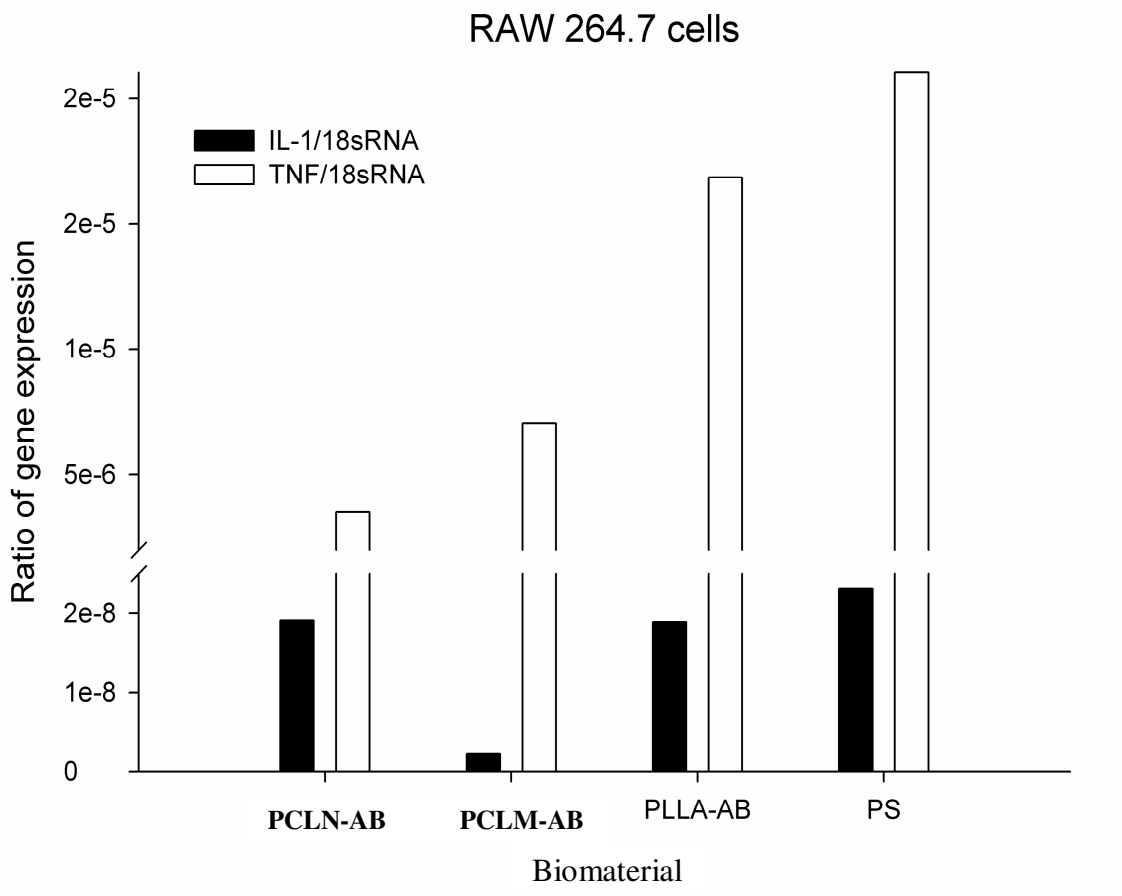

Figure 6.7. Expression of IL-1β and TNF-α in Raw264.7 macrophage cells in response to seeding on various AB/bioresorbable polymer composites and a PS control.

comparison to the PS, control which is widely used in cell culture plates as a non toxic material, all three tested composites had lower levels of IL-1β and TNF-α expression. This indicates lower activation of the macrophages by the composites, which may indicate the development of a mild inflammatory response when implanted. The results do not indicate that the inflammatory response is necessarily undesirable. It is also noteworthy that these results for AB/PCLM are somewhat contradictory to the MTT results for AB/PCLM. It is unclear that the gene expression ratio for AB/PCLM could be this low if very few viable cells were present, as was indicated by the MTT assay.

Conclusion

The AB/PCLN and AB/PLLA composites appeared to exhibit reasonable biocompatibility based on these *in vitro* tests described in this chapter. Both showed adequate cell growth, the cells maintained their morphology, and they showed low production of IL-1β and TNF-α. Due to the lower cell viability on the AB/PCLM and AB/PDX composites, these materials were less promising than the AB/PLLA and AB/PCLN composites. Another composite recently developed within the Redepenning research group is AB/polyglycolide (PG). By comparison to other studies, we anticipate that the PG in the AB/PG composites will resorb much move quickly than the PLLA in the AB/PLLA composites. The *in vitro* biocompatibility of this material is not yet known, but given the similarity between PG and PLLA it could be expected to behave similarly.

Regardless of the material chosen for future applications, it is highly likely that additional *in vitro* screening will be done. Because these materials are intended for use as bone graft materials, one good place to start would be to measure osteoclast and

osteoblast cell activity on the composites. Like the previous *in vitro* studies, thin discs of the composites will be seeded with bone marrow-derived stem cells and cultured under conditions designed to enhance osteoclastogenesis. The osteoclasts will be examined for cell activation status. The composites will be examined for signs of degradation using image analysis of culture microphotographs, histological evaluation using trichrome staining, and assays of bone and polymer breakdown products. This will include calcium release into the culture medium. This work will be performed in collaboration with Professor Paul Wooley's group at Via Christi Hospital in Wichita, KS.

Composites that perform well in the *in vitro* tests will undergo additional biocompatibility testing using the murine air pouch model.[35] These experiments will use a mouse osteolysis model. This model mimics the conditions that exist during wound healing after implantation of a foreign material into the body. Male BALB/c mice will be injected subcutaneously with 2.5 mL of air to form the air pouch. After 6 days a sterile saline solution is injected into the pouch and 2 days later the composite is implanted. The mice are sacrificed 14 days later and the fluid within the pouch is analyzed. Additionally histological and immunohistochemical evaluations will be conducted to determine the tissue inflammation status and morphology of the composite. Pathological analysis of the cell morphology at the interface between the inflammatory tissue and the composite will also be conducted. Bone density, bone volume fraction, and bone structure of the composites will be measured using microcomputerized tomography (MicroCT) imaging. Based on the biocompatibility results as well as the mechanical properties of the composite materials, the ultimate goal is to select a material to be used to repair a segmental bone defect. The defect will be introduced into the femur of a 200-250 g male

Lewis rat. The same section of bone from a donor rat will be processed and converted into a composite of AB/bioresorbable polymer using conditions preferred by our group. This composite rat femur, with dimensions similar to the femoral bone for which it is being substituted, will be implanted into the defect. The performance of the implant will be assessed through a variety of tests including histological, immunohistological, and biomechanical assessments.

References

1. Holt, D.J.; Chamberlain, L.M.; Grainger, D.W., Cell-cell signaling on co-cultures of macrophages and fibroblasts. *Biomaterials* **2010**, 31, 9382-9394.

2. Anderson J.M.; Gristina A.G.; Hanson S.R.; Harker L.A.; Johnson R.J.; Merritt K.; Naylor P.T.; Schoen F.J., Host reactions to biomaterial and their evaluation. In *Biomaterials science: An introduction to materials in medicine*, Ratner B.D.; Hoffman A.S.; Schoen F.J.; Lemons J.E., eds.; Academic Press: San Diego, California, 1996.

3. Anderson, J.M.; Rodriguez, A.; Chang, D.T., Foreign body Reaction to biomaterials. *Seminars in Immunology* **2008**, 20, 86-100.

4. Greenhalgh, D.G., The role of monocytes/macrophages in wound healing. In *Phagocyte Function: A Guide for Research and Clinical Evaluation*, Robinson, J.P.; Babcock, G.F., eds.; Wiley-Liss: New York, New York, 1998.

5. Valente, J.F.; Ogle, C.K.; Alexander, J.W., Monocytes and macrophages in solid organ transplantation: Important implications for the future of transplant immunology. In *Phagocyte Function: A Guide for Research and Clinical Evaluation*, Robinson, J.P.; Babcock, G.F., eds.; Wiley-Liss: New York, New York, 1998.

6. Wound healing. In *Biomaterials Science and Biocompatibility*, Silver, F.H.; Christiansen, D.L., eds.; Springer: New York, New York, 1999.

7. Hatefi, Y., The mitochondrial electron transport and oxidative phosphorylation system. *Annual Review of Biochemistry* **1985**, *54*, 1015-1069.

8. Chakrabarti, R.; Kundu, S.; Kumar, S., Vitamin A as an enzyme that catalyzes the reduction of MTT to formazan by vitamin c. *Journal of Cellular Biochemistry* **2000,** 80, 133-138.

9. Griffiths, G. D.; Lindsay, C. D.; Upshall, D. G., Examination of the toxicity of several protein toxins of plant origin using bovine pulmonary endothelial cells. *Toxicology* **1994,** 90, 11-27.

10. Lacy, A.; O'Kennedy, R., Studies on coumarins and coumarin-related compounds to determine their therapeutic role in the treatment of cancer. *Current Pharmaceutical Design* **2004,** 10, 3797-3811.

11. Melo, A. R.; Lasunskaia, E. B.; de Almeida, C. M. C.; Schriefer, A.; Kipnis, T. L.; da Silva, W. D., Expression of the virulence factor, BfpA, by enteropathogenic Escherichia coli is essential for apoptosis signaling but not for NF-kappa B activation in host cells. *Scandinavian Journal of Immunology* **2005,** 61, 511-519.

12. Mosmann, T., Rapid colorimetric assay for cellular growth and survival: Application to proliferation and cytotoxicity assays. *Journal of Immunological Methods* **1983**, 65, 55–63.

13. Hunt, M., Real time PCR. http://pathmicro.med.sc.edu/pcr/realtime-home.htm, July 1, 2010. Accessed August 6, 2011.

14. Ponchel, F.; Toomes, C.; Bransfield, K.; Leong, F.T.; Douglas, S.H.; Field, S.L.; Bell, S.M.; Combaret, V.; Puisieux, A.; Mighell, A.J.; Robinson, P.A.; Inglehearn, C.F.; Isaacs, J.D.; Markham, A.F., Real-time PCR based on SYBR-Green I fluorescence: An alternative to the TaqMan assay for a relative quantification of gene rearrangements, gene amplifications and micro gene deletions. *BMC Biotechnology* **2003**, 3, 18.

15. Pfaffl, M.W., A new mathematical model for relative quantification in real-time RT-PCR. *Nucleic Acids Research* **2001**, 29, 2002-2007.

16. Goidin, D.; Mamessier, A.; Staquet, M.J.; Schmitt, D.; Berthier-Vergnes, O., Ribosomal 18S RNA prevails over glyceraldehyde-3-phosphate dehydrogenase and beta-actin genes as internal standard for quantitative comparison of mRNA levels in invasive and noninvasive human melanoma cell subpopulations. *Analytical Biochemistry* **2001**, 295, 17-21.

17. Peng, F.; Yu, X.; Wei, M., In vitro cell performance on hydroxyapatite particles/poly(L-lactic acid) nanofibrous scaffolds with an excellent particle along nanofiber orientation. *Acta Biomaterialia* **2011**, 7, 2585-2592.

18. Li, J.; Zheng, W.; Zheng, Y.F.; Lou, X., Cell responses and hemocompatibility of g-HA/PLA composites. *Science China Life Sciences* **2011**, 54, 366-371.

19. Jeong, S.I.; Ko, E.K.; Yum, J.; Jung, C.H.; Lee, Y.M.; Shin. H., Nanofibrous poly(lactic acid)/hydroxyapatite composite scaffolds for guided tissue regeneration. *Macromolecular Bioscience* **2007**, 8, 328-338.

20. Marques, A.P.; Reis, R.L.; Hunt, J.A., Cytokine secretion from mononuclear cells cultured *in vitro* with starch-based polymers and poly-L-lactide. *Journal of Biomedical Materials Research Part A* **2004**, 71, 419-429.

21. Hunt, J.A.; Callaghan, J.T., Polymer-hydroxyapatite composite versus polymer interference screws in anterior cruciate ligament reconstruction in a large animal model. *Knee Surgery, Sports Traumatology, Arthroscopy* **2008**, 16, 655-660.

22. Hojo, Y.; Kotani, Y.; Ito, M.; Abumi, K.; Kadosawa, T.; Shikinami, Y.; Minami, A., A biomechanical and histological evaluation of a bioresorbable lumber interbody fusion cage. *Biomaterials* **2005**, 26, 2643-2651.

23. Williams, J.B.; Irvine, J.W., Preparation of the inorganic matrix of bone. *Science* **1954**, 119, 771-772.

24. Wiegand, T.E., Resorbable Polymer-Hydroxyapatite Composites for Bone Trauma Treatment: Synthesis and Properties, Ph.D. dissertation, University of Nebraska, Lincoln, Nebraska, 2011.

25. Lee, S. H.; Kim, B. S.; Kim, S. H.; Choi, S. W.; Jeong, S. I.; Kwon, I. K.; Kang, S. W.; Nikolovski, J.; Mooney, D. J.; Han, Y. K.; Kim, Y. H., Elastic biodegradable poly(glycolide-co-caprolactone) scaffold for tissue engineering. *Journal of Biomedical Materials Research Part A* **2003,** 66A, 29-37.

26. Stolt, M.; Viljanmaa, M.; Sodergard, A.; Tormala, P., Blends of poly(epsilon-caprolactone-b-lactic acid) and poly(lactic acid) for hot-melt applications. *Journal of Applied Polymer Science* **2004,** 91, 196-204.

27. Zhang, J.; Wang, L. Q.; Wang, H. J.; Tu, K. H.; Liu, L., Amphiphilic block copolymers based on methoxy poly(ethylene glycol) and either crystalline or amorphous poly(caprolactone-b-lactide): Synthesis, solid-state and aqueous solution characterizations. *Journal of Applied Polymer Science* **2007,** 105, 915-927.

28. Zhong, Z. Y.; Ankone, M. J. K.; Dijkstra, P. J.; Birg, C.; Westerhausen, M.; Feijen, J., Calcium methoxide initiated ring-opening polymerization of epsilon-caprolactone and L-lactide. *Polymer Bulletin* **2001,** 46, 51-57.

29. Zhang, Y.; Zhang, Q.; Cheng, K.; Xu, J., Monocarboxyl-end-grouped polycaprolactam with an adjustable molecular weight. *Journal of Applied Polymer Science* **2004**, 92, 722-727.

30. Holmes, B.S.; Moniz, W.B.; Ferguson, R.C., NMR study of nylon 66 in solution (^{1}H, ^{13}C, and ^{15}N NMR using adiabatic J cross polarization). *Macromolecules* **1982**, 15, 129-132.

31. Ziats, N.P.; Miller, K.M.; Anderson, J.M., In vitro and in vivo interactions of cells with biomaterials. *Biomaterials* **1988** 9, 5-13.

32. ter Steege, J.C.; van de Ven, M.W.; Forget, P.P.; Brouckaert, P.; Buurman, W.A., The role of endogenous IFN-gamma, TNF-alpha and IL-10 in LPS-induced nitric oxide release in a mouse model. *Cytokine* **1998** 10, 115-123.

33. Douglas, S.D.; Tuluc, F., Morphology of monocytes and macrophages. In *Williams Hematology 8th ed*., Lichtman, M.A.; Kipps, T.J.; Seligsohn, U.; Kaushansky, K.; Prchal, J.T., eds.; McGraw-Hill: New York, New York, 2010.

34. Dalby, M.J.; Riehle, M.O.; Sutherland, D.S.; Agheli, H.; Curtis, A.S.G., Changes in fibroblast morphology in response to nano-columns produced by colloidal lithography. *Biomaterials* **2004**, 25, 5415-5422.

35. Ottaviani, R. A.; Wooley, P. H.; Song, Z.; Markel, D. C., Inflammatory and immunological responses to hyaluronan preparations using a murine biocompatibility model. *Journal of Bone and Joint Surgery-American Volume* **2007,** 89, 148-157.